A Combinatorial Maf Transcription Factor Code Establishes Synaptic Heterogeneity Critical for Normal Hearing Function

HARVARD UNIVERSITY
Graduate School of Arts and Sciences

DISSERTATION ACCEPTANCE CERTIFICATE

The undersigned, appointed by the

Division of Medical Sciences

Program in Neuroscience

have examined a dissertation entitled

A Combinatorial Maf Transcription Factor Code Establishes Synaptic Heterogeneity Critical for Normal Hearing Function

presented by Isle M. Bastille

candidate for the degree of Doctor of Philosophy and hereby certify that it is worthy of acceptance.

Signature: Thomas Schwarz
Thomas Schwarz (Dec 2, 2022 13:35 EST)

Typed Name: Dr. Thomas Schwarz

Signature: RosalindA Segal
RosalindA Segal (Dec 2, 2022 14:00 EST)

Typed Name: Dr. Rosalind Segal

Signature: gordon fishell
gordon fishell (Dec 2, 2022 13:19 EST)

Typed Name: Dr. Gordon Fishell

Signature: Mark Rutherford
Mark Rutherford (Dec 2, 2022 13:11 EST)

Typed Name: Dr. Mark Rutherford

Date: December 01, 2022

A Combinatorial MAF Transcription Factor Code Establishes Synaptic Heterogeneity Critical for Normal Hearing Function

A dissertation presented

by

Isle M. Bastille

to

The Division of Medical Sciences

in partial fulfillment of the requirements

for the degree of

Doctor of Philosophy

in the subject of

Neuroscience

Harvard University

Cambridge, Massachusetts

December 2022

Dissertation advisor: Lisa V. Goodrich Isle M. Bastille

A Combinatorial MAF Transcription Factor Code Establishes Synaptic Heterogeneity Critical for Normal Hearing Function

Abstract

Spiral ganglion neuron (SGN) synaptic, functional, and molecular diversity is critical for hearing function. Heterogeneous inner hair cell (IHC)-SGN synapses transduce complex sound information from the ear to the brain. Type I SGNs encode the frequency, timing, and intensity of the sounds we hear. Each Type I SGN creates one to two synapses onto a single IHC. Immunohistochemical analyses have found variations in the subunit composition and volume of glutamate receptor puncta among SGN postsynaptic terminals. Synapses develop during the first postnatal week in mice and acquire their mature heterogeneous properties by one month. Single-cell RNA sequencing has shown that Type I SGNs can be divided into three molecularly distinct subtypes (IA, IB and IC). However, the molecular drivers of SGN synaptic heterogeneity remain elusive. MAF family transcription factors stand out as excellent candidates due to their known roles in synapse development. To define the contributions of MAFB and CMAF to synapse development and heterogeneity, we examined their expression patterns and assessed conditional knock-out strains for changes in synaptic morphology, auditory response, and gene expression. We used 10X single-cell RNA sequencing (scRNAseq) to independently assess c*Maf* and *Mafb* RNA expression levels across Type 1 SGN subtypes and to detect changes to synaptic genes in knockout strains. We have found that single-knockouts of CMAF and MAFB have both opposing and additive synaptic and functional phenotypes, with particularly severe deficits in double knockout animals. CMAF and MAFB are expressed in complementary patterns across SGN molecular subtypes and transcriptional analyses confirm that CMAF and MAFB contribute to subtype-specific and overall synaptic gene expression in SGNs. Here, we show

that these transcription factors create a combinatorial code across SGN subtypes to establish the synaptic heterogeneity that is critical for normal hearing function.

Table of Contents

List of Figures

List of Tables

Acknowledgements

"People are not a means to an end. They are the end." Josh Pan, PhD

I am so thankful for all the people that have carried me to this point. Not only because they have supported my endeavors, but because they have enriched my life with meaning. The privilege of having this moment to acknowledge these people is just as rewarding as the scientific work itself.

It is impressive when a weed grows through concrete. But I find it even more impressive that there are places on Earth that have grown rainforests. The Goodrich lab is a rainforest of curiosity, collaboration, and kindness all mixed with an abundance of scientific rigor and humor. I am so lucky to have been able to do this work in such a hospitable and stimulating environment. I am especially grateful to Austen Sitko for her continuous encouragement and contributions to this project. I am also thankful to Lucy Lee, my talented collaborator on this project and an fearless lab manager who has rescued us all from equipment meltdowns, orange ceiling goop and rogue birds. The ethos of the lab is modeled by Lisa Goodrich. I could not have asked for a more inspiring and patient mentor. I have learned so much from her guidance and watching how she navigates science, leadership, and life with the utmost integrity.

Beyond the Goodrich lab, I have found several oases of support and compassion. I am thankful to the department administrative staff including Karen Harmin, Susan Jackson and Soha Ashrafi. They are the forest rangers that have protected and promoted a vision of inclusivity and progress in the department culture. I was immensely fortunate for the feedback that Pascal Kaeser, Constance Cepko, Thomas Schwarz and Rachel Wilson provided as members of my dissertation advisory committee and student advisory committee. I am also grateful to Gordon Fishell, Mark Rutherford and Rosalind Segal for serving on my dissertation examination committee. I'm thankful for the staff at the Bauer Sequencing Core and the Neurobiology Imaging facility who have contributed to these scientific discoveries.

My favorite discovery in graduate school has been the friends I've found in fellow PiN students. I am so thankful for the countless weekends spent exploring and sharing interesting ideas about biology and the world while simultaneously laughing to tears. These are the people I would go to space with because they have taught me more about neutron stars and dark matter in a single Friday night than I would have ever learned in a lifetime. They would also be the best company and bring the best snacks. Andrew Landau, Jasmine Reggiani, Daniel Gilliam, Rich Hakim, and Aniqa Tasnim, I'm ready when you are.

I am thankful to Jessica Gutchess and Ivan Santiago for riding along with me all these years. Thank you for unquestioningly buckling up next to me when the ride got choppy. Thank you for always packing an extra parachute.

Knowing Win Gillis has been akin to exploring every corner of the universe without even leaving the safety and comfort of my living room. Thankful is an understatement.

I am grateful to my whole family for their love and humor. I am especially thankful to my mother and my father who have sacrificed so much for me and taught me to live passionately, genuinely and without fear. They are as different from each other as the wind and the tides. But they have both taught me to always keep moving, with and for the world.

CHAPTER ONE

Introduction

The sense of hearing provides animals with rich information about the surrounding environment. Sound information is used to localize danger or food and to communicate within and across species. This information can be detected over large distances and dynamic ranges. For example, humans can detect sound intensities over 100 decibels and frequencies from 20 hertz to 20 kilohertz[1,2]. Our impressive sense of hearing also gives us the ability to appreciate music while simultaneously conferring the ability to filter out unfavorable sounds.

Highly adapted structures within the mammalian inner ear encode and relay sound information to the brain. Within the inner ear, mechanosensitive hair cells create synapses with primary afferent spiral ganglion neurons (SGNs) which transmit sound information to the brain[3]. To reliably transduce complex sound information, these synapses are heterogeneous in form and function[4]. While much work has been done to characterize the morphological development and physiology of cochlear synapses, insight into the genetic mechanisms that establish and fine tune synaptic heterogeneity remains elusive. Recent work understanding the overall genetic heterogeneity of SGNs has provided a molecular handle for investigating the genetic regulation of SGN synaptic diversity[5–7].

OVERVIEW OF COCHLEAR WIRING

Sound vibrations first travel through the middle ear and to the basilar membrane in the cochlea. In humans and mice, there are four rows of mechanically sensitive hair cells that transduce basilar membrane vibrations into graded electrochemical signals. There is one row of inner hair cells which behave as sound detectors and three rows of outer hair cells which function as sound amplifiers. Hair cells synaptically transmit information to bipolar spiral ganglion neurons (SGNs), which send sound information to the brain. Specifically, presynaptic densities, known as ribbons, line the bottom surface of hair cells. These ribbons cluster synaptic vesicles that release glutamate onto postsynaptic glutamate receptors in SGN terminals (**Figure 1.1, inset**). If the opening of postsynaptic receptors causes sufficient depolarization, SGNs will

fire an action potential. SGN axons coalesce into the VIIIth cranial nerve to relay sound information to target cells in the brain for further processing. Therefore, SGNs are critical conduits between the auditory environment and the brain[3].

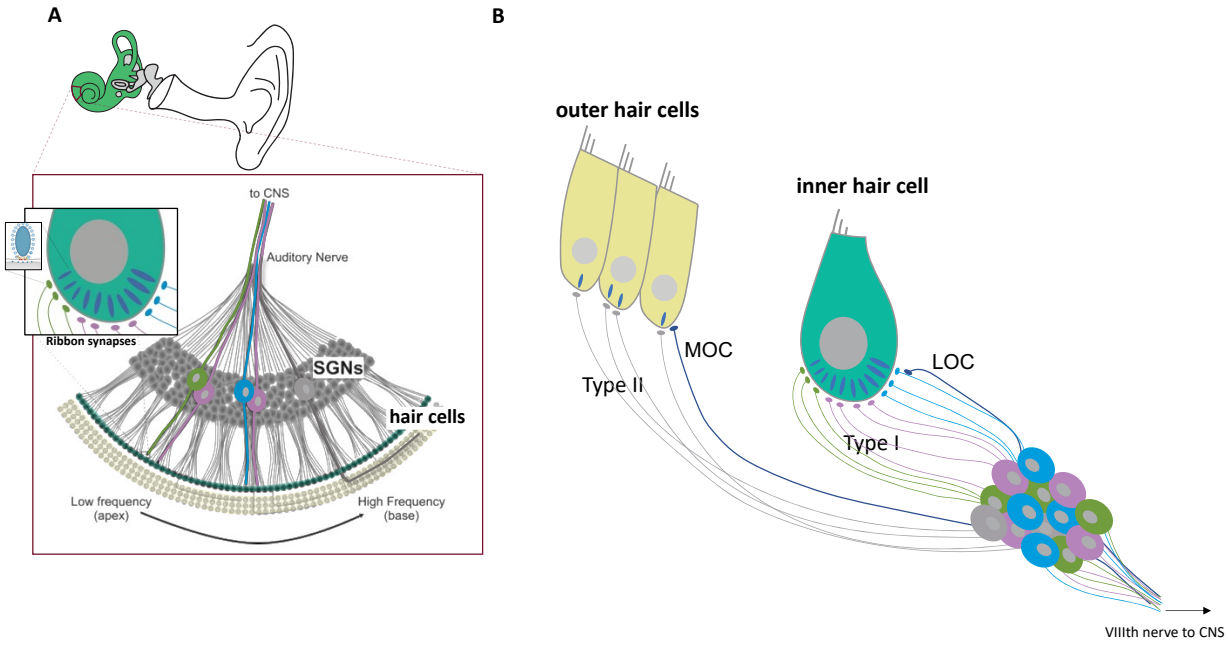

Figure 1.1. Organization of cells in the cochlea. (A) A top-down view of a segment of the cochlea showing the spiraling rows of outer and inner hair cells attached to radiating bundles from Type I and Type II SGNs. Type II SGNs project to the outer hair cells and turn towards the base (dark grey). Type I SGNs project out to inner hair cells (green, purple, blue). The inset shows a zoomed-in view of Type I SGN ribbon synapses on the bottom of a single inner hair cell. Each of the presynaptic ribbons (blue) is studded with glutamatergic vesicles (shown in smaller inset) **(B)** A schematic showing how afferent spiral ganglion and efferent (MOC= medial olivocochlear and LOC= lateral olivocochlear) neurons are organized in a cross-section of the cochlea. Type II SGNs synapse onto multiple outer hair cells, while most Type I SGNs synapse onto one inner hair cell. MOC efferent neurons synapse onto outer hair cells and LOC efferent neurons synapse onto the peripheral processes of Type I SGNs.

Electrophysiological and morphological diversity across SGNs increases the functional encoding capacity of SGNs as a population. The most salient difference across SGNs is between Type I and Type II SGNs, which receive synaptic input from inner and outer hair cells, respectively. A single Type II SGN sends a projection towards the base of the cochlea and receives *en passant* input from multiple outer hair cells (**Figure 1.1A**). These cells are thought to function as auditory nociceptors and mounting evidence indicates that they serve a protective function in noxious sound environments[8,9]. Type II SGNs are unique to mammals and comprise approximately 5% of the total SGN population[10]. Meanwhile, Type I SGNs encode all the information about the frequency, timing, and intensity of sounds. Each Type I SGN receives input from one to two inner hair cells and each inner hair cell synapses onto approximately 10-20 SGNs depending on species and tonotopic location[3,11–13] (**Figure 1.1B**). SGN electrophysiological properties are also regulated by the olivocochlear feedback system which extends processes from the auditory brainstem into the cochlea. Lateral and medial olivocochlear (LOC and MOC) efferent neurons form neuromodulatory synapses onto the peripheral processes of type I SGNs and onto outer hair cells, respectively.

As a population, Type I SGNs must reliably encode an immense range of sound frequencies and intensities while also preserving precise information about the timing of sounds. The divergence from a single graded hair cell potential into multiple, spiking SGNs allows for the segmentation of sound information into different neural representations. Therefore, to fully encode sound, Type I SGNs are both specialized and diverse in their response properties to synaptic input[6,14–16]. Insight into how Type I SGNs develop and maintain heterogenous properties to meet these demands has come from decades of work investigating the development, electrophysiology, synaptic properties, and molecular constitution of Type I SGNs. Many studies have found an association between the electrophysiological, synaptic, and molecular profiles of Type I SGNs and their synaptic position on inner hair cells in the pillar to modiolar axis (modiolar = closer to SGN cell bodies, pillar = closer to the tallest hair cell

stereocilia) (**Figure 1.2A**). The concordance between molecular, electrophysiological, and synaptic data provides a handle for further understanding how SGN synaptic properties emerge and contribute to the functional encoding of sound. For the rest of this thesis, I will focus on synaptic, molecular, and electrophysiological properties within mammalian Type I SGNs (referred to as “SGNs" for simplicity). There is further interesting diversity and specialization within Type II SGNs as well as across invertebrates and non-mammals that is outside of the scope of this thesis.

Electrophysiological properties of SGNs

Diversity in SGN electrophysiological response properties is essential for the complete encoding of all features of sound[14,16]. Hair cells are organized tonotopically along the basilar membrane. The characteristic frequency of a cell along this axis refers to the preferential sound frequencies that the cell encodes. Hair cells in the apex of the cochlea have low characteristic frequencies and those in the base have higher characteristic frequencies. SGNs are aligned to hair cells in this tonotopic axis and vary correspondingly in their tonotopic responses to sound frequencies[17,18](**Figure 1.1A**).

SGNs with identical frequency tuning contain further electrophysiological heterogeneity. SGNs encode increasing sound intensity, or loudness, as an increase in action potential spike rate. However, ethologically relevant sound intensities can span several orders of magnitude. To tile this immense range, SGNs vary in evoked and cell-intrinsic electrophysiological properties[2]. *In vitro* recordings have shown that SGNs have diverse responses to injected currents[19]. Whole-cell patch recording and single-cell labeling of SGNs in acute cochlear preparations from rats have shown that SGNs display a wide range of biophysical properties across postnatal development and into maturity. Across the first three weeks of postnatal development, SGN maximum conductances and current thresholds increase while latencies become shorter[20]. Electrophysiological heterogeneity persists in adult animals. Single unit

recordings along with dye tracing in the cat found that mature SGNs can be divided into physiologically distinct groups based on their spontaneous firing rates and thresholds (defined as the lowest sound intensity that elicits a spike). These groups include low spontaneous firing rate (SR)/high threshold SGNs, medium SR/medium threshold SGNs, and high SR/low threshold SGNs. The dynamic range of sound intensity encoding also seemed to covary with these properties. High SR SGNs encoded a more limited range of sound intensities while low SR SGNs encoded a wider range[21]. Together, these electrophysiological groups are thought to convey the large range of sound intensities required for normal hearing[2].

Synaptic heterogeneity of SGNs

Along the tonotopic axis, the number of synapses between inner hair cells and SGNs differ widely, peaking at the frequency range where the cochlea is most sensitive to sound. For mice, synapse number peaks around 17-20 synapses per hair cell at the 16 kHz region of the cochlea[3,22]. Meanwhile, regardless of tonotopic location, a single inner hair cell converts mechanical information into a graded receptor potential that drives diverse firing in 10-20 SGNs[13]. Heterogeneity in individual IHC-SGN synaptic properties contributes to the electrophysiological diversity across SGNs required for encoding a complete representation of sound. Assessments of dye-filled neurons after recording have shown that the electrophysiological subclasses of SGNs differ in their projection patterns and synaptic properties in the pillar to modiolar axis of one hair cell. Low SR SGNs synapse preferentially onto the modiolar side of the hair cell, apposed to larger presynaptic ribbons while high SR SGNs preferentially synapse onto the pillar side of the hair cell apposed to smaller presynaptic ribbons[4] (**Figure 1.2A,B**). Recordings from intact rat cochlear preps followed by single fiber labeling has shown that the firing properties of SGNs are correlative with their synaptic contact location on the bottom of the hair cell in the pillar to modiolar axis[20]. Presynaptic ribbons and postsynaptic patches of glutamate receptors can be clearly visualized by immunohistochemistry

and confocal microscopy. Each GLUR2 punctum is a cluster of GLUR2-containing AMPA receptors in the postsynaptic membrane of one SGN. CTBP2 is a transcription factor that is identical to the B domain of RIBEYE, the core component of presynaptic ribbons[23]. Staining for CTBP2 marks the presynaptic ribbon. These stains reveal the tight apposition and varying sizes of pre- and postsynaptic puncta (**Figure 1.2C**).

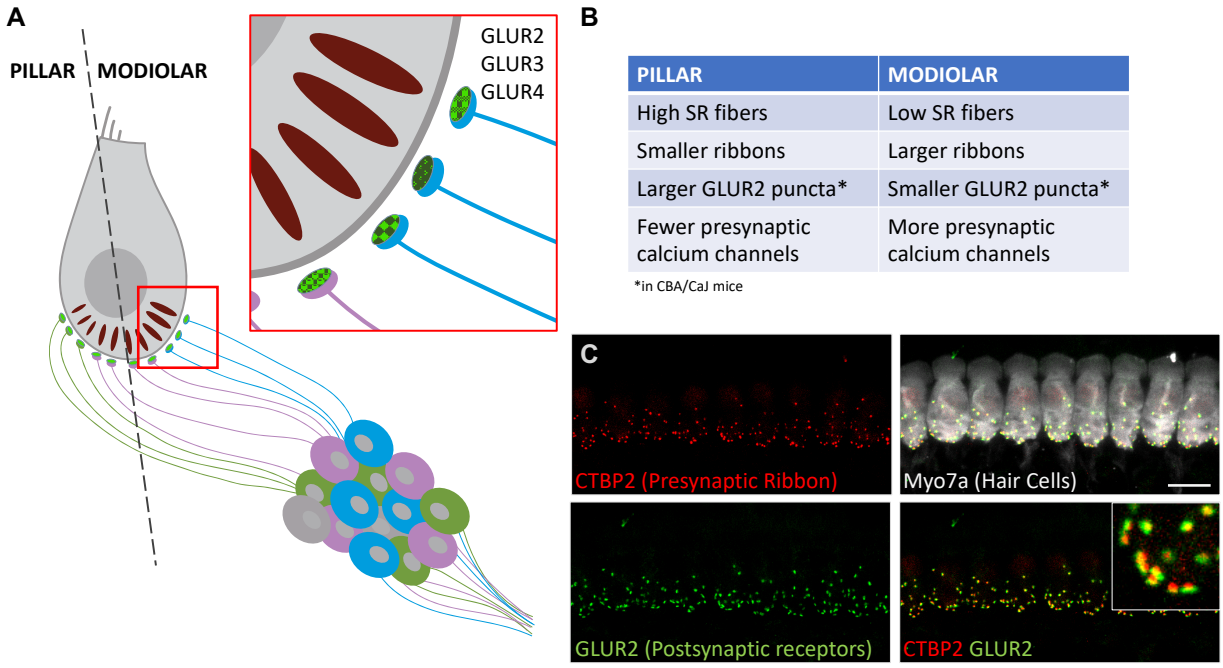

Figure 1.2. Morphological and molecular diversity across SGNs. (A) A schematic summary of the organization of projections and synapses between inner hair cells and Type I SGNs. Further heterogeneity across SGN fibers in GLUR subunit composition is shown in the red inset. **(B)** Summary table of morphological and electrophysiological properties of pillar and modiolar synapses. **(C)** CTBP2 staining marks presynaptic ribbons and GLUR2 marks postsynaptic glutamate receptors. MYO7A is used to visualize hair cells.

Beyond size differences in presynaptic ribbons, presynaptic release properties and calcium dynamics have been shown to vary in the pillar to modiolar axis. The number of inferred Ca^{2+} channels and Ca^{2+} currents are larger on the modiolar side of the hair cell. Modiolar Ca^{2+}

channels open at more depolarized hair cells potentials compared to pillar localized channels[24,25]. Patch-clamp recording combined with glutamate and calcium imaging in explanted cochleae of young adult mice has shown that ribbons differ in voltage dependence of release as well as the degree of calcium coupling to the release of synaptic vesicles across the pillar to modiolar axis[26]. The size of the presynaptic density has also been shown to vary in this axis[27].

SGNs differ in their postsynaptic properties as well. Patch clamp recordings and immunohistochemistry have shown that postsynaptic currents in SGNs are mediated α-amino-3-hydroxy-5-methylisoxazole-4-propionic acid (AMPA) receptors. Tetrameric AMPA receptors are responsible for the fast, large excitatory currents observed at the IHC-SGN synapse. Mature SGNs contain AMPA receptors that express variable amounts of GLUR2, GLUR3, and GLUR4 subunits[28–32](**Figure 1.2, inset**). AMPA receptors that contain GLUR2 are known to have similar conductances of Na+ and K+ as other combinations but greatly reduced conductances of Ca^{2+} due to RNA editing that replaces a glutamine amino acid with a charged arginine amino acid[33,34]. Therefore, although many postsynaptic AMPA receptors are calcium impermeable, SGNs also contain calcium permeable AMPA receptors[32,35]. Extensive work has characterized heterogeneity in the volume of glutamate receptor puncta in the postsynaptic membrane of SGNs that correlates with the electrophysiological differences in thresholds and firing rates. There is large variability in the volume of GLUR puncta across individual SGNs. In certain strains of mice such as CBA/CaJ, there are generally larger GLUR puncta are observed on the pillar side of the hair cell and smaller GLUR puncta are observed on the modiolar side[4,9,36]. Postsynaptic recordings have shown that pillar and modiolar SGN currents differ in amplitude in response to different presynaptic current rates. Pillar synapses produce larger EPSCs while modiolar synapses produce smaller EPSCs in response to high presynaptic release rates[37]. Both pre- and postsynaptic properties as well as differential expression of receptors and ion channels likely combine to produce response diversity among SGNs.

SGNs are molecularly distinct

Along the tonotopic axis, SGNs express diverse neurotrophins, calcium binding proteins, and ion channels that likely correspond to the distinct demands of encoding low and high frequency sound[38]. Electrophysiological and immunohistochemical findings hinted that SGNs within similar frequency ranges contain further molecular heterogeneity that corresponds to the distinct postsynaptic response properties in the pillar to modiolar axis. It was not until recent years that studies utilizing single-cell RNA sequencing (scRNAseq) have found definitive molecular subtypes of SGNs that differ both across and within different locations along the tonotopic axis[5–7]. Three independent studies have shown that Type I SGNs can be divided into three molecular subtypes named type IA, IB, and IC (**Figure 1.3**). These three groups are found along the entire tonotopic axis and can be distinguished by varying expression levels of cell adhesion molecules, neurotransmitter receptors, ion channels, and transcription factors. Several genes emerged as useful markers that molecularly delineate these subtypes. For example, the calcium binding protein, calretinin (CALB2), is differentially expressed across SGNs; Type IA, IB, and IC SGNs express high, medium and low relative levels of *Calb2* respectively. CALB2 expression across SGN fibers varies in the pillar to modiolar axis. High CALB2 expressing cells preferentially synapse onto the pillar side of the hair cell and likely correspond to high SR neurons. Meanwhile, type IB and IC SGNs express mid and low levels of Calb2 respectively and synapse onto the modiolar side of the hair cell and likely correspond to medium and low SR SGNs (**Figure 1.3**). Furthermore, type IC neurons are preferentially affected by aging, which is consistent with the preferential vulnerability of low SR SGNs to age-related hearing loss[6,39,40]. These findings provide molecular insight and access into the characteristics of the previously observed electrophysiological, morphological, and synaptic groups.

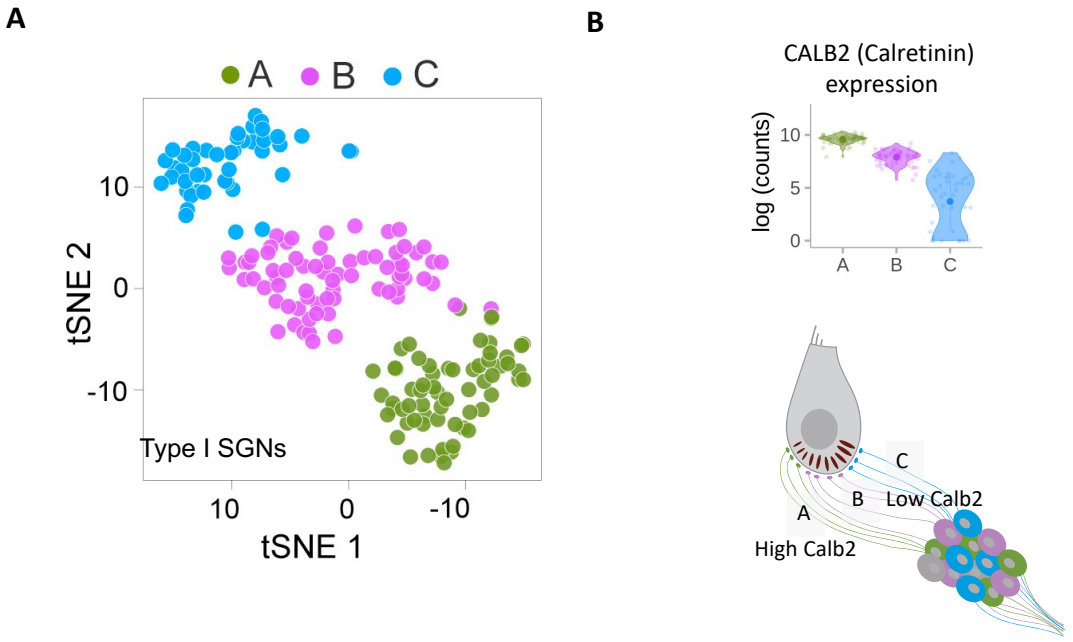

Figure 1.3. Molecular diversity across SGNs. (A) Type I SGNs cluster into three distinct groups by single cell RNAseq. **(B)** Violin plot of Calb2 expression levels across Type I SGN subtypes and schematic of SGN molecular subtype projection patterns. *TSNE and Violin Plot from (Shrestha…Goodrich, 2018).*

The development of distinct SGN subtypes

A series of prenatal developmental steps dictate development of general SGN fate. In mice, SGN precursors originate in the otic placode, an ectodermal thickening located next to the 5th and 6th rhombomeres of the hindbrain. This otic placode invaginates and detaches as the otic vesicle. Between embryonic day (E)9.5 and E12.5 in the mouse, neuroblasts delaminate from the otic vesicle and coalesce to form the cochlear-vestibular ganglion[41]. Subsequently, this ganglion separates into the spiral and vestibular ganglion. By E13.5, most SGNs have exited the cell cycle. SGNs begin to send peripheral processes out to the hair cell region around

E14.5. SGN processes coalesce to form the radial bundles characteristic of the mature wiring pattern around E15/ E16[42].

Key transcriptional cascades over the course of development sequentially differentiate otic progenitors into fully mature SGNs. The transcription factor GATA3 acts repeatedly during development to direct SGN production and coordinate multiple aspects of SGN differentiation. Knockout of *Gata3* in post-delamination neurons (around E9.5) resulted in defects in cochlear wiring. Furthermore, sustained developmental expression of GATA3 is important for inducing SGN differentiation and suppressing vestibular ganglion neuron (VGN) identity in later stages of development. RT-PCR confirmation of microarray data in *Gata3* cKO mice showed the upregulation of several VGN genes[43,44]. By late embryogenesis, certain SGNs are already exhibiting bias towards IB/IC subtype fates due to their expression of the transcription factor RUNX1[45]. At birth, immature ribbon synapses can be observed at the base of the cochlea. These synapses contain clusters of ribbons and emerging AMPA receptor clusters in the developing postsynaptic density[46].

Postnatally, each SGN subtype acquires the exquisitely precise and heterogeneous synaptic properties, refined connections with inner hair cells, and expression of other subtype specific genes that determine their ultimate subtype identity and electrophysiological potential[47]. During the first postnatal week in mice, SGN subtype identities and gene expression are refined to resemble mature patterns[6]. The number of ribbons peaks toward the end of the first postnatal week[48]. RIBEYE aggregates are transported to the basolateral surface of the hair cell as ribbon precursors that undergo dynamic refinement, fusing, and pruning. By the onset of hearing, around postnatal day (P)12 in mice, ribbon numbers are close to adult level. Differences in pillar and modiolar ribbon size are most evident around P15[49]. Spatial gradients of GLUR puncta size are evident as early as the puncta have coalesced into quantifiable units around P14[13]. Meanwhile, Cav1.3 channels are localized to the bottom of the hair cell in the first postnatal week. Around P14, these channels become segregated near ribbons. At this time, AMPA

receptors form more discrete, denser, ring-like puncta centered directly across presynaptic ribbons[22]. Between P17 and P34, presynaptic ribbons elongate while the surface area of postsynaptic densities (PSDs) decreases. Additionally, the spatial gradient of PSD morphology decreases, with pillar PSDs decreasing the most in surface area during this time[27]. There is further segregation in pillar to modiolar synapse development. For instance, pillar synapses do not mature electrophysiologically until after P20[37]. This has been corroborated by studies showing that the biophysics of neurons contacting the modiolar face of the hair cell change faster with age than do pillar-contacting neurons[20].

Little is known about the molecular pathways that initiate ribbon synapse formation. Thyroid hormone is broadly important for the overall maturation of the ribbon synapse. In animals that lack thyroid follicular cells, synapse pruning does not occur and synaptic puncta numbers remain elevated into adulthood. Furthermore, IHCs retain immature presynaptic properties containing multiple ribbons apposed to a single GLUR2 punctum[47]. Synapse development depends on intrinsic transcriptional programs that guide SGN development overall. Previous work identified the transcription factor GATA3 as a regulator of SGN development and gross SGN wiring. In mutants with GATA3 selectively deleted from SGNs, there was significant downregulation of two MAF transcription factors, MAFB and CMAF[44]. The transcription factor MAFB is expressed downstream of GATA3 and is critical in SGNs for the proper development of the PSD. Knocking out *Mafb* from SGNs results in the downregulation of GLUR2 staining in SGN peripheral processes. However, not all SGN synapses were affected in *Mafb* KOs, suggesting the involvement of other factors in synaptic development[50]. The transcription factor CMAF is similar in structure to MAFB and is also expressed downstream of GATA3 in SGNs[44]. However, the function of CMAF in SGNs is unknown.

The MAF transcription factors

Several properties of CMAF and MAFB suggest that they can work together and separately to regulate gene transcription. MAFB and CMAF are part of a family of large MAF transcription factors that possess the evolutionarily conserved basic and leucine zipper domain (bZIP) at their C-terminus. The leucine zipper confers the capacity for homo- and heterodimerization with other transcription factors and with each other. Dimerization results in combinatorial DNA binding sites conferred by each individual DNA binding site in the dimer. This feature expands the regulatory repertoire of each bZIP transcription factor and provides the means to integrate with other transcription factors to regulate gene expression in a nuanced way[51]. Next to the bZIP domain is a homologous region known to mediate DNA binding called the ancillary DNA binding domain. Cooperation between the bZIP domain and an adjacent ancillary DNA-binding domain regulates DNA binding of these proteins. CMAF and MAFB have identical DNA binding sites. When these proteins homodimerize or heterodimerize with other large MAF factors, the DNA binding site from each protein conjoins into a palindromic DNA recognition sequence known as MAF recognition elements or MAREs. On the N-terminus, CMAF and MAFB both have a transcriptional domain that consists of 100 amino acids. Meanwhile, CMAF and MAFB differ in the linker region between the ancillary DNA binding site and the transcriptional domain. The linker region is longer in CMAF and contains glycine and histidine repeats while the linker domain in MAFB contains histidine repeats (**Figure 1.4**).

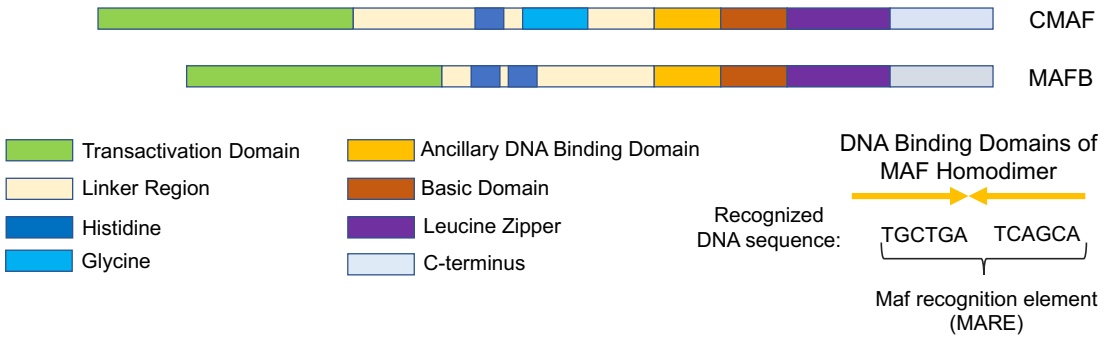

Figure 1.4 Molecular Structure of CMAF and MAFB. The structural domains of CMAF and MAFB include the transactivation domain, the linker region, the ancillary DNA binding domain, and the basic leucine zipper. MAF homodimers have conjoined DNA binding domains called MAF recognition elements (MAREs) that recognize palindromic sequences of DNA.

Despite having identical DNA binding and transcriptional domains, CMAF and MAFB can have differential control over gene expression. CMAF and MAFB have overlapping and distinct compatibility for dimerization with other transcription factors. For example, MAFB can dimerize with CJUN while CMAF cannot and both CMAF and MAFB can dimerize with CFOS[52]. The precise combinations of dimers and the extent of dimerization can have different genetic outcomes[53,54]. However, the DNA binding sequences of bZIP heterodimers cannot simply be inferred by the conjoined DNA binding sites from each individual transcription factor in the dimer. This indicates that there is emergent DNA binding that is difficult to predict. Emergent DNA binding often depends on the variable spacing between each DNA binding domain in the dimer that is likely dictated by the context-specific dimerization geometry and chemistry of the two transcription factors[51].

CMAF and MAFB are known to act as key regulators of terminal differentiation in many tissues including bone, kidney, lens and blood. Regulators of terminal differentiation are

important for the expression of mature identity features. For example, MAFB is important for the expression of insulin and glucagon in pancreatic endocrine cells whose primary function is to secrete these two hormones[52]. Within the central nervous system, CMAF and MAFB are important for synaptic differentiation. CMAF is critical for the proper differentiation of Pacinian corpuscles, afferent mechanoreceptors in the skin that detect high frequency vibrations[55]. CMAF and MAFB have been found to have antagonistic roles in the postnatal development of cortical interneuron synapses. Specifically, *cMaf* knockout cortical interneurons had more excitatory synapses on proximal dendrites while *Mafb* knockouts had fewer. Meanwhile, double knockout neurons had similar synaptic counts compared to control. In concordance, *cMaf* knockout mice had larger amplitude excitatory postsynaptic currents (EPSCs) while *Mafb* knockouts had smaller amplitude EPSCs[56].

Both CMAF and MAFB are expressed in SGNs[44,50]. Immunohistochemical stains qualitatively reveal heterogenous expression of MAFB in the spiral ganglion indicating that MAFB might be differentially expressed across SGN subtypes. Additionally, some, but not all GLUR2 puncta were downregulated in *Mafb* knockouts[50]. Previous studies on MAFB in SGNs were performed prior to our current appreciation of the close correspondence between molecular and synaptic heterogeneity across SGNs. Therefore, the transcription factors that dictate the differentiation and diversification of SGN synaptic properties remain elusive. We hypothesize that CMAF and MAFB are differentially expressed across SGN subtypes and have subtype-specific effects on SGN synaptic development and gene expression.

Utilizing intersectional mouse genetics, analyses of synaptic morphology, functional hearing measurements, and single-cell RNA sequencing, my thesis aims to uncover the role of CMAF and MAFB in establishing SGN synaptic properties necessary for functional hearing. Considering the observation that some, but not all synapses were affected in *Mafb* knockouts, my work first assesses the synaptic and functional effects of knocking out *cMaf* and *Mafb* alone and together across SGNs (**Chapter 2**). This data identifies both synergistic and antagonistic

effects of CMAF and MAFB on SGN synaptic properties and functional output. I then leverage our current insights into the molecular subtypes of SGNs to characterize CMAF and MAFB expression patterns across SGN subtypes (**Chapter 3**). This analysis reveals that CMAF and MAFB are expressed in complementary patterns across SGN subtypes. From these findings, I parse out the relative contributions of each of these transcription factors to SGN synaptic gene expression. Using scRNAseq, I compare the molecular profiles of mutant and control SGNs to reveal overlapping and distinct differentially expressed synaptic and synaptic plasticity genes in *cMaf* and *Mafb* single and double knockout mice (**Chapter 4**). I also find that CMAF and MAFB contribute to SGN subtype-specific synaptic gene expression. With this data, I posit that CMAF and MAFB create combinatorial MAF transcription factor "code" that instructs the execution of subtype-specific synaptic properties. This work provides insight into the transcriptional programs that dictate SGN synaptic diversity.

CHAPTER TWO

Antagonistic and synergistic contributions of CMAF and MAFB to SGN synaptic properties and synchronous firing

Isle M. Bastille and Lisa V. Goodrich designed all experiments. IMB, Lucy Lee, and Austen Sitko collected and stained all cochlea. IMB and LL created synaptic reconstructions. Evan Hale and LL measured auditory brainstem responses. IMB analyzed all quantitative data.

INTRODUCTION

Several decades of work have revealed electrophysiological and morphological heterogeneity in spiral ganglion neuron (SGN) peripheral synapses that transmit auditory information from the ear to the brain. While many studies have gone on to characterize the molecular composition of these synapses, little is known about the transcriptional events that fine tune and ensure synaptic patterning required for proper hearing. Understanding the logic of synaptic transcriptional programs will reveal downstream gene expression profiles and proteins that diversify the functional output of SGN molecular subtypes.

SGN peripheral synapses with inner hair cells are made up of presynaptic ribbons directly apposed to postsynaptic glutamate receptors. Postnatally, presynaptic ribbons and postsynaptic densities are pruned, consolidated, and aligned as pre- and postsynaptic pairs[27,49]. Synapses are spread across the bottom surface of the hair cell and contain different sizes of pre- and postsynaptic puncta, which can be directly visualized by fluorescent immunohistochemistry and confocal microscopy. This heterogeneity contributes to the diverse electrophysiological potential of each SGN and is crucial for the collective encoding of a large range of sound intensities[16].

The transcription factors MAFB and CMAF are excellent candidates for understanding the transcriptional programs that contribute to diverse SGN synaptic properties. CMAF regulates synaptic features in the cortex and peripheral somatosensory system[55]. In fact, in cortical interneurons, CMAF and MAFB have been shown to have opposing effects on interneuron excitability and synaptic development. CMAF knockout interneurons contain more excitatory postsynaptic puncta while MAFB knockout interneurons contain fewer[56]. Furthermore, MAFB directs post-synaptic differentiation in SGN peripheral synapses. The loss of MAFB results in a downregulation of GLUR2 puncta and presynaptic ribbons as early as postnatal day (P)6[50]. However, not all synaptic puncta are diminished in MAFB mutants, implicating the involvement of other factors that contribute to the establishment and fine tuning of SGN synaptic

properties. CMAF is expressed in SGNs and is identical in structure to MAFB in its DNA binding and transactivation domains. MAFB and CMAF have shared and unique dimerization partners, which could result in similar and dissimilar DNA binding sites and downstream target genes[52]. We hypothesize that CMAF contributes in distinct, overlapping, and combinatorial ways as MAFB to the establishment of peripheral SGN synapses.

We used conditional transgenic mice and cochlear wholemount synapse analysis to show that CMAF and MAFB contribute in both opposing and additive ways to SGN synaptic properties. By measuring the auditory brainstem responses (ABRs) in *cMaf* and *Mafb* single and double mutants, we demonstrate that CMAF and MAFB also contribute in opposing and additive ways to auditory sensitivity.

RESULTS AND DISCUSSION

To assess the contributions of CMAF and MAFB to SGN synaptic properties, we collected cochleae from *Mafb* and *cMaf* single and double knockout mutants and control littermates for wholemount staining. To knockout *Mafb* and *cMaf* from SGNs, we crossed *Bhlhe22*$^{Cre/+}$ (*B5*$^{Cre/+}$) animals to double floxed *cMaf* and floxed *Mafb* animals (*Mafb*$^{fl/fl}$;*cMaf*$^{fl/fl}$). In the cochlea, *B5*$^{Cre/+}$ is expressed in SGNs. We collected ears from 8-12 week old littermates with a total of 10 double conditional knockout animals (*cMaf/Mafb*^{dKO}, *B5*$^{Cre/+}$;*Mafb*$^{fl/fl}$;*cMaf*$^{fl/fl}$), 8 Mafb conditional knockout animals (*Mafb*^{CKO}, *B5*$^{Cre/+}$;*Mafb*$^{fl/fl}$;*cMaf*$^{fl/+}$), 9 cMaf conditional knockout animals (*cMaf*^{CKO}, *B5*$^{Cre/+}$;*Mafb*$^{fl/+}$;*cMaf*$^{fl/fl}$) and 15 controls (Control/NoCre, *Mafb*$^{fl/fl}$;*cMaf*$^{fl/fl}$). Immunohistochemistry for CMAF in cochlear sections confirmed the loss of CMAF protein from dKO and *cMaf*^{CKO} animals (**Figure 2.1A-C**). MAFB antibodies that provided strong signal in adult animals were discontinued before we could stain dKO animals. However, MAFB expression peaks in SGNs around postnatal day 6 (P6)[50]. We have been able to stain P6 control (Control, *Mafb*$^{fl/+}$) and *Mafb* knockout (*Mafb*$^{CKO/GFP}$, *B5*$^{Cre/+}$;*Mafb*$^{fl/GFP}$) animals to confirm the downregulation of MAFB with a similar combination of alleles as dKO animals (**Figure**

2.1D,E). Previous studies have also used this floxed *Mafb* allele to successfully knock down MAFB alone and together with CMAF[50,56,57].

The degree of SGN peripheral neurite extension to hair cells could affect IHC-SGN synaptogenesis. Therefore, we assessed if there were any gross changes to SGN wiring patterns in the cochlea. After staining for neurofilament (NFH) in wholemount cochleae, we saw no gross changes to wiring in *cMaf* and *Mafb* single and double mutants (**Figure 2.1F-I**). While differences in neurofilament staining intensity were present, SGN peripheral processes in mutants were still reaching the hair cell area, stained by parvalbumin (PVALB) in qualitatively equal proportions as controls. By staining for choline acetyltransferase (ChAT) we were also able to confirm that there were no gross defects in efferent neuron wiring in the cochlea across genotypes (**Figure 2.1F-I**).

Figure 2.1. *cMaf* and *Mafb* are not required for gross cochlear wiring. (A-C) Anti-CMAF immunostaining of cochlear sections in P66 control (*cMaf*$^{fl/fl}$;*Mafb*$^{fl/fl}$) **(A),** *cMaf*^{CKO} (*B5*$^{Cre/+}$*;cMaf*$^{fl/fl}$;*Mafb*$^{fl/+}$) **(B),** and *cMaf/Mafb*^{DKO} (*B5*$^{Cre/+}$*;cMaf*$^{fl/fl}$;*Mafb*$^{fl/fl}$) **(C),** animals confirms CMAF is downregulated in mutant SGNs. **(D-E)** Anti-MAFB immunostaining of cochlear sections in P6 control (*Mafb*$^{fl/+}$) **(D)** and *Mafb*$^{CKO/GFP}$ (*B5*$^{Cre/+}$;*Mafb*$^{fl/GFP}$) animals confirms MAFB is downregulated in mutant SGNs. (**F-I)** Confocal image stacks of cochlear wholemounts in P42 control (*cMaf*$^{fl/fl}$;*Mafb*$^{fl/fl}$) **(F),** *cMaf*cKO (*B5*$^{Cre/+}$*;cMaf*$^{fl/fl}$;*Mafb*^{fl}+) **(G),** *Mafb*cKO (*B5*$^{Cre/+}$*;cMaf*^{fl}/+;*Mafb*$^{fl/fl}$) **(H),** and *cMaf/Mafb*dKO (*B5*$^{Cre/+}$*;cMaf*$^{fl/fl}$;*Mafb*$^{fl/fl}$) **(I),** immunostained for neurofilament (NFH) to label all neuronal processes, parvalbumin (PVALB) to label hair cells and choline acetyltransferase (ChAT) to label efferent neuron processes reveal no gross changes to cochlear wiring in *cMaf* and *Mafb* single and double mutants. Scale bar in all images = 20μm.

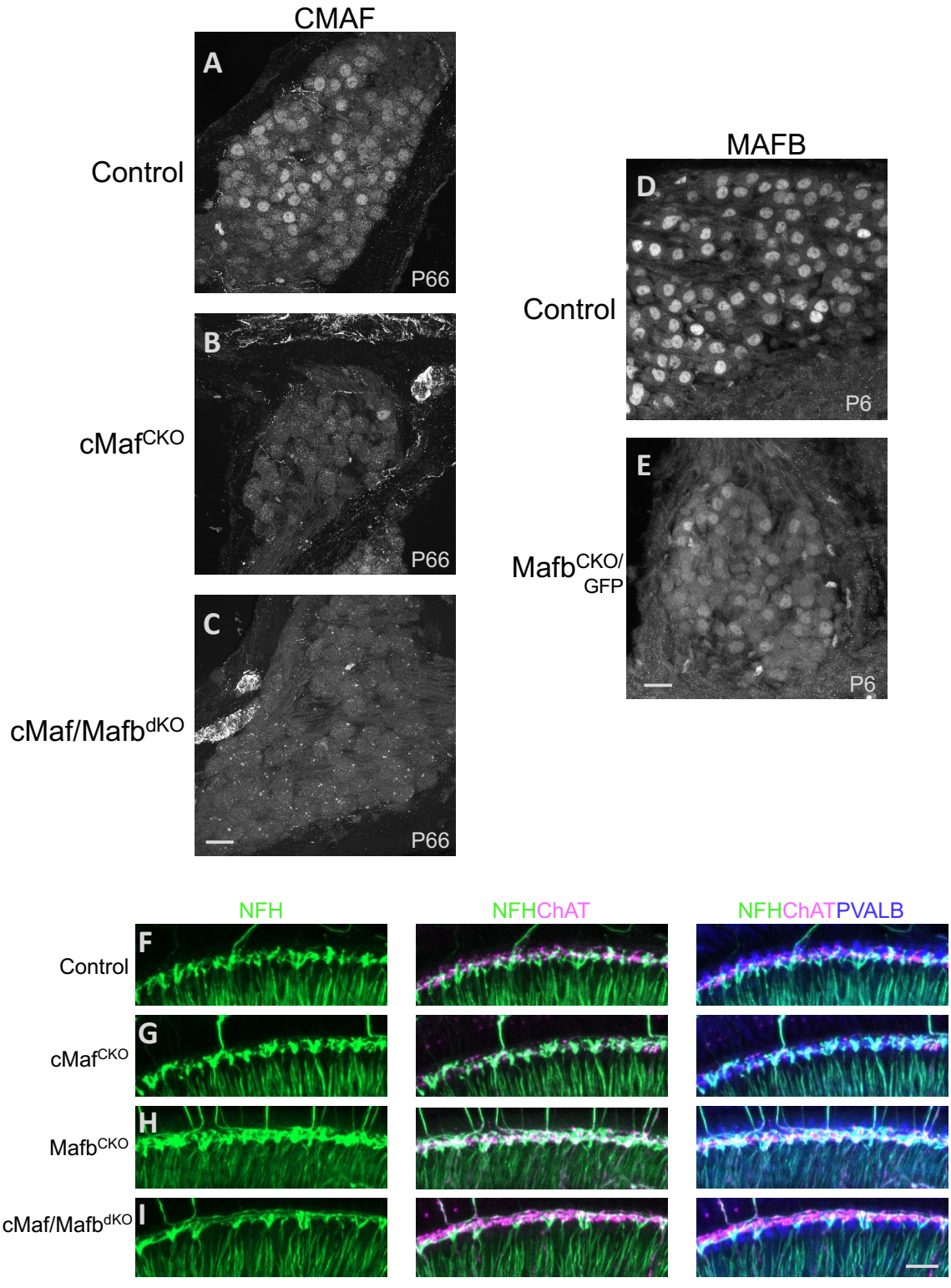
CMAF
MAFB
Control
cMaf^CKO
cMaf/Mafb^dKO
Control
Mafb^CKO/GFP
A
B
C
D
E
P66
P6
NFH
NFHChAT
NFHChATPVALB
Control
cMaf^CKO
Mafb^CKO
cMaf/Mafb^dKO
F
G
H
I

To measure synapses in *cMaf* and *Mafb* mutants, we stained for the presynaptic ribbon marker, CTBP2 which labels the B domain of the ribbon scaffolding protein RIBEYE[23], the postsynaptic glutamate receptor GLUR2, and the calcium binding protein CALB2 to stain hair cells. In these stains, each ribbon punctum is a single presynaptic ribbon and each GLUR2 punctum is a cluster of postsynaptic glutamate receptors from one SGN peripheral neurite. We chose CALB2 as a hair cell marker due to its reliability in delineating the entire perimeter of each hair cell as opposed to other hair cell markers that are mainly cytosolic. We adapted staining protocols that optimized for sensitivity to staining postsynaptic glutamate receptors[58]. Specifically, this involved shorter tissue post-fixation and decalcification that allowed for higher signal to noise for notoriously difficult synaptic stains. This staining protocol allowed us to detect very small glutamate receptor puncta that may have been missed by older methods in our lab. We then captured confocal image stacks of hair cells and synapses (**Figure 2.2A,B**) from the 8 and 16kHz regions of the cochlea of each mouse. Each stack contained 10-12 inner hair cells. Staining and imaging was done in 4 batches which all included control animals. Imaging and staining parameters were kept constant across the four batches, and great care was taken to avoid oversaturating any pixels during imaging.

We created 3D reconstructions of GLUR2 puncta in the 8kHz and 16kHz frequency regions of the cochlea and ribbon reconstructions for the 8kHz region in Imaris (**Figure 2.2C**). These reconstructions allowed us to export measurements of synaptic punctum volumes and relative location between synaptic puncta. We chose to compare synaptic volume over staining intensity because intensity values varied across controls from different staining batches. Meanwhile, the reconstructions generated in Imaris for synaptic puncta were generated using a 'local contrast background subtraction' which is capable of compensating for overall differences in background intensity in the images that could affect changes in the volume of reconstructed puncta. Using this technique, synaptic puncta volumes were similar across controls from

different staining batches. The entirety of these experiments and analyses were done blind to genotype.

To investigate the combined contribution of CMAF and MAFB, we first quantified synapses in dKO mice (**Figure 2.2A,B**). Quantification revealed no change to synapse number, defined as pairs of aligned pre- and post-synaptic puncta (**Figure 2.2D**). Furthermore, there was no significant difference in the number of orphan ribbons per hair cell, or ribbons without an opposing GLUR2 punctum (**Figure 2.2E**). Orphan ribbons are usually found after noise- or chemically-induced synaptopathy where degeneration of SGN peripheral processes results in unpaired ribbons[36,59]. Similar numbers of synapses and paired ribbons in dKOs compared to controls further suggests that SGN peripheral processes are reaching inner hair cells and creating synaptic pairs. However, dKOs contained significantly more orphan GLUR2 puncta per hair cell, or GLUR2 puncta that are not closely apposed to a ribbon (**Figure2.2B, yellow arrowheads; Figure 2.2F**). Orphan GLUR2 puncta are also found in immature cochleae where developing postsynaptic densities contact the hair cell prior to the anchoring of a presynaptic ribbon in that location[49]. It is possible that GLUR2 orphans in dKO mice are the result of afferent contacts that are never paired with a presynaptic ribbon or abnormal pruning of paired ribbons. Further work is needed to investigate these mechanisms.

Although there were no changes in the number of synapses, dKO mice had qualitatively aberrant pre- and post-synaptic puncta sizes and spacing along the bottom of the hair cell (**Figure 2.2A,B**). By extracting volumetric measurements from each synaptic punctum, we found that control and dKO mice had no difference in mean GLUR2 punctum volume. However, the distribution of GLUR2 puncta volume was wider in double knockout mice (**Figure 2.2G**). The interquartile range of the distribution of GLUR2 volume was significantly larger in dKO mice compared to controls (**Figure 2.2H**). By plotting the pillar to modiolar and apical (top of the hair cell) to basal (bottom of the hair cell) positional coordinates of each GLUR2 punctum, we found that the positional distribution of synapses was smaller in dKO (**Figure 2.2I**). When we

measured the GLUR2 interpunctum distance, or the shortest distance between GLUR2 puncta, we found that GLUR2 puncta were closer together in dKO animals compared to controls (**Figure 2.2J**), in line with our qualitative observations**.** Presynaptic ribbons were also closer together in dKO animals (**Figure 2.2K**). Altogether, these results indicate that dKO are still creating synaptic pairs, however, the loss of *cMaf* and *Mafb* results in dysregulation of SGN peripheral synaptic volume and spacing.

Dysregulation in synaptic spacing and volume is also qualitatively similar in stains for GLUR4 puncta, although GLUR4 puncta have not been quantified. Nevertheless, GLUR4 puncta in dKOs also have qualitatively irregular spacing and sizing, mirroring GLUR2 phenotypes (**Figure 2.2L,M**). These observations suggest that the effects of knocking out both *cMaf* and *Mafb* are not confined to GLUR2 AMPA subunits but are affecting mechanisms that contribute to overall AMPA receptor aggregation.

Figure 2.2. *cMaf/Mafb*^{DKO} (dKO) mice have aberrant peripheral SGN synapses. Wholemount synapse staining of GLUR2 and CTBP2 in the 8kHz region of 8-12 week old control (NoCre) (**A**) and *cMaf/Mafb*^{DKO} (dKO, *B5*$^{Cre/+}$*;cMaf*$^{fl/fl}$;*Mafb*$^{fl/fl}$) (**B**) mice. Hair cells were stained by CALB2 (not shown) and are outlined in the merged panels. Orphan GLUR2 puncta are denoted by yellow arrowheads. GLUR2=cyan, Ribbons(CTBP2)=Red, Scale bar, 5μm. **(C)** Representative reconstructions of GLUR2 and CTBP2 puncta from a control animal. **(D)** Average number of synapses per hair cell in control and *cMaf/Mafb*^{DKO} mice (p=0.448, Mann Whitney Rank Sum). Number of orphan ribbons (p=0.088, Mann Whitney Rank Sum) **(E)** and GLUR2 puncta (p<0.001, Mann Whitney Rank Sum) **(F)** per hair cell. **(G)** Distribution of GLUR2 puncta volumes in control and *cMaf/Mafb*^{DKO} mice. **(H)** Average interquartile range of GLUR2 puncta volumes in control and *cMaf/Mafb*^{DKO} mice (p<0.001, Mann Whitney Rank Sum). **(I)** Plots of all individual GLUR2 puncta across animals in the pillar to modiolar and basilar to apical axis of the hair cell. Average GLUR2 **(J)** and ribbon **(K)** inter-punctum distance in control and *cMaf/Mafb*^{DKO} mice (p<0.001, Mann Whitney Rank Sum). **(M-N)** GLUR2 and GLUR4 stain in control and *cMaf/Mafb*^{DKO} mice. Scale bar, 5μm. All measurements from N=12 controls and N=10 *cMaf/Mafb*^{DKO} mice. In all barplots **(D-F, H,J,K),** each dot represents average measurements from a single mouse with standard error. All density plots **(G, F)** represent distributions from all synaptic puncta measured in the 8kHz region.

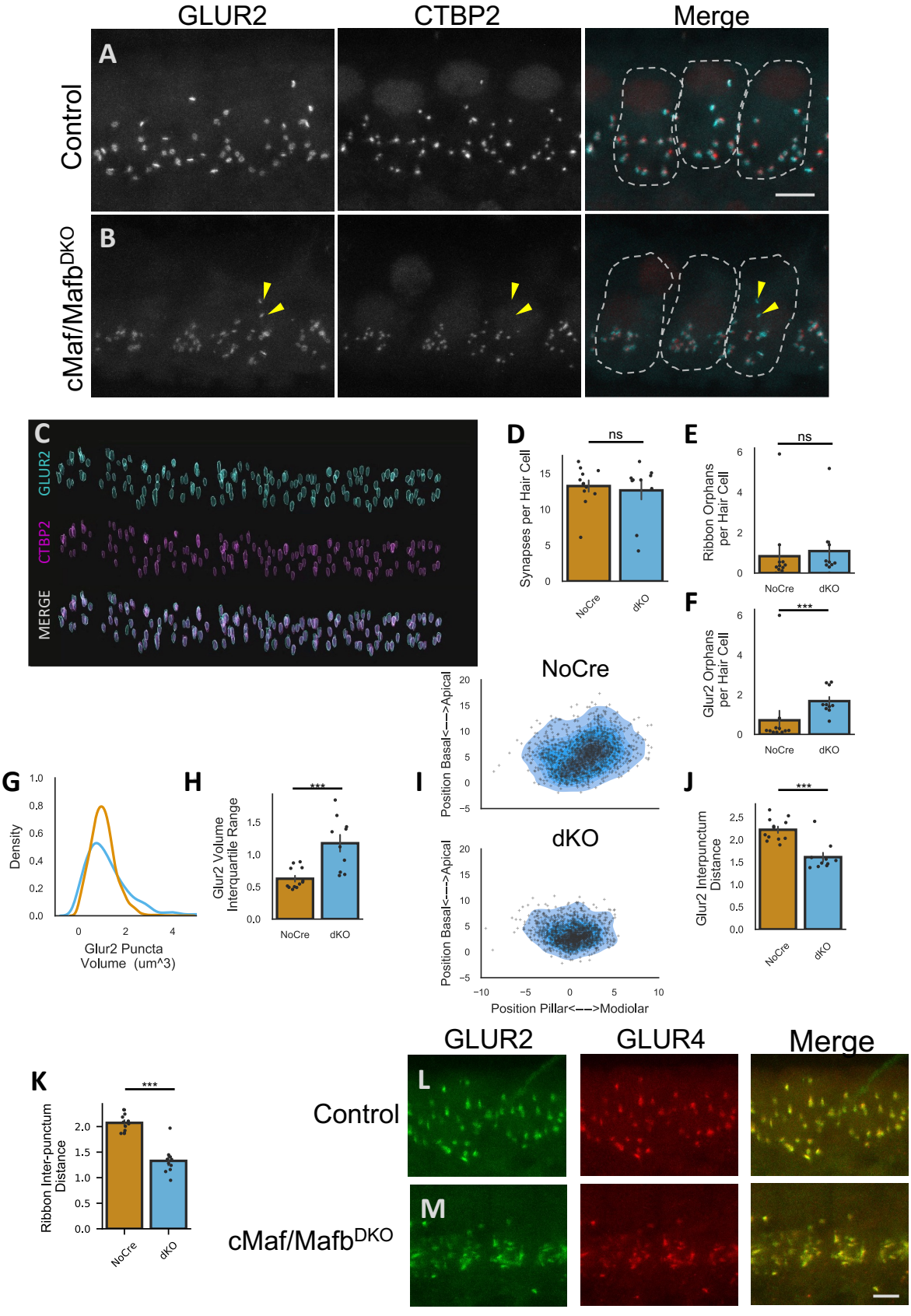
GLUR2
CTBP2
Merge
A
Control
B
cMaf/MafbDKO
C
GLUR2
CTBP2
MERGE
D
ns
Synapses per Hair Cell
NoCre
dKO
E
ns
Ribbon Orphans per Hair Cell
NoCre
dKO
F
***
Glur2 Orphans per Hair Cell
NoCre
dKO
G
Density
Glur2 Puncta Volume (um^3)
H
***
Glur2 Volume Interquartile Range
NoCre
dKO
I
NoCre
dKO
Position Basal<--->Apical
Position Pillar<--->Modiolar
J
***
Glur2 Interpunctum Distance
NoCre
dKO
K
***
Ribbon Inter-punctum Distance
NoCre
dKO
GLUR2
GLUR4
Merge
Control
L
cMaf/MafbDKO
M

cMaf/Mafb dKO phenotypes could reflect dysregulation in synaptic differentiation and maturation. At earlier developmental stages in wildtype (CBA/CAJ) animals, synaptic puncta appear small and clustered together. Postnatally, both ribbons and postsynaptic densities undergo a period of consolidation and refinement. Postsynaptic densities first develop independently of ribbons and eventually become tethered to ribbons through intercellular synaptic adhesion molecules[27,49]. Both presynaptic ribbons and postsynaptic densities transform from small, clustered puncta to consolidated and aligned pre- and postsynaptic pairs that are spread across the bottom of the hair cell[13]. Double knockout synapses qualitatively mirror underdeveloped synapses. One interpretation is that the loss of both *cMaf* and *Mafb* results in aberrant SGN synaptic differentiation.

The mechanisms that determine presynaptic ribbon properties have long been postulated to be entirely dictated by the inner hair cell alone[60]. However, emerging evidence indicates that molecular differentiation in SGNs can drive presynaptic changes in hair cells. CMAF and MAFB are only expressed in SGNs and are not expressed in hair cells in the cochlea. Yet, *cMaf/Mafb* dKO presynaptic ribbons are closer together than controls. Data from our lab has shown that knocking out the transcription factor RUNX1 from SGNs causes changes to overall SGN subtype identity. Shifts in subtype identity result in shifts in both GLUR2 and presynaptic ribbon punctum size, demonstrating that postsynaptic changes can influence presynaptic ribbon properties[45]. Additionally, knocking out the 1C-specific transcription factor *Pou4f1* results in increases in voltage sensitivity of presynaptic calcium channels[61]. Therefore, it is possible that abnormal presynaptic ribbon patterning in *cMaf/Mafb* dKO mice is driven by aberrations in postsynaptic development.

These results indicate that both CMAF and MAFB are critical for establishing mature SGN synaptic properties. However, the relative contributions of *cMaf* and *Mafb* to SGN synaptic properties are unknown. Previous studies have shown that the loss of MAFB results in loss of GLUR2 puncta and presynaptic ribbons[50]. Meanwhile, the role of *cMaf* alone has not been

investigated at this synapse. Therefore, we next wanted to investigate the respective roles of *cMaf* and *Mafb* to the synaptic phenotype observed in the double mutants.

CMAF and MAFB have opposing and synergistic effects on SGN synaptic properties

To investigate how CMAF and MAFB each contribute to the synaptic phenotype observed in *cMaf/Mafb* double knockouts, we compared synaptic properties in *cMaf* (*cMaf*^{CKO}, *B5*$^{Cre/+}$*;Mafb*$^{fl/+}$*;cMaf*$^{fl/fl}$) and *Mafb* (Mafb^{CKO}, *B5*$^{Cre/+}$*;Mafb*$^{fl/fl}$*;cMaf*$^{fl/+}$) single mutants to control (NoCre, *cMaf*$^{fl/fl}$;*Mafb*$^{fl/fl}$) and double knockout (dKO, *B5*$^{Cre/+}$*;Mafb*$^{fl/fl}$*;cMaf*$^{fl/fl}$) littermates (**Figure 2.3 A-D**). Each of the single mutants from these crosses was heterozygous for the other factor. We quantified GLUR2 puncta from the 8kHz and 16kHz region of the cochlea and ribbons from the 8kHz region. Utilizing the same approaches as in the previous section, we found no change in the number of synapses across *cMaf*^{CKO}, *Mafb*^{CKO}, dKO, and control (NoCre) animals (**Figure 2.3E**). We found a moderate, but statistically insignificant increase in GLUR2 orphans in *cMaf*^{CKO} animals compared to controls and fewer GLUR2 orphans in *Mafb*^{CKO} animals compared to dKO animals. Meanwhile, we saw no significant change in the number of ribbon orphans per hair cell across genotypes (**Figure 2.3G**).

Antagonistic effects on volume were observed in the 8kHz and 16kHz region of the cochlea in *cMaf*^{CKO} and *Mafb*^{CKO} mice. Qualitatively, we noticed that *cMaf*^{CKO} postsynaptic GLUR2 puncta (**Figure 2.3B**) appeared larger while *Mafb*^{CKO} GLUR2 puncta (**Figure 2.3C**) appeared smaller compared to controls (**Figure 2.3A**). By plotting the distribution of GLUR2 puncta volumes, we found that *cMaf*^{CKO} GLUR2 puncta were significantly larger while *Mafb*^{CKO} GLUR2 puncta were significantly smaller compared to both the control and dKO mice. (**Figure 2.3H-I,M-N**). These antagonistic trends on volume were also apparent when we plotted the average GLUR2 punctum size per animal (**Figure 2.3J,O**). Average punctum volume of *cMaf*^{CKO} mice was significantly larger than controls in the 16kHz region (**Figure 2.3O**) and showed a

trend for larger puncta in the 8kHz region (**Figure 2.3J**). On the other hand, *Mafb*^{CKO} mice showed a trend for reduced average GLUR2 punctum volume compared with controls and a significant decrease compared with *cMaf*^{CKO} mice in both frequency regions. dKO animals showed no changes in GLUR2 puncta volume compared with controls, possibly due to the antagonistic effects of knocking out each factor.

Although the differences in GLUR2 puncta volumes across genotypes were subtle, we found that the distributions of GLUR2 volumes in *cMaf*^{CKO}, *Mafb*^{CKO} and dKO mice had larger interquartile ranges compared to controls (**Figure 2.3K,P**). Larger variance in punctum volume underscores the dysregulation in synaptic properties that is influenced by both MAF factors. Combined with GLUR2 volume comparisons, these data indicate that a subset of GLUR2 puncta are becoming larger in *cMaf*^{CKO} mice while a subset of GLUR2 puncta are becoming smaller in *Mafb*^{CKO} mice. Furthermore, while the inter-punctum distances were mildly changed in *cMaf*^{CKO} and *Mafb*^{CKO} animals, the dKO animals exhibited closely clustered GLUR2 puncta **Figure 2.3L,Q**). These findings highlight the additive effects that these two transcription factors have on SGN postsynaptic properties.

A previous study demonstrated that *Mafb*^{CKO} animals had fewer GLUR2 puncta[50]. Meanwhile, we observed an average decrease in GLUR2 puncta volume in *Mafb*^{CKO} animals with no overall change in numbers of GLUR2 puncta. This is likely due to changes in the staining protocol optimized for detecting synaptic puncta. In these stains, we were able to detect small GLUR2 puncta in the *Mafb*^{CKO} animals that might have been missed with older, less sensitive staining methods. Therefore, the *Mafb*^{CKO} synaptic phenotype in this study is in agreement with the previously observed phenotype.

Presynaptic properties were also affected in *cMaf*^{CKO}, *Mafb*^{CKO}, and dKO animals. When we compared ribbon volume across genotypes, we found that the ribbons in *cMaf*^{CKO}, *Mafb*^{CKO} and dKO animals were smaller than in controls (**Figure 2.3R-T**). The interquartile range of ribbon volumes was not significantly changed across genotypes (**Figure 2.3U**). Meanwhile, the

inter-punctum distance between ribbons was moderately decreased in both *cMaf*^{CKO} and *Mafb*^{CKO} animals and severely decreased in the dKO animals, suggesting potential additive effects of *cMaf* and *Mafb* on ribbon spacing (**Figure 2.3V**). In the cochlea, CMAF and MAFB are expressed in SGNs and not hair cells. Therefore, these data offer further insight into postsynaptic influence on presynaptic size and distribution mediated by *cMaf* and *Mafb* expressed in SGNs.

Figure 2.3 CMAF and MAFB have opposing and additive effects on SGN synapses. (A-D) Wholemount synapse immunostaining of GLUR2 and CTBP2 in the 8kHz region of control (NoCre), *Mafb*^{CKO}, *cMaf*^{CKO} and *cMaf/Mafb*^{DKO} (dKO) littermates. Hair cells were stained by CALB2 (not shown) and are outlined in dashed lines in the merge panels. Scale bar, 5μM. **(E)** Number of synapses per hair cell (Kruskal-Wallis, p=0.328). **(F)** Number of GLUR2 orphans per hair cell (Kruskal-Wallis, p=0.002). **(G)** Number of ribbon orphans per hair cell (Kruskal-Wallis, p=0.165). **(H,I)** Distribution of 8kHz GLUR2 puncta volumes in control (NoCre), *Mafb*^{CKO}, *cMaf*^{CKO} and dKO animals (Kruskal-Wallis, p<0.001). **(J)** Median 8kHz GLUR2 puncta volumes per animal across genotypes (Kruskal-Wallis, p=0.039). **(K)** Mean interquartile range of 8kHz GLUR2 puncta volumes per mouse across genotypes (Kruskal-Wallis, p<0.001). **(L)** Mean 8kHz GLUR2 inter-punctum distance per animal across genotypes (Kruskal-Wallis, p<0.001) **(M,N)** Distribution of 16kHz GLUR2 puncta volumes in control, *Mafb*^{CKO}, *cMaf*^{CKO} and dKO animals (Kruskal-Wallis, p<0.001). **(O)** Median 16kHz GLUR2 puncta volumes per animal across genotypes (Kruskal-Wallis, p<0.001). **(P)** Mean interquartile range of 16kHz GLUR2 puncta volumes per mouse across genotypes (Kruskal-Wallis, p<0.001). **(Q)** Mean 16kHz GLUR2 inter-punctum distance per animal across genotypes (Kruskal-Walils, p<0.001). (**R,S**) Distributions of 8kHz ribbon volumes across all genotypes (Kruskal-Wallis, p<0.001). (**T**) Median 8kHz ribbon volumes per animal across genotypes (Kruskal-Wallis, p=0.0265). **(U)** Mean 8kHz interquartile range of ribbon volumes across all genotypes (Kruskal-Wallis, p=0.690). (**V**) Mean 8kHz ribbon inter-punctum distance per animal across genotypes (Kruskal-Wallis, p<0.001). All plots were quantified from one cochlea from 10 double knockout animals (*cMaf/Mafb*^{DKO}, *B5*$^{Cre/+}$*;Mafb*$^{fl/fl}$*;cMaf*$^{fl/fl}$), 8 *Mafb* knockout animals (Mafb^{CKO}, *B5*$^{Cre/+}$*;Mafb*$^{fl/fl}$*;cMaf*^{fl}/+), 9 *cMaf* knockout animals (*cMaf*^{CKO}*, B5*$^{Cre/+}$*;Mafb*^{fl}/+*;cMaf*$^{fl/fl}$) and 15 controls (NoCre, *Mafb*$^{fl/fl}$*;cMaf*$^{fl/fl}$) except for any analyses with ribbons (**E-G, R-V**) which were from the 8kHz region and had N=2 fewer controls and N=4 fewer *Mafb* knockout animals due to complications with ribbon staining. Outer perimeter of boxes in boxplots **(H, M, R)** show the interquartile range and the median line

Figure 2.3 (Continued) and whiskers show the entire range of the data excluding outliers calculated as a function of the interquartile range, each dot represents a single synaptic punctum. In bar plots **(E-G, J-L, O-Q, T-V)**, vertical line denotes the standard error, each dot represents the average within a mouse. All density plots **(I, N, S)** represent distributions of individual synaptic puncta across genotypes. Significant differences amongst groups that had a Kruskal-Wallis p-value<0.05 were followed with pair-wise post-hoc Dunn test, p values can be found in **Table S2.3**. Asterisks shown as shorthand for pair-wise p-values ($p<0.05$= *, $p<0.01$= **, $p<0.001$= ***).

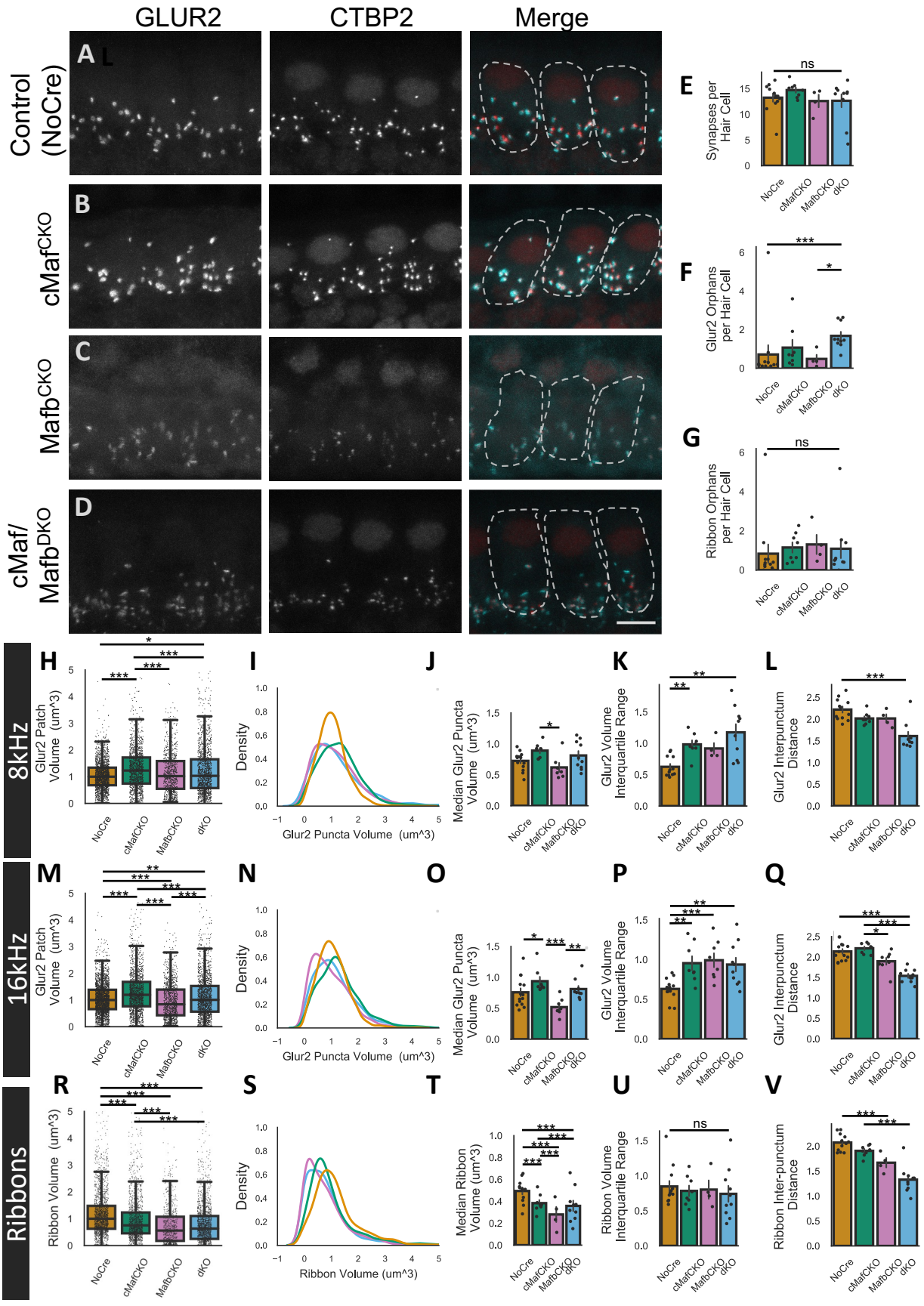
GLUR2
CTBP2
Merge
Control (NoCre)
cMafCKO
MafbCKO
cMaf/ MafbDKO
A
B
C
D
E
F
G
H
I
J
K
L
M
N
O
P
Q
R
S
T
U
V
8kHz
16kHz
Ribbons
Synapses per Hair Cell
Glur2 Orphans per Hair Cell
Ribbon Orphans per Hair Cell
Glur2 Patch Volume (um^3)
Density
Glur2 Puncta Volume (um^3)
Median Glur2 Puncta Volume (um^3)
Glur2 Volume Interquartile Range
Glur2 Interpunctum Distance
Ribbon Volume (um^3)
Ribbon Volume (um^3)
Median Ribbon Volume (um^3)
Ribbon Volume Interquartile Range
Ribbon Inter-punctum Distance
NoCre
cMafCKO
MafbCKO
dKO
ns

Altered auditory sensitivity in *cMaf* and *Mafb* mutants

Ribbon synapses are critical for transmitting auditory information from IHCs to SGNs. To test if the varied synaptic effects observed in *cMaf* and *Mafb* mutants have functional consequences for auditory sensitivity, we recorded auditory brainstem responses (ABRs) from single and double knockout mice and control littermates. These measurements involve placing electrodes near the base of the skull of anesthetized mice to measure electric field potentials generated by synchronous firing of neurons at different steps along the ascending auditory pathway in response to sound stimuli. The first peak in the ABR corresponds to synchronous firing from SGNs. We presented pure tone bursts of 8,16, 32, and 45 kHz each at increasing sound pressure levels from 20dB to 90dB in 5dB increments to control animals (NoCre, $Mafb^{fl/fl};cMaf^{fl/fl}$, N=14), *cMaf* knockout ($cMaf^{CKO}$, $B5^{Cre/+};Mafb^{fl}/+;cMaf^{fl/fl}$, N=6) and *Mafb* knockout ($Mafb^{CKO}$, $B5^{Cre/+};Mafb^{fl/fl};cMaf^{fl/+}$, N=11) and double knockout (dKO, $B5^{Cre/+};Mafb^{fl/fl};cMaf^{fl/fl}$, N=9) littermates (**Figure 2.4A-D**). Auditory sensitivity is measured by identifying the lowest sound pressure level, or threshold, that elicits a brainstem response. We analyzed ABRs across all frequencies and found that the ABR threshold was elevated for controls animals beyond 32 kHz (**Figure 2.4E**). Therefore, we only analyzed the ABR responses to 8 and 16kHz stimuli to avoid confounds of high frequency hearing loss characteristic of certain strains of mice[62]. The remaining frequency ranges include the region of highest sensitivity for mice (16kHz)[22].

We found that loss of CMAF and MAFB had differing effects on ABR thresholds. $Mafb^{CKO}$ animals had significantly elevated thresholds at 16kHz compared to controls. Meanwhile, $cMaf^{CKO}$ animals had similar thresholds as controls at 8kHz and 16kHz (**Figure 2.4E**). These results corroborate previous observations of elevated ABR thresholds in *Mafb* mutants[50]. Meanwhile, dKO animals had markedly elevated thresholds compared to all the other genotypes. The difference between thresholds between $Mafb^{CKO}$, dKO and control mice was

significant for all comparisons at 8kHz and 16kHz ($p<0.05$, post-hoc Dunn's multiple comparison's test, **Table S2.4**) except between *Mafb*^{CKO} and dKO animals in the 16kHz region ($p=0.099$, post-hoc Dunn's multiple comparison's test, **Table S2.4**). These exacerbated effects on threshold in dKO animals suggest that *cMaf* and *Mafb* have synergistic roles in establishing auditory threshold. In further support of this finding, dKO animals had higher thresholds compared to *Mafb*^{CKO} animals in the 8kHz region. In this experiment, the only difference between *Mafb*^{CKO} animals (*B5*$^{Cre/+}$*;Mafb*$^{fl/fl}$*;cMaf*$^{fl/+}$) and dKO littermates (*B5*$^{Cre/+}$*;Mafb*$^{fl/fl}$*;cMaf*$^{fl/fl}$) was a single copy of *cMaf.* Therefore, elevated ABR thresholds in dKO animals compared to *Mafb*^{CKO} animals further indicates that *cMaf* and *Mafb* are jointly contributing auditory thresholds. There were no significant differences in distortion product otoacoustic emissions (DPOAE) thresholds across genotypes (**Figure 2.4F**). Since DPOAE are indicators of hair cell function, these results suggest that changes in hair cell function were not responsible for any observed changes in ABR threshold.

Figure 2.4. Changes in auditory sensitivity in Maf mutants. Auditory brainstem responses (ABRs) and distortion product otocacoustic emissions (DPOAEs) were recorded from 8-12 week old control animals (NoCre, *Mafb*$^{fl/fl}$*;cMaf*$^{fl/fl}$, N=14, orange), *cMaf* knockout (*cMaf*^{CKO}, *B5*$^{Cre/+}$*;Mafb*$^{fl/+}$*;cMaf*$^{fl/fl}$, N=6, green), *Mafb* knockout (Mafb^{CKO}, *B5*$^{Cre/+}$*;Mafb*$^{fl/fl}$*;cMaf*$^{fl/+}$, N=11, magenta), and double knockout (dKO, *B5*$^{Cre/+}$*;Mafb*$^{fl/fl}$*;cMaf*$^{fl/fl}$, N=9, blue), littermates (**A-D**) Average ABR waveforms recorded after presentation of a 16kHz stimulus at different sound intensity levels across genotypes. Bootstrapped 68% confidence intervals shown by shaded bands. (**E**) ABR threshold measurements across frequencies (p_{8kHz}<0.001, p_{16kHz}<0.001, p_{32kHz}=0.213, p_{45kHz}=0.326, Kruskal-Wallis). Significant differences amongst groups that had a Kruskal-Wallis p-value<0.05 were followed with pair-wise post-hoc Dunn test, p-values can be found in **Table S2.4**. (**F**) DPOAE thresholds across all frequencies. Standard error shown by vertical bars (all comparisons not significant, p>0.05, Kruskal-Wallis).

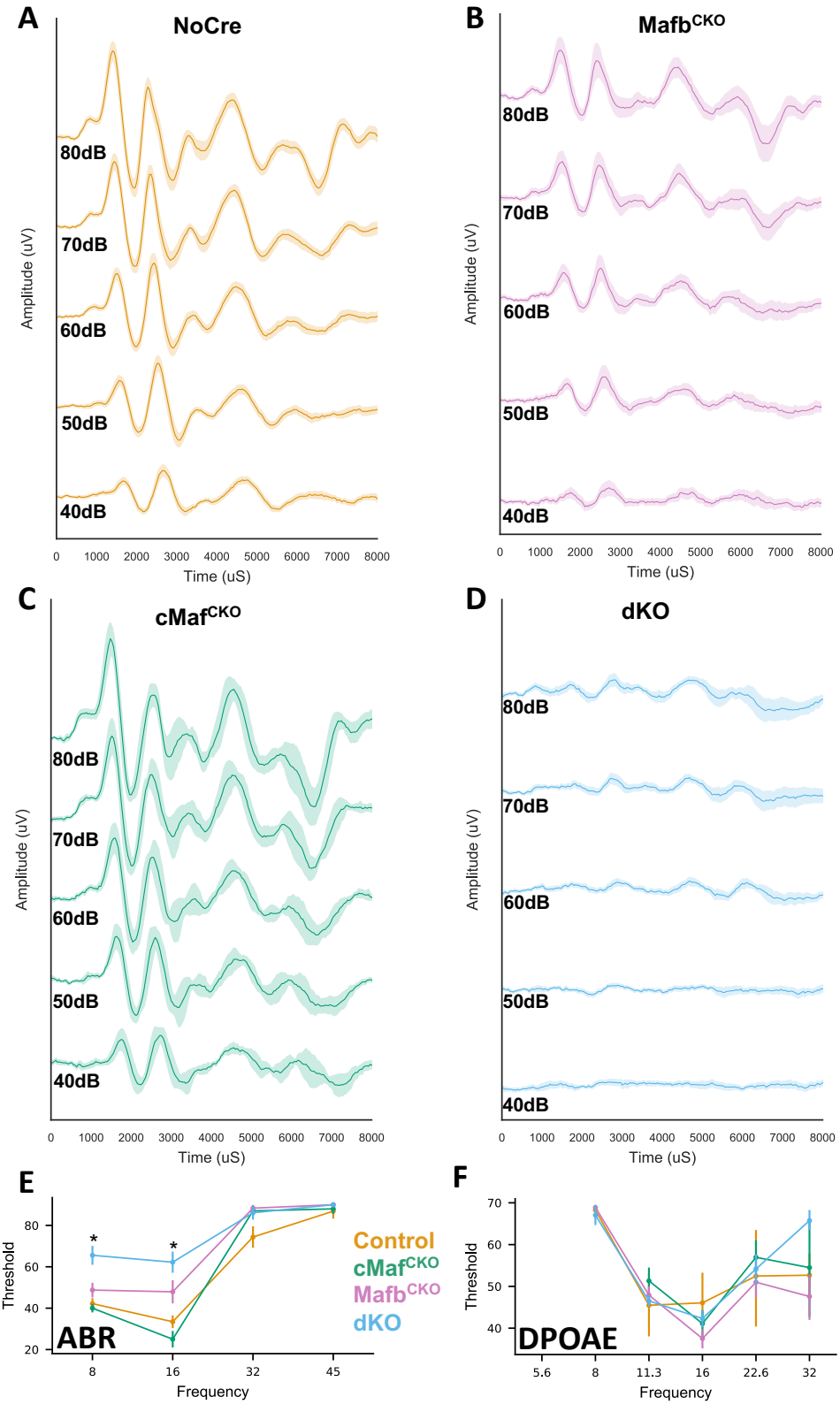
A
NoCre
80dB
70dB
60dB
50dB
40dB
Amplitude (uV)
0 1000 2000 3000 4000 5000 6000 7000 8000
Time (uS)
B
Mafb^CKO
80dB
70dB
60dB
50dB
40dB
Amplitude (uV)
0 1000 2000 3000 4000 5000 6000 7000 8000
Time (uS)
C
cMaf^CKO
80dB
70dB
60dB
50dB
40dB
Amplitude (uV)
0 1000 2000 3000 4000 5000 6000 7000 8000
Time (uS)
D
dKO
80dB
70dB
60dB
50dB
40dB
Amplitude (uV)
0 1000 2000 3000 4000 5000 6000 7000 8000
Time (uS)
E
Threshold
80
60
40
20
*
*
ABR
8 16 32 45
Frequency
Control
cMaf^CKO
Mafb^CKO
dKO
F
Threshold
70
60
50
40
DPOAE
5.6 8 11.3 16 22.6 32
Frequency

From these ABR waveforms, we were able to extract key measurements that correspond to the strength and speed of synchronous firing. The first peak (P1) of the ABR waveform corresponds to synchronous SGN firing. The amplitude of P1 corresponds to the degree of synchronous firing of SGNs[63] (**Figure 2.5A-B**). *Mafb*^{CKO} animals had significantly smaller P1 amplitudes than controls and *cMaf*^{CKO} animals across most sound intensities at 8kHz and 16kHz (**Figure 2.5C,E**). This result confirms previous measurements that found smaller P1 amplitudes in *Mafb* mutants compared to controls[50]. On the other hand, P1 amplitudes in *cMaf*^{CKO} animals showed a trend for increased P1 amplitudes compared to control and significantly higher P1 amplitudes than *Mafb*^{CKO} animals at many sound pressure levels (**Figure 2.5C,E**). These effects were most pronounced at 16kHz and demonstrate opposing effects of CMAF and MAFB on P1 amplitude. dKO animals had severely decreased responses across most sound pressure levels compared to all other genotypes at both 8kHz and 16kHz (**Figure 2.5C,E**). Meanwhile, both *cMaf*^{CKO} and *Mafb*^{CKO} animals had delayed latencies to peak 1 (**Figure 2.5D,F).** These results corroborate previous work demonstrating that *Mafb* mutants exhibit delayed peak 1 latencies[50]. Furthermore, this result confirms that *cMaf* is involved in proper auditory function. Although *cMaf* mutants showed trends for larger P1 amplitudes (**Figure 2.5C,E**), the timing of the synchronous response was delayed (**Figure 2.5D,E**), indicating that *cMaf* mutant SGNs are aberrantly encoding sound. dKO latencies were not plotted because the first peak in these mutants was so variable and broad that latencies were difficult to interpret.

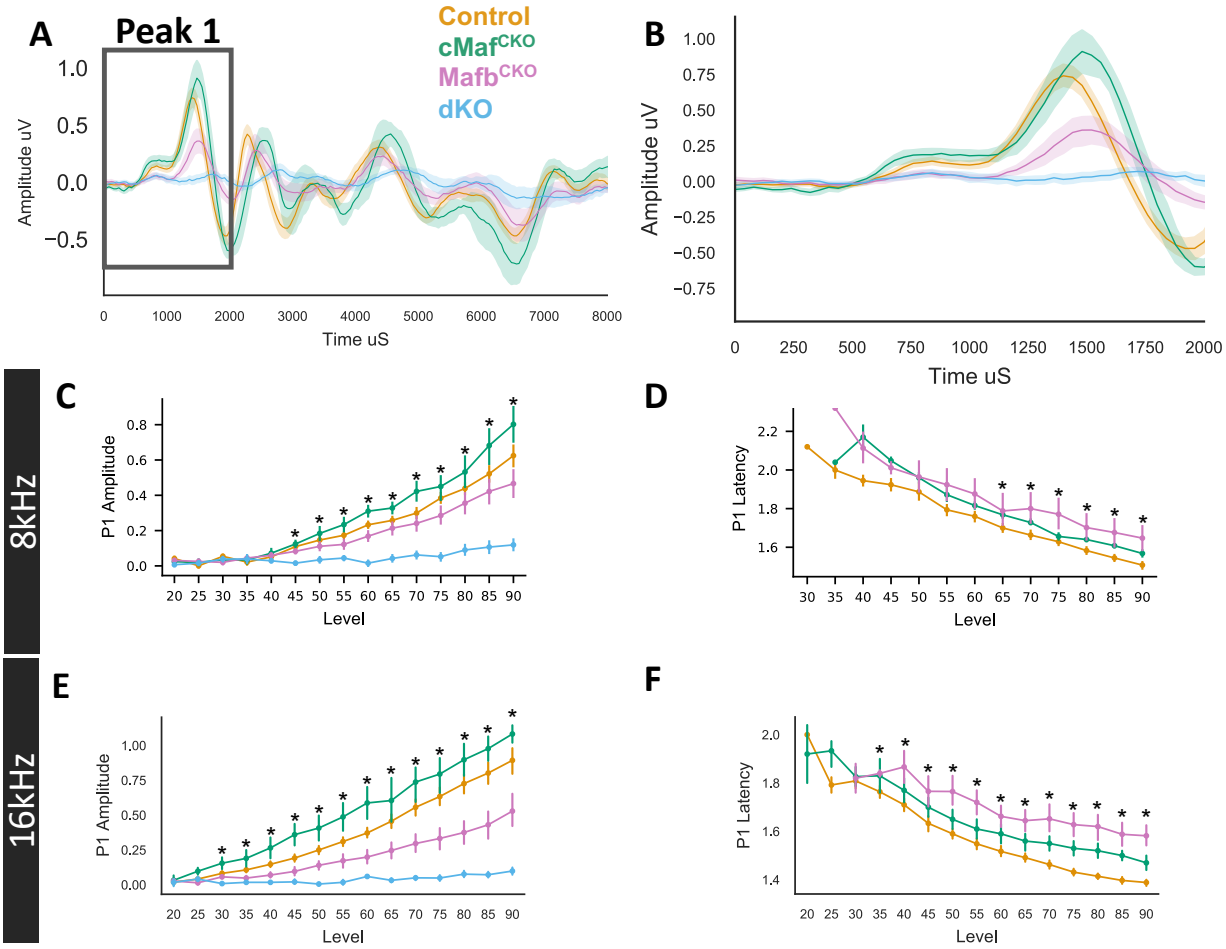

Figure 2.5. *cMaf* and *Mafb* have opposing and additive effects on auditory function. (A) Overlaid average ABR waveforms across genotypes in response to a 16kHz, 80dB sound stimulus in control animals (NoCre, *Mafb*$^{fl/fl}$;*cMaf*$^{fl/fl}$, N=14, orange), *cMaf* knockout (*cMaf*^{CKO}, *B5*$^{Cre/+}$;*Mafb*$^{fl/+}$;*cMaf*$^{fl/fl}$, N=6, green), *Mafb* knockout (Mafb^{CKO}, *B5*$^{Cre/+}$;*Mafb*$^{fl/fl}$;*cMaf*$^{fl/+}$, N=11, magenta), and double knockout (dKO, *B5*$^{Cre/+}$;*Mafb*$^{fl/fl}$;*cMaf*$^{fl/fl}$, N=9, blue), littermates. Peak 1 (P1) is outlined in a gray box. (**B**) Zoomed in view of peak 1 from **(A).** (**C**) P1 amplitude across all sound pressure levels for an 8kHz stimulus. (**D**) P1 latency across sound pressure levels for an 8kHz stimulus. (**E**) P1 amplitude across all sound pressure levels for a 16kHz stimulus. (**F**) Peak 1 latency across sound pressure levels for a 16kHz stimulus. Shaded regions on average

Figure 2.5 (Continued) waveforms show 68% bootstrapped confidence interval and bars on remaining plots show standard error. Comparisons with an asterisk were statistically significant ($p<0.05$, Kruskal-Wallis). Significant differences amongst groups that had a Kruskal-Wallis p-value<0.05 were followed with a pairwise post-hoc Dunn test. Kruskal-Wallis p-values and pairwise post-hoc Dunn p-values can be found in **Table S2.5**.

These data indicate that MAFB and CMAF have both antagonistic and additive effects on SGN functional output. These findings also corroborate the complementary and opposing synaptic phenotypes in each of these mutants. The opposing changes in P1 amplitude in *cMaf* and *Mafb* single mutants could be explained by the opposing changes in GLUR2 puncta volume in these mutants. *cMaf* single mutants had larger GLUR2 puncta volumes, which could result in larger excitatory postsynaptic currents (EPSCs) and a larger amplitude response. Meanwhile, the smaller GLUR2 volumes in the *Mafb* mutants could result in smaller EPSCs and a smaller amplitude response as well as elevated threshold. The increased latency of response in *cMaf* and *Mafb* mutants could be a result of the larger variability in GLUR2 puncta size or smaller synaptic spacing. This larger GLUR2 puncta variability could result in more variable EPSCs across SGNs and therefore, more variable spike timing and decreased synchrony leading to a peak response. Meanwhile, aberrant synaptic spacing could make it harder to segregate presynaptic calcium domains and result in abnormal vesicle release patterns. However, these hypotheses require more investigation to definitively connect the synaptic phenotypes observed with the functional phenotypes.

Mafb^{CKO} animals in this analysis had smaller GLUR2 puncta, increased P1 ABR latencies, increased ABR thresholds, and decreased P1 amplitudes. These results reflect previously published phenotypes in *Mafb* mutants despite mutants in this analysis being heterozygous for *cMaf*. Similarly, we have described an increase in GLUR2 volume in *cMaf* mutants despite these mutants being heterozygous for *Mafb* (*B5*$^{Cre/+}$*;Mafb*$^{fl/+}$*;cMaf*^{fl}*/ cMaf*^{fl}*).* We

independently confirmed the increase in GLUR2 volume in *cMaf* mutants with both copies of *Mafb* (*B5*$^{Cre/+}$;*cMaf*$^{fl/fl}$) (**Figure 2.6A,B**). We also observed a subtle increase in P1 amplitude and unchanged ABR thresholds in these *cMaf* mutants **(Figure 2.6C,D**). These results suggest that the missing *Mafb* copy in cMaf mutants (*B5*$^{Cre/+}$;*Mafb*$^{fl/+}$;*cMaf*^{fl}/ *cMaf*^{fl}) has minimal effects on the synapse and ABR phenotypes and that changes observed in these animals would be primarily driven by the loss of *cMaf*.

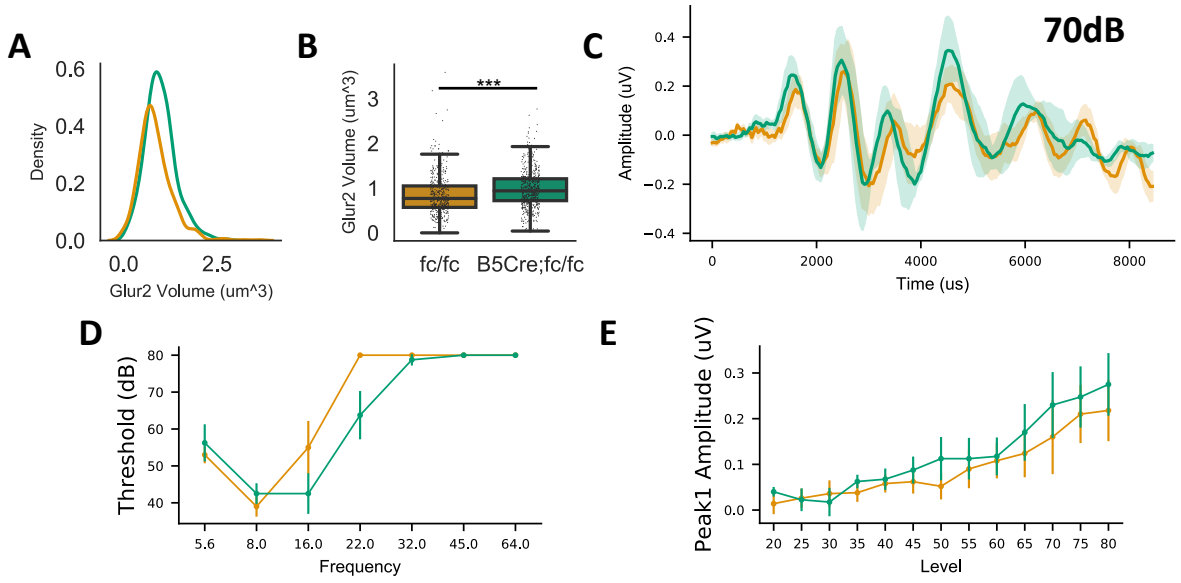

Figure 2.6. *cMaf* mutants with both copies of *Mafb* corroborate synaptic and ABR phenotypes of *cMaf* mutants heterozygous for *Mafb*. (A) Distributions of GLUR2 puncta volume in control (orange, *cMaf*$^{fl/fl}$, N=4) and *cMaf*^{CKO} (green, *B5*$^{Cre/+}$;*cMaf*$^{fl/fl}$, N=5) cochlear wholemounts. **(B)** *cMaf*^{CKO} animals have larger GLUR2 puncta volume than controls ($p<0.001$, t-test). **(C)** Average ABR waveform for a 70dB, 16kHz stimulus in *cMaf*^{CKO} and control animals. **(D)** ABR thresholds across stimulus frequencies in *cMaf* mutants and control animals. **(E)** Peak1 ABR amplitudes across stimulus sound intensities in *cMaf* mutants and control animals.

cMaf and *Mafb* single mutants had opposing effects on GLUR2 punctum volume (**Figure 2.3H-J,M-O**) and peak 1 ABR amplitude (**Figure 2.5C,E**) and exhibited mild effects on synapse interpunctum distances (**Figure 2.3L,Q**) and ABR threshold (**Figure 2.4E**) compared to controls and double knockouts. Meanwhile, double mutants exhibited exacerbated effects on synaptic interpunctum distances (**Figure 2.3L,Q**), ABR thresholds (**Figure 2.4E**) and peak 1 amplitudes (**Figure 2.5C,E**) and intermediate effects on GLUR2 volume (**Figure 2.3H-J,M-O**) compared to single mutants. Importantly, single and double mutants all had distinct ABR and synaptic phenotypes. Together, these results are suggestive of the additive and opposing effects of each factor on synaptic properties and auditory function.

How could CMAF and MAFB have both opposing and additive effects on SGN synaptic properties and auditory function? SGN synaptic heterogeneity is dictated in part by the molecular heterogeneity across SGN subtypes. Therefore, one possibility is that CMAF and MAFB have different expression patterns across subtypes of SGNs.

METHODS

Animal Models

Bhlhe22$^{Cre/+}$ (*B5*$^{Cre/+}$, MGI:4440745), *cMaf*^{fl} (MGI:5316775) and *Mafb*^{fl} (MGI:5581666) are all previously described. Animals were maintained on a mixed background. Animal work was conducted in compliance with protocols approved by the Institutional Animal Care and Use Committee at Harvard Medical School.

Immunohistochemistry

Animals were anesthetized via isoflurane exposure in an open-drop chamber and subsequently perfused with 7.5-10mL of cold 4% paraformaldehyde (PFA) in 1X PBS. Both temporal bones were dissected and cold 4% PFA was perfused through the oval and round windows with a syringe. Temporal bones were then processed for the following two applications:

Wholemount immunohistochemistry

Temporal bones used for wholemount staining were drop-fixed in 5mL of 4% PFA at room temperature and transferred to 10% EDTA overnight at 4C. Cochlea were then micro-dissected and transferred to blocking solution (16%v/v normal donkey serum, 3%v/v Triton-X in 1xPBS) overnight at 4ºC. Cochlear turns were stained overnight with anti-Calb2 (1:1000), anti-CTBP2 (1:500) and anti-GluR2 (1:500) and subsequently with corresponding secondaries at 37ºC overnight. Rinses after primary and secondary antibody were done using 1% PBST for 10 minutes at room temperature.

Immunostaining in cryosections

Temporal bones used for cryosectioning and staining were drop-fixed overnight at 4ºC in 4% PFA in 1x PBS and then transferred to 120mM EDTA for three consecutive nights. Cochleae were then removed from temporal bones embedded for sectioning. 18um cochlear sections were washed 1x for 5 minutes in 1x PBS and then 2x for 5 minutes in 0.25% Triton X-100 in 1x PBS. Sections were blocked with 5%v/v normal donkey serum and 0.3% Triton X-100 in 1x PBS. Sections were stained with rabbit anti-MAFB (1:250) or rabbit anti CMAF (1:250) for four hours at room temperature. After rinsing with 1x PBS, sections stained with appropriate secondary antibodies at 4ºC overnight. Sections were then rinsed with 1x PBS for 10 minutes. The second wash contained DAPI at 1mg/uL.

Image acquisition

All tissues were imaged using a Leica SP8 point-scanning confocal microscope with HyD and photomultiplier tube (PMT) detectors. For wholemounts, frequency maps were generated by taking 10X stacks of the cochlear tubes and using the Measure_Line ImageJ plugin available through the Histology Core at Mass Eye and Ear (Boston, MA). Synaptic puncta were then

captured using HyD detectors while hair cells were captured using PMT detectors using a 63x oil-immersion objective (voxel size= 0.901 x 0.901 x 0.299um^3) Special attention was taken not to oversaturate any pixels in channels that were to be used for intensity-based morphometric quantification.

Image analysis

Pre- and post-synaptic puncta were reconstructed semi-automatically using the “Surfaces” function in Imaris. A local contrast-background subtraction algorithm was applied to all z-stacks for thresholding. All reconstructions were created and reviewed with the researcher blinded to genotype. Inaccuracies in automatic segmentation were corrected manually. Reconstructions located outside the volume of hair cells were excluded from analysis. Image-based coordinates of reconstructed puncta were transformed into hair cell-centric coordinates using the “Reference Frames” function in Imaris. Each hair cell-centric coordinate system was defined with the following three planes: an XZ plane bisecting the hair cell through its plane of symmetry, a YZ plane bisecting the nucleus through the plane parallel to the tilt of the hair cell, and an XY plane tangential to the basolateral pole of the hair cell. Metrics regarding the size and localization of reconstructed pre- and postsynaptic puncta were exported into Excel for further analysis.

Auditory Brainstem Responses (ABR) and Distortion Products Otoacoustic Emissions (DPOAE)

Mice were anesthetized by intraperitoneal injection of ketamine (100mg/kg), xylaxine (10mg/kg) and meloxicam (1mg/kg) was administered for analgesia. Additional ketamine (30-40 mg/kg) was administered as needed to maintain the anesthetic plane throughout the procedure. Animals were placed on a 37ºC heating pad (ATC1000, World Precision Instruments). ABRs and DPOAEs were measured using a custom acoustic system (Eaton-Peabody Laboratories, Massachusetts Eye and Ear) in an electrically shielded and sound attenuating room. All recordings were performed with the researcher blinded to genotype.

ABRs were recorded from three subcutaneous needle electrodes: a recording electrode caudal to the pinna, a reference electrode at the vertex, and a ground electrode by the tail. ABR stimuli were presented from 20 to 90 dB SPL in 5 dB steps at 8, 16, 32, and 45 kHz. Each stimulus was presented as a 5-ms tone-pip at a rate of 31/s, with a 0.5 ms rise-fall time and alternating polarities. Responses were amplified 10,000x, filtered with a 0.3–3 kHz passband (P511, Grass), and averaged 512 times. Recordings with peak to peak amplitudes exceeding 15 μV were rejected as artifacts. ABR thresholds, amplitudes, and latencies were analyzed using ABR Peak Analysis software (v.1.1.1.9; Massachusetts Eye and Ear). ABR threshold was defined as the lowest stimulus level at which wave 1 could be identified by visual inspection.

DPOAEs were recorded from a probe-tube microphone aligned above the ear canal. In-ear calibrations were performed using the Cochlear Function Test Suite (v 2.36, Massachusetts Eye and Ear) prior to reach recording. DPOAE stimuli were presented at primary tones f1 and f2, where f2 varied from 5.6 to 32 kHz in half-octave steps. Primary tones had a frequency ratio of f2/f1 = 1.2 and a level difference of L1 = L2 + 10. Levels of f2 were incremented in 10 dB steps from 0 dB to 70 dB SPL. The distortion products at 2f1-f2 were temporally and spectrally averaged. Iso-response contours were generated by the Cochlear Function Test Suite software for various criterion response amplitudes. DPOAE threshold was defined as the f1 level required to produce a DPOAE of 5 dB SPL.

Statistics

All statistical analysis was done in Python. Normality of each distribution was tested using the Shapiro-Wilk test. If both groups showed a normal distribution, a parametric t-Test or ANOVA was used. Otherwise, the non-parametric Mann-Whitney Rank Sum or Kruskal-Wallis Test was applied.

CHAPTER THREE

Complementary expression patterns of CMAF and MAFB across SGN subtypes

Isle M. Bastille and Lisa V. Goodrich designed all experiments. Andrea Yung and Chester Chia collected tissues for sequencing. IMB conducted all downstream computational analysis. IMB performed all histology, data visualization, and statistics. Lucy Lee created cell reconstructions in Imaris.

INTRODUCTION

Previous work from our lab has revealed that the transcription factor, MAFB, is involved in the development of the SGN postsynaptic density[50]. In this work, we have discovered that CMAF and MAFB are contributing in diverse ways to the establishment of SGN properties and hearing function. The loss of *cMaf* results in larger GLUR2 puncta volume (**Figure2.3H-J,M-O**) and larger peak 1 ABR amplitudes (**Figure2.5C,E**) while the loss of *Mafb* results in smaller GLUR2 puncta volume (**Figure2.3H-J,M-O**) and smaller P1 ABR amplitudes (**Figure2.5C,E**). Knocking out both *cMaf* and *Mafb* results in decreased spacing between synaptic puncta (**Figure2.2J, Figure2.3L,Q**), an increase in the variance of synaptic volumes (**Figure2.2H, Figure2.3K,P**) and more GLUR2 orphans (**Figure2.2F, Figure2.3F**) compared to control and single mutant animals. Single mutants of *cMaf* and *Mafb* had milder decreases in synaptic spacing than double mutants (**Figure 2.3L,Q**). Single mutants also had delayed peak 1 ABR latencies (**Figure 2.5D,F**). It remains unclear how CMAF and MAFB contribute in additive and opposing ways to SGN synaptic properties.

SGN molecular subtypes differ in peripheral synaptic morphology. Previous work used sparse labeling with tamoxifen-induced expression of Ai14 ($Mafb^{CreERT2}$;Ai14/+) followed by immunohistochemistry of subtype markers to localize single fibers of SGN subtypes in the pillar to modiolar axis along the base of the inner hair cell. 1A SGNs highly express the calcium binding protein CALB2, while 1B SGNs express lower amounts of CALB2, and 1C SGNs express the lowest amount of CALB2. Staining for CALB2 with sparse single-fiber labeling revealed that 1A peripheral processes form pillar-localized synapses that are apposed to larger presynaptic ribbons compared to other subtypes[6]. Furthermore, the transcription factor Runx1 controls the composition of SGN subtypes. Knocking out Runx1 results in fewer 1B and 1C SGNs in favor of 1A SGNs. This shift in overall molecular identity results in a shift in synaptic properties. Runx1 knockout SGNs have more 1A-like molecular profiles and subsequently

adopted 1A-like synaptic properties[45]. These results suggest that the fine tuning of synaptic morphology across SGN subtypes is interrelated with diverse synaptic gene expression profiles across SGNs.

SGN molecular subtypes express shared and distinct synaptic genes. These genes include postsynaptic receptors, synaptic intercellular adhesion molecules, potassium, sodium and calcium channels[6]. However, the transcriptional determinants that drive subtype-specific differences in synaptic gene expression are unknown. Considering the overlapping and distinct synaptic and functional phenotypes we have observed in *cMaf* and *Mafb* single and double mutants, I hypothesize that CMAF and MAFB are differentially expressed across SGN subtypes and have subtype-specific effects on the expression of SGN synaptic genes. In this chapter, I will explore the first part of this hypothesis by measuring *cMaf* and *Mafb* expression levels across SGN subtypes.

RESULTS AND DISCUSSION

RNA expression profiles across mature SGN subtypes

To assess the expression of *cMaf* and *Mafb* across SGN subtypes, we first used fluorescent *in situ* hybridization in wildtype (CD1, N=5) cochlear sections. *In situs* revealed complementary *cMaf* and *Mafb* RNA expression patterns across SGNs. SGNs with qualitatively higher amounts of *cMaf* puncta are also high for *Calb2,* a marker that is highest in 1A SGNs. Meanwhile, cells that are lower in *Calb2* and *cMaf* are higher in *Mafb* (**Figure 3.1A-C**).

To quantitatively assess *cMaf* and *Mafb* levels across SGN subtypes, we turned to single-cell RNA sequencing. This offered us an unbiased measure of *cMaf* and *Mafb* across SGN subtypes. We began by micro-dissecting the spiral ganglion from the cochleae of P27-P30 mice (N=3, 6 cochleae). We created a single cell suspension and encapsulated and

generated barcoded single cell libraries using the 10X Genomics platform. These libraries were sequenced and computationally analyzed to pull out and cluster SGNs (**Figure 3.1D)**

This dataset included 1039 SGNs that clustered into the three previously identified clusters, 1A, 1B and 1C. We identified each subtype cluster by its expression of previously identified marker genes such as *Calb2* and *Lypd1* (**Figure 3.1E**). We then assayed the RNA expression levels of *cMaf* and *Mafb* across these clustered subtypes.

By plotting the expression levels, we found that *cMaf* and *Mafb* were expressed in complementary patterns across SGN subtypes (**Figure 3.1F,G**). *cMaf* expression was significantly higher in the 1A SGNs, and lower in 1B and 1C SGNs (**Figure3.1I**), while *Mafb* was significantly higher in 1B and 1C SGNs and lower in the 1A subtype cluster (**Figure 3.1J**). These complementary expression patterns are exemplified by plotting the expression levels and the percent of cells expressing each transcription factor across subtypes. The percent of cells expressed includes any cells that had an expression level above 0 for each factor. *cMaf* is detected in more cells at a higher level in the 1A population while *Mafb* is detected at lower levels and in fewer 1A SGNs. Conversely, *Mafb* is detected in more cells at a higher level in the 1B and 1C population while *cMaf* is detected at lower levels and in fewer 1B and 1C SGNs (**Figure 3.1H**).

Figure 3.1. Complementary expression of *cMaf* and *Mafb* across SGNs. (A) *In-situ* hybridization of *Mafb* and **(B)** *cMaf* and **(C)** *Calb2* (merged with *cMaf* and *Mafb*) on a cochlear section of a P30 mouse. **(A'-C')** Zoom in view of cells in A-C. Yellow outlines delineate high *Calb2* expressing cells. Gray outlines delineate low *Calb2* expressing cells. Scale bar, 10μm **(D)** Schematic of single-cell collection protocol. The spiral ganglion was dissected out of the temporal bone of P27-P30 mice and dissociated into a single cell suspension. We then used the 10X Genomics platform to encapsulate individual cells and generate barcoded single-cell libraries for sequencing. **(E)** UMAP plot summarizing sequencing data from 1039 SGNs (N=3). SGNs cluster into three molecularly distinct subtypes, 1A, 1B, and 1C as identified by the expression of the 1A enriched marker, *Calb2,* the 1B/1C enriched marker, *Runx1,* and the 1C enriched marker *Lypd1.* **(F)** UMAP representation of *cMaf* expression across SGN subtype clusters demonstrates that *cMaf* is higher in the 1A cluster, lower in the 1B cluster, and lowest in the 1C cluster ($p<0.001$, Wilcoxon rank sum with Bonferroni correction). **(G)** UMAP representation of *Mafb* expression across SGN subtype clusters demonstrating that *Mafb* is higher in 1B and 1C SGNs and lower in 1A SGNs ($p<0.001$, Wilcoxon rank sum with Bonferroni correction). Red denotes higher expression while cyan denotes lower expression. **(H)** Dotplot summarizing relative *cMaf* and *Mafb* expression across SGN subtypes. The color denotes the relative expression across SGN subtypes. Red denotes higher relative expression while cyan denotes lower relative expression. **(I)** Violin plot of *cMaf* expression across subtypes. **(J)** Violin plot of *Mafb* expression across subtypes. Mean values are represented by a gray dot.

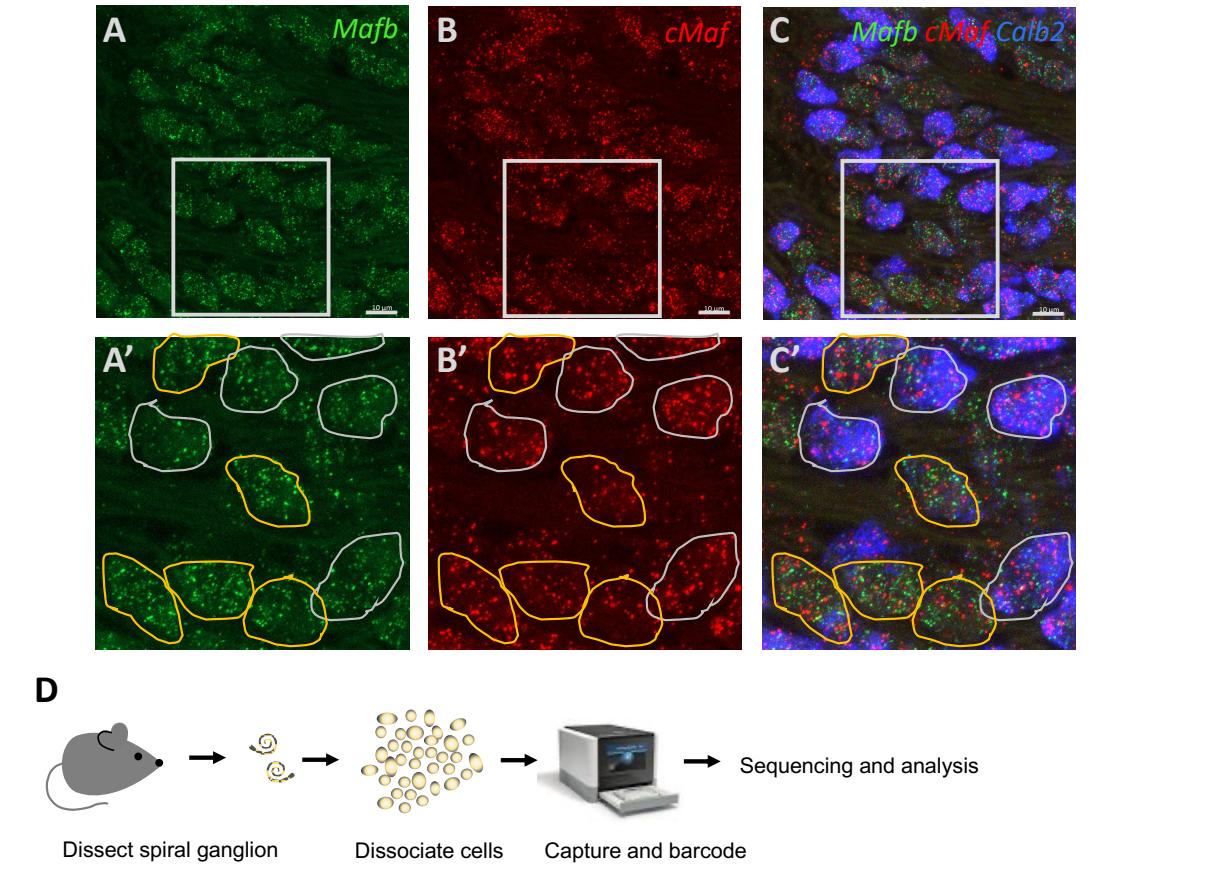
A
Mafb
B
cMaf
C
Mafb cMaf Calb2
A'
B'
C'
D
Dissect spiral ganglion
Dissociate cells
Capture and barcode
Sequencing and analysis
E
1A
1B
1C
Calb2
Runx1
Lypd1
High
Low
Expression Level
UMAP2
UMAP1
F
cMaf
High
Low
Expression Level
G
Mafb
High
Low
Expression Level
H
1C
1B
1A
Identity
Maf
Mafb
Features
Percent Expressed
40
50
60
70
Average Expression
1.0
0.5
0.0
-0.5
-1.0
I
Maf
Expression Level
2.0
1.5
1.0
0.5
0.0
1A
1B
1C
Identity
J
Mafb
Expression Level
1.5
1.0
0.5
0.0
1A
1B
1C
Identity

CMAF protein is expressed at different levels across molecularly distinct mature SGNs

cMaf and *Mafb* RNA expression levels are complementary across mature SGN subtypes. To assess if CMAF adult protein expression reflected adult RNA expression profiles, we stained for CMAF in P27-P30 mice (N=3) (**Figure 3.2A**). As a proxy for subtype identification, we also stained for CALB2 which is highest in 1A SGNs, lower in 1B SGNs, and lowest in 1C SGNs. We took confocal image stacks of the middle turn of the cochlea and created single cell reconstructions in Imaris. By creating single cell reconstructions of stained cells in Imaris, we were able to quantify CMAF staining intensity across the cell bodies of individual SGNs (**Figure 3.2GE**). To account for technical differences in staining intensity across animals, we standardized (z-scored) the staining intensity across cells for each animal so that the mean staining intensity for each animal is 0 and the standard deviation across cells is 1. This allowed us to aggregate data between animals. When we plotted the z-scored CMAF staining intensity versus the z-scored CALB2 staining intensity, we found that higher CALB2- expressing cells had higher CMAF expression (**Figure 3.2B**). This result validates the previously observed higher *cMaf* in 1A SGNs and lower *cMaf* in 1B and 1C SGNs. We were unable to measure adult MAFB protein expression because MAFB protein exits the nucleus after the first postnatal week and the antibody available is not sensitive enough to make quantitative assessments in adults.

CMAF and MAFB are expressed at different levels across molecularly distinct SGNs during synaptogenesis

Postnatal day 6 (P6) is the stage of peak synaptogenesis in the cochlea[46]. To assess if complementary *cMaf* and *Mafb* RNA expression patterns were reflected at the protein level at this stage, we stained for CMAF or MAFB protein in postnatal day 6 cochlear sections (**Figure3.2C,E**). However, SGN subtype identity is still in the process of consolidating at this age and cannot be segregated by adult markers such as CALB2[6]. To mark developing 1B and 1C subtypes, we used *NetrinG1*$^{Cre/+}$ crossed to *Ai14*, a ROSA26-LSL-tdTomato fluorescent

reporter (*NtnG1*$^{Cre/+}$*;Ai14/+*). *NtnG1*$^{Cre/+}$ is expressed in a subset of 1B and 1C SGNs at this stage. Therefore, at P6, tdTomato (Ai14) labeling driven by *NtnG1*$^{Cre/+}$ is consistent with a 1B or 1C identity, but unmarked cells might also take on a 1B or 1C identity as the animal matures. *NetrinG1*$^{Cre/+}$ is also expressed in a subset of myelinating glia at this stage. However, marked glia are readily distinguishable from neurons by the smaller size of their cell body, more intense tdTomato expression and fried-egg-like morphology. Additionally, we stained for CALB2 which is diffusely expressed across all SGNs at this stage but not expressed in glia. Therefore, we could definitively distinguish tdTomato+ neurons from tdTomato+ glia in 3D reconstructions (**Figure 3.2GE**).

To compare levels of CMAF and MAFB across molecularly distinct SGNs at P6, we stained *NtnG1*$^{Cre/+}$*;Ai14/+* mice (N=5, postnatal day 6) and took confocal image stacks at middle turns of the cochlea. Keeping the location of the cochlea consistent is important because apical, middle, and basal regions of the cochlea contain different proportions of SGN subtypes and mature at different rates[6]. We found that tdTomato+ cells had higher MAFB staining intensity (**Figure 3.2C,G**) and lower CMAF staining intensity (**Figure 3.2D,F**) than tdTomato- cells. These results suggest that CMAF and MAFB expression levels are already biased to different SGN subtypes at P6, the age of peak synaptogenesis[46]. These protein expression patterns are also consistent with the *cMaf* and *Mafb* adult RNA expression profiles (**Figure 3.1H**). Diverging CMAF and MAFB expression profiles could result in differential synaptic gene regulation across SGN subtypes at this early stage.

Figure 3.2. CMAF and MAFB are expressed in distinct subsets of SGNs. (A) Immunolabeling of CMAF and CALB2 in cochlear sections of P28-P30 wildtype mice (N=5). CALB2 is differentially expressed in SGN subtypes at this stage (highest in 1A SGNs, lowest in 1C SGNs) **(B)** Positive correlation between standardized (z-scored) CMAF staining intensity and standardized CALB2 staining intensity (R^2=0.55, p<0.001). **(C)** Fluorescent tdTomato labeling of *NtnG1*$^{Cre/+}$*;Ai14/+* cells (red) with immunolabeling for MAFB (green) and CALB2 (white) in P6 mice (N=4). CALB2 captures all SGNs at this developmental stage. **(D)** Fluorescent tdTomato labeling of *NtnG1*$^{Cre/+}$*;Ai14/+* cells (red) with immunolabeling for CMAF (green) and CALB2 (white) in P6 mice (N=4). CALB2 captures all SGNs at this developmental stage. **(E)** Example Imaris reconstruction of cells in **(D)**. Each individual SGN cell body reconstruction is a different color. Glia were excluded by the intensity of tdTomato, smaller cell body size, fried-egg like morphology and lack of CALB2 expression. **(F)** Quantification of standardized MAFB staining intensity in *NtnG1*$^{Cre/+}$*;Ai14/+* labeled and unlabeled P6 SGNs. Each dot corresponds to a single reconstructed cell. (p=<0.001, Mann-Whitney Rank sum with Bonferroni correction). **(G)** Quantification of standardized CMAF staining intensity in *NtnG1*$^{Cre/+}$*;Ai14/+* labeled and unlabeled P6 SGNs. Each dot corresponds to a single reconstructed cell (p=<0.001, Mann-Whitney Rank sum with Bonferroni correction).

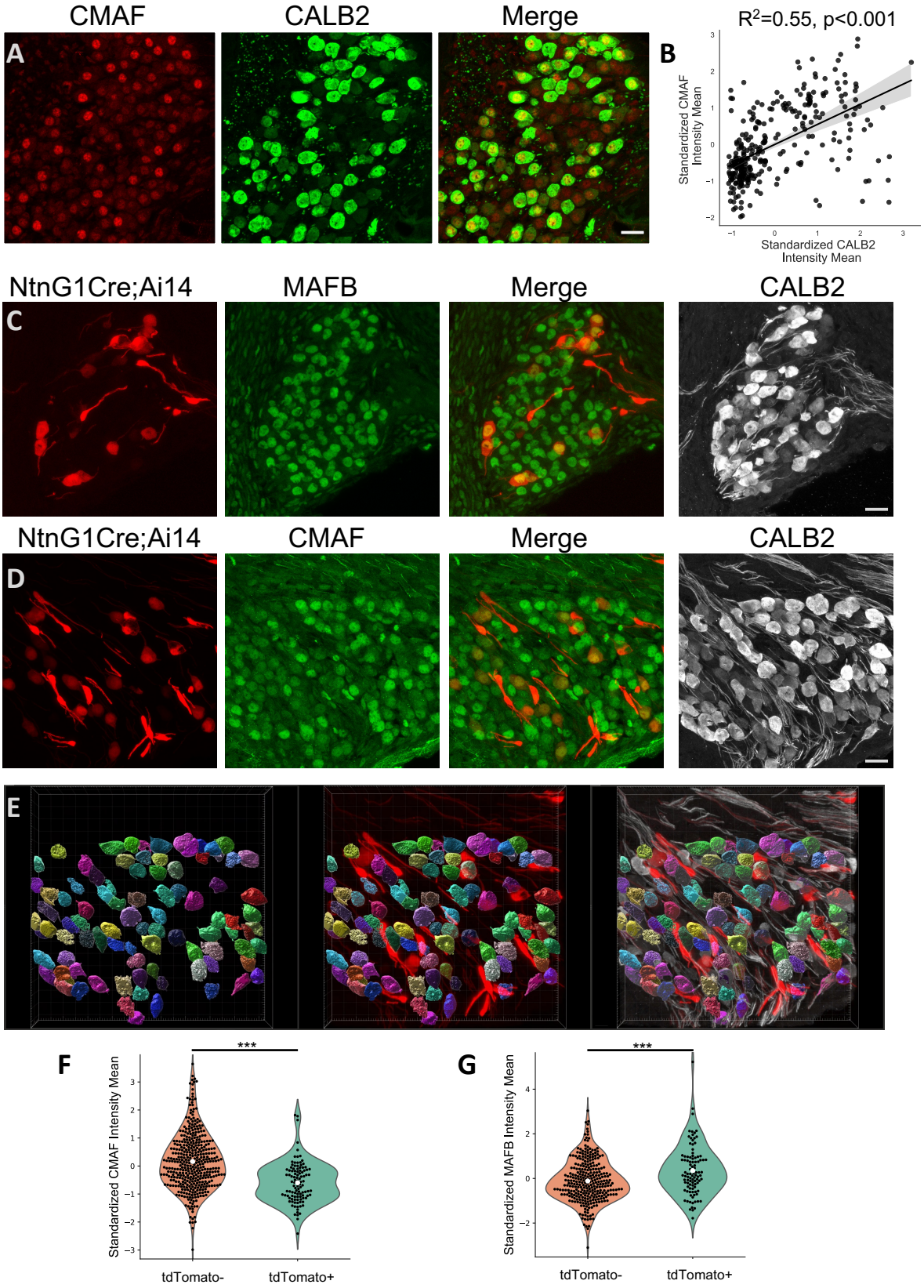
CMAF
CALB2
Merge
A
B
R²=0.55, p<0.001
Standardized CMAF Intensity Mean
Standardized CALB2 Intensity Mean
NtnG1Cre;Ai14
MAFB
Merge
CALB2
C
NtnG1Cre;Ai14
CMAF
Merge
CALB2
D
E
F
***
Standardized CMAF Intensity Mean
tdTomato-
tdTomato+
G
***
Standardized MAFB Intensity Mean
tdTomato-
tdTomato+

Several previously published datasets of mature SGN transcriptomes also reflect complementary *cMaf* and *Mafb* expression patterns in SGNs[6,7,64]. Transcriptomes from postnatal day three (P3) SGNs show that *Mafb* is similarly expressed at similar levels in 1A SGNs as in 1B and 1C SGNs, suggesting that 1A SGNs downregulate *Mafb* over postnatal development. Meanwhile, *cMaf* expression patterns at P3 reflect adult expression patterns[7]. These expression data corroborate the *cMaf* and *Mafb* expression patterns we have found across SGN subtypes in both adult and P6 tissue.

CMAF and MAFB have been used as molecular markers of distinct neurons in the spinal cord[65]. They are also both expressed in overlapping and distinct developing and mature cortical interneurons[56]. While gene expression changes have been studied in *cMaf/Mafb* double knockout cortical interneurons, little is known about the relative contributions of CMAF and MAFB to neuronal differentiation and gene expression. CMAF and MAFB are playing antagonistic and synergistic roles in establishing SGN synaptic properties and hearing function (**Chapter 2**). Furthermore, they are expressed in complementary patterns across SGN subtypes (**Figure 3.1**). These observations suggest that CMAF and MAFB could have subtype specific effects on gene expression across SGNs.

METHODS

Animal Models

NetrinG1$^{Cre/+}$ mice were kindly provided by Fan Wang (Duke University) and Rosa26-LSL-tdTomato (*Ai14*; Jax strain 007914) was previously described. Animals were maintained on a C57BL/6 background. Animal work was conducted in compliance with protocols approved by the Institutional Animal Care and Use Committee at Harvard Medical School.

Histology

All animals were anesthetized via isoflurane by the open-drop method and perfused with cold 4% paraformaldehyde (PFA) in 1x PBS. Both temporal bones were dissected out and PFA was perfused through the oval and round windows with a syringe. Temporal bones were decalcified for 72 hours in 120mM EDTA in 1x PBS. Cochlea were then cryopreserved in 30% sucrose in 1x PBS for 24 hours at 4°C and then in 30% sucrose in NEG for 24 hours at 4°C. Cochleae were then removed from temporal bones embedded for sectioning. 18um cochlear sections were washed 1x for 5 minutes in 1x PBS and then 2x for 5 minutes in 0.25% Triton X-100 in 1x PBS. Sections were blocked with 5%v/v normal donkey serum, 10% FAB fragments and 0.3% Triton X-100 in 1x PBS. Sections were stained with mouse anti-HuD (1:50), rabbit anti cMaf (1:250), rabbit anti Mafb (1:250) and goat anti Calb2 (1:500) for four hours at room temperature. After rinsing with 1x PBS, sections stained with appropriate secondary antibodies at 4°C overnight. Sections were then rinsed with 1x PBS for 10 minutes. The second wash contained DAPI at 1mg/µL. Tissues were imaged using a Leica SP8 point-scanning confocal microscope with HyD and photomultiplier tube (PMT) detectors.

Hybridized Chain Reaction Fluorescent In Situ Hybridization

Mice on a CD1 background (P29-P30) were perfused with ice-cold, RNAse-free 4% PFA in 1x PBS. Cochlea were flushed with PFA through the oval window and post-fixed overnight at 4°C. Cochlea were decalcified for three nights in RNAse-free 120 mM EDTA in 1x PBS at 4°C prior to cryopreserving in a sucrose gradient of 10% thenand 30% sucrose and embedding in NEG-50. 20 µm cryosections were thawed at room temperature for 10 minutes and incubated at 50°C for 15 minutes. Sections were fixed ten minutes with ice-cold, RNAse-free 4% PFA in 1x PBS and washed twice with RNAse-free 0.1% Triton X-100 in 1x PBS (PBST). Sections were then treated with 1 µg/mL Proteinase K for 10 minutes. and then washed twice with RNAse-free 0.1%

PBST. Sections were fixed for a second time with ice-cold, RNAse-free 4% PFA in 1x PBS for 10 minutes, and then washed twice with RNAse-free 0.1% PBST. After drying, Molecular Instrument's Multiplexed HCR RNA-Fluorescent In Situ Hybridization protocol was followed. (https://files.molecularinstruments.com/MI-Protocol-RNAFISH-FrozenTissue-Rev3.pdf), using 1 pmol of *Mafb*, *cMaf*, and *Calb2* probes synthesized by Molecular Instruments. Sections were imaged on a Zeiss LSM800 confocal microscope.

Single-cell RNA sequencing

Temporal bones were extracted, and the spiral ganglion was microdissected from the cochlea in cold Leibovitz L-15 buffer. Cells were then treated with collagenase type IV followed by papain for 25 minutes each at 37°C. The cells were passed through ovomucoid as recommended for the Papain Dissociation System and then passed through a 40μum cell strainer. Dissociated cells were resuspended in cold EBSS. Cell concentration was estimated by counting cells on a hemocytometer. Cells were then loaded into a single cell chip from 10x Genomics following manufacturer's recommendations. Datasets were processed with the Chromium single-cell 3' library and gel bead kit v2.0. cDNA libraries were generated according to the manufacturer's directions. The final libraries were sequenced on an Illumina NovaSeq SP.

Bioinformatics Analysis

Alignment

Raw reads were converted to fastq files using the cellranger pipeline from 10X Genomics v 3.0.1. Reads were then aligned to the to the mouse reference genome (mm10) in a Linux-based high performance computing cluster at Harvard Medical School.

Normalization

The aligned data was imported into R and analyzed for statistical analysis and graphical representation. The library was normalized by fitting the gene counts to a regularized binomial

regression function implemented by the scTransform package for Seurat using all default settings and regression on percent mitochondrial reads[66].

Clustering

Clustering was performed using the Seurat FindClusters command using 30 principle components. SGNs were identified by the expression of neuronal genes such as Tubb3 and Nefh. Subtypes of SGNs were identified by the expression of subtype specific markers previously identified (Calb2, Lypd1, and Runx1). Differential expression was tested using the FindAllMarkers command on the SCT assay and probing for significant difference of cMaf and Mafb across SGN clusters.

Statistics

Statistical analysis for histological quantification was done in Python. Normality of each distribution was tested using the Shapiro-Wilk test. If both groups showed a normal distribution, a parametric t-Test or ANOVA was used. Otherwise, the non-parametric Mann-Whitney Rank Sum or Kruskal-Wallis Test was applied. Statistical analysis for differentially expressed genes was done in R. Differential gene expression was tested using a Wilcoxon rank sum test with Bonferroni post-hoc correction.

CHAPTER FOUR

CMAF and MAFB have broad and subtype-specific effects on SGN synaptic gene expression

Isle M. Bastille and Lisa V. Goodrich designed all experiments. IMB, Chester Chia and Andrea Yung and Lucy Lee collected SGN transcriptomes. IMB conducted all bioinformatics analysis.

INTRODUCTION

SGN synaptic, functional, and molecular diversity is critical for hearing function. SGN molecular subtypes have diverse gene expression profiles that encode a variety of synaptic proteins and ion channels needed for mature physiological function. SGNs exhibit heterogeneity in the size and composition of AMPA receptor clusters and postsynaptic scaffolds[28–32]; however, the transcriptional mechanisms that drive SGN postsynaptic diversification and specialization remain elusive. The transcription factor MAFB was previously found to play a role in SGN postsynaptic differentiation. Specifically, *Mafb* mutants had decreased GLUR2 puncta compared to controls[50]. However, this study was conducted prior to our current understanding of the molecular heterogeneity across SGNs. Therefore, previous work may have missed information on subtype-specific effects of *Mafb*. In fact, *Mafb* knockouts had reduced, but not absent functional hearing and synapses[50]. This partial phenotype suggests that other transcription factors could be contributing to SGN postsynaptic development. The related transcription factor, CMAF, is also expressed in SGNs. How CMAF and MAFB contribute to gene expression across SGN subtypes is still unknown.

MAFB and CMAF have the potential to regulate distinct and overlapping sets of genes. MAFB and CMAF are basic leucine zipper (bZIP) transcription factors[44,50]. The leucine zipper promotes homo- and heterodimerization with other transcription factors and with each other. Dimerization results in combinatorial DNA binding sites conferred by each individual DNA binding site in the dimer. This feature expands the regulatory repertoire of each bZIP transcription factor and provides the means to integrate with other transcription factors to regulate gene expression in a nuanced way[51]. Despite having identical DNA binding and transactivation domains, CMAF and MAFB have overlapping and distinct compatibility for dimerization with other transcription factors. In effect, CMAF and MAFB can have overlapping and distinct control over gene expression.

The constellation of phenotypes observed in single and double mutants is consistent with combinatorial regulation by MAFB and CMAF. The loss of cMaf results in larger GLUR2 puncta (**Figure 2.3H-J, M-O**) and higher peak 1 ABR amplitudes (**Figure 2.5C,E**) while the loss of Mafb results in smaller GLUR2 puncta volume (**Figure 2.3H-J, M-O**) and smaller peak 1 ABR amplitudes (**Figure 2.5C,E**). Knocking out both *cMaf* and *Mafb* results in exacerbated effects on synaptic spacing between pre- and postsynaptic puncta (**Figure 2.2J**), more GLUR2 orphans (**Figure 2.2F**) and severely dysfunctional ABRs (**Figure 2.4D-E, Figure 2.5A-F**) compared to single knockouts and control animals. Distinct synaptic and functional phenotypes in single mutants suggest that CMAF and MAFB are transcriptionally regulating distinct sets of genes. Meanwhile, exacerbated phenotypes in double mutants suggest that CMAF and MAFB could also be regulating overlapping sets of genes. CMAF and MAFB are expressed in complementary patterns across SGN subtypes: *cMaf* is highest in 1A SGNs, medium in 1B, and low in 1C SGNs, while *Mafb* is higher in 1B and 1C SGNs and lower in 1A SGNs (**Figure 3.1F-J**). Therefore, I hypothesize that CMAF and MAFB have both subtype-specific and combinatorial effects on SGN synaptic gene expression.

RESULTS AND DISCUSSION

To assess subtype-specific changes in gene expression conferred by *Mafb* and *cMaf* alone or together, I adopted a single cell transcriptomic approach. Single-cell RNA sequencing allows for quantitative measurements of differentially expressed genes across SGN subtypes. We collected transcriptomes from *cMaf* and *Mafb* single and double knockout mice and assessed resultant overall and subtype-specific changes in gene expression compared to control animals. We began by micro-dissecting the spiral ganglion from the cochleae of P27 *cMaf* conditional knockouts ($cMaf^{CKO}$, $B5^{Cre/+}$; $cMaf^{fl/fl}$, N=3) and littermate control ($B5^{Cre/+}$; $cMaf^{fl/+}$, N=3) animals. We dissociated the tissue into a single-cell suspension and created single cell cDNA libraries using the 10X 3'V2.0 Genomics platform. These libraries were sequenced and computationally

analyzed to pull out neuronal transcriptomes from knockout and control animals. After filtering out low-quality cells with high mitochondrial content, we proceeded with analysis of 1005 control SGNs and 1015 *cMaf*^{CKO} SGNs. Control SGNs normally cluster into three molecularly distinct subgroups[6]. However, unsupervised clustering analysis of combined control and *cMaf*^{CKO} transcriptomes revealed four distinct clusters (**Figure 4.1A**). Two clusters included cells from both genotypes whereas the other two clusters contained either control or mutant cells (**Figure 4.1B**). By analyzing the expression of previously identified SGN subtype marker genes, we found that the two overlapping clusters were 1B and 1C SGNs, as defined by their expression of 1B/1C genes *Runx1* and *Slc17a6* and expression of 1C specific gene *Lypd1* (**Figure 4.1F-H**). *Runx1* is a key transcriptional determinant in the development of 1B and 1C SGNs[45].

We determined that the remaining two clusters were 1A SGNs that segregated by genotype. Control and *cMaf*^{CKO} 1A clusters both expressed the 1A marker genes *Pcdh20* and *Rxrg. Calb2,* previously identified to be highly expressed in 1A neurons, was downregulated in *cMaf*^{CKO} SGNs. However, the 1A *cMaf*^{CKO} cluster had higher relative levels of *Calb2* compared to the 1B and 1C *cMaf*^{CKO} clusters (**Figure 4.1C-E**). Meanwhile, neither control 1A SGNs nor *cMaf*^{CKO} 1A SGNs expressed 1B or 1C marker genes (**Figure 4.1F-H**). It is possible that 1B and 1C SGNs from both genotypes were co-clustered while 1A mutant and control SGNs segregated into separate clusters due to larger gene expression changes in 1A SGNs when *cMaf* is knocked out.

Figure 4.1 Single-cell sequencing reveals segregated control and *cMaf*^{CKO} 1A SGNs. (A) UMAP plot summarizing sequencing data of 1005 control SGNs (*B5*$^{Cre/+}$*; cMaf*$^{fl/+}$, N=3) and 1015 *cMaf*^{CKO} SGNs (*B5*$^{Cre/+}$*; cMaf*$^{fl/fl}$, N=3). **(B)** UMAP plot showing contributions from each genotype. **(C-E)** Expression of 1A SGN markers in control and *cMaf*^{CKO} SGNs. **(F-H)** Expression of 1B and 1C SGN markers in control and *cMaf*^{CKO} SGNs. The color denotes the relative expression across 1A,1B, and 1C control and *cMaf*^{CKO} SGNs. Dark purple denotes higher relative expression while gray denotes lower relative expression.

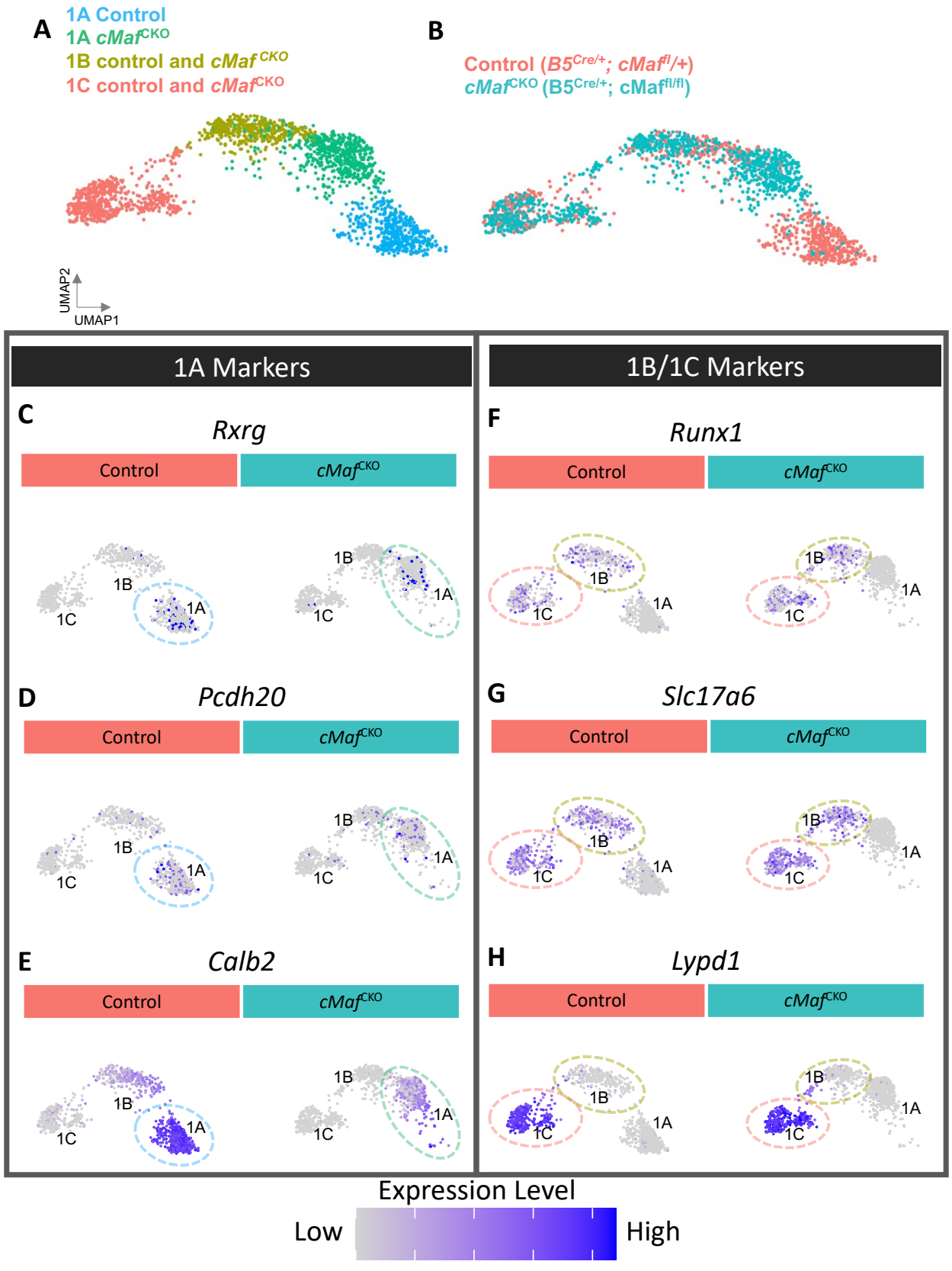
A
1A Control
1A cMafCKO
1B control and cMafCKO
1C control and cMafCKO
UMAP2
UMAP1
B
Control (B5Cre/+; cMaf fl/+)
cMafCKO (B5Cre/+; cMaf fl/fl)
1A Markers
1B/1C Markers
C
Rxrg
F
Runx1
D
Pcdh20
G
Slc17a6
E
Calb2
H
Lypd1
Control
cMafCKO
1A
1B
1C
Expression Level
Low
High

Once mutant and control SGNs were clustered, we assessed gene expression changes in *cMaf*^{CKO} animals. To assess overall gene expression changes across SGNs, we compared the transcriptomes of all control SGNs to transcriptomes of all *cMaf*^{CKO} SGNs (**Figure 4.2A**). By doing so, we increased the statistical power to capture a wide range of gene expression changes that could then be independently assessed for differential expression by subtype. This approach also allowed us to conduct an unbiased gene ontology analysis on differentially expressed genes across all SGN subtypes before focusing on changes in synaptic and neuronal gene expression by subtype. Genes that were considered differentially expressed had statistically different expression (Bonferonni adjusted p-value < 0.05) and log2fold change greater than 0.25 between control and knockout SGNs (**Figure4.2A, gray lines**). This list comprised 173 downregulated genes and 100 upregulated genes (**Table S4.1**). We ran the list of 273 upregulated and downregulated genes through a gene ontology analysis in PANTHER (**Table S4.2**). Differentially expressed genes in *cMaf*^{CKO} SGNs were associated with gene ontologies related to synaptic development, synaptic function, neuronal development, neuronal function, ribosomal assembly, translation, and cellular metabolism. Considering the synaptic phenotypes we have observed in *cMaf* mutants, we focused our analysis on all genes that were classified as being involved in synaptic or neuronal function, development, and maintenance. These 87 genes were from the following gene ontologies: postsynaptic density organization (GO:0097106), chemical synaptic transmission (GO:0007268), axo-dendritic transport (GO:0008088), neuron projection maintenance (GO:1990535), neuron projection extension (GO:1990138), regulation of cation channel activity (GO:2001257), cellular divalent inorganic cation homeostasis (GO:0072503), regulation of membrane potential (GO:0042391), regulation of neurotransmitter levels (GO:0001505), and synaptic vesicle endocytosis (GO:0048488).

To assess subtype-specific changes in neuronal and synaptic gene transcription, we compared the expression of all 87 synaptic and neuronal genes from the gene ontology analysis in

cMaf^{CKO} and control SGNs of each subtype. Among the 87 synaptic and neuronal genes, 34 are normally differentially expressed across control SGN subtypes (**orange dots, Figure 4.2B**). Sixty-four of these genes were differentially expressed overall between control and *cMaf*^{CKO} SGNs but were not differentially expressed when we assayed by subtype (**peach background, Figure 4.2B**). For example, *Dst* was modestly downregulated in all three SGN subtypes in *cMaf*^{CKO} animals. However, downregulation of *Dst* was not significant when considered by subtype. *Dst* was only significantly downregulated when all control SGNs were compared to all *cMaf*^{CKO} SGNs. All synaptic and neuronal genes that were differentially expressed overall but not by subtype in *cMaf*^{CKO} SGNs are denoted with a gray bar and peach background (**Figure 4.2B)**.

Meanwhile, twenty-three genes were differentially expressed in at least one subtype in *cMaf*^{CKO} SGNs compared to controls. Genes that were differentially expressed in individual subtypes in *cMaf*^{CKO} SGNs compared to controls are denoted with a black bar and purple (differentially expressed in 3 subtypes), green (differentially expressed in 2 subtypes), or blue (differentially expressed in 1 subtype) background (**Figure 4.2B**). Six of the 23 subtype-differentially expressed genes were differentially expressed across 3 subtypes (**purple background, Figure 4.2B, Figure 4.2D,E**). Three of the 23 subtype-differentially expressed genes were differentially expressed across 2 subtypes (**green background, Figure 4.2B, Figure 4.2D,E**). 14 of the 23 subtype-differentially expressed genes were differentially expressed across 1 subtype (**blue background, Figure 4.2B, Figure 4.2F**).

Of the 23 genes that were differentially expressed in individual subtypes in *cMaf* knockouts, 17 are normally differentially expressed across control SGN subtypes (**orange dots, purple, green and blue background, Figure 4.2B**). For example, *Rph3a* is normally highly expressed in control 1C SGNs. However, in *cMaf* mutants, *Rph3a* was significantly upregulated in 1A SGNs with non-significant changes in 1B and 1C SGNs (**Figure 4.2B,F**).

Subtype-specific gene expression changes in *cMaf*^{CKO} SGNs were biased to 1A SGNs, where *cMaf* is most highly expressed in control SGNs (**Figure 3.1F,H,I; Figure 4.2C**). Eighteen out of the 23 subtype-differentially expressed genes were differentially expressed in *cMaf*^{CKO} 1A SGNs compared to control 1A SGNs. Fewer were differentially expressed in *cMaf*^{CKO} 1B (10/23) and 1C (7/23) SGNs compared to 1B and 1C control SGNs respectively (**Figure 4.2C**).

Subtype-differentially expressed genes in *cMaf*^{CKO} SGNs had larger log2fold changes (log2FC) from control in 1A SGNs than in 1B and 1C SGNs. In order to compare log2FC across subtypes, the gene had to be differentially expressed in more than one subtype in *cMaf*^{CKO} SGNs compared to controls. We therefore assessed only genes that had at least a 10% difference in the degree of change in at least two subtypes (**Table S4.3**). We found 6 out of 9 of these genes had larger log2FC from controls in the 1A and 1B *cMaf*^{CKO} subtypes than 1C *cMaf*^{CKO} SGNs. *Mafb* and *Uchl1* showed the highest fold upregulation from control in *cMaf*^{CKO} 1A SGNs (**Figure 4.2D**), whereas *Calb2* showed the highest fold downregulation from control in *cMaf*^{CKO} 1A SGNs (**Figure 4.2E**). *Ubb* (**Figure 4.2E**) was significantly changed in 1A and 1C SGNs. *Sncg* (**Figure 4.2D**) and *Mt2* (**Figure 4.2E**) were the only two genes that showed larger log2FC in 1B and 1C *cMaf*^{CKO} SGNs compared to control. Meanwhile, of the 14 genes that were significantly changed in only one subtype, 11 were differentially expressed in 1A *cMaf*^{CKO} SGNs (**Figure 4.2F**). These results indicate that *cMaf* has larger effects on 1A and 1B synaptic and neuronal gene expression compared to 1C SGNs.

We wanted to validate if differentially expressed genes in *cMaf*^{CKO} SGNs were changed at the protein level. The calcium binding protein *Calb2* was the most significantly differentially expressed gene in 1A and 1B SGNs *cMaf*^{CKO} subtypes (p_A=6.18E-162, $log2FC_A$=3.21; p_B=9.43E-50, $log2FC_B$=1.658, Bonferroni adjusted p-value, Wilcoxon Rank Sum) (**Figure 4.2E, Table S4.3**). *Calb2* is highest expressed in control 1A SGNs and lowest expressed in control 1C

SGNs. *Calb2* was most downregulated in 1A SGNs and least downregulated in 1C SGNs in *cMaf* knockouts compared to controls (**Figure 4.2E,G**). We validated the downregulation with immunohistochemistry of CALB2 protein in *cMaf* knockout animals (**Figure 4.2I**). The exact function of CALB2 in SGNs is unknown and relatively little is known about the mechanisms of *Calb2* genetic regulation. CALB2 is known to act as a calcium buffer in cells across the body and the loss of Calb2 in cerebellar Purkinje cells results in aberrant increases in neuronal excitability[67,68]. Therefore, dysregulation of CALB2 expression in *cMaf*^{CKO} SGNs could contribute to altered synaptic physiology.

Mafb regulation by *cMaf* in a subtype-dependent manner could contribute to the complementary expression patterns of *cMaf* and *Mafb* across SGNs subtypes. *Mafb* was upregulated in cMaf knockout SGNs compared to control SGNs. This upregulation was strongest in *cMaf* knockout 1A SGNs (**Figure 4.2D,H**), where *cMaf* is relatively most expressed and *Mafb* is relatively least expressed in control animals (**Figure 3.1F-J**). This upregulation of *Mafb* in *cMaf* knockout 1A SGNs flattened the graded expression of Mafb across SGNs subtypes with respect to control animals (**Figure 4.2H**). Thus, in mutants, *Mafb* was no longer differentially expressed in 1B and 1C SGNs compared to 1A SGNs. We qualitatively validated the upregulation of MAFB protein with immunohistochemistry in *cMaf* knockout animals (**Figure 4.2J**).

The upregulation of *Mafb* could be partially compensating for the loss of *cMaf.* However, it is likely that *Mafb* is also regulating a distinct set of genes, consistent with the distinct synaptic (**Figure 2.3H-J,M-O**) and functional phenotypes (**Figure2.4B,C,E, Figure 2.5C-F**) observed in *cMaf* and *Mafb* mutants. *Mafb* upregulation in 1A and 1B *cMaf*^{CKO} SGNs could potentially rescue some aspects of *cMaf* function while also causing abnormal *Mafb* target gene expression patterns across SGN subtypes. In other words, the genes that *Mafb* transcriptionally regulates are likely partially but not completely overlapping with *cMaf*-regulated genes. Moreover, this result suggests that *cMaf* is potentially repressing *Mafb* expression in 1A SGNs compared to 1B

and 1C SGNs. To distinguish which genes are targeted uniquely by *Mafb,* it is necessary to assess gene expression changes in *Mafb* mutants and *cMaf/Mafb* double mutants.

Figure 4.2. Single-cell sequencing reveals overall and subtype-specific changes in gene expression in *cMaf*^{CKO} SGNs. (A) Volcano plot denoting differentially expressed genes between control SGNs (*B5*$^{Cre/+}$*; cMaf*$^{fl/+}$*,* N=3, n=1005) and *cMaf*^{CKO} SGNs SGNs (*B5*$^{Cre/+}$*; cMaf*$^{fl/fl}$*,* N=3, n=1015). Cyan, genes downregulated in *cMaf*^{CKO} with an average log2 fold change >0.25 and P<0.05 (Wilcoxon rank sum test, Bonferroni post-hoc correction). Magenta, genes upregulated in *cMaf*^{CKO} SGNs with an average log2 fold change >0.25 and P<0.05 (Wilcoxon rank sum test, Bonferroni post-hoc correction). Gray lines denote cutoff of 0.25 log2fold change and a p-value of 0.05. **(B)** Dot plot of differentially expressed synaptic and neuronal genes in *cMaf*^{CKO} SGNs. 23 genes that were differentially expressed in at least one subtype in *cMaf*^{CKO} SGNs are denoted by the black bar. Purple background: genes that were differentially expressed in all three SGN subtypes in *cMaf*^{CKO} SGNs. Green background: genes that were significantly differentially expressed in two SGN subtypes in *cMaf*^{CKO} SGNs. Blue background: genes that were significantly differentially expressed in one SGN subtype in *cMaf*^{CKO} SGNs. Peach background: 64 genes that were differentially expressed overall when comparing all control and *cMaf*^{CKO} SGNs and not differentially expressed in individual subtypes. The color of the dot denotes the relative expression across 1A,1B, and 1C control and *cMaf*^{CKO} SGNs. Dark purple denotes higher relative expression while gray denotes lower relative expression. The size of the dot represents the percent of cells that had an expression level above 0. Orange circle next to gene name denotes genes that are differentially expressed across SGN subtypes in control animals. **(C)** Subtype-specific differentially expressed genes. Magenta, genes that were upregulated in *cMaf*^{CKO} SGN subtypes compared to control. Cyan, genes that were downregulated in *cMaf*^{CKO} SGN subtypes compared to control. **(D)** Heatmap of relative log2fold change of genes that were upregulated in at least two subtypes in *cMaf*^{CKO} SGNs. Warmer colors denote a larger upregulation. ns= subtype comparisons that were not significant (p>0.05, Wilcoxon rank sum test, Bonferroni post-hoc correction) **(E)** Heatmap of relative log2fold change of genes that were downregulated in at least two subtypes in *cMaf*^{CKO} SGNs. Warmer colors

Figure 4.2 (Continued) denote a larger downregulation. ns= subtype comparisons that were not significant (p>0.05, Wilcoxon rank sum test, Bonferroni post-hoc correction) **(F)** Volcano plot denoting genes that were differentially expressed in one SGN subtype in *cMaf*^{CKO} SGNs. The color of the point denotes which subtype the gene was differentially expressed in. (Orange=1A, Green=1B, Pink=1C). **(G,H)** Split violin plots denoting distributions of **(G)** *Calb2* and **(H)** *Mafb* expression across subtypes in control (orange) and *cMaf*^{CKO} SGNs (blue). **(I)** CALB2 expression in cryosections of control (*cMaf*$^{fl/fl}$) and knockout (*B5*$^{Cre/+}$*; cMaf*$^{fl/fl}$) cochlea. Green, CALB2. Blue, HuD, a neuronal cell body marker. **(J)** MAFB expression in cryosections of control (*cMaf*$^{fl/fl}$) and knockout (*B5*$^{Cre/+}$*; cMaf*$^{fl/fl}$) cochlea. Red, MAFB. Scale bar=20μm. For all panels a gene was considered differentially expressed if it had a P value<0.05 (Wilcoxon rank sum test, Bonferroni post-hoc correction).

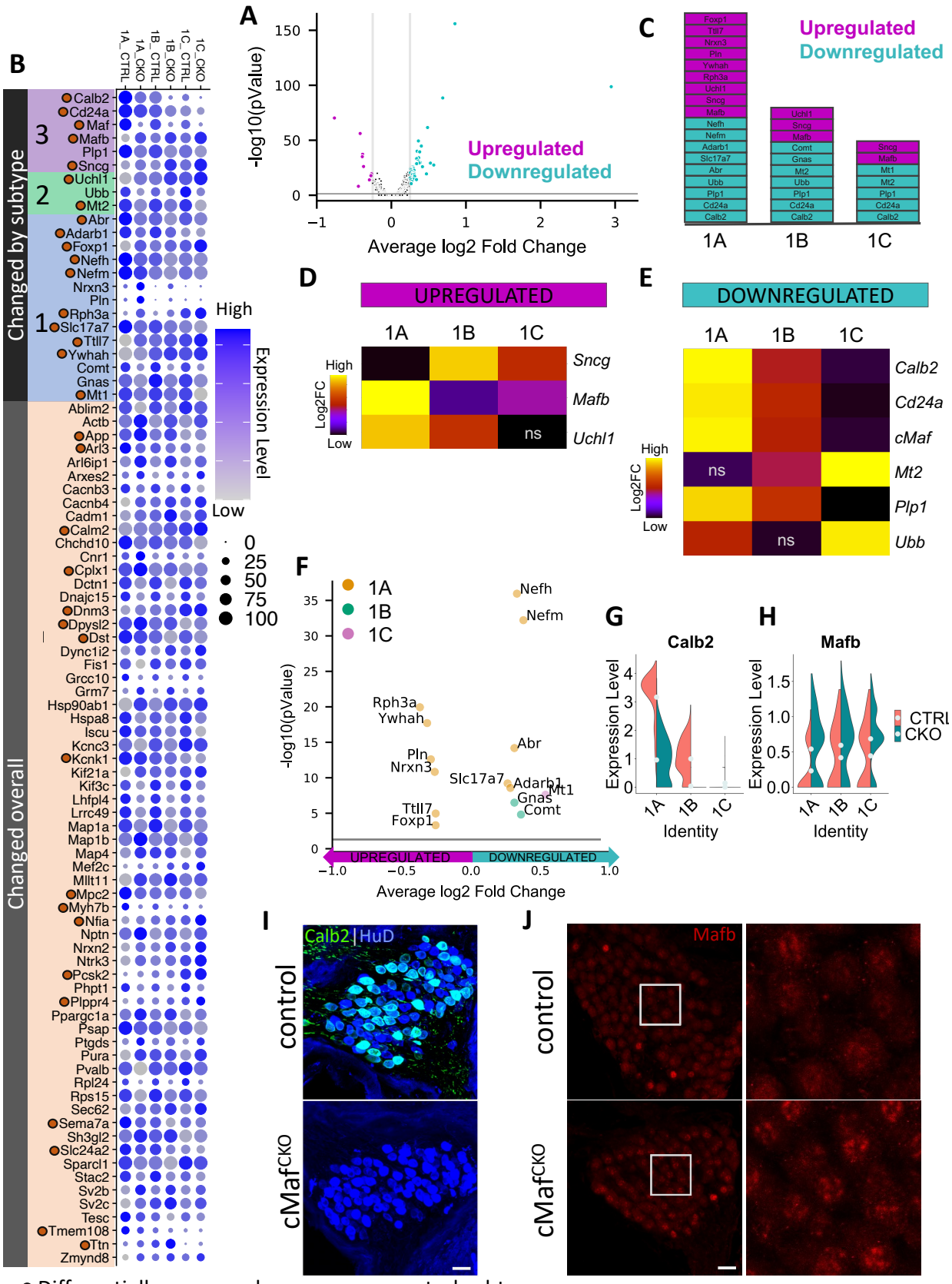

● Differentially expressed genes across control subtypes

Using the same analysis, we assessed differentially expressed genes in *Mafb* mutants. Briefly, *Mafb* mutant (*Mafb*^{CKO}, *B5*$^{Cre/+}$*;Mafb*$^{fl/GFP}$, N=3) and control (*Mafb*$^{fl/+}$, N=4) cochleae were microdissected and dissociated into a single-cell suspension. The *Mafb*^{GFP} allele is a knock-in global null mutation that replaces the *Mafb* coding sequence with *GFP.* Single-cell libraries were generated using the 10X 3'V3.1 Genomics platform. This was an updated version of the 10X technology capable of detecting almost double the amount of genes per cell as the previous version used with the *cMaf* mutants[69]. After quality filtering, this dataset contained 1056 control SGNs and 961 *Mafb*^{CKO} SGNs. When *Mafb*^{CKO} and control SGNs were clustered together, they segregated into three overlapping clusters (**Figure 4.3A,B**). These clusters corresponded to type 1A, 1B, and 1C SGNs as identified using known subtype marker genes (**Figure 4.3C**). Unlike the *cMaf*^{CKO}, all *Mafb*^{CKO} SGNs co-clustered with controls, indicating that Mafb is not causing differential gene expression in genes that drive subtype clustering.

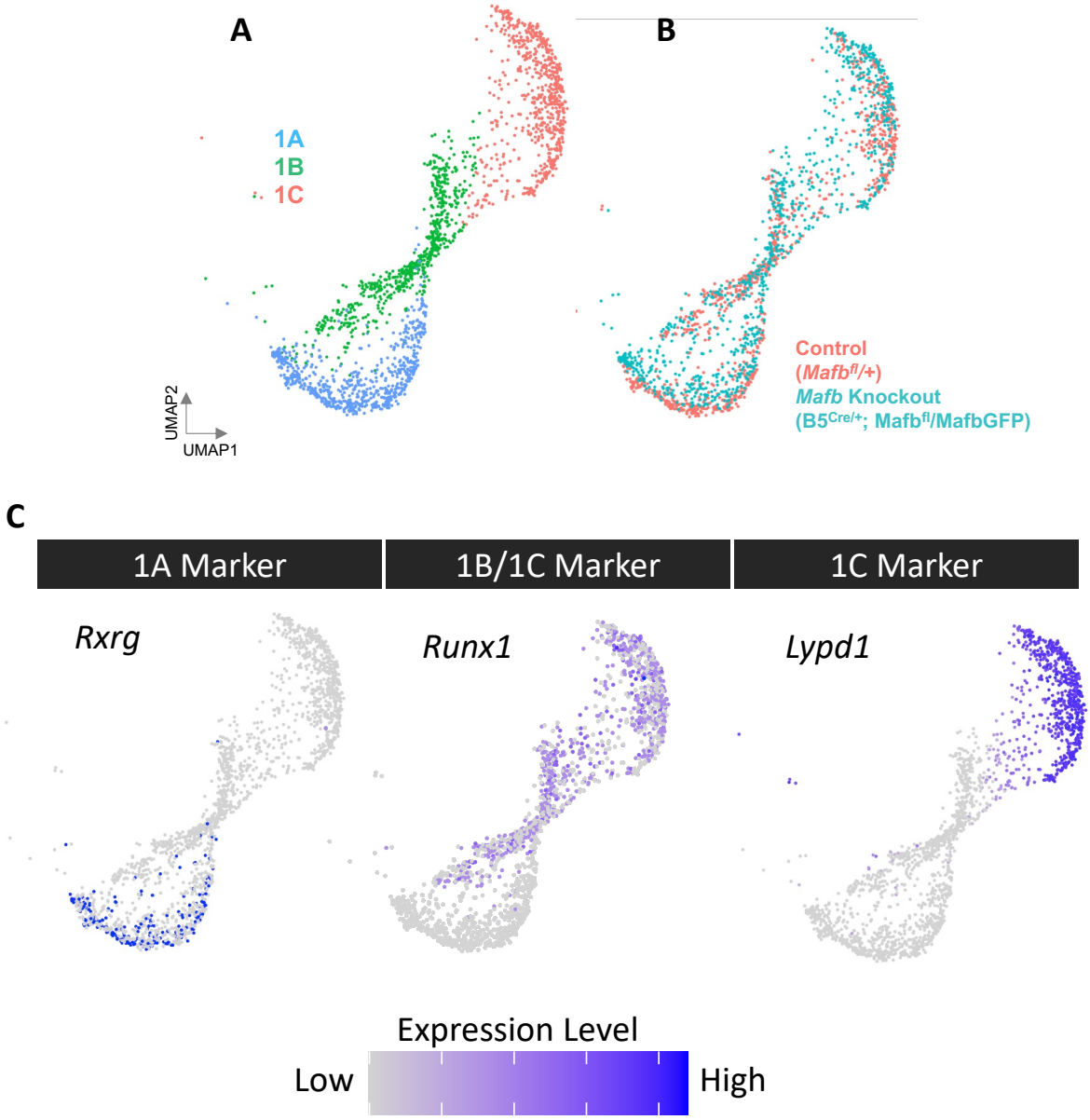

Figure 4.3 Single-cell sequencing of control and *Mafb*^{CKO} SGNs. (A) UMAP plot summarizing sequencing data of 1056 control SGNs (*Mafb*$^{fl/+}$, N=3) and 961 *Mafb*^{CKO} SGNs (*B5*$^{Cre/+}$*; Mafb*$^{fl/GFP}$, N=4). **(B)** UMAP plot showing contributions from each genotype. **(C)** Expression of SGN subtype markers in control and *Mafb*^{CKO} SGNs. The color denotes the

Figure 4.3 (Continued) relative expression across 1A,1B, and 1C control and *cMaf*^{CKO} SGNs. Dark purple denotes higher relative expression while gray denotes lower relative expression.

We first assessed overall gene transcription changes in *Mafb* knockout SGNs. Genes that were considered differentially expressed had statistically different expression (Bonferonni adjusted p-value < 0.05) and log2fold change greater than 0.25 between control and knockout SGNs (**Figure 4.4A, gray lines**). 153 genes were differentially downregulated while 157 were differentially upregulated (**Table S4.4**). We ran the resultant list of 313 up and downregulated genes through a gene ontology analysis in PANTHER (**Table S4.5**). Differentially expressed genes in *Mafb*^{CKO} SGNs were associated with gene ontologies related to synaptic development, synaptic function, neuronal development, neuronal function, ribosomal assembly, translation, and cellular metabolism. Considering the synaptic phenotypes we have observed in *Mafb* mutants, we focused on the genes that were classified as being involved in synaptic or neuronal function, development, and maintenance. These resulting 72 genes were significantly enriched for the following gene ontologies: glutamatergic synapse (GO:0098978), dendritic spine (GO:0043197), voltage-gated potassium channel complex (GO:0008076), postsynaptic density (GO:0014069), integral component of synaptic membrane (GO:0099699), neuronal cell body (GO:0043025), axon (GO:0030424).

To assess subtype-specific changes in neuronal and synaptic gene transcription in *Mafb*^{CKO} SGNs, we compared the expression of all 72 synaptic and neuronal genes from the gene ontology analysis in *Mafb*^{CKO} SGNs to control SGNs by subtype. Forty-three genes were not significantly changed when we assayed by subtype. For example, *Cdh9* was subtly downregulated across SGNs. The downregulation of *Cdh9* was not significantly changed when considered by subtype, but is significantly downregulated when all control SGNs are compared to all *Mafb*^{CKO} SGNs. Meanwhile, twenty-nine genes were significantly changed in at least one

subtype in *Mafb*^{CKO} SGNs compared to controls (**black bar, Figure 4.4B, Table S4.6**). Of the 29 genes that were differentially expressed in a subtype-specific manner in *Mafb*^{CKO} SGNs, more genes were significantly differentially expressed in 1C SGNs (21 out of 29 genes) than 1B SGNs (13 out of 29 genes) and 1A SGNs (12 out of 29 genes) **(Figure 4.4C**). Five of the 29 subtype-differentially expressed genes were differentially expressed across 3 subtypes (**purple background, Figure 4.4B, Figure 4.4D,E**). Seven of the 29 subtype-differentially expressed genes were differentially expressed across 2 subtypes (**green background, Figure 4.4B. Figure 4.4D,E**). Of the 29 genes that were differentially expressed in individual subtypes in *Mafb*^{CKO} SGNs, 17 were differentially expressed across 1 subtype (**blue background, Figure 4.4B, Figure 4.4F**).

Thus, subtype-specific gene expression changes in *Mafb*^{CKO} SGNs were biased to 1B and 1C SGNs, where *Mafb* expression levels are highest in control SGNs. We assessed the genes that had at least 10% difference in the degree of change across at least two subtypes in *Mafb* knockout compared to control SGNs. We found that 11 out of 13 of these genes had the largest log2fold change in 1B and/or 1C SGNs, where *Mafb* is most highly expressed in controls (**Figure 4.4D,E**). We also observed that 10 of the 17 genes that were differentially expressed in only one subtype were changed in 1B or 1C SGNs (**Figure 4.4F**). These results suggest that *Mafb* has differential effects on 1B and 1C synaptic and neuronal gene expression patterns that reflect the control levels of *Mafb*.

Figure 4.4. Single-cell sequencing reveals overall and subtype-specific changes in gene expression in *Mafb^{CKO}* SGNs. (A) Volcano plot denoting differentially expressed genes between 1056 control SGNs (*Mafb$^{fl/+}$,* N=3) and 961 *Mafb^{CKO}* SGNs (*B5$^{Cre/+}$; Mafb$^{fl/GFP}$,* N=4). Cyan, genes downregulated in *Mafb^{CKO}* with an average log2 fold change >0.25 and P<0.05 (Wilcoxon rank sum test, Bonferroni post-hoc correction). Magenta, genes upregulated in *Mafb^{CKO}* SGNs with an average log2 fold change >0.25 and P<0.05 (Wilcoxon rank sum test, Bonferroni post-hoc correction). Gray lines denote cutoff of 0.25 log2fold change and a P-value of 0.05. **(B)** Dot plot of differentially expressed synaptic and neuronal genes in *Mafb^{CKO}* SGNs. 23 genes that were differentially expressed in at least one subtype in *Mafb^{CKO}* SGNs are denoted by the black bar. Purple highlight, genes that were differentially expressed in each of the three SGN subtypes in *Mafb^{CKO}* SGNs. Green highlight, genes that were significantly differentially expressed in two SGN subtypes in *Mafb^{CKO}* SGNs. Blue highlight, genes that were significantly differentially expressed in one SGN subtype in *Mafb^{CKO}* SGNs. Peach highlight, genes that were differentially expressed overall when comparing all control and *Mafb^{CKO}* SGNs and not differentially expressed in individual subtypes. The color of the dot denotes the relative expression across 1A,1B and 1C control and *Mafb^{CKO}* SGNs. Dark purple denotes higher relative expression while gray denotes lower relative expression. The size of the dot represents the percent of cells that had an expression level above 0. Orange circle next to gene names, genes that are differentially expressed across SGN subtypes in control animals. Asterisk denotes genes that were also differentially expressed in *cMaf^{CKO}* SGNs. **(C)** Subtype-specific differentially expressed genes. Magenta, genes that were upregulated in *Mafb^{CKO}* SGN subtypes compared to control. Cyan, genes that were downregulated in *Mafb^{CKO}* SGN subtypes compared to control. **(D)** Heatmap of relative log2fold change of genes that were upregulated in at least two subtypes in *Mafb^{CKO}* SGNs. Warmer colors denote a larger upregulation. ns= subtype comparisons that were not significant (p>0.05, Wilcoxon rank sum test, Bonferroni post-hoc correction) **(E)** Heatmap of relative log2fold change of genes that were downregulated in at least

Figure 4.4 (Continued) two subtypes in *Mafb*^{CKO} SGNs. Warmer colors denote a larger downregulation. ns= subtype comparisons that were not significant (p>0.05, Wilcoxon rank sum test, Bonferroni post-hoc correction) **(F)** Volcano plot denoting genes that were differentially expressed in one SGN subtype in *Mafb*^{CKO} SGNs. The color of the point denotes which subtype the gene was differentially expressed in (Orange=1A, Green=1B, Pink=1C). For all panels a gene was considered differentially expressed if it had a P value<0.05 (Wilcoxon rank sum test, Bonferroni post-hoc correction).

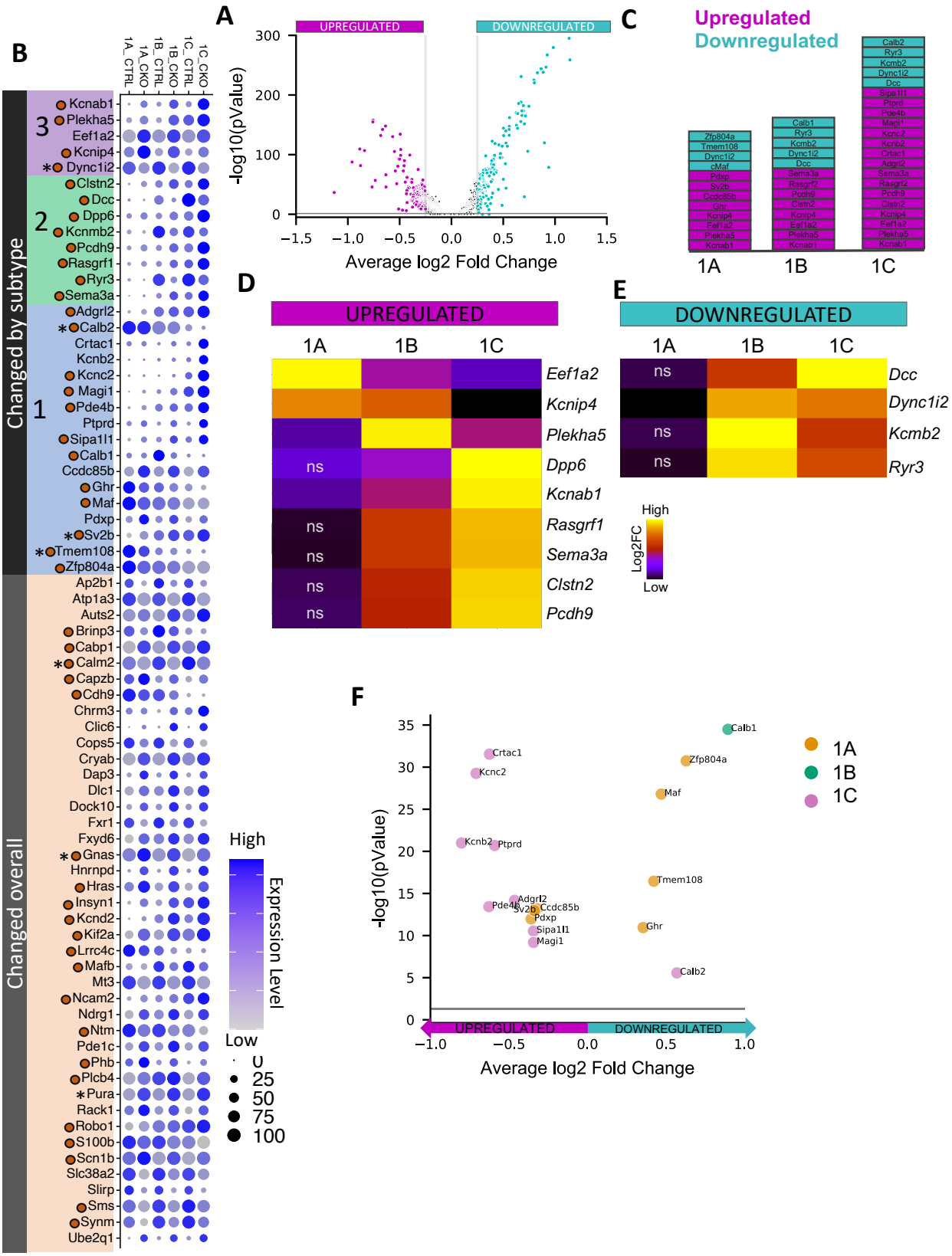

●Differentially expressed genes across control subtypes
∗Changed in *cMaf* CKOs

Genes that were differentially expressed in both *cMaf*^{CKO} and *Mafb*^{CKO} SGNs were changed in both congruent and antagonistic directions. From the synaptic and neuronal genes analyzed in *cMaf*^{CKO} and *Mafb*^{CKO} datasets, 7 were differentially changed in both single mutants **(Figure 4.4B, asterisk**). Four of the seven genes were changed in the same direction in *cMaf*^{CKO} and *Mafb*^{CKO} SGNs. *Sv2b* and *Pura* were upregulated in *cMaf*^{CKO} and *Mafb*^{CKO} while *Calb2* and *Tmem108* were downregulated in *cMaf*^{CKO} and *Mafb*^{CKO}. Meanwhile, three genes were changed in opposing directions. *Dync1i2* and *Calm2* were downregulated in *Mafb*^{CKO} SGNs and upregulated in *cMaf*^{CKO} SGNs. On the other hand, *Gnas* was upregulated in *Mafb*^{CKO} SGNs and downregulated in *cMaf*^{CKO} SGNs (**Figure 4.2B, Figure 4.4B**). However, these two datasets were collected with different versions of the 10X barcoding technology. Therefore, *Mafb* knockout transcriptomes had many more genes per cell and rigorous comparison of the overlap between differentially expressed genes from these two datasets is not feasible with these data. Additionally, *cMaf* was downregulated in 1A SGNs in *Mafb* knockouts. Considering the upregulation of *Mafb* in *cMaf* knockouts (**Figure 4.2D,H,J**), it is possible that *cMaf* and *Mafb* regulate each other, with *cMaf* repressing *Mafb* and *Mafb* enhancing the expression of *cMaf*. Therefore, some of the differentially expressed genes in each dataset are potentially due to changes in the other factor.

To understand how *cMaf* and *Mafb* work together to regulate SGN gene expression, we collected transcriptomes from double knockout (dKO, *B5*$^{Cre/+}$*;Mafb*$^{fl/fl}$*;cMaf*$^{fl/fl}$, N=3) SGNs and control (*Mafb*$^{fl/fl}$*;cMaf*$^{fl/fl}$, N=3) littermates. We used the 10X 3'V3.1 Genomics platform and pipeline for processing dKO and control SGNs. After quality filtering, this dataset contained 907 control SGNs and 705 dKO SGNs. Unsupervised graph-based clustering revealed that while control SGNs still formed three distinct clusters that corresponded to 1A, 1B, and 1C SGN subtypes, dKO neurons formed one cluster (**Figure 4.5 A,B**). Most of the cells in the dKO

cluster expressed 1B and 1C genes such as *Lypd1* and *Runx1* and completely lacked the expression of the 1A marker genes *Rxrg* and *Calb1* (**Figure 4.5C**). dKO neurons did not cluster with control 1B and 1C neurons and had lower expression of *Lypd1* compared to 1C neurons in controls. There was subtle segregation of *Lypd1* expression in dKO SGNs, suggesting a low degree of molecular diversification within this cluster(**Figure 4.5C**). However, despite lower *Lypd1* levels in a proportion of double knockout SGNs, dKO SGNs formed one amalgamated cluster (**Figure 4.5A**). Recent work has shown that the sustained expression of *Runx1* directs SGNs to a 1B/1C subtype identity while 1A SGNs downregulate *Runx1* over development[45,64]. The lack of subtype-segregated *Runx1* expression as well as the complete lack of 1A markers suggests that double knockout SGNs are potentially arrested at earlier stages of development. These results suggest that *cMaf* and *Mafb* function together to properly differentiate SGNs.

When we compared the transcriptomes of control and double knockout SGNs, we found that there were 1254 significantly differentially expressed genes (**Figure 4.6A, Table S4.7**). This list was longer than the list of differentially expressed genes in either of the single knockouts, suggesting that there are combinatorial effects of *cMaf* and *Mafb* on gene expression. When we ran this list through a gene ontology analysis, we found that these genes were enriched for many synaptic and neuronal processes, such as retrograde trans-synaptic signaling by trans-synaptic protein complex (GO:0098942, p= 7.64E-04), synaptic membrane adhesion (GO:0099560 p= 2.13E-09), synapse maturation (GO:0060074, p= 8.05E-06), peripheral nervous system neuron differentiation (GO:0048934, p= 3.07E-04), regulation of postsynaptic density assembly (GO:0099151, p= 4.19E-04) , excitatory postsynaptic potential (GO:0060079, p=2.68E-04), synaptic vesicle cycle (GO:0099504, p= 2.03E-08) and presynapse assembly (GO:0099054, p=6.72E-05) (**Table S4.8**). This gene ontology analysis supports combined roles of cMaf and Mafb in SGN differentiation and synaptic development.

Figure 4.5 Single-cell sequencing of control and *cMaf/Mafb*^{DKO} (dKO) SGNs. (A) UMAP plot summarizing sequencing data of double knockout (dKO, *B5*$^{Cre/+}$*;Mafb*$^{fl/fl}$*;cMaf*$^{fl/fl}$, N=3, n=705) SGNs and controls (*Mafb*$^{fl/fl}$*;cMaf*$^{fl/fl}$, N=3, n=907). **(B)** UMAP plot showing contributions from each genotype. **(C)** Expression of SGN subtype markers in control and dKO SGNs. The color denotes the relative expression across 1A,1B, and 1C control and *cMa/Mafbf*^{DKO} SGNs. Dark purple denotes higher relative expression while gray denotes lower relative expression.

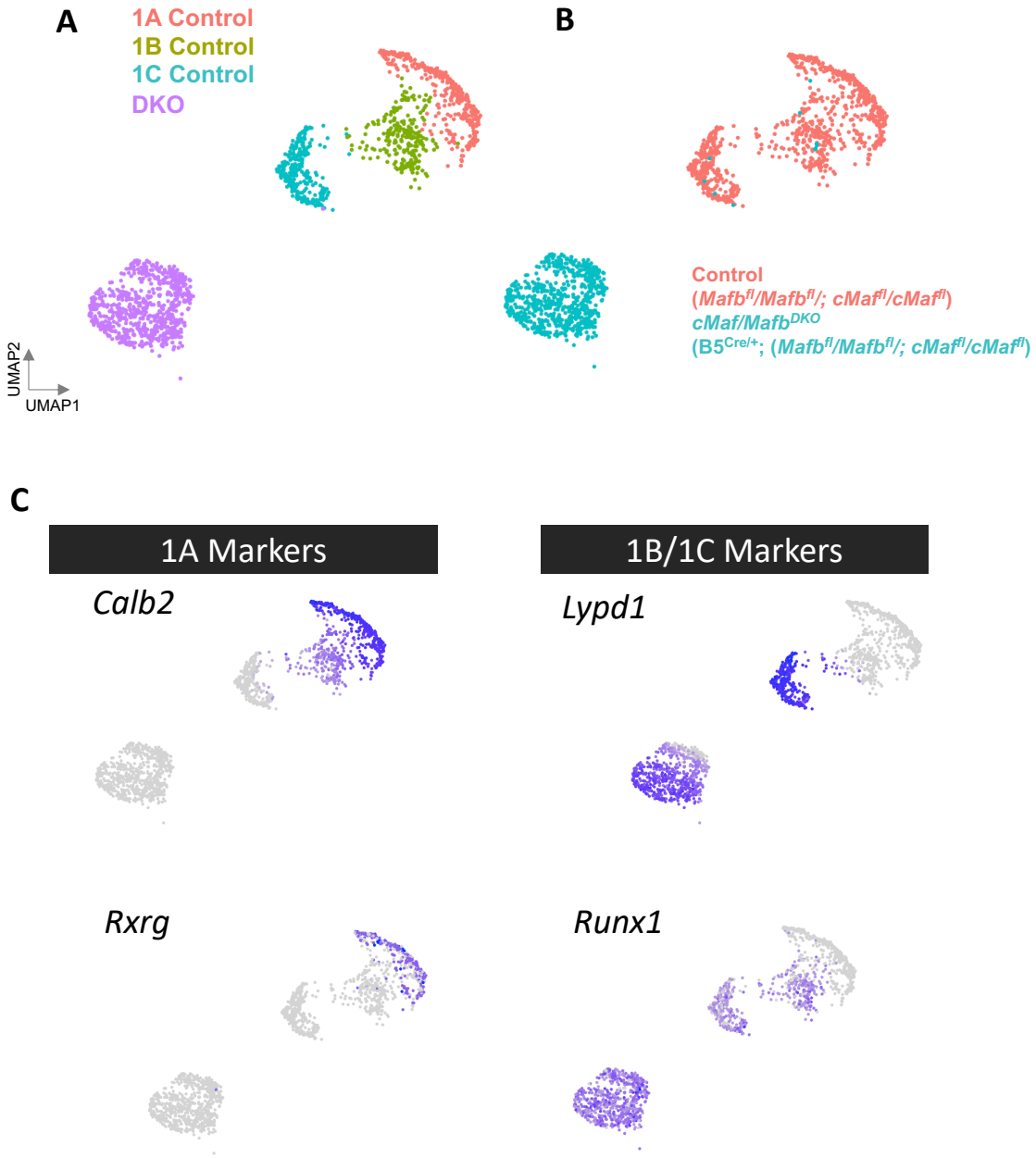

We wanted to know how the top differentially regulated genes in dKO SGNs were differentially expressed in *Mafb*^{CKO} and *cMaf*^{CKO} SGNs. We took genes that were at least 30% up or downregulated in dKO neurons and checked to see if they were differentially expressed in *Mafb*^{CKO} and *cMaf*^{CKO} SGNs. This list comprised 98 genes that were the most differentially

expressed genes in dKO SGNs. Eight of these genes were changed in both *Mafb*^{CKO} and *cMaf*^{CKO} SGNs single mutant scRNAseq datasets (**purple background, Figure 4.6B**). These genes likely correspond to genes that CMAF and MAFB both regulate. Six genes were significantly changed only in *cMaf*^{CKO} SGNs (**green background, Figure 4.6B**). These genes are likely CMAF-specific target genes. Since the *cMaf* transcriptomes were collected on older versions of the 10X technology, it is likely that the number of *cMaf*-specific regulated genes are underestimated. Fifty-two genes were changed only in *Mafb*^{CKO} SGNs, which likely correspond to MAFB-specific target genes (**blue background, Figure 4.6B**). Thirty-two genes were only significantly changed in dKO SGNs and not significantly changed in either single knockout dataset (**yellow background, Figure 4.6B**). These results suggest that the effects that cMaf and Mafb have overlapping, distinct, and synergistic effects on synaptic gene expression in SGNs.

When we analyzed the expression of the double knockout top differentially regulated genes in *cMaf* mutant SGNs by subtype, we found that most of these genes were differentially regulated in *cMaf* mutants in 1A SGNs (**Figure 4.6C**). Meanwhile, in the *Mafb* mutants, most of these genes were differentially regulated in 1C and 1B SGNs (**Figure 4.6D**). These results corroborate the previously observed subtype-specific activity of *cMaf* and *Mafb*.

Figure 4.6. Single-cell sequencing of *cMaf/Mafb*^{DKO} (dKO) SGNs reveals synergistic and subtype-specific effects on gene expression. (A) Volcano plot denoting differentially expressed genes between double knockout (dKO, *B5*$^{Cre/+}$*;Mafb*$^{fl/fl}$*;cMaf*$^{fl/fl}$, N=3, n=705) SGNs and control (*Mafb*$^{fl/fl}$*;cMaf*$^{fl/fl}$, N=3, n=907) SGNs. Cyan, genes downregulated in *cMaf/Mafb*^{DKO} with an average log2 fold change >0.25 and P<0.05 (Wilcoxon rank sum test, Bonferroni post-hoc correction). Magenta, genes upregulated in cMaf/*Mafb*^{DKO} SGNs with an average log2 fold change >0.25 and P<0.05 (Wilcoxon rank sum test, Bonferroni post-hoc correction). Gray lines denote cutoff of 0.25 log2fold change and a P-value of 0.05. **(B)** Dot plot of top 30% differentially expressed genes in *cMaf/Mafb*^{DKO} in *cMaf, Mafb* and *cMaf/Mafb*^{DKO} datasets. The color represents whether these genes were upregulated (Magenta) or downregulated (Cyan) in knockout SGNs. Control expression of these genes across SGN subtypes is on the left. The color denotes the relative expression across 1A,1B, and 1C SGNs. Dark purple denotes higher relative expression while gray denotes lower relative expression. The size of the dot represents the percent of cells that had an expression level above 0. Purple highlight, genes that were differentially expressed in both *cMaf*^{CKO} and *Mafb*^{CKO} SGNs. Green highlight, genes that were differentially expressed in *cMaf*^{CKO} SGNs. Blue highlight, genes that were differentially expressed in *Mafb*^{CKO} SGNs. Yellow highlight, genes that were only differentially expressed in dKO SGNs. **(C)** Genes that were differentially expressed in *cMaf*^{CKO} SGNs by subtype. **(D)** Genes that were differentially expressed in *Mafb*^{CKO} SGNs by subtype. For all panels a gene was considered differentially expressed if it had a P value<0.05 (Wilcoxon rank sum test, Bonferroni post-hoc correction).

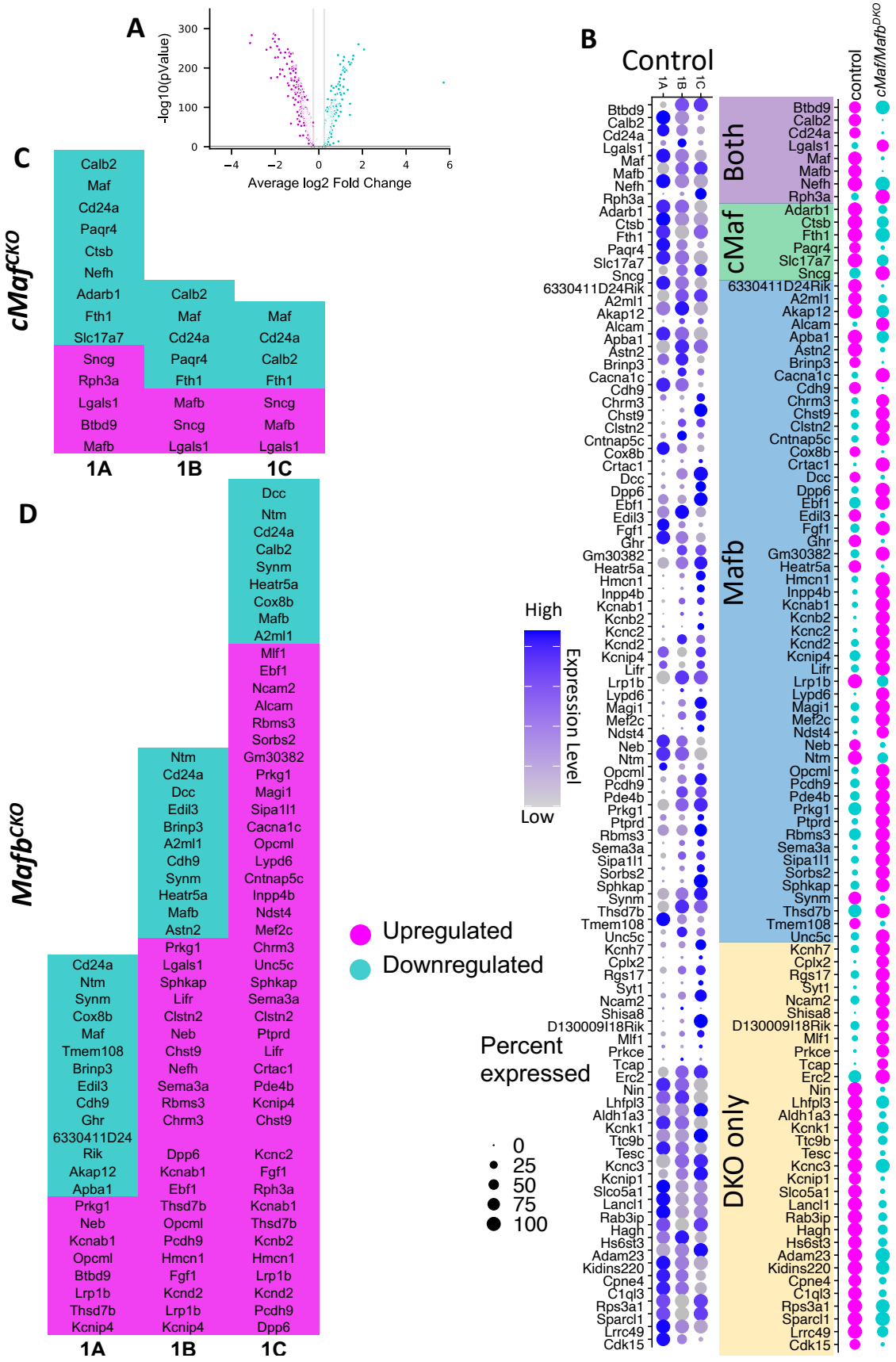
A
-log10(pValue)
Average log2 Fold Change
B
Control
control
cMaf/Mafb^DKO
Both
cMaf
Mafb
DKO only
High
Low
Expression Level
Percent expressed
0
25
50
75
100
C
cMaf^CKO
1A
1B
1C
D
Mafb^CKO
1A
1B
1C
Upregulated
Downregulated

These data provide insight into an emerging model of combinatorial transcriptional regulation of SGN synaptic development. CMAF and MAFB are expressed in complementary patterns across SGNs (**Figure 3.1F-J**). CMAF and MAFB complementary expression patterns are likely self-reinforcing. The loss of CMAF upregulates the expression of MAFB in 1A and 1B SGNs (**Figure 4.2D,H**) while the loss of MAFB downregulates the expression of CMAF in 1A SGNs (**Figure 4.4F**). CMAF and MAFB expression patterns are also influenced by upstream determinants of SGN subtype identity such as neuronal activity and the transcription factors Runx1 and Gata3[6,44,45]. CMAF and MAFB have distinct (**Figure 4.2B, Figure 4.4B**) and overlapping (**Figure 4.6B)** effects on SGN synaptic gene expression as confirmed by analysis of differentially expressed genes in single and double mutant single-cell RNA sequencing datasets. CMAF and MAFB broadly regulate neuronal and synaptic gene expression across SGN subtypes (**Figure 4.2B, Figure 4.4B**) and also regulate several synaptic genes in a subtype-specific manner (**Figure 4.2C-F, Figure 4.4C-F, Figure 4.6C,D**). Differentially expressed genes in *cMaf* and *Mafb* single and double mutants include pre- and postsynaptic molecules as well as ion channels and intercellular adhesion molecules. The expression of certain genes such as *Adarb1, Abr,* and *Ywhah* are primarily regulated by CMAF. Meanwhile, the expression of certain genes such as *Dcc, Cdh9, Dpp6,* and *Kcnab1* are primarily regulated by MAFB. Genes such as *Rph3a, Cd24a,* and *Calb2* are regulated by both transcription factors independently and genes such as *Ncam2* and *Cplx2* are regulated by CMAF and MAFB in combination. These overlapping and differential effects on SGN synaptic gene transcription are poised to provide nuanced and combinatorial control over SGN synaptic properties, consistent with the phenotypes we have observed.

METHODS

Animal Models

Bhlhe22^{Cre} (*B5*^{Cre}, MGI:4440745), *cMaf*^{fl} (MGI:5316775), *Mafb*^{GFP} (MGI:3663168), and *Mafb*^{fl} (MGI:5581666) are all previously described. Animals were maintained on a mixed background. Animal work was conducted in compliance with protocols approved by the Institutional Animal Care and Use Committee at Harvard Medical School.

Histology

All animals were anesthetized via isoflurane by the open-drop method and perfused with cold 4% paraformaldehyde (PFA) in 1x PBS. Both temporal bones were dissected out and PFA was perfused through the oval and round windows with a syringe. Temporal bones were decalcified for 72 hours in 120mM EDTA in 1x PBS. Cochlea were then cryopreserved in 30% sucrose in 1x PBS for 24 hours at 4°C and then in 30% sucrose in NEG for 24 hours at 4°C. Cochleae were then removed from temporal bones embedded for sectioning. Cochlear sections were washed 1x for 5 minutes in 1x PBS and then 2x for 5 minutes in 0.25% Triton X-100 in 1x PBS. Sections were blocked with 5%v/v normal donkey serum, 10% FAB fragments, and 0.3% Triton X-100 in 1x PBS. Sections were stained with mouse anti-HuD (1:50), rabbit anti cMaf (1:250), rabbit anti Mafb (1:250), and goat anti Calb2 (1:500) for four hours at room temperature. After rinsing with 1x PBS, sections were stained with appropriate secondary antibodies at 4°C overnight. Sections were then rinsed with 1x PBS for 10 minutes. The second wash contained DAPI at 1mg/µL.

Single-cell RNA sequencing

Temporal bones were extracted and the spiral ganglion was microdissected from the cochlea in cold Leibovitz L-15 buffer. Cells were then treated with collagenase type IV followed by papain for 25 minutes each at 37°C. The cells were passed through ovomucoid as recommended for the Papain Dissociation System and then passed through a 40µm cell strainer. Dissociated cells

were resuspended in cold EBSS. Cell concentration was estimated by counting cells on a hemocytometer. Cells were then loaded into a single cell chip from 10x Genomics following manufacturer's recommendations. Datasets were processed with the Chromium single-cell 3' library and gel bead kit v3.1. cDNA libraries were generated according to the manufacturer's directions. The final libraries were sequenced on an Illumina NovaSeq SP.

Bioinformatics Analysis

Alignment

Raw reads were converted to fastq files using the cellranger pipeline from 10X Genomics v 3.0.1. Reads were then aligned to the mouse reference genome (mm10) in a Linux-based high performance computing cluster at Harvard Medical School.

Normalization

The aligned data was imported into R for statistical analysis and graphical representation. The library was normalized by fitting the gene counts to a regularized binomial regression function implemented by the scTransform package for Seurat using all default settings and regression on percent mitochondrial reads[66].

Clustering

Clustering was performed using the Seurat FindClusters command using 30 principle components. SGNs were identified by the expression of neuronal genes such as *Tubb3* and *Nefh*. Subtypes of SGNs were identified by the expression of subtype specific markers previously identified (*Calb2*, *Lypd1,* and *Runx1*).

Differential Gene Expression and Gene Ontology Analysis

Differential expression was tested using the FindAllMarkers command on the SCT assay and probing for significantly regulated genes between control and mutant SGNs from each genotype. Genes were considered differentially expressed in mutant SGNs if they were significantly changed ($P<0.05$) at a Log2Fold change greater than 0.25. Differentially expressed genes were subjected to Gene Ontology term enrichment analysis in PANTHER. All genes that

were classified into synaptic and neuronal gene ontology categories were used for subsequent subtype specific gene expression analysis.

Subtype gene expression analysis

Differential expression of synaptic and neuronal genes from Gene Ontology term enrichment analysis was tested using the FindAllMarkers command on the SCT assay and probing for significantly regulated genes between control and mutant SGNs by subtype. Genes were considered differentially expressed in mutant SGNs if they were significantly changed ($P<0.05$) at a Log2Fold change greater than 0.25. Many genes were changed by subtype but had similar log2fold changes across subtypes. To filter out genes that were similarly changed across the three subtypes, we calculated the range of the log2fold change across subtypes per gene. When we plotted the distribution of the range of the log fold changes per gene, we found a clear demarcation in the distribution around where the genes had a range in log2fold change around 0.15. We considered all genes that had a log2fold change range of >0.15 as differentially changed across subtypes. All genes that were significantly differentially regulated in one subtype were included in this analysis.

Statistics

Statistical analysis for histological quantification was done in Python. Normality of each distribution was tested using the Shapiro-Wilk test. If both groups showed a normal distribution, a parametric t-Test or ANOVA was used. Otherwise, the non-parametric Mann-Whitney Rank Sum or Kruskal-Wallis (KS) Test was applied. Statistical analysis for differentially expressed genes was done in R. Differential gene expression was tested using a Wilcoxon rank sum test with Bonferroni post-hoc correction.

CHAPTER FIVE

Concluding remarks

Neuronal and synaptic diversity is critical for encoding rich information about our environment. The ability to discriminate between diverse types of sensation is reflected in the existence of functionally and morphologically specialized sensory neurons and receptors. Sensory neuron diversification is coordinated by gene programs that endow sensory neurons with properties needed for robust encoding of the complex sensory environment. Spiral ganglion neurons (SGNs) functionally, molecularly, and synaptically diversify to encode complex sound information. I have provided insight into gene expression programs that jointly contribute to the tuning of synaptic and functional properties of SGNs for functional hearing. These data provide insight into an emerging model of combinatorial transcriptional regulation of SGN synaptic development (**Figure 5.1**).

SGN synaptic heterogeneity is required for encoding sound

Precise synaptic refinement is necessary for creating diverse, high-fidelity synapses with low temporal jitter that encode an enormous range of sound intensities and frequencies. SGN peripheral synapses with inner hair cells are made up of presynaptic ribbons directly apposed to postsynaptic glutamate receptors. Heterogeneity in SGN synaptic properties contributes to the diverse electrophysiological potential of each SGN and is crucial for the collective encoding of complex sound information (**Figure 1.2**)[16]. In the mature cochlea, SGNs segregate into three molecularly distinct subtypes (1A, 1B and 1C). Postnatally, each SGN subtype acquires exquisitely precise and heterogeneous synaptic properties, refined connections with inner hair cells, and expression of subtype-specific genes[6,47]. Presynaptic ribbons, calcium channels, postsynaptic receptors and postsynaptic densities are postnatally refined and aligned to create functional synapses[46,49]. Furthermore, spatial gradients of SGN subtype fibers, ribbon and GLUR punctum size emerge postnatally along the bottom of the inner hair cell and are maintained throughout maturity[13,27]. 1A neurons project onto the pillar side of the hair cell, while

1B and1C SGNs innervate the modiolar side (**Figure 1.2, Figure 1.3**)[6]. Little is known about the transcriptional events that coordinate the expression of distinct synaptic proteins in different SGN subtypes.

The transcription factors MAFB and CMAF are excellent candidates for understanding the transcriptional programs that contribute to diverse SGN synaptic properties. In cortical interneurons, both CMAF and MAFB have been shown to have opposing effects on interneuron excitability and synaptic development. CMAF knockout interneurons contain more excitatory postsynaptic puncta while MAFB knockout interneurons contain fewer[56]. Furthermore, CMAF regulates synaptic features in the somatosensory system[55]. MAFB directs post-synaptic differentiation in SGN peripheral synapses. The loss of MAFB results in fewer GLUR2 puncta and presynaptic ribbons as early as postnatal day 6[50]. However, not all synaptic puncta are diminished in MAFB mutants, implicating the involvement of other factors that contribute to the establishment and fine tuning of SGN synaptic properties. CMAF is expressed in SGNs and is identical in structure to MAFB in its DNA binding domain and transactivation domain (**Figure 1.4**). MAFB and CMAF have shared and unique dimerization partners which could result in shared and unique DNA binding sites and downstream target genes[52]. Whether CMAF and MAFB jointly regulate SGN synaptic properties is unknown. In this thesis, I demonstrate that CMAF and MAFB contribute in opposing, overlapping, and combinatorial ways to the establishment of peripheral SGN synaptic properties and gene expression (**Figure 5.1**).

Figure 5.1. Working model of CMAF and MAFB combinatorial regulation of SGN synaptic gene expression. CMAF and MAFB regulate distinct, overlapping, and emergent sets of synaptic genes in SGNs. Complementary expression patterns of CMAF and MAFB result in subtype-specific gene regulation. CMAF and MAFB have stronger influences on gene expression in 1A and 1B/1C SGNs respectively. CMAF represses expression of MAFB in 1A SGNs while MAFB promotes expression of CMAF in 1A SGNs, reinforcing complementary expression patterns. CMAF and MAFB separately, jointly, and synergistically regulate synaptic genes to establish SGN synaptic properties. Synapses in control, *cMaf*^{CKO} , *Mafb*^{CKO} and dKOs are schematized as hair cells with presynaptic ribbons (red) and postsynaptic GLUR2 puncta (green). Upstream determinants of SGN subtype identity also contribute to SGN properties and CMAF and MAFB expression patterns. Pillar to modiolar positional gradient of GLUR puncta sizes is represented for clarity but not present in all strains of mice. All strains of mice exhibit substantial variability of GLUR puncta sizes regardless of position.

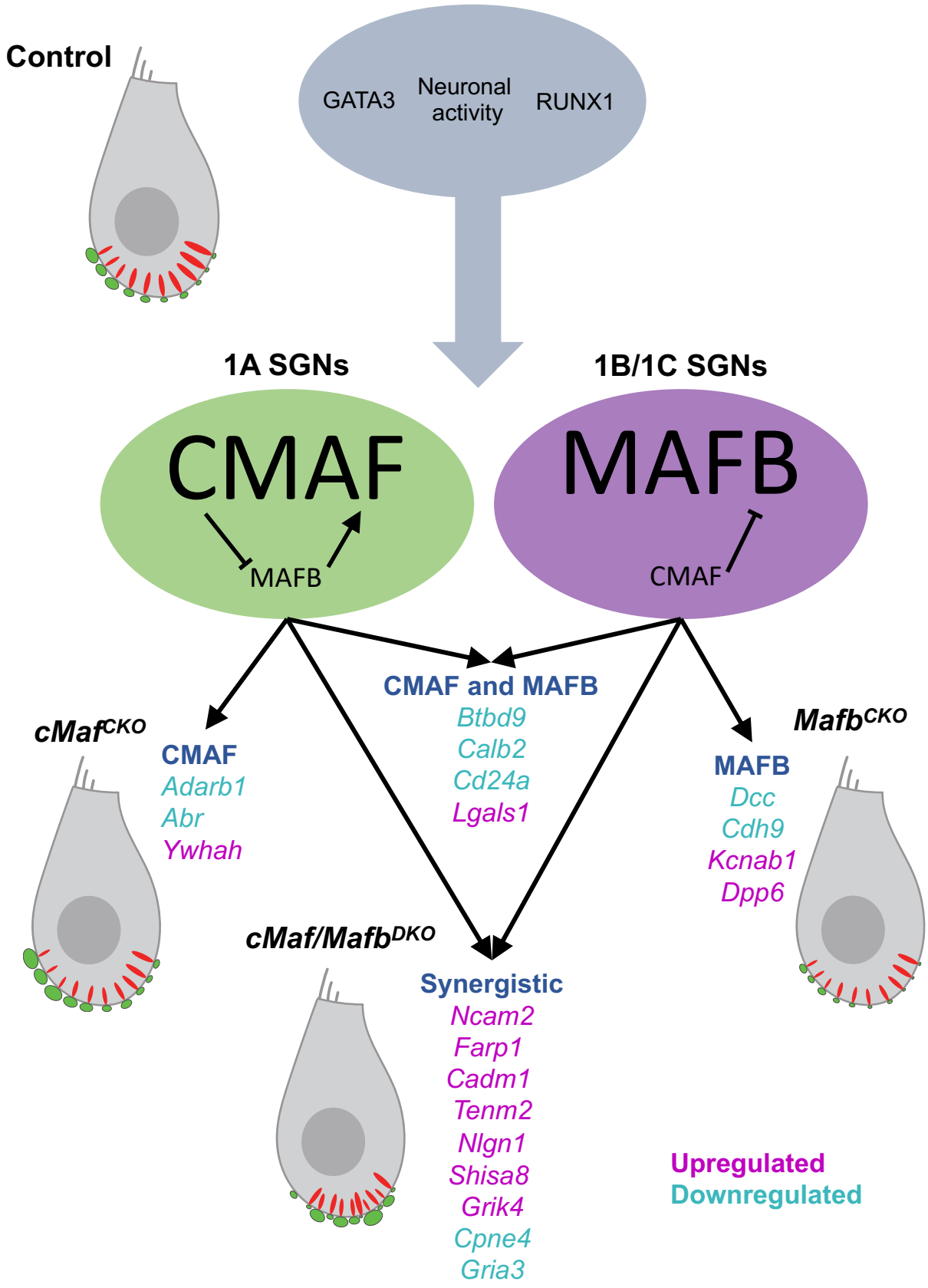
Control
GATA3
Neuronal activity
RUNX1
1A SGNs
1B/1C SGNs
CMAF
MAFB
MAFB
CMAF
CMAF and MAFB
Btbd9
Calb2
Cd24a
Lgals1
cMafCKO
CMAF
Adarb1
Abr
Ywhah
MafbCKO
MAFB
Dcc
Cdh9
Kcnab1
Dpp6
cMaf/MafbDKO
Synergistic
Ncam2
Farp1
Cadm1
Tenm2
Nlgn1
Shisa8
Grik4
Cpne4
Gria3
Upregulated
Downregulated

CMAF and MAFB have opposing and combinatorial effects on SGN peripheral synaptic properties and hearing function

The transcription factors CMAF and MAFB have opposing effects on SGN synaptic properties. These effects are reflected histologically and functionally. The loss of *cMaf* results in increases in GLUR2 puncta volume, while the loss of *Mafb* results in decreases in GLUR2 puncta volume compared to control animals (**Figure 2.3H-J,M-O,** schematized in **Figure 5.1**). Auditory responses were also affected in distinct and opposing ways in *cMaf* and *Mafb* mutants. *Mafb* mutants had elevated auditory brainstem response (ABR) thresholds compared to control animals while *cMaf* mutant ABR thresholds were unaltered (**Figure2.4E**). Peak 1 (P1) of an ABR recording corresponds to synchronous firing from SGNs[63]. *Mafb* mutants had significantly decreased peak 1 (P1) ABR amplitudes while *cMaf* mutants had slightly but insignificantly larger P1 ABR amplitudes (**Figure 2.5C,E**). Meanwhile, *cMaf/Mafb* double mutants had greatly exacerbated P1 amplitudes compared to either of the single mutants. The emergence of a distinct phenotype in the double mutant suggests that *cMaf* and *Mafb* synergistically contribute to auditory function. Overall, these distinct functional and synaptic phenotypes in *cMaf* and *Mafb* mutants argue that *cMaf* and *Mafb* either regulate distinct sets of synaptic genes and/or antagonistically regulate similar sets of synaptic genes.

CMAF and MAFB also have combinatorial effects on SGN synaptic properties and hearing function. Functional and synaptic phenotypes were exacerbated when both *cMaf* and *Mafb* were knocked out. *cMaf/Mafb* double mutants exhibited severe dysregulation in pre- and postsynaptic puncta spacing (**Figure 2.3L,Q,V**), and more GLUR2 orphans (**Figure 2.1F**) than controls and single mutants (schematized in **Figure 5.1**). Furthermore, double mutants had severely diminished P1 ABR amplitudes (**Figure 2.5C,E**), and elevated ABR thresholds (**Figure 2.4E**) compared to control and single knockout animals. Compounding synaptic and functional effects in the double mutants could be explained by additive or synergistic effects of CMAF and

MAFB on distinct sets of genes and/or by redundant regulation of genes that share dependency on both family members.

CMAF and MAFB have broad and subtype-specific effects on synaptic gene expression

To understand the molecular origin of the single and double mutant phenotypes, we assayed gene expression by single-cell RNA sequencing. Our results suggest that CMAF and MAFB act both in parallel and synergistically. Although the levels vary, CMAF and MAFB are expressed in all SGNs and regulate several genes in all subtypes. We found several genes that were differentially expressed when we compared pooled SGN subtypes between control and single mutant transcriptomes (**peach background, Figures 4.2B, 4.4B**). Some of these genes were differentially expressed in all three subtypes when comparing control to single or double mutants. To find which of these genes were regulated in a subtype-specific manner, we compared control and single mutant transcriptomes by subtype. This analysis revealed several genes that were regulated in a subtype-specific manner, with CMAF playing a dominant role in 1As and MAFB in the 1Bs and 1Cs (**black bar, Figures 4.2B, 4.4B; Figure 4.2C-F; Figure 4.4C-F; Figure 4.6C,D)**. Thus, the complementary expression patterns of CMAF and MAFB across SGN subtypes contribute to complementary subtype-specific synaptic gene regulation (summarized in **Figure 5.1**).

Subtype-differentially expressed genes in cMaf knockouts

Synaptic gene expression changes in *cMaf* knockouts were biased to 1A neurons, where *cMaf* is normally most expressed. A total of 23 genes related to synaptic function were changed in a subtype-specific manner in at least one subtype in *cMaf* knockout SGNs (**black bar, Figure 4.2B**). Of these, eighteen out of the 23 subtype-differentially expressed genes were changed in 1A SGNs, 10 out of 23 were changed in 1B SGNs, and 7 out of 23 were changed in 1C SGNs

compared to controls (**Figure 4.2C**). Furthermore, of the 9 genes that changed in multiple SGN subtypes in *cMaf* knockouts, 6 had larger log2fold changes in 1A SGNs than in 1B and 1C SGNs (**Figure 4.2D,E**). Of the remaining 14 genes that changed in only 1 subtype of *cMaf* knockout SGNs, 11 showed significant up- or downregulation only in 1A SGNs (**Figure 4.2F**).

Subtype-differentially expressed genes in Mafb knockouts

Just as *cMaf* mutants showed stronger gene expression changes in 1A SGNs, *Mafb* mutants showed strongest effects in 1B and 1C SGNs, where *Mafb* is normally most expressed (**Figure 3.1G,H,J; Figure 4.4C-F**). A total of 29 synapse-related genes changed in a subtype-specific manner in at least one subtype of *Mafb* knockout SGNs. Of the 29 genes that changed expression in a subtype-specific manner in *Mafb* mutant SGNs, more genes were significantly up- or downregulated in 1C SGNs (21 out of 29 genes) than 1B SGNs (13 out of 29 genes) or 1A SGNs (12 out of 29 genes) **(Figure 4.4C**). Eleven of the 13 that changed expression in multiple SGN subtypes in *Mafb* knockouts had larger log2fold changes in 1B and 1C SGNs than in 1A SGNs. These results demonstrate that CMAF and MAFB have complementary influence on synaptic gene expression across SGN subtypes, consistent with their complementary expression patterns.

CMAF and MAFB regulate distinct and overlapping sets of genes. We found that many genes changed expression in each single mutant, but not the other, compared to respective controls (**Figure 4.2B, Figure 4.4B**). CMAF and MAFB could have mutually exclusive DNA binding affinity for these genes, which could result in differential regulation. Some examples of these genes are *Adarb1* and *Dcc,* which are differentially expressed in *cMaf* and *Mafb* mutants respectively (**Figure 5.1**). At the same time, CMAF and MAFB regulate overlapping sets of genes. These genes were differentially expressed in both single knockout and double mutant

datasets (**Figure 4.2B, Figure 4.4B, Figure 4.6B**) and could have binding sites for both CMAF and MAFB in regulatory sequences. Some examples of these genes include *Btbd9, Calb2, Lgals2,* and *Cd24a* (**Figure 4.6B, Figure 5.1**). Most of these genes are more heavily reliant on one MAF factor over the other. For example, *Calb2* is primarily *cMaf* dependent, but *Mafb* seems to drive low level expression of *Calb2* on its own. Further experiments using techniques such as Cleavage Under Targets and Release Using Nuclease (CUT&RUN) could reveal overlapping and distinct DNA binding sites of CMAF and MAFB in SGNs.

Synergistic genetic contributions of CMAF and MAFB

CMAF and MAFB work together to regulate a large set of genes. Each *cMaf* and *Mafb* single-cell RNA sequencing dataset revealed 273 and 313 differentially expressed genes between control and mutant transcriptomes respectively. Double knockout SGNs had 1254 differentially expressed genes compared to control SGNs. This set of differentially expressed genes in double knockouts is larger than the sum of each single knockout set. Hundreds of genes changed expression only in the double knockouts providing evidence for the synergistic contributions of CMAF and MAFB to SGN gene expression.

Synergistic regulation by CMAF and MAFB contributes not only to synaptic development but also appears to be essential for SGN subtype diversification. Double mutant SGNs did not segregate or co-cluster with control SGN subtypes (**Figure 4.5A,B**) and formed one cluster that expressed 1B/1C marker genes and lacked expression of 1A marker genes (**Figure 4.5C**). These data indicate that the loss of both *cMaf* and *Mafb* causes defects in SGN subtype diversification. Emerging work is investigating gene transcription profiles in SGNs across embryonic and early postnatal development[64]. Further analysis could compare differentially expressed genes in double knockouts to gene expression in younger SGNs prior to subtype diversification. This analysis could provide insight into whether and how double knockout SGNs

are being prevented from diversifying and maturing. Altogether, these data indicate that distinct, overlapping, and synergistic gene expression changes could contribute to the varied synaptic phenotypes observed in *cMaf* and *Mafb* single and double mutants.

Genes downstream of CMAF and MAFB genes provide insight into synaptic and functional phenotypes

Rather than one causal gene, it is likely that groups of differentially expressed genes in the *cMaf* and *Mafb* single and double mutants encode proteins that contribute to the synaptic and functional phenotypes observed. *cMaf* knockouts had larger GLUR2 puncta (**Figure2.3 H-J,M-O**)**,** delayed P1 ABR latencies (**Figure 2.5D,F**) and had slightly, but statistically insignificant larger P1 ABR amplitudes than controls (**Figure 2.5C,E**). *cMaf* also had subtype-specific effects on SGN gene expression (**Figure 4.2C-F, Figure 4.6C**). Therefore, differentially regulated genes and proteins in *cMaf* knockouts involved in GLUR2 postsynaptic development, function, and plasticity could contribute to the synaptic and functional phenotypes that we observed.

Proteins involved in synaptic plasticity could result in abnormal synaptic scaling in *cMaf* knockouts. For example, the genes *Abr, Ywhah,* and *Adarb1* were differentially expressed in *cMaf* mutants compared to controls. All three of these genes encode proteins that are involved in mechanisms of developmental and adult postsynaptic plasticity. *Abr* and *Adarb1* were downregulated in *cMaf* knockouts while *Ywhah* was upregulated. *Abr* encodes the Active Breakpoint Cluster-Related protein, a RacGTPase known to be localized to hippocampal excitatory synapses and directly interact with the postsynaptic scaffolding protein PSD-95. Downregulation of the ABR protein results in an increase in RAC1, a Rho- GTPase known to cause increases in AMPAR clustering and in miniature excitatory postsynaptic currents (mEPSCs)[70,71]. Therefore, the downregulation of *Abr* in *cMaf* mutant 1A neurons could result in increases in RAC1 and subsequent increases in GLUR2 punctum size and EPSC amplitude.

Larger EPSCs could contribute to the increases in ABR (auditory brainstem response) P1 amplitude observed in *cMaf* mutants. Measurements of RAC1 in *cMaf* mutants as well as experiments assessing GLUR2 puncta volume in available and viable *Abr* knockout (MGI:107771) and/or *Rac1* conditional knockout (MGI:J:83457) mice could provide insight into the involvement of this pathway in SGN peripheral synaptic development and plasticity.

Downregulation of *Adarb1* in *cMaf* mutants could also contribute to synaptic and functional phenotypes. ADARB1 is an RNA editing enzyme known for the Q/R editing of GLUR2 AMPAR subunits, which render these subunits impermeable to calcium[33,34]. Downregulation of *Adarb1* could result in increased calcium permeability of AMPARs in *cMaf* mutants. Previous studies have shown that blockade of calcium permeable AMPARs protects SGNs from noise-induced excitotoxicity and cochlear synaptopathy[32]. In the brain, calcium influx is thought to mediate excitotoxic trauma. *cMaf* mutants have similar numbers of synapses as controls (**Figure 2.3E**), suggesting that downregulation of *Adarb1* and increases in calcium permeability in *cMaf* mutants are not causing cochlear synaptopathy. Alternatively, increased calcium permeability through AMPARs could result in increases in AMPAR receptor insertion into the postsynaptic membrane[72]. Furthermore, GLUR2 subunits that are unedited by ADARB1 show a slower recovery from desensitization and are not able to respond as rapidly to trains of impulses as channels with edited subunits[33,34]. Downregulation of *Adarb1* could thus result in clusters of glutamate receptors that are not able to respond as rapidly to sound input, contributing to the delayed P1 ABR latencies observed in *cMaf* mutants.

Meanwhile, *Ywhah* encodes the 14-3-3η protein which is a positive regulator of actin stabilization and insertion of NMDARs in postsynaptic membranes[73,74]. Upregulation of this protein could result in increased NMDAR-mediated plasticity in *cMaf* mutants that could also result in increases in AMPAR insertion into the SGN postsynaptic membrane. Increased AMPAR insertion could result in the larger GLUR2 punctum size observed in *cMaf* mutants. More work, including electrophysiological and calcium imaging experiments combined with

genetic perturbations of these genes, is needed to investigate the functional roles of these synaptic plasticity proteins at the IHC-SGN synapse.

Mafb regulated genes could contribute to the synaptic and functional dysregulation observed in *Mafb* mutants. *Mafb* knockouts had decreases in GLUR2 punctum volume (**Figure 2.3H-J,M-O**), decreases in P1 ABR amplitude (**Figure 2.5C,E**) and increases in P1 ABR latency (**Figure 2.5D,F**). *Mafb* also had subtype-specific effects on SGN gene expression (**Figure 4.4C-F, Figure 4.6D**). Therefore, genes that contribute to SGN synaptic formation likely contribute to *Mafb* mutant phenotypes.

The changes in gene expression in *Mafb* mutants point to additional synaptic phenotypes that we would have not detected using our methods. For example, it is difficult to capture developmental events by observing mature synapses. Distinct expression of cell surface adhesion and signaling molecules across SGN peripheral processes could promote discrete, local synaptic connection patterns during development. Therefore, different levels of adhesion and signaling molecules could contribute to the correct matching of each SGN subtype and presynaptic ribbon within different hair cell domains.

DCC could contribute to local miswiring in *Mafb* mutants. *Dcc* is differentially expressed across SGN subtypes in control animals (**Figure 4.6B**). *Dcc* was one of the most differentially downregulated genes in 1B and 1C *Mafb* mutant SGNs (**Figure 4.4E**). DCC is a transmembrane receptor for Netrin-1 and is involved in axon guidance[75]. DCC is also important for regulating the assembly of peripheral auditory circuits. Mice that are mutants for *Dcc* have reduced ribbon synapses and aberrant peripheral and central innervation patterns[76]. These studies were conducted in mice that had global deletion of *Dcc.* Therefore, the effect of SGN-restricted downregulation of *Dcc* is still unknown. We did not observe any changes to mature gross wiring in the cochlea of *Mafb* mutants (**Figure 2.1F,H**). However, it is possible that the decrease in *Dcc* expression in *Mafb* mutants results in local miswiring of SGN peripheral processes during development. Local miswiring could result in SGNs aberrantly targeting

different areas in the hair cell. SGN molecular subtypes segregate in the pillar to modiolar axis of the hair cell[6]. Perhaps local targeting modulated by DCC is required to establish the proper pattern of terminals. Thus, although our data demonstrate that *Mafb* mutant SGNs create similar numbers of synapses as controls (**Figure 2.3E**), the downregulation of *Dcc* could result in aberrations in proper pre- and postsynaptic pairing that ultimately results in reduced mature GLUR2 puncta volume and SGN function. Developmental assessment and direct labeling of SGN subtype fibers in *Mafb* mutants could reveal local miswiring patterns affected by DCC. Another intercellular adhesion molecule that could be involved in establishing proper GLUR2 puncta volume is CDH9. *Cdh9* is differentially expressed across SGN subtypes in control animals (**Figure 4.6B**). CDH9 regulates postsynaptic morphology and the formation of synapses[77]. Therefore, downregulation of *Cdh9* could also result in decreased GLUR2 puncta size.

Proteins that cause aberrant SGN firing properties could contribute to *Mafb* ABR deficits. The genes that encode several potassium channel subunits and auxiliary proteins such as DPP6 and KCNAB1 were significantly upregulated in *Mafb* mutant SGNs. In hippocampal neurons, DPP6 and KCNAB1 alter the kinetics of potassium channels, which alter action potential kinetics. KCNAB1 broadens the width of action potentials[78]. Meanwhile, DPP6 causes increases in A-Type K^+ currents and subsequent decreases in dendritic excitability[79]. Therefore, it is possible that increases of DPP6 and KCNAB1 in *Mafb* knockouts could result in reduced, temporally smeared action potentials that contribute to dysregulated synaptic development and dysfunctional ABRs.

The genes that CMAF and MAFB jointly regulate could provide insight into mechanisms of SGN synaptic differentiation. CMAF and MAFB work alone and together to establish proper postsynaptic volume (**Figure 2.3H-J, M-O**), distribution (**Figure 2.3L,Q**), and alignment (**Figure 2.2F, Figure 2.3F**) of peripheral SGN synapses. Additionally, *cMaf* and *Mafb* mutant SGNs do not cluster with control SGNs and also do not segregate into discrete subtype clusters (**Figure**

4.5A,B). Therefore, *cMaf* and *Mafb* could be working together to properly differentiate SGNs. *Cpne4* encodes Copine-4 (CPNE4), which is a calcium-dependent membrane binding protein. *Cpne* is drastically downregulated in *cMaf/Mafb* double mutant SGNs. This protein is known to be involved in neuronal and dendritic differentiation in the hippocampus and retina. Overexpression of CPNE4 in retinal ganglion cells results in cytoskeletal and dendritic morphology changes[80]. *Cpne* downregulation in *cMaf/Mafb* double mutant SGNs could be contributing to synaptic and dendritic differentiation in SGNs.

The mechanisms that determine SGN-IHC synaptic properties have long been postulated to be primarily dictated by presynaptic input from hair cell ribbons[60]. However, emerging evidence is revealing that pre- and postsynaptic development, refinement, and maintenance is orchestrated by the interplay of hair cell and SGN intrinsic genetic programs as well as spontaneous and evoked activity[6,45,61,82].

The phenotypes we have observed provide additional evidence of the postsynaptic influence on presynaptic properties. We have observed changes to presynaptic hair cell ribbon volume (**Figure 2.3R-T**) and spacing (**Figure 2.2K, Figure 2.3V**) in *cMaf* and *Mafb* mutants. The closely spaced pre- and postsynaptic puncta in CMAF/MAFB double knockouts suggest that synaptic spacing could be influenced by postsynaptic signals. Immature hair cells contain closely spaced ribbons that ultimately fuse to form single mature ribbons. Afferent fibers are found apposed to the inner hair cell before ribbons arrive at the basal surface of the hair cell. Postsynaptic densities develop independently of ribbons and eventually become tethered to ribbons through intercellular synaptic adhesion molecules[49]. *cMaf* and *Mafb* could be working together to differentiate SGN postsynaptic properties that send retrograde signals to hair cells.

Aberrations in postsynaptic development in *cMaf* and *Mafb* mutants could disrupt intercellular signaling mechanisms that independently impact synapse development. The differentially expressed genes in *cMaf/Mafb* double knockout animals in this study offer a starting point for investigating possible postsynaptic molecules that contribute to synaptic

patterning and maturation. Candidate molecules include retrograde synaptic signaling and intercellular adhesion molecules. *cMaf/Mafb* double mutant animals had several differentially regulated genes that fit these gene ontology categories, including *Farp1, Cadm1, Tenm2,* and *Nlgn1* (**Figure 4.6B, Figure 5.1, Table S4.7**). All of these genes encode proteins that are expressed at postsynaptic membranes and promote synaptic adhesion with presynaptic membranes. In fact, NLGN1 is a postsynaptic adhesion molecule known to be important for cochlear ribbon synapse formation[81]. How these molecules function together and separately to modulate intercellular signals that promote SGN synaptic differentiation remains to be explored.

To our knowledge, this is the first identification of combinatorial transcriptional regulation of genes that control synaptic differentiation in SGNs (**Figure 5.1**). Although many questions about the mechanisms of SGN synaptic diversification and functional tuning remain unanswered, the data here provide a stepping stone for future investigation.

Broadened understandings of transcriptional mechanisms of SGN synaptic differentiation

Previous work has established an important role for neuronal activity in diversifying SGN subtypes consistent with the well-established effects of spontaneous and experience-dependent activity on neural circuit assembly. One possibility is that CMAF and MAFB act as conduits between incoming activity and synaptic refinement. Neuronal activity stimulates the expression of immediate early genes (IEGs) such as cFOS and cJUN. The expression of IEGs go on to induce a second wave of transcription, the products of which encode proteins that are localized to or act at synapses[83,84]. Both CMAF and MAFB can dimerize with cFOS, while only MAFB can dimerize with cJUN. CMAF and MAFB can also heterodimerize with each other and homodimerize with themselves[52]. This ability for homo- and heterodimerization provides a basis for combinatorial and synergistic control of gene expression[51]. Additionally, the ability to dimerize with neuronal IEGs

provides an additional axis of genetic regulation that integrates neuronal activity to dictate SGN gene expression.

Dimerization could be a potential mechanism by which CMAF and MAFB affect overlapping and distinct genes. The precise combinations of dimers and the extent of dimerization can have different transcriptional outcomes[53]. It has been shown that mutations that force MAFB to only form homodimers result in binding of symmetrical MAF recognition element (MARE) DNA binding sites (**Figure 1.4**). Meanwhile, MAFB mutants that could only form heterodimers with cFOS had entirely different DNA binding preferences[54].

The extent of hetero- and homodimerization between these transcription factors could depend on the relative stoichiometries and binding preferences of available dimerization partners. The complementary expression patterns of *cMaf* and *Mafb* results in different stoichiometries of CMAF and MAFB across SGN subtypes that could result in differing amounts of hetero- and homodimers and nuanced mechanisms of genetic control. Further work assessing protein-protein interactions in SGNs is needed to investigate the extent of CMAF, MAFB, and IEG dimerization in the cochlea.

Considering the distinct and combinatorial contributions that *cMaf* and *Mafb* have on SGN synaptic properties, this data is a valuable resource for dissecting the mechanisms of SGN synaptic differentiation and maintenance. Although significant insights into SGN synaptic function have been made studying mouse models of SGN synaptic loss and degeneration, *cMaf* and *Mafb* mutants offer a model to study the specific synaptic properties without reducing overall synaptic number or drastically changing the wiring of the cochlea. Furthermore, the diverse functional hearing defects observed in *cMaf* and *Mafb* mutants provide insight into SGN genetic programs and synaptic properties that contribute to the functional encoding of sound. To our knowledge, this is the first identification of combinatorial transcriptional regulation of genes that control synaptic differentiation in SGNs. Thus, SGNs provide a tractable system to study the combinatorial transcriptional regulation that results in neuronal and synaptic differentiation.

APPENDIX

Table S2.3. Pairwise Post-hoc Dunn P-values for panels in Figure 2.3 with Kruskal-Wallis P<0.05.

Figure Panel							
2.3F	GluR2 Orphans per Hair cell			**DKO**	**CMAF**	**NOCRE**	**MAFB**
			DKO	1	0.125752	0.000191	0.026028
			CMAF	0.125752	1	0.05631	0.334863
			NOCRE	0.000191	0.05631	1	0.626938
			MAFB	0.026028	0.334863	0.626938	1
2.3H	8 kHz GLUR2 Puncta Volume			**DKO**	**CMAF**	**NOCRE**	**MAFB**
			DKO	1.00E+00	7.17E-07	1.24E-02	1.00E+00
			CMAF	7.17E-07	1.00E+00	6.79E-17	3.26E-07
			NOCRE	1.24E-02	6.79E-17	1.00E+00	6.92E-01
			MAFB	1.00E+00	3.26E-07	6.92E-01	1.00E+00
2.3J	8kHz Median GLUR2 Puncta Volume			**DKO**	**CMAF**	**NOCRE**	**MAFB**
			DKO	1	1	1	0.275712
			CMAF	1	1	0.409435	0.036005
			NOCRE	1	0.409435	1	1
			MAFB	0.275712	0.036005	1	1
2.3K	8kHz GLUR2 Interquartile Range			**MAFB**	**NOCRE**	**CMAF**	**DKO**
			MAFB	1	0.292191	1	1

			NOCRE	0.292191	1	0.009681	0.001346
			CMAF	1	0.009681	1	1
			DKO	1	0.001346	1	1
2.3L	8kHz GLUR2 Interpunctum Distance			**MAFB**	**NOCRE**	**CMAF**	**DKO**
			MAFB	1	1	1	0.500343
			NOCRE	1	1	1	0.000422
			CMAF	1	1	1	0.140996
			DKO	0.500343	0.000422	0.140996	1
2.3M	16 kHz GLUR2 Puncta Volume			**MAFB**	**NoCRE**	**CMAF**	**DKO**
			MAFB	1.00E+00	1.93E-35	1.38E-79	3.77E-44
			NoCRE	1.93E-35	1.00E+00	1.64E-20	3.03E-03
			CMAF	1.38E-79	1.64E-20	1.00E+00	4.54E-09
			DKO	3.77E-44	3.03E-03	4.54E-09	1.00E+00
2.3N	16kHz Median GLUR2 Patch Volume			**MAFB**	**NoCRE**	**CMAF**	**DKO**
			MAFB	1	0.070387	0.000531	0.003535
			NoCRE	0.070387	1	0.035824	0.16006
			CMAF	0.000531	0.035824	1	0.462424
			DKO	0.003535	0.16006	0.462424	1
2.3P	16kHz GLUR2 Interquartile Range			**MAFB**	**NoCRE**	**CMAF**	**DKO**
			MAFB	1	0.000871	0.881005	0.698225
			NoCRE	0.000871	1	0.001575	0.001811

			CMAF	0.881005	0.001575	1	0.818149
			DKO	0.698225	0.001811	0.818149	1
2.3Q	16kHz GLUR2 interpunctum distance			**MAFB**	**NoCRE**	**CMAF**	**DKO**
			MAFB	1	0.070387	0.018655	0.055359
			NoCRE	0.070387	1	0.39845	0.000036
			CMAF	0.018655	0.39845	1	0.000011
			DKO	0.055359	0.000036	0.000011	1
2.3R	Ribbon Volume			**DKO**	**NOCRE**	**CMAF**	**MAFB**
			DKO	1.00E+00	4.29E-59	4.48E-12	1.00E+00
			NOCRE	4.29E-59	1.00E+00	7.78E-16	2.08E-40
			CMAF	4.48E-12	7.78E-16	1.00E+00	1.66E-10
			MAFB	1.00E+00	2.08E-40	1.66E-10	1.00E+00
2.3T	Median Ribbon Volume			**DKO**	**NOCRE**	**CMAF**	**MAFB**
			DKO	1.00E+00	7.16E-60	7.47E-13	2.46E-01
			NOCRE	7.16E-60	1.00E+00	1.30E-16	3.46E-41
			CMAF	7.47E-13	1.30E-16	1.00E+00	2.76E-11
			MAFB	2.46E-01	3.46E-41	2.76E-11	1.00E+00
2.3V	Ribbon Interpunctum distance			**MAFB**	**NoCRE**	**CMAF**	**DKO**
			MAFB	1	0.02658	0.259578	0.281102
			NoCRE	0.02658	1	0.196169	0.000007

			CMAF	0.259578	0.196169	1	0.005114
			DKO	0.281102	0.000007	0.005114	1

Table S2.4. Pairwise post-hoc Dunn p-values for ABR thresholds in Figure 2.4 with Kruskal-Wallis P<0.05.

ABR Threshold_8kHz		**NOCRE**	**dKO**	**CMAFCKO**	**MAFBCKO**
	NOCRE	1	0.000086	0.528062	0.190049
	dKO	0.000086	1	0.000443	0.010009
	CMAFCKO	0.528062	0.000443	1	0.12175
	MAFBCKO	0.190049	0.010009	0.12175	1
ABR Threshold_16kHz		**NOCRE**	**dKO**	**CMAFCKO**	**MAFBCKO**
	NOCRE	1	0.000113	0.253636	0.020981
	dKO	0.000113	1	0.000185	0.099143
	CMAFCKO	0.253636	0.000185	1	0.008485
	MAFBCKO	0.020981	0.099143	0.008485	1

Table S2.5. Pairwise post-hoc Dunn p-values for ABR thresholds in Figure 2.5 with Kruskal-Wallis P<0.05.

Comparison	**Kruskal-Wallis p-value**	**Pair-wise post-hoc Dunn**				
8kHz_90_P1Amp	7.57E-05		**NOCRE**	**dKO**	**CMAFCKO**	**MAFBCKO**
		NOCRE	1	0.000076	0.32956	0.187395

		dKO	0.00007 6	1	0.000065	0.008933
		CMAFCK O	0.32956	0.000065	1	0.050865
		MAFBCK O	0.18739 5	0.008933	0.050865	1
8kHz_85_P1Amp	1.11E-04		**NOCRE**	**dKO**	**CMAFCKO**	**MAFBCKO**
		NOCRE	1	0.000095	0.356363	0.235574
		dKO	0.00009 5	1	0.000094	0.007247
		CMAFCK O	0.35636 3	0.000094	1	0.071735
		MAFBCK O	0.23557 4	0.007247	0.071735	1
8kHz_80_P1Amp	1.01E-04		**NOCRE**	**dKO**	**CMAFCKO**	**MAFBCKO**
		NOCRE	1	0.000042	0.51354	0.184382
		dKO	0.00004 2	1	0.000179	0.006893
		CMAFCK O	0.51354	0.000179	1	0.104662
		MAFBCK O	0.18438 2	0.006893	0.104662	1

8kHz_75_P1Amp	9.45E-05		**NOCRE**	**dKO**	**CMAFCKO**	**MAFBCKO**
		NOCRE	1	0.000034	0.575791	0.132496
		dKO	0.000034	1	0.000217	0.009548
		CMAFCKO	0.575791	0.000217	1	0.096063
		MAFBCKO	0.132496	0.009548	0.096063	1
8kHz_70_P1Amp	1.15E-04		**NOCRE**	**dKO**	**CMAFCKO**	**MAFBCKO**
		NOCRE	1	0.000214	0.181282	0.306813
		dKO	0.000214	1	0.000044	0.009255
		CMAFCKO	0.181282	0.000044	1	0.039909
		MAFBCKO	0.306813	0.009255	0.039909	1
8kHz_65_P1Amp	1.08E-04		**NOCRE**	**dKO**	**CMAFCKO**	**MAFBCKO**
		NOCRE	1	0.000121	0.262228	0.319316
		dKO	0.000121	1	0.000066	0.00577
		CMAFCKO	0.262228	0.000066	1	0.067718

		MAFBCKO	0.319316	0.00577	0.067718	1
8kHz_60_P1Amp	2.36E-05		**NOCRE**	**dKO**	**CMAFCKO**	**MAFBCKO**
		NOCRE	1	0.000041	0.223316	0.143964
		dKO	0.000041	1	0.000019	0.009658
		CMAFCKO	0.223316	0.000019	1	0.023341
		MAFBCKO	0.143964	0.009658	0.023341	1
8kHz_55_P1Amp	6.86E-04		**NOCRE**	**dKO**	**CMAFCKO**	**MAFBCKO**
		NOCRE	1	0.000657	0.301055	0.136722
		dKO	0.000657	1	0.00035	0.056862
		CMAFCKO	0.301055	0.00035	1	0.034807
		MAFBCKO	0.136722	0.056862	0.034807	1
8kHz_50_P1Amp	0.003		**NOCRE**	**dKO**	**CMAFCKO**	**MAFBCKO**
		NOCRE	1	0.001043	0.490605	0.227433
		dKO	0.001043	1	0.001603	0.04188

		CMAFCKO	0.490605	0.001603	1	0.116994
		MAFBCKO	0.227433	0.04188	0.116994	1
8kHz_45_P1Amp	4.45E-04		**NOCRE**	**dKO**	**CMAFCKO**	**MAFBCKO**
		NOCRE	1	0.000128	0.623694	0.25547
		dKO	0.000128	1	0.000692	0.008739
		CMAFCKO	0.623694	0.000692	1	0.185705
		MAFBCKO	0.25547	0.008739	0.185705	1
8kHz_40_P1Amp	0.333					
8kHz_35_P1Amp	0.565					
8kHz_30_P1Amp	0.173					
8kHz_25_P1Amp	0.495					
8kHz_20_P1Amp	0.201					
16kHz_90_P1Amp	3.47E-05		**NOCRE**	**dKO**	**CMAFCKO**	**MAFBCKO**
		NOCRE	1	0.000014	0.518054	0.057026
		dKO	0.000014	1	0.000213	0.01513

		CMAFCKO	0.518054	0.000213	1	0.052272
		MAFBCKO	0.057026	0.01513	0.052272	1
16kHz_85_P1Amp	4.65E-05		**NOCRE**	**dKO**	**CMAFCKO**	**MAFBCKO**
		NOCRE	1	0.000017	0.576526	0.041912
		dKO	0.000017	1	0.000333	0.023241
		CMAFCKO	0.576526	0.000333	1	0.051638
		MAFBCKO	0.041912	0.023241	0.051638	1
16kHz_80_P1Amp	4.11E-05		**NOCRE**	**dKO**	**CMAFCKO**	**MAFBCKO**
		NOCRE	1	0.000022	0.478381	0.034824
		dKO	0.000022	1	0.000227	0.032063
		CMAFCKO	0.478381	0.000227	1	0.031979
		MAFBCKO	0.034824	0.032063	0.031979	1
16kHz_75_P1Amp	3.19E-05		**NOCRE**	**dKO**	**CMAFCKO**	**MAFBCKO**
		NOCRE	1	0.00001	0.615771	0.046859

		dKO	0.00001	1	0.000297	0.015411
		CMAFCKO	0.615771	0.000297	1	0.063047
		MAFBCKO	0.046859	0.015411	0.063047	1
16kHz_70_P1Amp	3.07E-05		**NOCRE**	**dKO**	**CMAFCKO**	**MAFBCKO**
		NOCRE	1	0.000011	0.578442	0.038789
		dKO	0.000011	1	0.000263	0.020061
		CMAFCKO	0.578442	0.000263	1	0.049355
		MAFBCKO	0.038789	0.020061	0.049355	1
16kHz_65_P1Amp	1.16E-04		**NOCRE**	**dKO**	**CMAFCKO**	**MAFBCKO**
		NOCRE	1	0.000039	0.578358	0.05427
		dKO	0.000039	1	0.000561	0.028807
		CMAFCKO	0.578358	0.000561	1	0.061787
		MAFBCKO	0.05427	0.028807	0.061787	1

16kHz_60_P1Amp	1.20E-04		**NOCRE**	**dKO**	**CMAFCKO**	**MAFBCKO**
		NOCRE	1	0.000107	0.401171	0.0243
		dKO	0.000107	1	0.00039	0.096218
		CMAFCKO	0.401171	0.00039	1	0.017814
		MAFBCKO	0.0243	0.096218	0.017814	1
16kHz_55_P1Amp	1.66E-04		**NOCRE**	**dKO**	**CMAFCKO**	**MAFBCKO**
		NOCRE	1	0.000097	0.431925	0.047036
		dKO	0.000097	1	0.000444	0.054336
		CMAFCKO	0.431925	0.000444	1	0.032878
		MAFBCKO	0.047036	0.054336	0.032878	1
16kHz_50_P1Amp	9.15E-05		**NOCRE**	**dKO**	**CMAFCKO**	**MAFBCKO**
		NOCRE	1	0.000049	0.401119	0.088387
		dKO	0.000049	1	0.000233	0.019619
		CMAFCKO	0.401119	0.000233	1	0.046467

		MAFBCKO	0.088387	0.019619	0.046467	1
16kHz_45_P1Amp	5.94E-04		**NOCRE**	**dKO**	**CMAFCKO**	**MAFBCKO**
		NOCRE	1	0.001379	0.164276	0.071941
		dKO	0.001379	1	0.000335	0.153351
		CMAFCKO	0.164276	0.000335	1	0.009534
		MAFBCKO	0.071941	0.153351	0.009534	1
16kHz_40_P1Amp	4.98E-04		**NOCRE**	**dKO**	**CMAFCKO**	**MAFBCKO**
		NOCRE	1	0.000566	0.304073	0.044838
		dKO	0.000566	1	0.000624	0.139207
		CMAFCKO	0.304073	0.000624	1	0.017203
		MAFBCKO	0.044838	0.139207	0.017203	1
16kHz_35_P1Amp	0.002		**NOCRE**	**dKO**	**CMAFCKO**	**MAFBCKO**
		NOCRE	1	0.000824	0.545277	0.035636
		dKO	0.000824	1	0.003193	0.195076

		CMAFCKO	0.545277	0.003193	1	0.041632
		MAFBCKO	0.035636	0.195076	0.041632	1
16kHz_30_P1Amp	0.006		**NOCRE**	**dKO**	**CMAFCKO**	**MAFBCKO**
		NOCRE	1	0.004587	0.229654	0.469733
		dKO	0.004587	1	0.00164	0.040707
		CMAFCKO	0.229654	0.00164	1	0.095856
		MAFBCKO	0.469733	0.040707	0.095856	1
16kHz_25_P1Amp	0.147					
16kHz_20_P1Amp	0.813					
8_90_P1Lat	0.002		**NOCRE**	**CMAFCKO**	**MAFBCKO**	
		NOCRE	1	0.161979	0.000405	
		CMAFCKO	0.161979	1	0.186154	
		MAFBCKO	0.000405	0.186154	1	

8_85_P1Lat	0.001		**NOCRE**	**CMAFCKO**	**MAFBCKO**	
		NOCRE	1	0.096574	0.000252	
		CMAFCKO	0.096574	1	0.246514	
		MAFBCKO	0.000252	0.246514	1	
8_80_P1Lat	0.004		**NOCRE**	**CMAFCKO**	**MAFBCKO**	
		NOCRE	1	0.157931	0.000995	
		CMAFCKO	0.157931	1	0.273443	
		MAFBCKO	0.000995	0.273443	1	
8_75_P1Lat	0.004		**NOCRE**	**CMAFCKO**	**MAFBCKO**	
		NOCRE	1	0.549463	0.000918	
		CMAFCKO	0.549463	1	0.057729	
		MAFBCKO	0.000918	0.057729	1	
8_70_P1Lat	0.007		**NOCRE**	**CMAFCKO**	**MAFBCKO**	
		NOCRE	1	0.206899	0.001546	

		CMAFCKO	0.206899	1	0.251854	
		MAFBCKO	0.001546	0.251854	1	
8_65_P1Lat	0.049		**NOCRE**	**CMAFCKO**	**MAFBCKO**	
		NOCRE	1	0.196813	0.016501	
		CMAFCKO	0.196813	1	0.586197	
		MAFBCKO	0.016501	0.586197	1	
8kHz_60_P1Lat	0.098					
8kHz_55_P1Lat	0.085					
8kHz_50_P1Lat	0.201					
8kHz_45_P1Lat	0.058					
8kHz_40_P1Lat	0.112					
8kHz_35_P1Lat	0.651					
8kHz_30_P1Lat	0.382					
8kHz_25_P1Lat	0.358					
8kHz_20_P1Lat	0.14					
16kHz_90_P1Lat	2.29E-04		**NOCRE**	**CMAFCKO**	**MAFBCKO**	
		NOCRE	1	0.101105	0.000046	

		CMAFCKO	0.101105	1	0.221992	
		MAFBCKO	0.000046	0.221992	1	
16kHz_85_P1lat	0.001		**NOCRE**	**CMAFCKO**	**MAFBCKO**	
		NOCRE	1	0.02357	0.000559	
		CMAFCKO	0.02357	1	0.85505	
		MAFBCKO	0.000559	0.85505	1	
16kHz_80_P1Lat	0.002		**NOCRE**	**CMAFCKO**	**MAFBCKO**	
		NOCRE	1	0.032732	0.000659	
		CMAFCKO	0.032732	1	0.781838	
		MAFBCKO	0.000659	0.781838	1	
16kHz_75_P1Lat	0.004		**NOCRE**	**CMAFCKO**	**MAFBCKO**	
		NOCRE	1	0.034074	0.002145	
		CMAFCKO	0.034074	1	0.951864	

		MAFBCKO	0.002145	0.951864	1	
16kHz_70_P1Lat	0.02		**NOCRE**	**CMAFCKO**	**MAFBCKO**	
		NOCRE	1	0.073684	0.00904	
		CMAFCKO	0.073684	1	0.948382	
		MAFBCKO	0.00904	0.948382	1	
16kHz_60_P1Lat	0.189					
16kHz_55_P1Lat	0.379					
16kHz_50_P1Lat	0.277					
16kHz_45_P1Lat	0.473					
16kHz_40_P1Lat	0.453					
16kHz_35_P1Lat	0.333					
16kHz_30_P1Lat	0.34					
16kHz_25_P1Lat	0.004					
16kHz_20_P1Lat	0.084					

Table S4.1. Differentially expressed genes in all *cMaf*^{CKO} mutant SGNs. Average log2 Fold from control. Bonferonni adjusted p-value, Wilcoxon rank sum

Gene	**avg_log2FC**	**p_val_adj**
Calb2	2.94760352	1.88E-99
Maf	0.85246135	9.89E-157

Rps19	0.68924953	3.37E-89
Ubb	0.56854326	3.36E-28
Cd24a	0.52414616	6.47E-30
mt-Atp6	0.4853265	2.66E-62
Mt2	0.47040673	3.80E-20
Plp1	0.41694275	1.16E-26
mt-Nd2	0.40202378	1.87E-45
Paqr4	0.38795274	2.09E-30
Rpl18a	0.38013726	3.58E-40
Rpl19	0.37343025	4.51E-30
Serf2	0.36634554	7.71E-35
Snrpn	0.36254897	4.39E-50
Cox7c	0.35972668	8.03E-32
Gpx4	0.35379326	3.45E-30
Rpl7	0.34485011	8.84E-41
Atp5g1	0.33971384	5.10E-34
Atp5l	0.33887864	1.97E-29
mt-Rnr1	0.33700887	6.17E-15
Mt1	0.31197975	6.72E-18
Rpl22l1	0.30661526	2.03E-19
mt-Nd5	0.30409503	1.07E-20
Gm8797	0.30345626	1.67E-23
Eef1a1	0.29936715	2.08E-15
Mrpl23-ps1	0.29346545	2.18E-25
Rasgrp2	0.29030831	1.74E-21

Comt	0.28891062	1.41E-25
Rps20	0.2875719	1.25E-26
Tmsb4x	0.2869126	4.96E-20
Acyp2	0.28538901	1.34E-19
mt-Atp8	0.27880579	5.72E-20
Rpl26	0.27411826	2.75E-13
Ndufa12	0.2724098	1.34E-22
Rpl36al	0.26657354	6.16E-24
Hspa8	0.26621263	2.81E-11
Rplp1	0.26432776	3.55E-25
Ctsb	0.2636792	7.52E-12
Paxbp1	0.26254534	8.88E-15
Gnas	0.2583368	1.36E-24
Lhfpl4	0.25732919	5.31E-17
Rpl36a	0.25355814	4.26E-21
Nefm	0.25141744	2.61E-16
Rps25	0.24996328	2.62E-13
Kif3c	0.24807928	3.49E-14
mt-Nd4	0.2386764	7.36E-22
Ccdc85b	0.23655478	4.58E-19
Ftl1	0.23448217	9.59E-09
Stac2	0.23383632	7.45E-13
Slc17a7	0.23162215	2.85E-12
Ndufs5	0.22927324	1.33E-11
Rps15a	0.22856772	3.06E-10

Chchd2	0.21993544	2.33E-21
mt-Co1	0.21789143	4.85E-08
Rpsa	0.21450298	4.41E-15
Abr	0.21398267	2.02E-12
Scrt1	0.21320947	1.21E-09
Selenow	0.21225341	2.15E-12
Gng3	0.21187419	1.30E-09
Rpl37	0.21082318	6.42E-08
Rps4x	0.20997152	2.65E-05
Tspan7	0.20815023	8.71E-08
Rps24-ps3	0.20814911	2.13E-14
Nefh	0.20802379	1.12E-19
Rps16	0.20745607	1.30E-12
Fth1	0.20648365	4.00E-12
Rps14	0.20346964	1.62E-09
Sparcl1	0.20221531	2.64E-20
Rps27a	0.20169195	2.75E-18
Rps3a3	0.2009356	3.26E-12
Adarb1	0.20048593	2.41E-08
Lancl1	0.19927951	9.29E-06
Fbxo40	0.19739736	4.08E-12
1110032F04Rik	0.19632718	1.25E-08
Fam32a	0.19573335	2.24E-13
Slc24a2	0.19514603	2.32E-07
Rpl28	0.19315362	1.01E-14

Rps15	0.19287924	9.92E-08
Jund	0.19280601	0.00073209
Rpl30	0.19212721	1.82E-10
Aes	0.19131846	1.32E-08
Lrrc49	0.19085677	2.42E-06
Cds1	0.19073092	1.91E-06
Mpc2	0.18918699	0.0009697
Ndufab1	0.18753124	4.55E-06
Emc10	0.18698941	5.74E-08
Eef1a2	0.18569639	5.72E-10
Gm10260	0.18484814	1.75E-08
Rpl24	0.18473436	8.42E-15
Ablim2	0.18472538	2.55E-07
Rpl18	0.18320912	8.28E-16
Rpl13	0.17963538	5.87E-13
Synm	0.17950835	3.81E-06
Isca1	0.17947096	4.25E-13
Susd4	0.17939804	1.19E-07
Myh7b	0.17708075	5.75E-17
Fam213b	0.1769907	2.72E-07
Phpt1	0.17657374	1.54E-07
Kcnc3	0.1764876	1.36E-08
Ndufb4	0.17507336	2.28E-13
Gm6977	0.17493729	4.72E-18
Dbi	0.17421337	0.02201119

Sema7a	0.17367758	2.61E-06
Pvalb	0.17266257	1.38E-10
Cox6a1	0.17256626	1.53E-05
Pdrg1	0.17255961	5.46E-08
Cox6c	0.16972134	6.19E-09
Gas5	0.16877566	0.00066516
Dstn	0.16702623	0.00037142
Dnajc15	0.16608191	1.25E-05
Rps17	0.16581207	1.37E-12
Gm43652	0.16252748	4.71E-11
Cxx1a	0.16122253	5.06E-05
Rplp0	0.15982634	0.00293335
Ndufb8	0.15940896	0.00780935
Gm1821	0.15845352	9.18E-14
Dst	0.15697993	0.00017939
Rpl27a	0.15689594	2.86E-06
Rpl36	0.15582158	3.40E-07
Kcnk1	0.15567874	0.00922943
Grcc10	0.1549417	1.21E-09
Ccdc155	0.15186582	1.84E-05
Hypk	0.15096809	2.34E-05
Iscu	0.15051625	0.00049406
Amph	0.1495594	0.00017358
Rpl14	0.1492125	0.00201318
Glrx3	0.14907593	1.23E-06

Eef1b2	0.14873809	0.00033466
Selenof	0.14794039	3.88E-05
Arl3	0.14446929	0.00188788
Rps3a1	0.14387106	0.00068764
Gm2830	0.1438061	0.00032937
Tma7	0.14314498	0.00914743
CT010467.1	0.14242941	1.53E-06
Fis1	0.14241577	0.00399451
AC153368.1	0.14208857	1.75E-10
Hspa12a	0.14133778	0.00295426
Fam103a1	0.14010546	1.27E-06
Ppip5k2	0.13814433	0.00040334
Map1a	0.13798792	4.74E-05
Ube2m	0.13791036	0.0056275
Plekha6	0.13785863	0.00240726
Eno1	0.13779669	0.02641957
Tesc	0.13703318	0.01389303
Dcp2	0.13526907	0.00024852
Endod1	0.13493943	0.038524
Pdp1	0.1327438	0.03221108
BC029722	0.1326189	0.01433357
Rps10	0.13252931	0.00528301
Chchd10	0.1308552	7.09E-05
Bola3	0.12976164	0.02586523
Cacnb3	0.12953782	0.00341667

Ndufs3	0.12869651	0.01938607
Ccdc124	0.12688337	0.00591314
Gm10039	0.12651762	0.03293262
Gpx6	0.12607813	1.50E-07
Snrpd2	0.12462765	0.00170666
Rpl3	0.12394107	2.85E-05
Rcan1	0.12183998	0.00068971
Lancl3	0.12069581	5.14E-07
Tpt1	0.12043524	0.00971564
Rps6	0.11546679	7.55E-05
Cox8a	0.11327893	3.45E-05
Dnajc13	0.11236337	0.00138059
Gm26917	0.11081282	0.0019046
Tmem108	0.11058447	0.00984427
Lmbr1	0.10972524	0.00018768
Psap	0.10847141	0.00140621
Dctn1	0.10806464	0.04134683
Pabpc1	0.10656812	0.01819388
Rpl31	0.1050949	0.00088563
Gm10925	0.10322523	0.00047523
Cd302	0.10047765	4.27E-06
Gm15543	-0.1002222	0.00041758
Olfm3	-0.1011941	2.90E-05
Myt1l	-0.1048815	0.03946843
Cplx1	-0.1060496	0.02005932

Mrps5	-0.1060783	0.04549104
Lgr5	-0.1081335	0.04732108
Fam133b	-0.1103531	0.0075775
B230334C09Rik	-0.1143681	0.00192633
Arxes2	-0.1145458	0.01826034
Ncoa7	-0.1176221	0.03840906
Zmynd8	-0.1184614	0.01010784
Efhd2	-0.1189329	0.00682422
Cpne6	-0.1190656	0.01775635
Fxyd3	-0.1203811	0.01306015
Cnr1	-0.1225277	0.02935242
Nsf	-0.122744	0.02051143
Atxn7l3b	-0.1270386	0.01306953
Pja2	-0.1272854	0.04304537
Plppr4	-0.1286903	0.03055068
Car12	-0.1293364	0.02729072
Mef2c	-0.1303867	0.00024609
St13	-0.136523	0.00760811
Mllt11	-0.1370598	0.00128341
Hsp90ab1	-0.137222	3.25E-06
A330076H08Rik	-0.1378523	1.16E-13
Padi2	-0.1381973	4.87E-08
Prdx1	-0.1383773	0.00012302
Eif3j2	-0.1384829	1.68E-10
Metap2	-0.1394292	0.00273669

Pgam1	-0.1400173	0.00210985
Map4	-0.1412669	0.02181703
Kif21a	-0.1415419	0.02657903
Ntrk3	-0.1424526	0.00472715
Flywch1	-0.1441779	0.00062892
Lsamp	-0.144813	0.01312515
Sec62	-0.1459079	0.01169256
Atp5b	-0.147123	2.23E-05
Atp6v1e1	-0.1506294	7.66E-05
Dnm3	-0.1528738	0.00101736
Ppargc1a	-0.1534562	0.0140763
Zfhx3	-0.157405	0.00049029
Eno2	-0.1594124	1.40E-06
Snrnp27	-0.1599948	1.58E-07
Ywhah	-0.1607409	9.58E-10
Col27a1	-0.1609745	2.08E-08
Hbb-bs	-0.1609778	1.52E-07
Nfia	-0.1611601	0.00012757
Sv2b	-0.1613755	0.00106621
Pln	-0.1613921	1.14E-15
Aldoc	-0.1627428	0.00057888
Pcsk2	-0.1634453	0.00029884
Map1b	-0.1636418	5.72E-10
Glo1	-0.1646498	1.05E-05
Camta1	-0.165278	6.20E-06

Nptn	-0.1657872	0.00030514
Akap12	-0.1660525	1.49E-05
Elavl2	-0.1662419	0.00148458
Sv2c	-0.1671223	0.00026692
Nrxn2	-0.1701542	1.65E-05
Nmt1	-0.1719924	1.63E-10
Chst2	-0.1737217	0.00035746
Cacnb4	-0.1738594	3.58E-06
Ptma	-0.1769854	1.45E-06
Grm7	-0.1779712	8.09E-11
Ttn	-0.1785793	1.16E-10
Arl6ip1	-0.1786997	3.52E-07
Gm14303	-0.180398	1.13E-11
App	-0.1821137	1.66E-06
Dpysl2	-0.1844654	2.68E-05
Nrxn3	-0.1887218	1.12E-20
Snhg14	-0.1939869	3.72E-06
Ttll7	-0.1968783	7.80E-10
Sh3gl2	-0.197366	9.66E-08
Son	-0.1976133	3.98E-08
Rpl38	-0.2027795	1.32E-08
Cpe	-0.2030387	3.36E-11
Slc38a1	-0.2032377	5.30E-08
Ddah1	-0.2048738	9.51E-07
Cpne9	-0.2052132	2.04E-08

Pura	-0.2055723	1.37E-09
Cadm1	-0.2077186	2.97E-10
Ckmt1	-0.208506	1.17E-05
Calm2	-0.2099708	4.03E-15
Dync1i2	-0.2101624	3.99E-10
Arglu1	-0.2170501	5.34E-10
2900097C17Rik	-0.2238165	2.28E-13
Actb	-0.2361901	1.18E-12
Foxp1	-0.237153	4.00E-12
Efr3a	-0.2400122	7.48E-14
tdTomato	-0.249731	1.29E-11
Uchl1	-0.2659589	3.47E-20
Rph3a	-0.2738312	1.60E-18
Rps29	-0.2769363	1.56E-18
Lgals1	-0.2943851	1.11E-14
Sncg	-0.3723942	7.38E-27
AC121965.1	-0.3851098	5.86E-38
Mafb	-0.3896065	7.93E-36
Atp5k	-0.4186481	6.82E-57
Ptgds	-0.4417233	7.75E-09
Malat1	-0.7627916	5.71E-71

Table S4.2. Gene ontology results from all differentially expressed genes in *cMaf*^{CKO} SGNs

GO process	Mus musculus - REFLIST (21997)	N cMaf genes	Expected Proportion	Fold Enrichment	False Discovery Rate
neuron cellular homeostasis (GO:0070050)	43	6	0.48	12.43	2.35E-03
presynaptic endocytosis (GO:0140238)	59	6	0.66	9.06	9.84E-03
synaptic vesicle endocytosis (GO:0048488)	59	6	0.66	9.06	9.77E-03
axo-dendritic transport (GO:0008088)	79	8	0.89	9.02	9.11E-04
mitochondrial respiratory chain complex assembly (GO:0033108)	93	9	1.04	8.62	3.84E-04
postsynaptic density organization (GO:0097106)	20	4	0.22	17.81	1.40E-02
postsynaptic specialization organization (GO:0099084)	22	4	0.25	16.19	1.83E-02
nucleoside triphosphate metabolic process (GO:0009141)	210	20	2.36	8.48	8.68E-10
purine ribonucleotide biosynthetic process (GO:0009152)	172	16	1.93	8.28	1.64E-07
purine nucleotide biosynthetic process (GO:0006164)	181	16	2.03	7.87	3.09E-07
synaptic vesicle recycling (GO:0036465)	68	6	0.76	7.86	1.76E-02
ribosomal large subunit biogenesis (GO:0042273)	68	6	0.76	7.86	1.75E-02
peptide metabolic process (GO:0006518)	524	46	5.88	7.82	1.15E-22
ribonucleotide biosynthetic process (GO:0009260)	184	16	2.07	7.74	3.66E-07
purine-containing compound biosynthetic process (GO:0072522)	189	16	2.12	7.54	5.00E-07
amide biosynthetic process (GO:0043604)	485	41	5.45	7.53	1.81E-19
ribose phosphate biosynthetic process (GO:0046390)	193	16	2.17	7.38	6.31E-07
energy derivation by oxidation of organic compounds (GO:0015980)	245	20	2.75	7.27	9.54E-09
transport along microtubule (GO:0010970)	167	12	1.88	6.4	1.71E-04
generation of precursor metabolites and energy (GO:0006091)	338	24	3.8	6.32	1.47E-09
neuron projection extension (GO:1990138)	85	6	0.95	6.29	4.51E-02

nucleotide biosynthetic process (GO:0009165)	228	16	2.56	6.25	5.10E-06
postsynapse organization (GO:0099173)	102	7	1.15	6.11	2.12E-02
nucleoside phosphate biosynthetic process (GO:1901293)	234	16	2.63	6.09	6.64E-06
cellular transition metal ion homeostasis (GO:0046916)	105	7	1.18	5.94	2.46E-02
ribonucleoprotein complex assembly (GO:0022618)	166	11	1.86	5.9	8.20E-04
ribonucleoprotein complex subunit organization (GO:0071826)	174	11	1.95	5.63	1.13E-03
cell growth (GO:0016049)	127	8	1.43	5.61	1.42E-02
cellular amide metabolic process (GO:0043603)	767	48	8.61	5.57	3.00E-18
purine ribonucleotide metabolic process (GO:0009150)	356	22	4	5.5	1.34E-07
cytoskeleton-dependent intracellular transport (GO:0030705)	199	12	2.23	5.37	7.68E-04
synaptic vesicle cycle (GO:0099504)	133	8	1.49	5.36	1.82E-02
purine nucleotide metabolic process (GO:0006163)	371	22	4.17	5.28	2.63E-07
ribonucleotide metabolic process (GO:0009259)	376	22	4.22	5.21	3.15E-07
developmental cell growth (GO:0048588)	121	7	1.36	5.15	4.82E-02
microtubule-based transport (GO:0099111)	208	12	2.34	5.14	1.07E-03
synapse organization (GO:0050808)	315	18	3.54	5.09	1.09E-05
ribose phosphate metabolic process (GO:0019693)	387	22	4.35	5.06	4.98E-07
cellular macromolecule biosynthetic process (GO:0034645)	725	41	8.14	5.04	8.85E-14
memory (GO:0007613)	160	9	1.8	5.01	1.29E-02
neuromuscular process (GO:0050905)	179	10	2.01	4.98	6.80E-03
purine-containing compound metabolic process (GO:0072521)	404	22	4.54	4.85	9.60E-07
vesicle-mediated transport in synapse (GO:0099003)	147	8	1.65	4.85	3.11E-02
developmental growth involved in morphogenesis (GO:0060560)	153	8	1.72	4.66	3.90E-02
axon development (GO:0061564)	419	21	4.7	4.46	7.17E-06
ribosome biogenesis (GO:0042254)	286	14	3.21	4.36	1.11E-03
learning (GO:0007612)	186	9	2.09	4.31	3.11E-02
rRNA processing (GO:0006364)	207	10	2.32	4.3	1.69E-02
cognition (GO:0050890)	356	17	4	4.25	2.00E-04

organonitrogen compound biosynthetic process (GO:1901566)	1218	58	13.68	4.24	2.72E-17
learning or memory (GO:0007611)	319	15	3.58	4.19	8.93E-04
axonogenesis (GO:0007409)	384	18	4.31	4.17	1.43E-04
trans-synaptic signaling (GO:0099537)	385	18	4.32	4.16	1.46E-04
cellular nitrogen compound biosynthetic process (GO:0044271)	1355	63	15.22	4.14	1.73E-18
regulation of cation channel activity (GO:2001257)	195	9	2.19	4.11	4.13E-02
nucleotide metabolic process (GO:0009117)	477	22	5.36	4.11	1.25E-05
cellular metal ion homeostasis (GO:0006875)	329	15	3.69	4.06	1.16E-03
nucleoside phosphate metabolic process (GO:0006753)	484	22	5.43	4.05	1.52E-05
cellular divalent inorganic cation homeostasis (GO:0072503)	225	10	2.53	3.96	2.92E-02
regulation of neurotransmitter levels (GO:0001505)	252	11	2.83	3.89	1.81E-02
regulation of transmembrane transporter activity (GO:0022898)	301	13	3.38	3.85	6.87E-03
synaptic signaling (GO:0099536)	425	18	4.77	3.77	4.59E-04
ribonucleoprotein complex biogenesis (GO:0022613)	402	17	4.51	3.77	8.28E-04
rRNA metabolic process (GO:0016072)	240	10	2.69	3.71	4.32E-02
regulation of transporter activity (GO:0032409)	315	13	3.54	3.68	9.87E-03
regulation of ion transmembrane transporter activity (GO:0032412)	291	12	3.27	3.67	1.62E-02
divalent inorganic cation homeostasis (GO:0072507)	268	11	3.01	3.66	2.88E-02
chemical synaptic transmission (GO:0007268)	366	15	4.11	3.65	3.52E-03
anterograde trans-synaptic signaling (GO:0098916)	366	15	4.11	3.65	3.49E-03
nucleobase-containing small molecule metabolic process (GO:0055086)	537	22	6.03	3.65	7.69E-05
neuron projection morphogenesis (GO:0048812)	517	21	5.81	3.62	1.51E-04
organophosphate biosynthetic process (GO:0090407)	471	19	5.29	3.59	4.71E-04
plasma membrane bounded cell projection morphogenesis (GO:0120039)	523	21	5.87	3.58	1.69E-04
cell projection morphogenesis (GO:0048858)	529	21	5.94	3.54	1.94E-04

cell part morphogenesis (GO:0032990)	556	22	6.24	3.52	1.29E-04
metal ion homeostasis (GO:0055065)	417	16	4.68	3.42	3.96E-03
modulation of chemical synaptic transmission (GO:0050804)	526	20	5.91	3.39	5.90E-04
regulation of trans-synaptic signaling (GO:0099177)	527	20	5.92	3.38	6.00E-04
microtubule-based movement (GO:0007018)	397	15	4.46	3.36	7.84E-03
cell morphogenesis involved in neuron differentiation (GO:0048667)	482	18	5.41	3.33	1.94E-03
cellular cation homeostasis (GO:0030003)	404	15	4.54	3.31	9.10E-03
macromolecule biosynthetic process (GO:0009059)	1272	47	14.28	3.29	6.31E-10
regulation of cation transmembrane transport (GO:1904062)	412	15	4.63	3.24	1.07E-02
cell junction organization (GO:0034330)	524	19	5.88	3.23	1.69E-03
cellular ion homeostasis (GO:0006873)	423	15	4.75	3.16	1.32E-02
regulation of neuron death (GO:1901214)	397	14	4.46	3.14	2.12E-02
cellular component morphogenesis (GO:0032989)	653	23	7.33	3.14	3.92E-04
neuron projection development (GO:0031175)	747	26	8.39	3.1	1.27E-04
regulation of membrane potential (GO:0042391)	467	16	5.24	3.05	1.19E-02
cation homeostasis (GO:0055080)	502	17	5.64	3.02	9.04E-03
behavior (GO:0007610)	720	24	8.08	2.97	5.59E-04
mitochondrion organization (GO:0007005)	452	15	5.08	2.96	2.37E-02
inorganic ion homeostasis (GO:0098771)	515	17	5.78	2.94	1.14E-02
regulation of ion transmembrane transport (GO:0034765)	525	17	5.9	2.88	1.36E-02
ion homeostasis (GO:0050801)	527	17	5.92	2.87	1.40E-02
organic substance biosynthetic process (GO:1901576)	2240	72	25.15	2.86	2.63E-13
biosynthetic process (GO:0009058)	2313	73	25.97	2.81	3.56E-13
neuron development (GO:0048666)	921	29	10.34	2.8	1.71E-04
organophosphate metabolic process (GO:0019637)	860	27	9.66	2.8	4.06E-04
cellular biosynthetic process (GO:0044249)	2150	67	24.14	2.78	1.43E-11
cellular homeostasis (GO:0019725)	618	19	6.94	2.74	1.13E-02

regulation of ion transport (GO:0043269)	769	23	8.63	2.66	3.69E-03
carbohydrate derivative biosynthetic process (GO:1901137)	538	16	6.04	2.65	4.26E-02
cell morphogenesis involved in differentiation (GO:0000904)	615	18	6.91	2.61	2.57E-02
positive regulation of cell death (GO:0010942)	689	20	7.74	2.59	1.43E-02
regulation of transmembrane transport (GO:0034762)	625	18	7.02	2.56	2.99E-02
protein-containing complex organization (GO:0043933)	1256	36	14.1	2.55	7.77E-05
gene expression (GO:0010467)	2412	69	27.08	2.55	3.12E-10
cell morphogenesis (GO:0000902)	785	22	8.81	2.5	1.16E-02
protein-containing complex assembly (GO:0065003)	1115	31	12.52	2.48	1.00E-03
nucleobase-containing compound biosynthetic process (GO:0034654)	793	22	8.9	2.47	1.30E-02
cellular nitrogen compound metabolic process (GO:0034641)	3235	89	36.33	2.45	2.57E-13
plasma membrane bounded cell projection organization (GO:0120036)	1174	32	13.18	2.43	8.91E-04
neuron differentiation (GO:0030182)	1147	30	12.88	2.33	2.96E-03
cell projection organization (GO:0030030)	1225	32	13.76	2.33	1.64E-03
carbohydrate derivative metabolic process (GO:1901135)	931	24	10.45	2.3	1.88E-02
heterocycle biosynthetic process (GO:0018130)	864	22	9.7	2.27	3.70E-02
aromatic compound biosynthetic process (GO:0019438)	876	22	9.84	2.24	4.25E-02
negative regulation of cell death (GO:0060548)	1118	28	12.55	2.23	1.19E-02
regulation of cell death (GO:0010941)	1767	44	19.84	2.22	1.70E-04
generation of neurons (GO:0048699)	1226	30	13.77	2.18	9.00E-03
cellular component biogenesis (GO:0044085)	2437	56	27.36	2.05	5.76E-05
cellular component assembly (GO:0022607)	2204	50	24.75	2.02	3.66E-04
regulation of programmed cell death (GO:0043067)	1592	36	17.88	2.01	8.34E-03
regulation of apoptotic process (GO:0042981)	1560	35	17.52	2	1.12E-02
neurogenesis (GO:0022008)	1396	31	15.68	1.98	3.08E-02
regulation of transport (GO:0051049)	1940	43	21.78	1.97	3.21E-03
establishment of localization in cell (GO:0051649)	1765	39	19.82	1.97	6.81E-03

nervous system development (GO:0007399)	2038	45	22.88	1.97	1.93E-03
cellular macromolecule metabolic process (GO:0044260)	2348	51	26.37	1.93	1.00E-03
regulation of localization (GO:0032879)	2297	47	25.79	1.82	7.65E-03
cell development (GO:0048468)	1915	39	21.5	1.81	3.35E-02
nucleobase-containing compound metabolic process (GO:0006139)	2510	51	28.18	1.81	4.17E-03
organonitrogen compound metabolic process (GO:1901564)	4762	96	53.47	1.8	4.94E-07
organelle organization (GO:0006996)	2886	57	32.41	1.76	3.49E-03
regulation of biological quality (GO:0065008)	3833	75	43.04	1.74	1.67E-04
cellular aromatic compound metabolic process (GO:0006725)	2729	53	30.64	1.73	1.05E-02
cellular metabolic process (GO:0044237)	6217	120	69.81	1.72	9.90E-09
heterocycle metabolic process (GO:0046483)	2655	51	29.81	1.71	1.73E-02
protein metabolic process (GO:0019538)	3741	70	42.01	1.67	1.76E-03
organic cyclic compound metabolic process (GO:1901360)	2966	54	33.3	1.62	3.10E-02
cellular component organization or biogenesis (GO:0071840)	5606	102	62.95	1.62	1.71E-05
nitrogen compound metabolic process (GO:0006807)	6312	113	70.88	1.59	5.20E-06
cellular component organization (GO:0016043)	5412	96	60.77	1.58	1.69E-04
primary metabolic process (GO:0044238)	6871	120	77.15	1.56	5.26E-06
transport (GO:0006810)	3760	65	42.22	1.54	3.05E-02
establishment of localization (GO:0051234)	3923	67	44.05	1.52	2.93E-02
metabolic process (GO:0008152)	7979	136	89.59	1.52	1.12E-06
organic substance metabolic process (GO:0071704)	7593	125	85.26	1.47	6.36E-05
macromolecule metabolic process (GO:0043170)	5824	91	65.4	1.39	3.27E-02
cellular process (GO:0009987)	15352	211	172.38	1.22	5.29E-06
sensory perception of chemical stimulus (GO:0007606)	1235	1	13.87	0.07	2.55E-03
sensory perception of smell (GO:0007608)	1133	0	12.72	< 0.01	9.19E-04
electron transport coupled proton transport (GO:0015990)	5	3	0.06	53.43	8.95E-03

energy coupled proton transmembrane transport, against electrochemical gradient (GO:0015988)	5	3	0.06	53.43	8.88E-03
ribosomal small subunit assembly (GO:0000028)	19	6	0.21	28.12	6.45E-05
cytoplasmic translation (GO:0002181)	111	34	1.25	27.28	2.87E-31
neuron projection maintenance (GO:1990535)	10	3	0.11	26.72	3.16E-02
mitochondrial electron transport, cytochrome c to oxygen (GO:0006123)	12	3	0.13	22.26	4.67E-02
mitochondrial electron transport, NADH to ubiquinone (GO:0006120)	26	6	0.29	20.55	2.38E-04
proton motive force-driven ATP synthesis (GO:0015986)	67	15	0.75	19.94	1.59E-11
proton motive force-driven mitochondrial ATP synthesis (GO:0042776)	62	13	0.7	18.67	1.10E-09
ATP biosynthetic process (GO:0006754)	83	15	0.93	16.09	2.22E-10
oxidative phosphorylation (GO:0006119)	105	18	1.18	15.27	2.67E-12
positive regulation of signal transduction by p53 class mediator (GO:1901798)	30	5	0.34	14.84	5.22E-03
aerobic electron transport chain (GO:0019646)	54	9	0.61	14.84	8.93E-06
purine ribonucleoside triphosphate biosynthetic process (GO:0009206)	94	15	1.06	14.21	7.96E-10
mitochondrial ATP synthesis coupled electron transport (GO:0042775)	63	10	0.71	14.14	2.74E-06
NADH dehydrogenase complex assembly (GO:0010257)	57	9	0.64	14.06	1.26E-05
mitochondrial respiratory chain complex I assembly (GO:0032981)	57	9	0.64	14.06	1.24E-05
purine nucleoside triphosphate biosynthetic process (GO:0009145)	95	15	1.07	14.06	8.45E-10
ATP synthesis coupled electron transport (GO:0042773)	65	10	0.73	13.7	3.51E-06
metallo-sulfur cluster assembly (GO:0031163)	26	4	0.29	13.7	3.00E-02
iron-sulfur cluster assembly (GO:0016226)	26	4	0.29	13.7	2.99E-02
ribonucleoside triphosphate biosynthetic process (GO:0009201)	99	15	1.11	13.49	1.34E-09
nucleoside triphosphate biosynthetic process (GO:0009142)	110	15	1.24	12.14	4.90E-09
ribosome assembly (GO:0042255)	60	8	0.67	11.87	1.71E-04

respiratory electron transport chain (GO:0022904)	87	11	0.98	11.26	3.98E-06
ATP metabolic process (GO:0046034)	160	20	1.8	11.13	1.43E-11
aerobic respiration (GO:0009060)	144	18	1.62	11.13	2.46E-10
ribosomal small subunit biogenesis (GO:0042274)	72	9	0.81	11.13	6.90E-05
electron transport chain (GO:0022900)	98	11	1.1	10	1.05E-05
translation (GO:0006412)	357	40	4.01	9.98	1.02E-22
cellular respiration (GO:0045333)	176	19	1.98	9.61	4.76E-10
purine ribonucleoside triphosphate metabolic process (GO:0009205)	187	20	2.1	9.52	1.83E-10
peptide biosynthetic process (GO:0043043)	381	40	4.28	9.35	4.84E-22
ribonucleoside triphosphate metabolic process (GO:0009199)	192	20	2.16	9.28	2.45E-10
purine nucleoside triphosphate metabolic process (GO:0009144)	193	20	2.17	9.23	2.55E-10
proton transmembrane transport (GO:1902600)	59	6	0.66	9.06	9.91E-03

Table S4.3. Subtype differentially expressed genes in *cMaf*^{CKO} SGNs. Average log2 Fold from control. Bonferonni adjusted p-value, Wilcoxon rank sum.

1A SGNs	**Gene**	**avg_log2FC**	**p_val_adj**
	Calb2	3.24069856	6.18E-162
	Maf	0.949435	1.62E-80
	Cd24a	0.615437	3.81E-46
	Plp1	0.479109	7.44E-04
	Nefm	0.378144	6.12E-33
	Nefh	0.331538	1.12E-36
	Abr	0.313059	6.48E-15
	Ubb	0.304916	6.76E-04
	Adarb1	0.283989	2.67E-09
	Slc17a7	0.26404	6.19E-10
	Lhfpl4	0.257431	1.58E-06
	Ttll7	-0.25472	1.08E-05
	Foxp1	-0.25528	4.89E-04
	Nrxn3	-0.26135	1.47E-11
	Sncg	-0.28248	2.04E-05
	Pln	-0.28954	2.48E-13

	Ttn	-0.31514	3.18E-19
	Ywhah	-0.31629	1.95E-18
	Rph3a	-0.36844	1.14E-20
	Uchl1	-0.43808	1.93E-20
	Mafb	-0.47893	8.66E-22
1B SGNs			
	Calb2	1.657977	9.43E-50
	Maf	0.699526	6.01E-24
	Cd24a	0.545066	7.61E-08
	Plp1	0.40102	2.82E-06
	Comt	0.360466	1.53E-05
	Gnas	0.313049	3.19E-07
	Uchl1	-0.27527	4.24E-02
	Sncg	-0.47521	1.59E-04
1C SGNs			
	Mt2	0.645472	1.97E-08
	Ubb	0.589296	3.27E-10
	Mt1	0.537283	2.46E-08
	Cd24a	0.463322	2.62E-12
	Maf	0.459973	4.10E-22
	Calb2	0.282693	1.24E-10
	Kif3c	0.28258	2.56E-03
	Plp1	0.279097	3.42E-04
	Mafb	-0.33153	1.30E-06
	Sncg	-0.3959	9.68E-08

Table S4.4. Differentially expressed genes in all *Mafb*^{CKO} SGNs. Average log2 Fold from control. Bonferonni adjusted p-value, Wilcoxon rank sum.

Gene	**avg_log2FC**	**p_val_adj**
mt-Atp8	1.14368659	1.71E-259
Rps29	1.13621953	8.13E-296
Rpl38	0.98347717	2.37E-280
Cd24a	0.93903091	2.36E-79
Rpl41	0.92480709	7.92E-268
Rps28	0.91343743	2.00E-247
Mt1	0.8977929	1.45E-120

Rpl35a	0.88534232	8.13E-239
Atp5k	0.86572594	9.46E-245
Rps21	0.82992036	5.64E-238
Ndufb1-ps	0.80042624	3.90E-221
Rpl37	0.79735706	1.08E-225
Rps27	0.74807139	7.96E-182
Ntm	0.73716848	2.47E-106
Rpl39	0.71435083	1.52E-165
Dstn	0.70468095	2.84E-152
Dcc	0.70422772	4.05E-30
Atp5md	0.69514653	3.26E-174
Cox7c	0.69419983	6.90E-183
Mt3	0.68128362	1.82E-166
Atp5e	0.68040392	4.45E-174
mt-Nd4	0.67251839	1.27E-231
Rpl37a	0.67161956	1.03E-188
Tuba1b	0.66964079	4.13E-156
Atp5mpl	0.64888987	1.50E-186
Ndufa5	0.63992514	1.71E-169
Ndufa3	0.63812377	4.78E-145
Nmt1	0.63028703	4.90E-151
Tomm7	0.62778441	8.40E-150
Cox6c	0.62514263	1.19E-170
Rpl36	0.55996641	9.79E-163
Rpl34	0.55861897	5.43E-148
Ndufa1	0.55788036	3.38E-133
Ndufc1	0.55715681	4.81E-143
Sec61g	0.54010889	7.34E-115
Ryr3	0.52743506	1.63E-44
Cox17	0.52643778	4.66E-120
Atp5j2	0.524811	1.34E-140
Skp1a	0.52091328	2.12E-85
Uqcr11	0.50371468	1.22E-132
Rplp2	0.50240858	4.50E-145
mt-Nd4l	0.50084926	2.74E-59
Dync1i2	0.48973427	6.26E-115
Cdk8	0.48842698	9.64E-16
Hypk	0.4862124	7.42E-96
Romo1	0.47269489	1.70E-102

Rps26	0.46992316	1.39E-95
Atp5l	0.4583757	4.56E-117
Mt2	0.45335156	2.25E-42
Msantd4	0.43360642	5.08E-73
Ramac	0.42907337	1.90E-70
mt-Nd2	0.42076248	2.88E-119
Cops9	0.41828138	9.49E-75
Ndufa2	0.41657312	1.23E-99
Rpl36a	0.41014175	7.99E-68
Ndufb2	0.40762021	1.33E-83
Cfl2	0.40526415	1.08E-92
Edil3	0.39759261	4.41E-36
Snrpn	0.39621954	1.64E-78
Morf4l1	0.3933533	3.40E-123
Synm	0.39242904	5.86E-58
Cbx3	0.38902246	6.32E-72
Uqcr10	0.38870559	1.41E-90
Eif2s2	0.38858036	7.19E-85
Kcnmb2	0.38726868	5.59E-29
Galnt14	0.38353793	2.02E-55
Uqcrq	0.38330882	2.82E-74
Gnl3l	0.38124086	4.79E-71
Calb1	0.37790484	1.32E-18
Dnm1l	0.36747161	1.25E-75
Pdap1	0.36600821	5.16E-65
Cox8b	0.36141833	2.93E-08
Mgp	0.35796421	4.52E-26
1110004F10Rik	0.35520406	1.61E-47
Brinp3	0.35098584	1.78E-26
Rps2	0.35036397	4.83E-50
Rpl30	0.3503115	5.07E-77
Calm2	0.34622393	5.26E-77
Zfp804a	0.34616433	1.80E-14
Rps15a	0.34363115	5.68E-70
Rpl22l1	0.34329923	4.61E-49
mt-Nd5	0.33678651	3.69E-52
Efemp1	0.33576036	1.03E-50
Cox7a2	0.33575039	4.76E-74
Lancl3	0.33528453	2.21E-31

Rps8	0.33049437	1.13E-98
Ndufa4	0.32974187	2.63E-76
Cdh9	0.32929077	1.53E-18
Slc38a2	0.32654946	1.57E-53
Ighm	0.32551043	1.19E-38
3110039M20Rik	0.32300561	1.02E-38
Pet100	0.32099692	1.41E-44
Cox7b	0.32029869	7.91E-40
Cox6b1	0.31905278	6.96E-51
Ubl5	0.31889639	1.72E-56
Dzank1	0.31437838	1.07E-37
Cd302	0.31315789	3.00E-54
Sms	0.31279483	2.21E-56
Ap2b1	0.31214431	3.21E-37
Cd59a	0.31165295	1.10E-48
Rpl6	0.31087534	2.29E-74
Fxr1	0.31074486	4.42E-38
Sem1	0.31028169	3.72E-50
S100b	0.31013746	1.48E-49
Rpl21	0.31005669	8.38E-59
Pygl	0.30715148	3.14E-29
Son	0.30335361	1.17E-69
Slirp	0.30330031	7.87E-37
Mrps21	0.30224479	1.78E-40
Nars	0.30180731	8.66E-60
Isca1	0.29899061	2.35E-35
Rps24	0.29787759	5.08E-65
Malat1	0.28681006	6.37E-32
Slc24a2	0.28471083	1.41E-25
Ttn	0.28406157	8.54E-20
Rpl24	0.28319778	8.01E-67
Phpt1	0.28237171	4.80E-45
Fau	0.28235331	8.30E-67
Prpf4b	0.28191161	2.74E-30
Sec62	0.28107803	1.71E-62
Cntnap5a	0.28087705	6.27E-33
Atpif1	0.27975717	1.25E-37
Cops5	0.27960929	1.70E-31
Mpz	0.27957705	2.39E-11

Bola2	0.27936296	1.48E-30
Pfdn1	0.27884465	6.25E-43
Elob	0.27857647	2.45E-47
Ghr	0.27849025	3.85E-17
Eif3j1	0.27683317	1.57E-29
Rplp1	0.27565184	1.84E-60
Heatr5a	0.2755887	7.23E-26
Ndufb4	0.27349657	1.90E-33
Atp1a3	0.27273074	2.16E-68
Hmgb1	0.27240117	7.41E-43
Rps17	0.2714094	2.20E-41
Ndufv3	0.27128967	7.03E-36
Aimp1	0.27090812	1.08E-30
Dpm3	0.26988494	3.37E-32
Gm1673	0.26835305	1.99E-30
Sgcz	0.2636867	0.00191534
Thoc7	0.26367395	3.42E-31
Rpl23	0.26300233	9.75E-52
Psmc1	0.26292188	2.83E-34
Tmem108	0.26088865	3.20E-08
Ide	0.26054877	3.79E-31
Tbca	0.25932886	1.76E-36
Ndrg4	0.25912889	6.66E-44
Anapc13	0.25693028	9.80E-25
Runx1	0.25566149	6.72E-20
Lrrc4c	0.25436034	1.47E-14
Gas5	0.25051471	7.79E-27
Ddx5	0.25033868	8.81E-43
Ncam2	-0.2500208	1.61E-09
Pdxp	-0.2501601	2.46E-20
Sipa1l1	-0.2502269	6.30E-25
Magi1	-0.2504314	8.83E-12
Capzb	-0.2510815	2.39E-17
Use1	-0.2520596	2.49E-28
Tpi1	-0.2524916	7.59E-23
Rack1	-0.2530278	4.75E-22
Smarca5	-0.2532027	5.74E-27
Sv2b	-0.2535216	7.21E-19
Egln2	-0.2537189	1.04E-25

Pou3f2	-0.2548863	8.07E-31
Eno1	-0.2549965	5.39E-14
Phb	-0.2561525	7.08E-25
Vav3	-0.2563486	5.70E-32
Fndc5	-0.2567972	6.05E-40
Mtch1	-0.2570782	3.57E-23
Timp3	-0.2573572	1.07E-15
Mosmo	-0.2583651	1.85E-24
Smim10l1	-0.2589427	3.54E-25
Ndn	-0.26005	5.27E-20
Dcaf8	-0.2602423	7.61E-26
Gm10076	-0.2614186	6.28E-47
Lgals1	-0.2620222	1.15E-15
Ehbp1	-0.2624655	6.63E-19
Cdv3	-0.2627106	9.56E-33
Rabac1	-0.264069	3.35E-32
Arglu1	-0.2644543	5.31E-27
Gpm6b	-0.2649419	3.10E-15
Slit3	-0.2653812	1.71E-15
Ccdc85b	-0.2667761	2.14E-29
Tmem160	-0.2676868	2.28E-25
Ndrg1	-0.2679405	4.44E-16
Fxyd6	-0.2709791	6.71E-18
Gnas	-0.2754828	3.78E-58
Ptp4a2	-0.2755613	5.69E-29
Cab39	-0.2757764	2.07E-26
Mitf	-0.2761792	5.14E-32
Vegfb	-0.2799166	1.45E-27
Ebf1	-0.2808181	6.48E-13
Akirin2	-0.2818785	5.93E-50
Fbll1	-0.2819808	1.31E-43
Celf2	-0.2821232	2.83E-23
Chst2	-0.2835977	5.55E-25
Them6	-0.2837852	7.11E-33
Dad1	-0.2838954	1.33E-24
Pgp	-0.2840357	6.78E-36
Ptov1	-0.284306	5.94E-21
Atrnl1	-0.2854095	3.86E-22
Rbms3	-0.2860786	9.23E-19

Crtac1	-0.2860899	5.19E-26
Arfgef1	-0.2872229	1.83E-38
Cyhr1	-0.2876114	4.26E-42
Ube2q1	-0.2886644	8.09E-44
Clic6	-0.2896384	2.09E-51
Sostdc1	-0.2899907	5.17E-19
Pcbp1	-0.2907885	1.92E-37
Kras	-0.2908871	3.65E-37
Ube2q2	-0.2909152	7.62E-34
Tln2	-0.2924031	7.15E-27
Adgrl2	-0.2933416	9.84E-10
Ube2e2	-0.2941493	5.76E-30
Ppm1a	-0.297617	1.62E-36
Plcb4	-0.297969	1.96E-35
Mprip	-0.2985639	9.14E-33
Ttc19	-0.3000444	7.64E-30
Tlk1	-0.3013062	1.01E-43
Larp1b	-0.3025596	1.18E-39
Robo1	-0.3035864	7.13E-10
Dap3	-0.303667	7.30E-41
Aopep	-0.3047998	3.14E-27
Ankrd40	-0.3051443	1.61E-35
Prkg1	-0.3068894	9.05E-16
Camk2n2	-0.3102524	9.97E-44
Golim4	-0.3108253	6.55E-32
Ctnna3	-0.3151819	3.46E-13
Basp1	-0.3177253	4.01E-24
Cabp1	-0.3216366	8.46E-76
Dlc1	-0.322718	8.24E-23
Tafa5	-0.3229102	2.23E-48
Auts2	-0.3247803	8.67E-34
Hras	-0.3251235	1.90E-39
Mef2c	-0.3254101	1.30E-26
Chrm3	-0.3254435	2.05E-23
Emc10	-0.3283543	1.43E-37
Ptprd	-0.3284857	1.28E-27
Hdac9	-0.329343	2.45E-22
Arhgdig	-0.3296115	1.58E-44
Dnajc21	-0.331318	1.65E-42

Dexi	-0.3322309	1.24E-39
Nav3	-0.3340964	1.06E-37
Ap2s1	-0.3343713	3.73E-39
Gkap1	-0.3352292	1.72E-47
Kcnc2	-0.3358797	2.21E-21
Sox2	-0.3372394	2.22E-46
Trpm3	-0.3400772	1.20E-16
Lars2	-0.3421192	4.99E-22
Maml2	-0.3434525	2.55E-25
Dock10	-0.3452295	1.06E-34
Lifr	-0.3455853	1.28E-41
Sgcd	-0.3468446	2.45E-25
Sema3a	-0.3471208	2.92E-22
Selenow	-0.3526803	1.85E-39
Insyn1	-0.3543894	4.81E-36
Kcnb2	-0.3548068	1.42E-18
C130073E24Rik	-0.3655056	5.74E-23
Trim44	-0.3670304	4.09E-45
Pcbp4	-0.3676823	6.77E-33
Qk	-0.3690951	2.75E-29
Cryab	-0.3691647	2.67E-25
Pde4b	-0.3758084	1.05E-12
Npas3	-0.3773951	3.21E-23
Tnrc6c	-0.3817885	4.04E-59
Col27a1	-0.3826415	2.50E-54
Rasgrf1	-0.3869898	3.81E-24
R3hdm2	-0.3892222	6.32E-55
Clstn2	-0.3895336	2.09E-34
Pura	-0.4017285	5.70E-100
Jund	-0.4073035	4.10E-45
Plekha5	-0.4132966	7.56E-47
Tmem47	-0.4193333	1.26E-43
Rph3a	-0.4282205	2.57E-20
Spire1	-0.4286377	1.37E-62
Pde1c	-0.4302142	1.51E-40
Cd63	-0.4342483	3.73E-35
Sphkap	-0.4350304	7.62E-07
Opcml	-0.4453503	1.25E-54
Sap30l	-0.4534016	1.23E-90

Smap1	-0.4571825	4.26E-82
Fgf1	-0.4644119	1.99E-73
Gls	-0.4654072	1.22E-73
Ptgds	-0.4724657	1.29E-07
Eid2	-0.4898151	2.52E-109
Hnrnpd	-0.4904975	1.78E-99
Eef1a2	-0.4943655	5.72E-135
Ankrd11	-0.5013014	4.38E-93
Zfp91	-0.5082541	2.81E-94
Chst9	-0.5100051	1.42E-09
Kcnab1	-0.51716	2.88E-81
Plp1	-0.5281022	5.38E-52
Ddhd1	-0.5417225	2.19E-73
Kif2a	-0.5503936	5.71E-106
Scn1b	-0.5673533	7.61E-131
Hmcn1	-0.6318031	2.13E-46
Thsd7b	-0.6326221	7.17E-67
1500004A13Rik	-0.6363862	1.21E-148
Cdkn1b	-0.6651899	6.54E-143
Trnp1	-0.6828044	9.00E-133
Kcnd2	-0.7356108	1.44E-57
Clec2l	-0.7569247	1.31E-158
Ube2m	-0.758404	1.25E-155
Pcdh9	-0.7662071	1.93E-46
Lrp1b	-0.8390339	1.88E-107
Camk1d	-0.8774615	2.52E-82
Cmss1	-0.8847627	3.63E-110
Kcnip4	-0.9591237	2.55E-88
Dpp6	-1.1317426	3.34E-37

Table S4.5. Gene ontology results from all differentially expressed genes in *Mafb*^{CKO} SGNs.

GO process	Mus musculus - REFLIST (21997)	N Mafb genes	Expected Proportion	Fold Enrichment	False Discovery Rate
polysomal ribosome (GO:0042788)	34	12	0.47	25.37	8.94E-11

mitochondrial proton-transporting ATP synthase complex, coupling factor F(o) (GO:0000276)	12	4	0.17	23.96	1.74E-03
proton-transporting ATP synthase complex, coupling factor F(o) (GO:0045263)	13	4	0.18	22.12	2.19E-03
mitochondrial respiratory chain complex IV (GO:0005751)	20	6	0.28	21.57	4.93E-05
respiratory chain complex IV (GO:0045277)	25	7	0.35	20.13	9.30E-06
respiratory chain complex I (GO:0045271)	50	14	0.7	20.13	2.05E-11
NADH dehydrogenase complex (GO:0030964)	50	14	0.7	20.13	1.93E-11
mitochondrial respiratory chain complex I (GO:0005747)	50	14	0.7	20.13	1.82E-11
cytochrome complex (GO:0070069)	37	10	0.51	19.43	3.82E-08
respiratory chain complex (GO:0098803)	87	23	1.21	19	2.13E-18
cytosolic large ribosomal subunit (GO:0022625)	61	16	0.85	18.86	1.08E-12
mitochondrial respirasome (GO:0005746)	86	22	1.2	18.39	2.42E-17
respirasome (GO:0070469)	95	24	1.32	18.16	1.47E-18
respiratory chain complex III (GO:0045275)	12	3	0.17	17.97	2.59E-02
mitochondrial respiratory chain complex III (GO:0005750)	12	3	0.17	17.97	2.56E-02
cytosolic ribosome (GO:0022626)	108	27	1.5	17.97	1.63E-20
mitochondrial proton-transporting ATP synthase complex (GO:0005753)	20	5	0.28	17.97	6.79E-04
cytosolic small ribosomal subunit (GO:0022627)	45	11	0.63	17.57	1.40E-08
proton-transporting ATP synthase complex (GO:0045259)	21	5	0.29	17.12	8.04E-04
inner mitochondrial membrane protein complex (GO:0098800)	142	29	1.98	14.68	2.37E-20
proton-transporting two-sector ATPase complex, proton-transporting domain (GO:0033177)	22	4	0.31	13.07	1.10E-02
small ribosomal subunit (GO:0015935)	80	14	1.11	12.58	2.95E-09
polysome (GO:0005844)	76	13	1.06	12.3	1.53E-08
ribosomal subunit (GO:0044391)	195	30	2.71	11.06	2.19E-18
oxidoreductase complex (GO:1990204)	121	17	1.68	10.1	5.66E-10
ribosome (GO:0005840)	229	32	3.19	10.05	1.73E-18
large ribosomal subunit (GO:0015934)	120	16	1.67	9.58	4.31E-09
COP9 signalosome (GO:0008180)	35	4	0.49	8.22	4.54E-02
mitochondrial protein-containing complex (GO:0098798)	288	32	4.01	7.99	3.73E-16

voltage-gated potassium channel complex (GO:0008076)	76	8	1.06	7.57	6.77E-04
proton-transporting two-sector ATPase complex (GO:0016469)	50	5	0.7	7.19	2.38E-02
potassium channel complex (GO:0034705)	90	8	1.25	6.39	1.91E-03
transmembrane transporter complex (GO:1902495)	372	30	5.17	5.8	7.69E-12
transporter complex (GO:1990351)	394	30	5.48	5.47	2.43E-11
dendritic spine (GO:0043197)	200	13	2.78	4.67	3.00E-04
neuron to neuron synapse (GO:0098984)	433	28	6.02	4.65	3.89E-09
neuron spine (GO:0044309)	205	13	2.85	4.56	3.79E-04
mitochondrial inner membrane (GO:0005743)	540	34	7.51	4.53	8.68E-11
Z disc (GO:0030018)	130	8	1.81	4.42	1.68E-02
postsynaptic density (GO:0014069)	394	24	5.48	4.38	2.19E-07
sarcolemma (GO:0042383)	166	10	2.31	4.33	4.66E-03
asymmetric synapse (GO:0032279)	402	24	5.59	4.29	3.02E-07
organelle inner membrane (GO:0019866)	585	34	8.14	4.18	5.42E-10
ribonucleoprotein complex (GO:1990904)	714	41	9.93	4.13	8.15E-12
I band (GO:0031674)	143	8	1.99	4.02	2.78E-02
sarcomere (GO:0030017)	197	11	2.74	4.01	4.30E-03
postsynaptic specialization (GO:0099572)	434	24	6.04	3.98	1.08E-06
myofibril (GO:0030016)	222	12	3.09	3.89	2.99E-03
mitochondrial membrane (GO:0031966)	725	39	10.09	3.87	1.49E-10
mitochondrial envelope (GO:0005740)	778	40	10.82	3.7	2.76E-10
myelin sheath (GO:0043209)	215	11	2.99	3.68	8.35E-03
contractile fiber (GO:0043292)	235	12	3.27	3.67	4.63E-03
cation channel complex (GO:0034703)	223	11	3.1	3.55	1.09E-02
membrane protein complex (GO:0098796)	1217	57	16.93	3.37	3.25E-13
postsynapse (GO:0098794)	741	33	10.31	3.2	4.21E-07
integral component of synaptic membrane (GO:0099699)	227	10	3.16	3.17	3.96E-02
ion channel complex (GO:0034702)	294	12	4.09	2.93	2.72E-02
glutamatergic synapse (GO:0098978)	517	21	7.19	2.92	6.65E-04
dendrite (GO:0030425)	740	28	10.29	2.72	1.12E-04
dendritic tree (GO:0097447)	743	28	10.34	2.71	1.19E-04
synapse (GO:0045202)	1434	53	19.95	2.66	8.58E-09
envelope (GO:0031975)	1192	44	16.58	2.65	3.15E-07
organelle envelope (GO:0031967)	1192	44	16.58	2.65	3.08E-07
neuronal cell body (GO:0043025)	734	27	10.21	2.64	2.60E-04

somatodendritic compartment (GO:0036477)	1064	36	14.8	2.43	6.12E-05
plasma membrane protein complex (GO:0098797)	599	20	8.33	2.4	1.45E-02
mitochondrion (GO:0005739)	1888	63	26.26	2.4	8.21E-09
cell body (GO:0044297)	822	27	11.43	2.36	1.75E-03
axon (GO:0030424)	732	24	10.18	2.36	4.42E-03
cell junction (GO:0030054)	2081	64	28.95	2.21	1.13E-07
catalytic complex (GO:1902494)	1698	48	23.62	2.03	1.65E-04
neuron projection (GO:0043005)	1563	43	21.74	1.98	8.93E-04
protein-containing complex (GO:0032991)	5761	154	80.14	1.92	1.33E-16
organelle membrane (GO:0031090)	2459	62	34.21	1.81	1.65E-04
cytosol (GO:0005829)	3881	97	53.99	1.8	2.25E-07
plasma membrane bounded cell projection (GO:0120025)	2392	56	33.28	1.68	4.01E-03
cell projection (GO:0042995)	2635	61	36.66	1.66	2.64E-03
intracellular non-membrane-bounded organelle (GO:0043232)	4498	99	62.57	1.58	6.16E-05
non-membrane-bounded organelle (GO:0043228)	4499	99	62.59	1.58	6.05E-05
cytoplasm (GO:0005737)	11536	233	160.48	1.45	5.55E-15
intracellular organelle (GO:0043229)	12654	235	176.03	1.34	2.66E-10
organelle (GO:0043226)	12965	240	180.36	1.33	9.73E-11
intracellular anatomical structure (GO:0005622)	14305	263	199	1.32	7.45E-14
intracellular membrane-bounded organelle (GO:0043231)	11585	212	161.16	1.32	3.05E-07
membrane-bounded organelle (GO:0043227)	12045	216	167.56	1.29	9.89E-07
cellular anatomical entity (GO:0110165)	19206	299	267.17	1.12	9.76E-09
cellular_component (GO:0005575)	21007	303	292.23	1.04	2.69E-02

Table S4.6. Subtype differentially expressed genes in *Mafb* mutants. Average log2 Fold from control. Bonferonni adjusted p-value, Wilcoxon rank sum.

	Gene	**avg_log2FC**	**p_val_adj**
1A SGNs	**Zfp804a**	0.6278571	1.80E-31
	Maf	0.4693227	1.60E-27
	Tmem108	0.4217905	3.53E-17
	Ghr	0.3538498	1.13E-11
	Dync1i2	0.3443381	1.20E-20

	Kcnab1	-0.2752266	1.10E-14
	Plekha5	-0.286566	6.18E-09
	Ccdc85b	-0.3212108	6.57E-14
	Sv2b	-0.3382362	1.09E-13
	Pdxp	-0.3588071	1.06E-12
	Eef1a2	-0.6511596	1.12E-67
	Kcnip4	-1.0987118	8.79E-49
1B SGNs	**Calb1**	0.893896	3.27E-35
	Ryr3	0.8539711	1.04E-48
	Kcnmb2	0.6526982	1.56E-29
	Dcc	0.6055467	1.33E-22
	Dync1i2	0.5794788	5.27E-46
	Clstn2	-0.3082799	1.06E-05
	Rasgrf1	-0.3323189	2.69E-04
	Sema3a	-0.3541896	1.10E-09
	Dpp6	-0.4178149	3.94E-04
	Kcnab1	-0.4467812	5.38E-19
	Eef1a2	-0.4539061	2.61E-39
	Plekha5	-0.5429139	1.04E-30
	Pcdh9	-0.5773611	1.77E-11
	Kcnip4	-1.0503399	6.04E-37
1C SGNs	**Dcc**	1.0501715	9.59E-58
	Ryr3	0.5814886	1.62E-25
	Calb2	0.5691855	2.70E-06
	Dync1i2	0.5543416	6.37E-49
	Kcnmb2	0.3670485	1.88E-09
	Magi1	-0.3438083	6.53E-10
	Sipa1l1	-0.3442383	2.90E-11
	Eef1a2	-0.3687813	1.49E-25
	Plekha5	-0.3789161	7.24E-15
	Adgrl2	-0.464398	6.63E-15
	Rasgrf1	-0.5118382	2.15E-14
	Sema3a	-0.5350682	7.04E-13
	Clstn2	-0.578106	9.00E-23
	Ptprd	-0.5909842	2.03E-21
	Crtac1	-0.6241373	2.87E-32
	Pde4b	-0.6280312	3.69E-14

	Kcnip4	-0.6714618	1.54E-15
	Kcnc2	-0.709611	5.55E-30
	Kcnab1	-0.7429333	4.58E-48
	Kcnb2	-0.8018819	1.01E-21
	Pcdh9	-1.1368104	3.06E-38
	Dpp6	-1.7795106	4.13E-49

Table S4.7. Differentially expressed genes in dKO SGNs. Average log2 Fold from control. Bonferonni adjusted p-value, Wilcoxon rank sum.

Genes	**avg_log2FC**	**p_val_adj**
Calb2	5.72473724	1.90E-161
Fth1	2.1250146	1.42E-251
Nin	1.85105638	4.02E-264
Astn2	1.61283587	4.24E-237
6330411D24Rik	1.57301521	2.39E-224
Maf	1.50981729	5.81E-217
Lhfpl3	1.45317679	4.47E-212
Dcc	1.44625414	2.32E-81
Cd24a	1.44600024	3.64E-111
Aldh1a3	1.39886211	1.38E-219
Ctsb	1.38562047	5.39E-218
Cdh9	1.32570314	2.26E-144
Kcnk1	1.2728517	4.04E-198
Ttc9b	1.1997152	2.08E-198
Tesc	1.19627543	7.53E-193
Kcnc3	1.17631139	7.93E-233
Kcnip1	1.1688574	7.27E-137
Adarb1	1.15809524	6.86E-174
Slco5a1	1.15127867	2.61E-204
Nefh	1.14561072	5.21E-225
Mafb	1.13672023	1.51E-199
Lancl1	1.12751869	4.29E-197
Ghr	1.12642778	6.26E-152
Ntm	1.0641012	8.21E-118
Rab3ip	1.05145638	8.55E-185
Slc17a7	1.03756435	2.71E-189

Neb	1.03552047	1.77E-94
Edil3	1.02356545	2.35E-133
Hagh	1.01804986	6.06E-185
Hs6st3	1.01561917	4.45E-107
Adam23	0.99238147	1.94E-177
Kidins220	0.99007084	1.11E-211
Akap12	0.9858607	1.86E-138
Synm	0.98507127	1.45E-157
Cpne4	0.95774777	4.69E-112
Heatr5a	0.93622515	1.70E-164
C1ql3	0.92700301	2.67E-148
Btbd9	0.91510459	6.05E-15
Tmem108	0.90801649	7.23E-77
Rps3a1	0.89421991	1.52E-157
Cox8b	0.89221251	1.27E-99
Sparcl1	0.8847632	4.97E-234
Brinp3	0.85577162	2.80E-107
Apba1	0.84207886	4.33E-135
Lrp1b	0.82060102	5.97E-98
Paqr4	0.81205694	1.49E-107
A2ml1	0.80659498	2.09E-106
Lrrc49	0.80542993	4.09E-156
Cdk15	0.79112267	1.12E-88
B3gat1	0.78775954	5.76E-68
Ehd3	0.76804329	1.60E-135
Mtss1	0.76314684	4.27E-120
Hapln4	0.76065829	2.32E-130
Gria3	0.7469534	5.75E-126
Sema7a	0.74314276	3.15E-121
Laptm4b	0.73848404	9.88E-120
Gas6	0.73262556	7.04E-124
Pdzd2	0.72810451	1.43E-92
Cntnap4	0.72036648	7.28E-91
Tubb4b	0.71833238	9.61E-85
Sv2c	0.71697776	1.34E-95
Sytl2	0.7137625	1.74E-122
Nefl	0.71229575	9.76E-95
Asic3	0.71031931	2.31E-95
Lancl3	0.70961812	5.74E-92

Prxl2b	0.69568313	4.07E-108
Syt3	0.69120255	3.34E-110
Paxbp1	0.68849156	6.69E-91
Resp18	0.68380839	3.99E-95
S100b	0.68326969	6.01E-107
Map2	0.68181239	9.29E-152
Gdpd1	0.68059263	8.84E-95
Lrrc4c	0.68031725	2.31E-52
Kcnh5	0.67836111	4.14E-107
Ugt8a	0.67289324	1.22E-102
Galntl6	0.67259778	1.12E-09
Rida	0.67191121	2.02E-81
3110039M20Rik	0.66701754	1.22E-107
Cd302	0.6665195	1.03E-94
Adgrg2	0.66412035	2.76E-107
Nefm	0.66234527	7.37E-122
Fgf10	0.6612551	5.12E-97
Fbxo40	0.65539186	1.89E-68
Pld5	0.6501294	9.81E-79
Clu	0.64586518	2.39E-76
Ccdc155	0.64001049	3.05E-80
Pcdh7	0.6340146	4.03E-56
Rabggtb	0.63393675	4.63E-100
Vstm2l	0.62439214	6.71E-92
Iqsec3	0.62071623	7.50E-114
Eif3f	0.61994293	5.03E-89
Ppip5k2	0.61836998	1.93E-92
Cacna1d	0.61725803	2.19E-73
Cds1	0.61516454	3.72E-89
Zfp804a	0.61452223	8.47E-42
Ttn	0.61282917	8.88E-30
Mpc2	0.61188981	1.42E-113
Hs3st1	0.60770861	1.63E-90
Dnajc13	0.60736913	5.83E-68
Ptprf	0.60654015	5.30E-91
1700021F05Rik	0.60551752	2.26E-73
Dync1i1	0.60462944	3.06E-122
Cntnap5a	0.60390718	4.79E-98
Car10	0.59405499	7.14E-66

Slc35f1	0.59271269	7.98E-58
Rab33a	0.59196254	4.89E-69
Psap	0.59126255	2.15E-107
Nat8l	0.58951311	1.03E-91
Tmem179	0.58426984	8.55E-89
Cox5a	0.58375092	1.80E-155
Ryr3	0.58290293	1.57E-43
1110032F04Rik	0.58273385	1.97E-77
Hapln1	0.57991009	1.23E-89
Mxra7	0.57781636	2.01E-75
Rasgrp2	0.5747475	3.66E-33
A530058N18Rik	0.57385321	6.37E-76
Mapk8ip3	0.57086541	4.13E-98
Sh3bgr	0.56893235	3.12E-36
Ptgds	0.56686052	2.00E-25
Fstl1	0.56559113	1.06E-67
Isl1	0.55937087	1.11E-100
Ablim2	0.55858767	1.11E-89
Park7	0.55813574	1.26E-142
Endod1	0.5576301	2.55E-85
Vat1l	0.55698852	1.00E-64
Trim37	0.55501367	3.73E-101
Tmbim4	0.55384588	1.52E-74
Hist3h2ba	0.54917423	2.82E-66
Tmem163	0.54874243	2.37E-70
Ank1	0.5484661	2.82E-81
Cryab	0.54417335	6.39E-39
Lmbr1	0.54144163	3.07E-50
Ypel3	0.5386189	1.16E-74
Msl3	0.53847394	1.60E-61
Cst6	0.53038658	6.94E-57
Pdrg1	0.52695847	1.05E-48
Spcs1	0.52489902	3.47E-69
Spock3	0.52330487	1.60E-73
Syt2	0.52330178	2.16E-104
C1qtnf4	0.52180985	7.42E-61
Sncaip	0.52149375	5.77E-58
Pygl	0.51912748	5.16E-54
Mdga1	0.51831299	1.51E-05

Sez6	0.51569792	8.16E-77
Ubxn1	0.51439937	4.22E-66
B3galt5	0.51347626	6.85E-77
Faim2	0.50999321	4.51E-35
Asb13	0.50727255	7.22E-68
Prox1	0.50726059	1.44E-55
Dbi	0.50715828	2.47E-43
Upp1	0.50079953	1.29E-55
Prpf19	0.49522683	4.65E-68
Lhfpl4	0.49517335	9.50E-62
Dpf3	0.49498139	2.57E-65
Prune2	0.49497651	1.32E-59
Lrrc7	0.4919257	1.79E-44
Mif	0.49149538	7.21E-64
Tfrc	0.49112816	2.47E-40
Snx6	0.49066781	2.24E-63
Stx7	0.48945628	8.87E-65
Scrt1	0.48376493	1.93E-60
Tubb3	0.48073707	1.52E-67
Tuba4a	0.47903606	4.64E-59
Sncb	0.47721211	1.55E-80
Auh	0.47695749	1.97E-73
Abhd3	0.47634608	1.44E-55
Rcan1	0.47594877	1.68E-57
Cdc14a	0.47521294	6.87E-55
Kif3c	0.47459966	7.39E-56
Lrrn1	0.47448862	3.67E-67
Nrxn3	0.4737164	1.17E-39
Chga	0.47160094	5.79E-82
Map1a	0.47142641	7.31E-100
Lmbrd1	0.47114024	8.12E-58
Fam57b	0.4710697	6.57E-64
Tmem196	0.47073758	1.81E-54
Cd59a	0.46593971	5.50E-60
Stac2	0.46580244	6.07E-57
Acyp2	0.46561305	4.02E-81
Iscu	0.46309883	3.96E-63
Mdh1	0.46214528	1.05E-29
Pcsk1n	0.46014112	1.36E-81

Ube2v1	0.45739035	5.62E-47
Fnta	0.45589424	8.46E-53
Ckb	0.45237007	6.32E-57
Rgma	0.45136507	7.21E-46
Cib2	0.44777588	2.61E-22
Atp5g1	0.44775042	8.70E-80
Them6	0.44458886	2.49E-57
Hmgb1	0.44406116	2.79E-64
Susd4	0.44024098	1.65E-65
Ndufb8	0.43922491	3.17E-83
Arl3	0.4362013	2.83E-72
Kcnmb2	0.43564691	3.01E-13
Golgb1	0.43523992	1.52E-50
Fgd4	0.43233016	4.66E-44
Klc1	0.43201955	4.69E-92
Dnajc15	0.43188468	6.52E-71
Lgi1	0.43142416	1.15E-42
Map1lc3b	0.43024079	1.59E-75
Rnasek	0.42962865	1.06E-76
Jak1	0.42871758	1.87E-45
Slc24a2	0.42839259	4.33E-29
Pfn1	0.42701182	3.92E-47
Abhd12	0.42609679	2.69E-51
Naca	0.42425446	1.01E-79
Rnf187	0.42406719	6.20E-74
Cep83	0.42296873	1.68E-47
Uqcrfs1	0.42295138	2.76E-47
Cuta	0.42064423	4.28E-47
Stmn3	0.42041775	7.88E-123
Gm16083	0.41959575	4.45E-50
Cltb	0.41924547	3.81E-62
Anxa5	0.41852484	1.59E-42
Ubl3	0.41772772	8.22E-63
Paip2	0.4157005	4.62E-74
Cuedc2	0.41376876	3.61E-44
Galnt17	0.41132644	4.56E-34
Gm1673	0.41124561	9.37E-55
Tubb5	0.41022032	5.77E-39
Epn3	0.40944111	4.07E-41

Ccbe1	0.40777427	6.98E-38
Smap2	0.40640689	6.91E-56
Fbxo34	0.40638601	2.13E-41
Ap2m1	0.40526084	3.08E-43
Osbpl3	0.40480626	6.42E-39
Fbxo21	0.40344106	7.56E-41
Scg3	0.4029318	8.50E-54
Ckmt1	0.40054336	1.26E-28
Ndufs7	0.39971731	9.77E-72
Zfyve28	0.3995404	2.57E-42
Tmem246	0.39884634	1.44E-46
Ndufv2	0.39788858	5.78E-51
Rpl29	0.39738944	1.67E-41
Calm3	0.39698486	1.59E-90
Col19a1	0.39561364	1.28E-48
Fhl1	0.39425633	1.71E-44
Gcsh	0.39417133	1.31E-44
Lamtor4	0.39412351	1.79E-53
Ccdc126	0.3940348	1.98E-47
Tecr	0.39381664	1.59E-55
Dstn	0.3930205	3.16E-32
Tmem30a	0.39262469	6.50E-67
Hint1	0.39255167	8.22E-100
Cd63	0.3921104	4.60E-17
Snn	0.39133137	8.33E-44
Prox1os	0.39117915	5.20E-47
Naa20	0.39004507	1.77E-42
Prdx5	0.38910433	1.13E-67
Ifitm10	0.3874218	2.11E-35
Fgf9	0.38682159	1.83E-45
Tmem147	0.38660978	8.31E-47
Panx2	0.38483562	1.38E-36
Rex1bd	0.38440952	2.09E-52
A330102I10Rik	0.38380069	1.30E-25
Ppa2	0.38353515	1.81E-49
Rtraf	0.38282099	5.98E-43
Mff	0.38114623	1.66E-50
Plpp1	0.37987239	7.15E-41
Ppa1	0.37822546	4.23E-50

Dpy30	0.37727424	5.67E-41
Pgm2l1	0.37457354	3.25E-39
Tmod1	0.37450351	6.60E-34
Idh3b	0.37259623	1.30E-30
Mgp	0.37252344	2.05E-05
Capn2	0.37238036	5.65E-38
Mpc1	0.37195267	1.07E-59
Glrx3	0.37174671	6.08E-45
Nr3c2	0.37109656	8.13E-27
Dlgap2	0.36903402	5.84E-34
Fam162a	0.36847925	1.89E-35
Herc1	0.36716696	3.09E-46
Hydin	0.36684772	5.19E-23
Dcp2	0.36619027	6.31E-33
Ndufs3	0.36596579	2.45E-31
Scn4b	0.36519712	3.35E-35
Pin1	0.36471253	1.24E-40
Eif4g3	0.36408727	3.15E-58
Glrx5	0.36218503	2.88E-42
Ndel1	0.36113128	5.90E-34
Ceacam10	0.36017225	3.50E-20
Btf3	0.35994827	4.03E-48
Tmem151a	0.35836188	4.58E-34
Eml4	0.35819673	6.06E-30
Rpl21	0.35757912	6.13E-56
Tmem132c	0.35678351	1.21E-36
Pla2g7	0.35632883	1.75E-21
Cox14	0.35597028	2.48E-56
Hmox2	0.35563185	4.64E-30
Tuba1b	0.35557647	1.31E-32
Ywhag	0.35512628	1.88E-71
4-Sep	0.35416338	1.32E-31
Oip5os1	0.35409707	6.29E-41
Uqcrc2	0.35364436	3.17E-41
Psmb3	0.35314447	7.65E-32
Etl4	0.35267298	5.24E-20
Kcna1	0.35195254	6.14E-46
6430548M08Rik	0.35171229	3.44E-30
Ran	0.35143631	1.27E-42

Fam89b	0.35078154	3.20E-31
Fbxw7	0.35041112	7.04E-33
Sf3b6	0.35019229	2.87E-38
Psenen	0.35007348	5.05E-31
Yif1b	0.34963843	1.79E-30
Cope	0.34947551	2.33E-26
Rpl10a	0.34928004	2.75E-40
Cst3	0.34880277	3.05E-40
Phb	0.34818042	9.98E-34
Tmem37	0.34814829	8.85E-45
Bnip3	0.34715508	1.40E-29
Myl12b	0.3470678	7.48E-39
Galnt9	0.34680095	3.01E-30
Nacc2	0.34653438	2.10E-46
Tmem59l	0.34519563	2.07E-24
Rnf123	0.34469717	7.34E-26
Atp6v1b2	0.34431882	2.34E-42
Tnfrsf21	0.34426711	1.30E-29
Ndufa4	0.34416863	3.80E-95
Kcnab3	0.3441237	2.56E-25
Hcrtr2	0.34292313	3.75E-16
Gstm5	0.34256736	3.05E-30
Ctsd	0.34228872	1.51E-21
Ndufa5	0.34092647	2.66E-55
Cyc1	0.34054623	1.61E-25
Olfm3	0.34037208	5.59E-22
Tspan17	0.33973673	3.78E-27
Pip4k2a	0.33919975	2.75E-33
Vps29	0.33696359	1.64E-28
Lingo1	0.33630632	9.20E-27
Galnt14	0.33600597	3.07E-26
Atp10a	0.33532133	3.91E-37
Ndufc2	0.33508848	1.53E-52
Tspan7	0.33400443	4.44E-26
Cpt2	0.33250815	1.13E-38
Coprs	0.3324848	3.25E-28
Snph	0.33166016	1.45E-36
Podxl2	0.33163431	1.36E-27
Reep1	0.3310257	8.32E-25

Guk1	0.33052715	8.51E-36
Mindy3	0.3299789	7.11E-27
Scp2	0.32911733	5.41E-29
Ghitm	0.32901462	1.75E-61
Pfdn4	0.32866211	1.88E-29
Mcub	0.32860082	1.56E-16
Laptm4a	0.32850485	4.39E-26
Abr	0.327977	5.12E-45
Tango2	0.32784315	1.59E-28
Sdhb	0.32752106	2.18E-26
Rxrg	0.32739698	2.40E-37
Cttnbp2	0.32436907	5.19E-23
Esrrg	0.32370676	2.71E-19
Mvb12a	0.32353016	6.72E-26
Grina	0.32281643	2.35E-29
Uchl5	0.32228907	6.19E-26
Rab3a	0.32143237	3.42E-39
Aco2	0.32126633	4.01E-33
Gm26782	0.32088913	2.51E-22
Syne1	0.32086943	5.09E-30
Nkain2	0.31990139	0.01477238
P2rx6	0.31976954	1.77E-37
Bex3	0.3194959	4.66E-42
Pfdn1	0.31895362	9.00E-41
Crybb1	0.31814315	5.01E-38
Scamp3	0.31793231	2.88E-27
Serf2	0.31774415	1.01E-40
Vamp1	0.31691219	3.01E-49
Amigo3	0.31613513	6.20E-29
Pqlc1	0.31604325	3.63E-36
Mkrn1	0.31527884	2.89E-29
Ndrg4	0.3147203	4.53E-41
Uqcc3	0.31449701	5.39E-23
Ahcyl2	0.31406255	2.55E-26
Kcnk10	0.31331941	1.00E-34
Rpl9	0.31278773	3.61E-65
Rpl11	0.31260322	7.33E-57
Arfgef3	0.31232152	1.45E-24
Car2	0.31172623	2.77E-29

Ap4s1	0.31149189	1.05E-24
Vwa7	0.31057061	3.37E-29
Slain2	0.31040063	9.70E-35
Wbp2	0.30969643	6.81E-27
Dynlrb1	0.30750233	4.69E-32
Limk1	0.30731913	9.21E-25
Ndufa6	0.30727769	2.62E-51
Trim54	0.30684542	5.91E-28
Rps24	0.30656837	1.27E-58
Ttc13	0.30621693	1.27E-26
Tomm34	0.30538665	6.55E-24
Gm37240	0.30457525	3.47E-18
Capns1	0.30437377	2.36E-26
Tmem160	0.30429007	9.81E-28
Pappa	0.30427895	4.05E-14
Dapk2	0.30371109	2.49E-33
2410004B18Rik	0.30315014	4.15E-27
Fam110b	0.30312212	3.75E-24
Atp5d	0.30260589	1.12E-40
Smim12	0.30235899	7.06E-23
Gm43305	0.30203779	7.85E-28
Znrd2	0.301966	1.81E-24
Ufc1	0.30176487	7.90E-30
Rpl10	0.3017375	4.92E-28
Sptan1	0.30171117	7.79E-48
Ndufab1	0.30093317	2.24E-43
Grm7	0.30067907	2.85E-13
Mrps21	0.30037596	5.46E-31
Syndig1	0.30014874	1.82E-23
2310061I04Rik	0.29984917	7.03E-20
Tdrp	0.29923289	2.89E-21
Mtus1	0.29907081	2.93E-22
Atp6v1f	0.29803962	4.03E-39
Fbxo22	0.29798203	5.97E-22
Asna1	0.29785859	4.34E-22
Bola3	0.2978298	1.27E-26
Pkm	0.2977659	7.97E-32
Lpcat4	0.29770924	6.87E-30
Gm34016	0.29750542	4.94E-23

Rnf115	0.29737396	2.79E-23
Fam98c	0.29683211	2.55E-22
Mir124-2hg	0.29635417	3.12E-21
Sipa1l2	0.29571075	2.77E-26
Fkbp8	0.29561741	8.55E-24
Arl2bp	0.29554125	8.23E-22
Rab11a	0.2950365	4.54E-23
Hebp2	0.29491223	2.79E-21
Aldoc	0.29472357	7.26E-22
Plxna1	0.29430468	9.41E-29
Rpl8	0.29389199	3.74E-49
Tomm5	0.29350394	2.82E-27
Tmcc3	0.29335837	1.80E-29
Apoo	0.29309289	1.08E-22
Tmem234	0.29286977	1.66E-23
Ndufb9	0.29192007	2.40E-50
Lgi3	0.29159867	8.94E-20
Commd3	0.29118822	5.60E-22
C1d	0.29113764	5.40E-23
Lrrn3	0.29069552	4.18E-23
Rpl14	0.29056212	1.32E-42
Fam78b	0.29037363	2.56E-26
Lgi2	0.28991211	7.79E-20
Ppia	0.28939704	7.45E-37
Tmx2	0.289146	5.87E-24
Capzb	0.2880227	3.16E-17
Rpl7	0.28799681	1.00E-35
Rnf227	0.28776634	3.71E-23
Gtf2a2	0.28764855	5.30E-22
Ndufb11	0.28747747	6.16E-39
Dctn1	0.28735523	3.37E-33
Psma5	0.28726604	1.04E-23
Kctd17	0.28705186	1.26E-28
Rell2	0.28644802	1.24E-25
Nrep	0.28637814	4.52E-20
Adcy1	0.28636271	3.84E-23
1700008O03Rik	0.28635077	9.47E-30
Egln2	0.28633353	1.55E-19
Emc4	0.28580743	3.75E-29

Ndufs2	0.28578052	3.74E-27
Abhd17a	0.28552087	1.46E-20
Tmco1	0.28503654	5.14E-22
Klhdc8a	0.28501488	1.25E-19
AA465934	0.28470956	3.23E-25
Ndufa11	0.28461074	1.43E-38
Atp5f1	0.2843622	6.13E-45
Pak1	0.28426222	4.21E-08
Rtl8a	0.28424654	5.19E-20
Rnf208	0.28414476	2.63E-20
Abcc5	0.28398271	1.03E-20
Psmb4	0.2833752	6.03E-25
Mtch2	0.28302959	4.37E-20
Ppp3cc	0.28205108	4.84E-24
Fis1	0.28157178	1.22E-26
Fkbp3	0.28152165	8.67E-38
Txndc15	0.28090511	1.73E-20
Vdac1	0.28065827	2.79E-37
Prnp	0.28014258	2.09E-18
St3gal6	0.27976346	9.64E-19
Mrps36	0.27958985	2.50E-20
Tsc22d3	0.27940758	6.13E-17
Ndufs4	0.2793294	2.17E-29
Cystm1	0.2784443	4.72E-23
Chchd10	0.27822335	1.56E-48
Tanc1	0.27746209	1.67E-15
Fkbp4	0.27734583	3.60E-27
Cfl1	0.27697455	2.80E-23
Eif3i	0.27660198	1.49E-18
Lrrk1	0.27589618	3.71E-15
Pink1	0.27561439	6.02E-22
Mrps24	0.27538943	7.79E-22
Rps11	0.27463117	4.95E-45
Me3	0.27426839	1.26E-18
Pfdn5	0.27405245	1.10E-33
Snrpn	0.27399565	3.59E-43
Tsr3	0.27305914	6.00E-19
Mrpl34	0.27277314	3.12E-26
Ankrd9	0.27274315	6.30E-20

Psmc4	0.27211822	2.99E-19
Grhpr	0.27207567	3.08E-21
Mrps11	0.27195771	2.40E-18
Dad1	0.27193188	2.09E-22
Isca2	0.27191062	5.30E-18
Tsen15	0.27165258	1.21E-21
Clta	0.2716284	7.52E-44
Thy1	0.27152359	1.54E-15
Med21	0.27147572	1.31E-18
Mtmr7	0.27111991	3.63E-23
Ethe1	0.27068537	1.71E-19
H1f0	0.27053635	1.52E-16
Gpx4	0.27029826	1.05E-51
Prdx3	0.27003851	3.10E-18
Extl2	0.26988396	7.13E-19
Psmb2	0.26945608	1.22E-20
Mrpl12	0.26905775	3.80E-22
Pigp	0.26868731	4.05E-19
Lysmd2	0.26860382	2.18E-18
Ccser2	0.2681928	7.97E-20
Rtl8b	0.26793742	2.47E-16
0610012G03Rik	0.26778996	7.46E-21
Lamtor2	0.26744951	6.51E-27
Atp5g2	0.26736823	4.81E-34
Eif3k	0.26725886	7.18E-19
Amph	0.26670472	6.54E-21
Mtfp1	0.26627663	1.62E-13
Cdh22	0.26627076	4.70E-29
Tmem74b	0.26607705	1.33E-24
Fat1	0.26553883	3.68E-17
Snx21	0.26515427	2.97E-20
Qrsl1	0.26505309	5.66E-23
Ndufb10	0.26500064	4.88E-27
Wdr83os	0.2642867	2.84E-18
Ccdc28a	0.26425324	3.33E-18
Fkbp2	0.26384507	3.97E-37
Hcn1	0.26368288	1.57E-13
Sesn3	0.26343039	7.35E-16
Bcat1	0.26298301	1.57E-16

Sod2	0.26297694	9.66E-29
Srxn1	0.26297694	6.83E-20
Ppp2r2b	0.26277188	7.03E-15
Fndc10	0.26276665	2.31E-20
Ndufb5	0.26251967	1.01E-33
Tnks1bp1	0.2624326	5.46E-26
Sema6a	0.26202326	0.00011455
Blvra	0.26198403	3.78E-17
Nop10	0.26198324	4.72E-22
Anapc11	0.26175396	1.57E-17
Acyp1	0.26153058	1.62E-16
Higd2a	0.26146509	1.09E-20
Spcs2	0.2606658	3.51E-17
Ncs1	0.26065414	7.77E-22
Tubg2	0.26058674	8.81E-19
Arf5	0.26045157	2.07E-22
Cox5b	0.26025886	1.35E-30
Rnf157	0.25990916	5.88E-20
Chrac1	0.25981791	1.31E-17
Fbxo2	0.2596899	1.04E-17
Mrpl23	0.25955091	8.43E-16
Trappc2	0.25858256	1.60E-14
Wasl	0.25847249	2.50E-21
Zfp706	0.25824314	5.20E-17
Vps28	0.25776747	4.01E-12
Ppp1cc	0.25772872	2.99E-16
Tmem229b	0.25754937	6.32E-11
Fkbp1a	0.25743026	6.19E-22
Lamtor5	0.25726489	3.90E-23
Crot	0.25689398	9.45E-23
C77080	0.25653784	1.23E-24
Dnajc19	0.25611277	2.99E-16
Armh4	0.2558164	6.63E-16
Ndufa3	0.25571742	3.68E-21
Pgk1	0.25568425	1.03E-20
Ndufs8	0.25561976	5.52E-18
Cbr1	0.25552717	5.35E-14
Eif1b	0.25542011	2.73E-32
Serpinb6a	0.2547914	3.11E-17

Parp1	0.25473208	6.55E-17
C1qbp	0.25466547	4.63E-18
Atp5c1	0.25444001	9.12E-23
Cend1	0.25405418	1.15E-31
Kras	0.25391761	6.12E-18
Tbcb	0.25306821	1.33E-21
Ccdc85b	0.25298844	2.57E-21
Rsrp1	0.25288639	3.27E-16
Tmem60	0.25285612	5.50E-16
B3gat3	0.2525	3.40E-17
Glyr1	0.25204768	1.87E-15
Gm16286	0.2520116	2.20E-17
Pdcd6	0.25175438	8.82E-18
Limch1	0.25162176	2.82E-13
Hsf4	0.25160896	1.59E-24
Slc25a3	0.25144416	9.30E-19
Fdx1	0.25132552	3.05E-17
Acbd6	0.25115106	1.42E-19
Cntfr	0.25110787	7.12E-17
Tpgs1	0.25082197	5.84E-16
Rpl6	0.2508198	1.35E-33
Rps10	0.25047626	2.86E-35
Mbnl2	-0.2500522	3.93E-35
Cdr2	-0.2501925	1.73E-16
Mfsd6	-0.2503844	1.47E-17
Hmgn3	-0.2505363	5.56E-26
Cbln4	-0.2505435	1.28E-36
Gm15543	-0.2506412	6.96E-32
Kif13a	-0.2515746	2.22E-19
Hipk2	-0.2516464	4.03E-20
Sorbs1	-0.2517726	2.08E-11
Fat3	-0.2524789	3.30E-10
Efhd2	-0.2529578	6.89E-17
Dtnb	-0.2532758	7.65E-15
Minar2	-0.2537572	1.05E-33
Chd9	-0.2538248	3.60E-18
Cpa6	-0.254024	5.16E-26
6430571L13Rik	-0.2540314	5.55E-29
Cntn5	-0.2541246	0.02096558

Klhl5	-0.2545028	1.62E-21
Vapa	-0.254664	1.24E-25
Smpx	-0.2548275	7.84E-16
Stmn1	-0.2550964	3.89E-12
Stat3	-0.2553643	8.63E-13
Lrp8	-0.2565603	2.09E-21
Rab11fip4	-0.2571963	1.45E-15
Rbfox2	-0.257268	3.08E-17
Flrt3	-0.2575258	2.62E-30
Phldb2	-0.2582977	8.12E-27
Arih1	-0.258494	1.05E-14
Fam168a	-0.2585756	3.01E-20
Fjx1	-0.2588828	1.26E-10
Sntg2	-0.2590372	3.98E-09
Cemip2	-0.2594583	3.21E-19
Gprasp1	-0.2610617	6.39E-24
AC149090.1	-0.2613822	4.36E-11
Hsp90ab1	-0.2615148	1.44E-62
Kcnk9	-0.261856	1.93E-19
Kcnk3	-0.2620354	1.05E-35
Grip1	-0.2623396	1.08E-09
Snx7	-0.2624045	9.94E-29
Zcchc17	-0.2625038	7.77E-15
Cblb	-0.262852	1.02E-18
Fosb	-0.2629527	6.73E-05
Sez6l	-0.2635993	1.05E-35
Sh3pxd2a	-0.2641357	1.78E-33
Snx10	-0.2652168	4.10E-21
Grxcr2	-0.2652366	4.06E-35
Clrn1	-0.2656482	3.90E-19
Rit2	-0.2659572	1.26E-16
A830018L16Rik	-0.2664229	1.04E-20
Mfhas1	-0.2679048	8.44E-19
Cxxc5	-0.2689912	6.22E-19
Plscr4	-0.2694555	3.71E-30
Lrtm2	-0.2700157	1.50E-40
Rev3l	-0.2700832	6.90E-12
Prrc2b	-0.2713753	5.10E-19
Khdrbs3	-0.2718129	3.87E-18

Syt7	-0.2719758	9.77E-22
Sgms1	-0.2720325	1.18E-23
Osbpl10	-0.2729046	4.66E-28
mt-Nd4	-0.273005	1.67E-48
Wwox	-0.2730112	9.63E-11
Id3	-0.2737617	7.41E-09
Rnf180	-0.2739247	4.54E-17
Ldlrad3	-0.274954	7.14E-18
Thra	-0.2756449	7.82E-18
Smap1	-0.2758074	6.61E-21
Gnaq	-0.2759661	1.74E-18
Lhx1os	-0.2762997	6.02E-09
Prkar2a	-0.2780503	9.16E-22
Rap1gap2	-0.278724	1.56E-15
Pitpnm3	-0.2810394	1.27E-35
Gadd45b	-0.2815397	1.61E-11
Sertm1	-0.2818441	7.61E-16
Dipk2a	-0.283173	1.70E-32
Trak1	-0.2832856	2.15E-19
6-Sep	-0.2836525	5.84E-21
Man1a2	-0.2839636	2.56E-22
Ext1	-0.2841499	2.44E-25
Ctnnbip1	-0.2847888	1.21E-24
Sik3	-0.2850643	8.53E-12
Arnt2	-0.2853997	7.90E-23
Dusp3	-0.2854044	2.99E-28
Ldb3	-0.2862738	1.31E-22
Ttyh2	-0.2864791	9.73E-30
Msi2	-0.2867997	3.28E-28
Ppm1h	-0.2869206	2.30E-17
Mbd5	-0.2869616	1.89E-20
Unc80	-0.2871265	8.03E-33
Eml6	-0.2871478	1.94E-19
Dok6	-0.2871493	6.81E-29
Snrk	-0.2877152	3.41E-23
Pou6f2	-0.2882855	2.62E-33
Osbpl1a	-0.2883109	5.92E-38
Kdm1a	-0.2887918	1.77E-26
Tpd52	-0.2890138	2.98E-28

Cep120	-0.2891537	1.53E-18
Gsk3b	-0.2892984	7.93E-34
Hivep3	-0.290177	1.04E-19
Jakmip2	-0.2903563	5.02E-12
B230219D22Rik	-0.2906359	1.40E-16
1700120C14Rik	-0.2907259	1.69E-29
Padi1	-0.2907259	2.87E-26
Smad7	-0.2907672	1.77E-35
Mb21d2	-0.2912051	3.03E-35
Gls	-0.2916268	3.21E-20
Glce	-0.2926694	1.61E-28
Ralgps2	-0.2929725	9.16E-24
Erc1	-0.2931668	6.72E-30
Ube2h	-0.2938077	5.72E-21
Fanca	-0.2939666	9.79E-39
Arid1b	-0.294092	4.39E-23
Jph4	-0.2941057	1.38E-24
Pakap.1	-0.2949261	1.18E-26
Ccdc162	-0.2978566	9.10E-20
Myo3b	-0.2985235	4.69E-42
Ctif	-0.298597	1.31E-21
Atp2c1	-0.2988478	2.50E-23
Myo6	-0.2993493	1.59E-19
Spock1	-0.2994182	2.33E-18
Zeb1	-0.2998512	5.68E-20
Phactr3	-0.3010709	2.98E-26
Zmynd8	-0.3012814	1.11E-24
Lrrtm4	-0.3014011	1.63E-07
Bach2	-0.3014131	1.24E-16
2900097C17Rik	-0.3014149	1.97E-42
Exoc4	-0.3014394	1.01E-23
Tmeff2	-0.3016735	1.10E-28
Tpbgl	-0.30201	6.98E-29
Lockd	-0.3027345	9.60E-35
Dscam	-0.3032642	3.89E-24
Uty	-0.3033508	3.28E-31
Pja2	-0.30519	9.99E-47
Pak3	-0.3058053	3.52E-20
Osbpl6	-0.3060204	3.33E-27

Stk39	-0.3064181	1.01E-29
Trnp1	-0.3085064	7.13E-38
Rps2	-0.3085114	5.26E-24
Cabp1	-0.3089288	6.21E-43
Ampd3	-0.3098121	2.02E-26
Pacs1	-0.3107218	1.94E-25
Spire1	-0.3115913	1.35E-22
Sgk1	-0.3120954	3.78E-17
Gm20631	-0.3126024	6.70E-42
Cdkn2d	-0.3138645	4.81E-22
Magi2	-0.3144777	1.27E-25
Ikzf2	-0.3147123	1.20E-43
Scn2a	-0.3148492	3.74E-26
Fbxl17	-0.3149274	2.53E-23
1700025G04Rik	-0.3155529	2.57E-22
Fkbp11	-0.3156418	3.16E-48
Sox11	-0.3157599	5.36E-16
Id2	-0.3158054	8.96E-23
Cpe	-0.3161021	4.16E-34
Npas3	-0.3162407	5.07E-11
Id4	-0.3166539	2.62E-40
Cxxc4	-0.3170642	1.43E-27
Kmt2a	-0.3173526	3.73E-26
Dock9	-0.317586	1.15E-26
Klf12	-0.3184081	7.57E-26
Kcnn2	-0.3191424	1.22E-14
Slk	-0.3192603	1.00E-29
Pex5l	-0.3200917	4.59E-28
Brinp2	-0.3203883	4.97E-25
Nudt4	-0.3218013	8.83E-34
Ankrd12	-0.3219084	5.77E-26
Prkag2	-0.322188	1.05E-29
A330015K06Rik	-0.3222597	2.98E-42
Chrdl1	-0.3228209	2.85E-40
Oasl2	-0.3236667	3.58E-32
Col24a1	-0.3237633	1.85E-34
Gprasp2	-0.3240574	1.85E-29
Crym	-0.3242392	1.31E-08
Gfod1	-0.3244571	6.99E-26

B3galt1	-0.3248814	1.81E-25
Zswim6	-0.3257305	2.87E-21
Sh3bgrl2	-0.3264388	7.41E-33
Nmt2	-0.3276437	1.91E-29
Cnr1	-0.3276565	5.50E-22
Phf14	-0.3278143	6.39E-30
Sgip1	-0.3284678	9.51E-32
Ptk7	-0.3285735	4.44E-39
Pcsk1	-0.3286216	2.46E-42
Fut8	-0.3289462	5.08E-29
Pawr	-0.3294422	2.32E-39
Hip1	-0.3295342	4.89E-19
Cacng5	-0.3298086	2.57E-47
Foxn3	-0.3300024	4.25E-22
Mtch1	-0.3301427	3.31E-31
Atp2b4	-0.3301957	7.28E-46
Abcd2	-0.330767	6.43E-28
Ahi1	-0.3314361	4.00E-26
Pirt	-0.3315131	5.34E-38
Slc44a1	-0.3324004	7.61E-39
Cadm3	-0.333292	2.09E-29
Ywhaq	-0.3344313	4.45E-41
Ptprn2	-0.334735	9.02E-32
Cacnb4	-0.3348099	2.47E-33
Epha5	-0.3348597	1.50E-24
Atp9a	-0.3353781	9.41E-34
Nyap2	-0.3369943	1.18E-38
Cmip	-0.3374225	2.51E-31
Agfg2	-0.3377164	7.61E-34
Plscr2	-0.3393044	1.52E-48
Atp8a1	-0.3393725	8.31E-25
Nrg2	-0.3404406	1.14E-27
mt-Atp8	-0.341498	3.82E-21
Ano6	-0.3418125	4.26E-33
Sptssb	-0.3419881	5.98E-46
Tnik	-0.3420399	4.10E-17
Adamts19	-0.3427627	3.44E-26
Rab15	-0.3436148	1.92E-30
Eml2	-0.3438757	1.18E-28

Zfand3	-0.34473	3.36E-33
Slitrk3	-0.3453445	1.14E-34
Gtf2ird1	-0.3473507	3.56E-25
Flrt1	-0.3480363	4.32E-48
Fmn1	-0.3484888	1.96E-20
Ralgapa2	-0.3485347	7.33E-27
Snap91	-0.3494043	1.05E-45
Nbea	-0.3499011	5.33E-27
Olfm2	-0.3500782	2.35E-38
Adamtsl1	-0.3501906	2.93E-24
Tmem25	-0.3514061	1.09E-32
Zfp608	-0.3514786	1.09E-27
Cask	-0.352289	2.13E-30
Ptprn	-0.3526029	4.47E-32
Tnni3k	-0.3552181	2.08E-48
Rbm20	-0.3564309	7.90E-33
Snx18	-0.3574678	9.13E-41
Kcnj3	-0.3576441	2.59E-27
Snhg11	-0.3584992	6.56E-43
Cadm2	-0.360288	1.59E-18
Tmod2	-0.360424	3.20E-42
Emb	-0.3609362	8.07E-37
Ddx3y	-0.3616038	3.42E-40
Tcerg1l	-0.362313	3.34E-27
Arglu1	-0.362548	9.11E-30
Chd3	-0.3631227	7.20E-33
Patj	-0.3642837	5.01E-44
11-Mar	-0.3655493	1.77E-32
Cited2	-0.3664874	8.05E-32
Scn2b	-0.3670518	3.01E-49
R3hdm2	-0.3683709	1.90E-37
Cd47	-0.3685013	3.98E-40
2900079G21Rik	-0.3689216	7.67E-30
Shank1	-0.3701143	7.42E-38
Malat1	-0.3723619	6.85E-75
Cadps	-0.3727056	1.04E-53
Syt4	-0.3732585	6.98E-36
Tmem164	-0.3743772	2.75E-51
Wwc1	-0.3760389	4.75E-53

Tmtc2	-0.3768538	3.61E-24
Acss2	-0.3774933	2.18E-37
Pcbp2	-0.3782639	1.58E-41
Efcab14	-0.3782869	1.51E-40
Adamts2	-0.3788782	7.77E-35
Smarca5	-0.3791087	2.97E-39
Dip2c	-0.380674	5.18E-40
Plod2	-0.3809612	1.25E-47
Pclo	-0.381578	3.20E-52
Agtpbp1	-0.3816021	4.55E-41
Slitrk5	-0.3821851	7.68E-61
Kcna2	-0.3823304	4.76E-54
Dlg2	-0.3825727	4.46E-38
Rarb	-0.3832564	3.71E-31
Ptprs	-0.3838232	4.47E-35
Fam155a	-0.3846795	2.51E-23
AI504432	-0.385193	5.22E-58
Klf7	-0.3860011	1.05E-35
Zmiz1	-0.3863155	1.47E-41
App	-0.3863941	1.37E-67
Pde4dip	-0.3866423	1.08E-52
Gpam	-0.3872152	1.16E-48
Trim36	-0.3880812	9.44E-43
Gata3	-0.3881704	1.89E-37
Nxn	-0.3886791	1.39E-44
Rprm	-0.3900551	5.32E-54
Eea1	-0.3900861	7.61E-39
Nectin3	-0.3901277	9.59E-55
Mmp16	-0.3901407	2.07E-45
Camk1d	-0.3909416	3.17E-10
Homer2	-0.3917694	3.79E-32
Scn1a	-0.3919761	2.46E-62
Fibin	-0.3931274	2.19E-58
Syn2	-0.3940373	5.41E-37
11-Sep	-0.3947551	4.74E-52
Agbl4	-0.395051	6.65E-36
Chd7	-0.3962603	1.31E-51
Gnb5	-0.3970793	3.79E-56
Thsd7a	-0.3972387	1.52E-32

Hgf	-0.3976245	9.94E-31
mt-Nd2	-0.3989061	1.69E-68
Map4	-0.4013724	7.15E-58
Csmd3	-0.4021912	2.84E-37
Hmbox1	-0.4026866	1.70E-45
Pura	-0.4046359	2.52E-64
Dpp10	-0.4054009	1.06E-51
Nav1	-0.4060603	2.37E-45
D130079A08Rik	-0.4065013	6.87E-23
Zeb2	-0.4066341	3.52E-38
Twf2	-0.4068075	3.41E-56
Srcin1	-0.4076851	8.83E-44
Otud7a	-0.4078856	3.10E-35
Kcnma1	-0.4093164	6.41E-51
Stat1	-0.4097505	6.44E-42
Eya1	-0.4107781	5.73E-21
Rapgef2	-0.4143319	2.39E-37
Auts2	-0.4155029	4.28E-41
Gm45321	-0.4155064	7.44E-50
Srl	-0.4163948	8.09E-61
Dab2ip	-0.4164599	3.84E-70
Serf1	-0.4179746	1.41E-44
Grid2	-0.4202705	1.54E-32
Hk1	-0.421102	1.40E-55
Xkr6	-0.4218497	1.31E-41
Csrnp3	-0.4227989	1.91E-41
Ppp1r12a	-0.4229894	1.08E-41
Casz1	-0.4235601	4.95E-35
Il1rapl1	-0.4240802	5.21E-25
Ralyl	-0.426602	4.04E-54
Camk2b	-0.4270763	6.01E-41
Meg3	-0.4273655	4.11E-66
Clec18a	-0.4277959	8.62E-51
Acsl1	-0.4283643	5.79E-41
Sv2a	-0.4290137	4.63E-63
Nalcn	-0.4309614	4.99E-46
Camta1	-0.4310786	1.34E-82
Cdh12	-0.4314684	3.90E-47
Rbms1	-0.4325785	5.59E-41

Jmjd1c	-0.4329373	2.77E-25
Ptp4a2	-0.4333005	5.79E-49
Prr16	-0.4346117	3.88E-56
Dock10	-0.4347344	9.00E-33
Astn1	-0.4359336	9.79E-47
Rapgef6	-0.4363377	3.08E-24
Trhde	-0.4368388	4.73E-36
Ttc19	-0.4379038	1.77E-56
Dlgap1	-0.4379462	9.72E-42
Ntng1	-0.4384128	5.32E-17
Nuak1	-0.4402675	9.11E-46
Dusp26	-0.4403828	4.27E-61
Shisal1	-0.4411787	1.27E-76
Napb	-0.4433396	4.83E-83
Celf2	-0.4440134	2.56E-45
L1cam	-0.4449863	5.24E-55
Gm2516	-0.4452187	2.81E-59
Cap2	-0.4465848	6.93E-48
Grtp1	-0.4471543	3.26E-50
Sgcz	-0.4487554	1.32E-08
Amer2	-0.4492977	1.87E-51
Nfib	-0.4495791	1.88E-40
Pkia	-0.4517306	4.02E-40
Prkd1	-0.4522684	4.26E-49
Plppr4	-0.4523046	4.93E-31
Grm8	-0.4545936	1.13E-35
Plce1	-0.4574344	6.98E-53
Gabrb3	-0.4575793	3.18E-45
Msrb3	-0.4585038	1.92E-53
Brinp1	-0.4592701	7.24E-37
Ccser1	-0.4594849	3.11E-49
Ptprm	-0.4598605	2.42E-33
Stxbp5l	-0.4623056	1.18E-41
Ntrk2	-0.4625058	2.00E-57
Uvrag	-0.4630018	1.57E-47
Cux2	-0.4646577	1.83E-57
Nsg2	-0.4669432	5.60E-79
Cyld	-0.4673309	6.47E-52
Samd5	-0.4678524	6.02E-54

Csnk1g3	-0.4679453	3.94E-61
Csmd2	-0.4679738	8.96E-47
Nbeal1	-0.4691392	3.99E-58
Myt1l	-0.4692397	2.86E-61
Cdh4	-0.4693099	6.15E-34
Acsl3	-0.4708253	2.19E-52
Pbx3	-0.4708455	8.17E-48
Eya4	-0.4712331	1.85E-54
Prkg2	-0.4715718	4.26E-61
Fam126a	-0.4716677	1.19E-37
Pcbp3	-0.4719382	3.77E-64
Igsf21	-0.4722892	1.51E-82
Ppfia2	-0.4726007	2.19E-48
Nlgn1	-0.4726702	2.08E-30
Ryr2	-0.472775	7.69E-49
Samd12	-0.4766337	4.31E-44
Hs3st2	-0.4773233	2.03E-51
Sulf2	-0.4844243	1.91E-65
Zbtb20	-0.4869196	1.44E-68
Slc2a13	-0.4874601	7.29E-44
Nedd4l	-0.4897469	7.36E-74
Dtna	-0.4899031	6.17E-41
Mtcl1	-0.4902844	3.83E-58
Kcna6	-0.4904929	1.82E-75
Pid1	-0.490529	4.20E-71
Zfhx4	-0.4909865	2.20E-58
Slit3	-0.4919125	4.41E-33
Tmem151b	-0.4933328	2.34E-75
Anp32b	-0.4937157	2.01E-57
Arid5b	-0.4937768	7.86E-31
Srgap1	-0.494952	6.28E-56
Chst8	-0.4956245	5.36E-52
Panx1	-0.4989866	6.27E-68
Junb	-0.4995481	6.13E-40
Man2a1	-0.5006229	2.08E-48
Nrxn2	-0.5008492	2.13E-68
Jun	-0.5010496	6.59E-22
Bdnf	-0.5011753	1.04E-62
Tbc1d8	-0.5041276	5.80E-63

Gm42372	-0.5060057	3.10E-62
Avil	-0.5073486	4.63E-61
Itga4	-0.5083133	2.69E-82
Itsn1	-0.5104591	7.70E-75
Kcnip2	-0.5116402	1.28E-67
Cadm1	-0.5123724	1.80E-83
Uchl1	-0.51324	6.53E-61
Utrn	-0.515649	1.63E-56
Cfap161	-0.5200493	2.26E-54
Pik3r3	-0.5202344	4.81E-39
Ttll7	-0.5203754	1.71E-118
Lypd6b	-0.5217912	4.06E-70
Zfp365	-0.5219169	1.29E-80
Pbx1	-0.5223223	5.70E-54
mt-Nd3	-0.5224342	3.37E-71
Art1	-0.5232217	2.92E-89
Ptma	-0.5238359	1.12E-51
Sdk2	-0.5238402	3.99E-49
Atp2b1	-0.5246092	6.53E-70
Gm45341	-0.5275048	2.89E-57
Mapt	-0.5280793	4.28E-90
Ifit1	-0.533639	6.05E-21
Runx1t1	-0.5338978	3.88E-81
Nebl	-0.5352982	5.22E-74
Tanc2	-0.5367551	1.68E-44
Arl15	-0.5399848	3.85E-55
Pdcd4	-0.542545	6.61E-73
Zfp536	-0.5455642	4.64E-61
A230057D06Rik	-0.5461916	3.84E-58
Cers6	-0.5479644	1.00E-76
Atp11a	-0.551062	2.98E-102
Sptb	-0.5526527	2.16E-68
Ust	-0.5550876	1.09E-96
1500004A13Rik	-0.5552498	6.07E-81
Cacna2d1	-0.5591108	1.47E-80
Usp25	-0.5591989	2.45E-70
Arhgap21	-0.5605956	1.47E-42
Mcu	-0.5607607	1.31E-82
Myo5b	-0.5705112	2.92E-81

Ctnna3	-0.5715016	3.66E-40
Dock3	-0.5720368	3.01E-91
Sv2b	-0.5723194	1.24E-80
Nrcam	-0.5729737	8.81E-85
Acbd7	-0.5749211	2.02E-76
Ctnnd2	-0.5785131	1.32E-99
Cacna2d3	-0.5786258	8.27E-92
C530008M17Rik	-0.5821142	4.48E-40
Dgkz	-0.5841468	2.44E-104
Rgs7	-0.5842008	8.13E-63
Tmem117	-0.5866449	2.24E-65
Pou4f1	-0.5867098	4.85E-76
Fgf13	-0.5875385	1.09E-75
Lrrc3b	-0.5877236	2.18E-103
D430041D05Rik	-0.5881891	2.62E-79
Plcd4	-0.590674	1.31E-77
Aopep	-0.5959258	5.62E-65
Pde4d	-0.5995668	8.18E-128
4930555F03Rik	-0.6011412	2.11E-69
Tln2	-0.6017905	1.34E-90
Srgap3	-0.6069353	6.14E-99
Ptms	-0.6085913	5.61E-88
Plxna4	-0.6126838	1.03E-75
Vamp2	-0.6140063	1.19E-106
Kctd1	-0.6157953	1.49E-86
Mpdz	-0.6175976	9.67E-110
Glis1	-0.620515	1.16E-65
Gpc6	-0.6222326	1.28E-81
Pkp4	-0.6233711	1.89E-91
Grik2	-0.6248736	1.84E-81
Lrfn5	-0.6257257	1.17E-87
Cyth3	-0.630581	1.24E-94
Atxn1	-0.6323978	1.57E-76
Parp8	-0.633259	5.81E-82
Fam227b	-0.6338721	2.81E-85
Slc10a7	-0.6339213	1.47E-86
Arf3	-0.6340828	2.09E-108
Slc35f4	-0.6344829	2.68E-79
Kitl	-0.6361859	1.89E-80

Kctd16	-0.6399083	9.29E-52
Tspan2	-0.6407397	1.36E-111
Rims4	-0.6432468	7.83E-90
Tmem47	-0.6444335	3.31E-73
Pdgfa	-0.6446973	5.00E-74
Rims3	-0.6456198	6.98E-70
Maml2	-0.6494012	2.28E-63
Nrn1	-0.6520108	3.14E-129
Frmd4a	-0.652713	2.42E-101
Ptpn5	-0.655686	3.30E-112
Pdk3	-0.6569002	1.44E-105
Zfp385b	-0.6591123	1.61E-101
Slc17a6	-0.6592947	5.30E-76
Dner	-0.660143	5.12E-125
Nme7	-0.6615068	4.57E-71
Plekha5	-0.6639796	2.96E-97
Phyhipl	-0.6645504	7.15E-108
Zfp521	-0.6806332	1.45E-87
Gm45323	-0.6828369	1.43E-83
Dock11	-0.6846915	1.40E-112
Rnf150	-0.6853192	2.70E-92
Phactr1	-0.6869566	1.47E-87
Cachd1	-0.6893862	6.54E-109
Fry	-0.690262	4.86E-106
Elmod1	-0.692518	1.55E-108
Adgrb3	-0.6956542	1.78E-62
Rab31	-0.6964497	1.02E-96
Kif21a	-0.7023995	1.22E-138
Kank1	-0.7024626	2.99E-108
Slc9a9	-0.7027541	1.53E-92
Cpne9	-0.7055884	7.89E-28
Cit	-0.7098249	2.32E-77
Mtus2	-0.7099371	1.32E-90
Nav3	-0.7101307	2.10E-104
Farp1	-0.7106122	4.45E-105
Lpin2	-0.7150257	1.14E-93
Cdk14	-0.7163444	4.69E-86
Sel1l3	-0.7250867	1.89E-133
Zfp462	-0.7253788	1.02E-106

Nrg3	-0.726363	1.57E-132
Onecut2	-0.7295831	2.98E-117
Scoc	-0.7296161	9.03E-150
Hivep2	-0.735613	2.61E-106
Bcl11a	-0.7363852	2.74E-116
Dach1	-0.73723	1.45E-89
Prkar2b	-0.7404225	9.03E-94
Ptprg	-0.74191	1.02E-108
Rasgef1b	-0.7431534	2.81E-113
Actn2	-0.7432172	2.03E-89
Cdkn1b	-0.7460107	9.68E-113
Dgki	-0.7466168	1.23E-96
Kif2a	-0.7498225	3.85E-128
Crim1	-0.7586709	4.00E-106
Epha3	-0.7606322	1.47E-91
Grxcr1	-0.7637167	1.32E-130
Elavl2	-0.7658255	1.32E-141
Rgs7bp	-0.7669835	4.07E-146
Pcp4l1	-0.7699908	2.69E-108
Insyn1	-0.7703675	1.34E-121
Nrxn1	-0.7714597	4.91E-151
Adgrl3	-0.7720746	1.38E-128
Unc5d	-0.774451	1.28E-86
Pcsk5	-0.7775284	8.46E-97
Anks1b	-0.7828873	2.86E-110
Angpt1	-0.7862884	1.12E-125
Slit2	-0.7934909	1.18E-76
Ppp3ca	-0.7985513	2.01E-131
Tenm2	-0.7989094	9.94E-93
Lrrtm3	-0.799999	6.18E-84
Kalrn	-0.8011593	1.85E-137
Xylt1	-0.8089614	1.99E-140
Col27a1	-0.8102459	7.50E-110
Dgkb	-0.8112978	7.28E-55
Celf4	-0.8126972	4.42E-135
Tenm3	-0.8258254	2.82E-102
Cacna1e	-0.8275996	3.29E-158
Foxp1	-0.8288758	4.06E-161
Serpini1	-0.8301081	1.74E-117

Ctnna2	-0.8355327	2.94E-141
Dnm3	-0.8366884	6.12E-147
Prkcb	-0.837725	5.07E-156
Pde10a	-0.8442124	2.10E-93
Grik4	-0.8455828	2.65E-116
Runx1	-0.8486233	1.77E-118
Scn3a	-0.8523817	2.40E-140
Sntg1	-0.8688631	3.31E-29
Mrvi1	-0.8769647	3.03E-160
Egr1	-0.8832476	1.01E-64
Macrod2	-0.9019288	8.79E-127
Lingo2	-0.9043875	2.21E-70
Rasgrf1	-0.9051097	2.73E-80
Nav2	-0.919352	3.53E-149
Tafa5	-0.9260733	1.41E-172
Frmpd1	-0.9331285	1.00E-156
Plxna2	-0.9431715	6.75E-172
Lgr5	-0.9505529	1.84E-115
Slc4a4	-0.9512219	1.08E-153
Epha7	-0.9525577	5.51E-140
Schip1	-0.9599374	5.14E-59
Mdga2	-0.9641745	1.70E-132
Ifi27	-0.9650174	4.17E-87
Slc35f3	-0.9693242	6.20E-173
Fos	-0.975314	3.25E-71
Ubash3b	-0.9843022	3.88E-162
Akap6	-0.9933825	4.85E-138
Etv1	-0.9941341	1.31E-170
Hdac9	-1.0123208	5.65E-157
Arpp21	-1.0134631	1.80E-154
Plcxd3	-1.0160376	5.24E-168
Plcb4	-1.0453531	2.15E-185
Tenm4	-1.0517026	9.80E-209
C130073E24Rik	-1.0558292	9.06E-151
Ncald	-1.062543	4.93E-210
Pcsk2	-1.062723	6.97E-136
Casq1	-1.069165	1.64E-205
Oxr1	-1.0717383	3.55E-201
Enox1	-1.0778751	4.06E-179

Kirrel3	-1.0840014	1.42E-123
Ptprq	-1.0908983	7.36E-141
Tmem178b	-1.0932548	2.02E-178
Galnt13	-1.0949733	3.34E-144
Robo1	-1.0951097	4.77E-138
Vav3	-1.1163589	4.47E-144
Ntrk3	-1.1212904	1.49E-208
Adgrl2	-1.1228997	2.16E-170
Plcxd2	-1.1263095	2.58E-207
Opcml	-1.1279564	5.93E-154
Lgals1	-1.1308393	1.46E-109
Erc2	-1.1386652	1.02E-201
Rbms3	-1.166212	2.69E-207
Mef2c	-1.1782068	4.48E-205
Alcam	-1.1782596	7.33E-210
Tcap	-1.1802294	1.24E-126
Magi1	-1.1816499	1.95E-198
Fgf1	-1.2015947	1.61E-199
Lypd6	-1.2087197	8.88E-240
Lifr	-1.2298532	3.81E-218
Prkce	-1.2317142	1.21E-202
Cntnap5c	-1.2546799	8.35E-171
Mlf1	-1.2596437	2.76E-149
Unc5c	-1.2621481	3.71E-173
D130009I18Rik	-1.2815039	4.95E-61
Shisa8	-1.284759	6.51E-240
Prkg1	-1.3018349	2.30E-189
Sorbs2	-1.3411187	1.25E-231
Ncam2	-1.343874	6.60E-200
Cacna1c	-1.3586613	1.47E-242
Ndst4	-1.3711436	1.46E-155
Sphkap	-1.4070902	4.83E-131
Sipa1l1	-1.4277752	5.79E-252
Chrm3	-1.4297441	7.89E-166
Syt1	-1.4730532	2.82E-216
Clstn2	-1.5483283	5.25E-243
Pde4b	-1.5724962	8.43E-181
Ebf1	-1.5799461	4.61E-230
Sncg	-1.6001054	7.37E-231

Rgs17	-1.6799446	1.37E-202
Ptprd	-1.7661052	2.00E-245
Gm30382	-1.7763178	5.42E-186
Cplx2	-1.7867999	2.90E-202
Thsd7b	-1.8076663	2.49E-246
Kcnab1	-1.833816	2.79E-276
Kcnh7	-1.8916771	6.59E-234
Chst9	-1.9089988	1.89E-180
Hmcn1	-1.9149805	2.63E-259
Inpp4b	-2.0031327	9.45E-288
Rph3a	-2.0039053	5.43E-268
Kcnc2	-2.0047295	4.82E-230
Crtac1	-2.0684752	5.46E-292
Sema3a	-2.1078204	5.09E-278
Kcnd2	-2.1780624	2.05E-250
Kcnip4	-2.1886783	1.02E-175
Pcdh9	-2.4081854	3.11E-251
Kcnb2	-3.0615438	6.43E-285
Dpp6	-3.1605418	5.00E-269

Table S4.8. Gene ontology results from all differentially expressed genes in dKO SGNs.

GO process	Mus musculus - REFLIST (21997)	N cMaf/ Mafb genes	Expected Proportion	Fold Enrichment	False Discovery Rate
regulation of mitochondrial electron transport, NADH to ubiquinone (GO:1902956)	4	4	0.22	18.09	1.35E-02
retrograde trans-synaptic signaling by trans-synaptic protein complex (GO:0098942)	5	4	0.28	14.47	2.12E-02
presynaptic active zone organization (GO:1990709)	6	4	0.33	12.06	3.11E-02
heparin biosynthetic process (GO:0030210)	6	4	0.33	12.06	3.10E-02
synaptic vesicle clustering (GO:0097091)	9	6	0.5	12.06	2.74E-03
regulation of relaxation of cardiac muscle (GO:1901897)	8	5	0.44	11.31	1.11E-02

retrograde trans-synaptic signaling (GO:0098917)	10	6	0.55	10.85	3.91E-03
regulation of synaptic vesicle membrane organization (GO:1901632)	11	6	0.61	9.87	5.53E-03
trans-synaptic signaling by trans-synaptic complex (GO:0099545)	11	6	0.61	9.87	5.51E-03
regulation of synaptic vesicle fusion to presynaptic active zone membrane (GO:0031630)	11	6	0.61	9.87	5.50E-03
synaptic membrane adhesion (GO:0099560)	28	15	1.55	9.69	2.30E-07
mitochondrial electron transport, NADH to ubiquinone (GO:0006120)	26	13	1.44	9.04	3.81E-06
cellular response to epinephrine stimulus (GO:0071872)	10	5	0.55	9.04	2.12E-02
response to epinephrine (GO:0071871)	10	5	0.55	9.04	2.11E-02
neuron projection maintenance (GO:1990535)	10	5	0.55	9.04	2.11E-02
negative regulation of collateral sprouting (GO:0048671)	10	5	0.55	9.04	2.10E-02
modification of postsynaptic actin cytoskeleton (GO:0098885)	10	5	0.55	9.04	2.10E-02
maintenance of synapse structure (GO:0099558)	21	10	1.16	8.61	1.40E-04
synapse maturation (GO:0060074)	19	9	1.05	8.57	4.12E-04
peripheral nervous system neuron development (GO:0048935)	13	6	0.72	8.35	9.91E-03
peripheral nervous system neuron differentiation (GO:0048934)	13	6	0.72	8.35	9.89E-03
neuronal action potential propagation (GO:0019227)	11	5	0.61	8.22	2.74E-02
glutamate secretion (GO:0014047)	11	5	0.61	8.22	2.74E-02
action potential propagation (GO:0098870)	11	5	0.61	8.22	2.73E-02
regulation of postsynaptic density assembly (GO:0099151)	14	6	0.77	7.75	1.29E-02
regulation of postsynaptic density organization (GO:1905874)	19	8	1.05	7.62	2.10E-03
negative regulation of amyloid fibril formation (GO:1905907)	12	5	0.66	7.54	3.53E-02
membrane depolarization during cardiac muscle cell action potential (GO:0086012)	12	5	0.66	7.54	3.52E-02
proton motive force-driven mitochondrial ATP synthesis (GO:0042776)	62	25	3.43	7.29	2.72E-10
proton motive force-driven ATP synthesis (GO:0015986)	67	27	3.7	7.29	3.95E-11

heterophilic cell-cell adhesion via plasma membrane cell adhesion molecules (GO:0007157)	50	20	2.76	7.24	3.63E-08
regulation of amyloid fibril formation (GO:1905906)	15	6	0.83	7.24	1.63E-02
presynapse assembly (GO:0099054)	20	8	1.11	7.24	2.72E-03
negative regulation of mitochondrial membrane potential (GO:0010917)	15	6	0.83	7.24	1.63E-02
neurotransmitter-gated ion channel clustering (GO:0072578)	15	6	0.83	7.24	1.62E-02
regulation of presynapse assembly (GO:1905606)	38	15	2.1	7.14	4.19E-06
regulation of modification of postsynaptic structure (GO:0099159)	13	5	0.72	6.96	4.52E-02
regulation of dendritic spine maintenance (GO:1902950)	13	5	0.72	6.96	4.51E-02
regulation of presynapse organization (GO:0099174)	42	16	2.32	6.89	2.42E-06
dendritic spine morphogenesis (GO:0060997)	21	8	1.16	6.89	3.44E-03
regulation of cAMP-dependent protein kinase activity (GO:2000479)	16	6	0.88	6.78	2.08E-02
dendrite self-avoidance (GO:0070593)	16	6	0.88	6.78	2.08E-02
positive regulation of synaptic vesicle recycling (GO:1903423)	16	6	0.88	6.78	2.08E-02
aerobic electron transport chain (GO:0019646)	54	20	2.99	6.7	9.96E-08
vocalization behavior (GO:0071625)	22	8	1.22	6.58	4.26E-03
presynapse organization (GO:0099172)	25	9	1.38	6.51	1.96E-03
regulation of excitatory synapse assembly (GO:1904889)	17	6	0.94	6.38	2.52E-02
postsynaptic density organization (GO:0097106)	20	7	1.11	6.33	1.16E-02
ATP biosynthetic process (GO:0006754)	83	29	4.59	6.32	9.00E-11
oxidative phosphorylation (GO:0006119)	105	35	5.8	6.03	1.42E-12
mitochondrial ATP synthesis coupled electron transport (GO:0042775)	63	21	3.48	6.03	1.67E-07
positive regulation of CREB transcription factor activity (GO:0032793)	18	6	1	6.03	3.11E-02
regulation of postsynaptic specialization assembly (GO:0099150)	18	6	1	6.03	3.11E-02
regulation of relaxation of muscle (GO:1901077)	18	6	1	6.03	3.10E-02
positive regulation of synapse assembly (GO:0051965)	80	26	4.42	5.88	4.46E-09
ATP synthesis coupled electron transport (GO:0042773)	65	21	3.59	5.84	2.52E-07

regulation of synaptic vesicle recycling (GO:1903421)	31	10	1.71	5.84	1.65E-03
heparan sulfate proteoglycan biosynthetic process (GO:0015012)	25	8	1.38	5.79	8.11E-03
membrane depolarization during action potential (GO:0086010)	25	8	1.38	5.79	8.09E-03
purine ribonucleoside triphosphate biosynthetic process (GO:0009206)	94	30	5.2	5.77	2.31E-10
postsynaptic specialization organization (GO:0099084)	22	7	1.22	5.76	1.72E-02
regulation of synaptic vesicle endocytosis (GO:1900242)	22	7	1.22	5.76	1.72E-02
retrograde axonal transport (GO:0008090)	22	7	1.22	5.76	1.72E-02
positive regulation of intracellular steroid hormone receptor signaling pathway (GO:0033145)	19	6	1.05	5.71	3.74E-02
purine nucleoside triphosphate biosynthetic process (GO:0009145)	95	30	5.25	5.71	2.82E-10
negative regulation of membrane potential (GO:0045837)	19	6	1.05	5.71	3.74E-02
NADH dehydrogenase complex assembly (GO:0010257)	57	18	3.15	5.71	3.50E-06
mitochondrial respiratory chain complex I assembly (GO:0032981)	57	18	3.15	5.71	3.48E-06
neuron projection organization (GO:0106027)	51	16	2.82	5.68	1.75E-05
regulation of synapse assembly (GO:0051963)	122	38	6.74	5.63	6.19E-13
clathrin-dependent endocytosis (GO:0072583)	29	9	1.6	5.61	4.34E-03
ribonucleoside triphosphate biosynthetic process (GO:0009201)	99	30	5.47	5.48	6.50E-10
synapse assembly (GO:0007416)	93	28	5.14	5.45	3.53E-09
positive regulation of mitochondrial fission (GO:0090141)	20	6	1.11	5.43	4.53E-02
axon regeneration (GO:0031103)	20	6	1.11	5.43	4.52E-02
regulation of vesicle fusion (GO:0031338)	27	8	1.49	5.36	1.15E-02
neuron recognition (GO:0008038)	51	15	2.82	5.32	7.53E-05
dendritic spine development (GO:0060996)	38	11	2.1	5.24	1.58E-03
respiratory electron transport chain (GO:0022904)	87	25	4.81	5.2	7.13E-08
regulation of neuron migration (GO:2001222)	57	16	3.15	5.08	5.77E-05
walking behavior (GO:0090659)	50	14	2.76	5.07	2.43E-04
adult walking behavior (GO:0007628)	47	13	2.6	5	5.41E-04

circadian behavior (GO:0048512)	29	8	1.6	4.99	1.60E-02
regulation of synaptic vesicle exocytosis (GO:2000300)	84	23	4.64	4.95	5.65E-07
nucleoside triphosphate biosynthetic process (GO:0009142)	110	30	6.08	4.93	5.25E-09
aerobic respiration (GO:0009060)	144	39	7.96	4.9	1.03E-11
regulation of protein localization to synapse (GO:1902473)	26	7	1.44	4.87	3.42E-02
neurotransmitter secretion (GO:0007269)	90	24	4.98	4.82	4.24E-07
signal release from synapse (GO:0099643)	90	24	4.98	4.82	4.22E-07
regulation of synapse organization (GO:0050807)	263	70	14.54	4.81	6.82E-21
regulation of synapse structure or activity (GO:0050803)	271	72	14.98	4.81	1.90E-21
electron transport chain (GO:0022900)	98	26	5.42	4.8	1.26E-07
dendrite morphogenesis (GO:0048813)	80	21	4.42	4.75	3.96E-06
regulation of dopamine secretion (GO:0014059)	42	11	2.32	4.74	3.10E-03
negative chemotaxis (GO:0050919)	42	11	2.32	4.74	3.09E-03
regulation of postsynapse organization (GO:0099175)	111	29	6.14	4.73	2.27E-08
chemical synaptic transmission, postsynaptic (GO:0099565)	50	13	2.76	4.7	8.98E-04
innervation (GO:0060384)	31	8	1.71	4.67	2.20E-02
cell differentiation in hindbrain (GO:0021533)	31	8	1.71	4.67	2.20E-02
cardiac muscle cell action potential involved in contraction (GO:0086002)	31	8	1.71	4.67	2.20E-02
regulation of dendrite extension (GO:1903859)	31	8	1.71	4.67	2.19E-02
heparan sulfate proteoglycan metabolic process (GO:0030201)	35	9	1.93	4.65	1.20E-02
positive regulation of axonogenesis (GO:0050772)	98	25	5.42	4.61	4.31E-07
positive regulation of axon extension (GO:0045773)	52	13	2.87	4.52	1.24E-03
action potential (GO:0001508)	96	24	5.31	4.52	1.12E-06
regulation of NMDA receptor activity (GO:2000310)	28	7	1.55	4.52	4.65E-02
neuron projection regeneration (GO:0031102)	28	7	1.55	4.52	4.65E-02
cardiac muscle cell action potential (GO:0086001)	36	9	1.99	4.52	1.39E-02
rhythmic behavior (GO:0007622)	32	8	1.77	4.52	2.52E-02

dendritic spine organization (GO:0097061)	40	10	2.21	4.52	7.79E-03
cell-cell adhesion via plasma-membrane adhesion molecules (GO:0098742)	197	49	10.89	4.5	1.28E-13
receptor clustering (GO:0043113)	61	15	3.37	4.45	4.03E-04
synapse organization (GO:0050808)	315	77	17.41	4.42	3.57E-21
cell junction maintenance (GO:0034331)	45	11	2.49	4.42	4.77E-03
excitatory postsynaptic potential (GO:0060079)	41	10	2.27	4.41	8.92E-03
cardiac muscle cell contraction (GO:0086003)	37	9	2.05	4.4	1.60E-02
cerebellar cortex formation (GO:0021697)	33	8	1.82	4.39	2.91E-02
regulation of neurotransmitter secretion (GO:0046928)	122	29	6.74	4.3	1.25E-07
synaptic vesicle exocytosis (GO:0016079)	59	14	3.26	4.29	1.03E-03
regulation of potassium ion transmembrane transport (GO:1901379)	93	22	5.14	4.28	8.36E-06
neuron projection extension (GO:1990138)	85	20	4.7	4.26	3.02E-05
protein localization to synapse (GO:0035418)	68	16	3.76	4.26	3.37E-04
dendrite development (GO:0016358)	145	34	8.02	4.24	8.49E-09
cellular respiration (GO:0045333)	176	41	9.73	4.21	1.38E-10
regulation of synaptic transmission, GABAergic (GO:0032228)	43	10	2.38	4.21	1.16E-02
regulation of dendritic spine morphogenesis (GO:0061001)	56	13	3.1	4.2	2.16E-03
positive regulation of cell junction assembly (GO:1901890)	125	29	6.91	4.2	1.91E-07
neuromuscular process controlling balance (GO:0050885)	69	16	3.81	4.19	3.89E-04
adult locomotory behavior (GO:0008344)	108	25	5.97	4.19	1.98E-06
transmission of nerve impulse (GO:0019226)	78	18	4.31	4.17	1.28E-04
axon extension (GO:0048675)	52	12	2.87	4.17	3.98E-03
regulation of postsynaptic membrane potential (GO:0060078)	65	15	3.59	4.17	7.38E-04
neuronal action potential (GO:0019228)	44	10	2.43	4.11	1.33E-02
synaptic transmission, glutamatergic (GO:0035249)	44	10	2.43	4.11	1.33E-02
mitochondrial respiratory chain complex assembly (GO:0033108)	93	21	5.14	4.08	2.83E-05
postsynapse organization (GO:0099173)	102	23	5.64	4.08	8.99E-06

homophilic cell adhesion via plasma membrane adhesion molecules (GO:0007156)	111	25	6.14	4.07	3.03E-06
ATP metabolic process (GO:0046034)	160	36	8.84	4.07	6.39E-09
regulation of calcineurin-NFAT signaling cascade (GO:0070884)	40	9	2.21	4.07	2.40E-02
calcium-ion regulated exocytosis (GO:0017156)	49	11	2.71	4.06	8.41E-03
cerebellar cortex morphogenesis (GO:0021696)	45	10	2.49	4.02	1.51E-02
glycosaminoglycan biosynthetic process (GO:0006024)	45	10	2.49	4.02	1.50E-02
regulation of long-term neuronal synaptic plasticity (GO:0048169)	36	8	1.99	4.02	4.38E-02
neurotransmitter transport (GO:0006836)	136	30	7.52	3.99	2.68E-07
synaptic vesicle recycling (GO:0036465)	68	15	3.76	3.99	1.10E-03
presynaptic endocytosis (GO:0140238)	59	13	3.26	3.99	3.26E-03
synaptic vesicle endocytosis (GO:0048488)	59	13	3.26	3.99	3.25E-03
regulation of calcineurin-mediated signaling (GO:0106056)	41	9	2.27	3.97	2.70E-02
regulation of microtubule polymerization (GO:0031113)	55	12	3.04	3.95	5.96E-03
vesicle-mediated transport in synapse (GO:0099003)	147	32	8.13	3.94	1.18E-07
multicellular organismal signaling (GO:0035637)	129	28	7.13	3.93	1.04E-06
regulation of cell junction assembly (GO:1901888)	222	48	12.27	3.91	1.86E-11
regulation of neurotransmitter transport (GO:0051588)	139	30	7.68	3.9	3.91E-07
regulation of axonogenesis (GO:0050770)	181	39	10.01	3.9	3.31E-09
purine ribonucleotide biosynthetic process (GO:0009152)	172	37	9.51	3.89	1.02E-08
regulation of dendrite morphogenesis (GO:0048814)	93	20	5.14	3.89	9.40E-05
positive regulation of potassium ion transport (GO:0043268)	52	11	2.87	3.83	1.20E-02
synaptic vesicle cycle (GO:0099504)	133	28	7.35	3.81	1.75E-06
regulation of potassium ion transport (GO:0043266)	114	24	6.3	3.81	1.40E-05
purine nucleotide biosynthetic process (GO:0006164)	181	38	10.01	3.8	1.02E-08
olfactory lobe development (GO:0021988)	43	9	2.38	3.79	3.44E-02
receptor localization to synapse (GO:0097120)	53	11	2.93	3.75	1.36E-02

developmental cell growth (GO:0048588)	121	25	6.69	3.74	1.09E-05
ribonucleotide biosynthetic process (GO:0009260)	184	38	10.17	3.74	1.50E-08
regulation of neuronal synaptic plasticity (GO:0048168)	73	15	4.04	3.72	2.05E-03
cell growth (GO:0016049)	127	26	7.02	3.7	7.65E-06
cellular response to retinoic acid (GO:0071300)	44	9	2.43	3.7	3.88E-02
phospholipid translocation (GO:0045332)	49	10	2.71	3.69	2.42E-02
positive regulation of calcium ion transmembrane transporter activity (GO:1901021)	49	10	2.71	3.69	2.42E-02
negative regulation of microtubule polymerization or depolymerization (GO:0031111)	49	10	2.71	3.69	2.42E-02
respiratory gaseous exchange by respiratory system (GO:0007585)	49	10	2.71	3.69	2.41E-02
cranial nerve development (GO:0021545)	54	11	2.99	3.68	1.52E-02
proteoglycan biosynthetic process (GO:0030166)	54	11	2.99	3.68	1.52E-02
positive regulation of dendrite morphogenesis (GO:0050775)	59	12	3.26	3.68	9.66E-03
purine ribonucleoside triphosphate metabolic process (GO:0009205)	187	38	10.34	3.68	2.19E-08
ribose phosphate biosynthetic process (GO:0046390)	193	39	10.67	3.66	1.51E-08
purine-containing compound biosynthetic process (GO:0072522)	189	38	10.45	3.64	2.74E-08
trans-synaptic signaling (GO:0099537)	385	77	21.28	3.62	5.14E-17
regulation of dendrite development (GO:0050773)	135	27	7.46	3.62	6.75E-06
regulation of neurotransmitter levels (GO:0001505)	252	50	13.93	3.59	9.01E-11
ribonucleoside triphosphate metabolic process (GO:0009199)	192	38	10.61	3.58	3.91E-08
negative regulation of protein polymerization (GO:0032272)	76	15	4.2	3.57	2.92E-03
purine nucleoside triphosphate metabolic process (GO:0009144)	193	38	10.67	3.56	4.42E-08
cellular component maintenance (GO:0043954)	61	12	3.37	3.56	1.19E-02
lipid translocation (GO:0034204)	51	10	2.82	3.55	3.03E-02
developmental growth involved in morphogenesis (GO:0060560)	153	30	8.46	3.55	2.20E-06
central nervous system neuron axonogenesis (GO:0021955)	46	9	2.54	3.54	4.89E-02

synaptic signaling (GO:0099536)	425	83	23.49	3.53	7.32E-18
cerebellar cortex development (GO:0021695)	67	13	3.7	3.51	8.43E-03
modulation of chemical synaptic transmission (GO:0050804)	526	102	29.08	3.51	9.94E-22
regulation of trans-synaptic signaling (GO:0099177)	527	102	29.13	3.5	1.05E-21
positive regulation of protein localization to plasma membrane (GO:1903078)	62	12	3.43	3.5	1.33E-02
regulation of extent of cell growth (GO:0061387)	124	24	6.85	3.5	4.94E-05
adult behavior (GO:0030534)	186	36	10.28	3.5	1.67E-07
aminoglycan biosynthetic process (GO:0006023)	52	10	2.87	3.48	3.37E-02
retina morphogenesis in camera-type eye (GO:0060042)	78	15	4.31	3.48	3.59E-03
cellular response to calcium ion (GO:0071277)	78	15	4.31	3.48	3.58E-03
protein localization to cell junction (GO:1902414)	99	19	5.47	3.47	5.86E-04
energy derivation by oxidation of organic compounds (GO:0015980)	245	47	13.54	3.47	1.10E-09
chemical synaptic transmission (GO:0007268)	366	70	20.23	3.46	1.50E-14
anterograde trans-synaptic signaling (GO:0098916)	366	70	20.23	3.46	1.47E-14
regulation of membrane potential (GO:0042391)	467	89	25.82	3.45	1.21E-18
regulation of calcium-mediated signaling (GO:0050848)	84	16	4.64	3.45	2.51E-03
regulation of dendritic spine development (GO:0060998)	84	16	4.64	3.45	2.50E-03
axo-dendritic transport (GO:0008088)	79	15	4.37	3.43	3.99E-03
membrane depolarization (GO:0051899)	53	10	2.93	3.41	3.73E-02
regulation of neurotransmitter receptor activity (GO:0099601)	69	13	3.81	3.41	1.02E-02
neuron projection morphogenesis (GO:0048812)	517	97	28.58	3.39	6.54E-20
regulation of synaptic plasticity (GO:0048167)	235	44	12.99	3.39	8.96E-09
positive regulation of cation channel activity (GO:2001259)	91	17	5.03	3.38	1.93E-03
modulation of excitatory postsynaptic potential (GO:0098815)	59	11	3.26	3.37	2.58E-02
response to calcium ion (GO:0051592)	129	24	7.13	3.37	8.81E-05
regulation of mitochondrial membrane potential (GO:0051881)	86	16	4.75	3.37	3.10E-03

central nervous system neuron development (GO:0021954)	97	18	5.36	3.36	1.33E-03
plasma membrane bounded cell projection morphogenesis (GO:0120039)	523	97	28.91	3.36	1.16E-19
cell projection morphogenesis (GO:0048858)	529	98	29.24	3.35	8.03E-20
regulation of microtubule polymerization or depolymerization (GO:0031110)	92	17	5.09	3.34	2.12E-03
negative regulation of protein depolymerization (GO:1901880)	76	14	4.2	3.33	8.07E-03
regulation of neuron projection development (GO:0010975)	549	101	30.35	3.33	3.37E-20
positive regulation of nervous system development (GO:0051962)	359	66	19.85	3.33	5.35E-13
regulation of axon extension (GO:0030516)	109	20	6.03	3.32	6.21E-04
positive regulation of neuron apoptotic process (GO:0043525)	88	16	4.86	3.29	3.77E-03
cell part morphogenesis (GO:0032990)	556	101	30.74	3.29	6.46E-20
nucleoside triphosphate metabolic process (GO:0009141)	210	38	11.61	3.27	2.80E-07
cell morphogenesis involved in neuron differentiation (GO:0048667)	482	87	26.65	3.27	6.37E-17
regulation of cation channel activity (GO:2001257)	195	35	10.78	3.25	1.20E-06
regulation of potassium ion transmembrane transporter activity (GO:1901016)	67	12	3.7	3.24	2.20E-02
axon development (GO:0061564)	419	75	23.16	3.24	2.47E-14
actin cytoskeleton reorganization (GO:0031532)	73	13	4.04	3.22	1.52E-02
axonogenesis (GO:0007409)	384	68	21.23	3.2	9.74E-13
neuron apoptotic process (GO:0051402)	113	20	6.25	3.2	9.36E-04
regulation of catecholamine secretion (GO:0050433)	68	12	3.76	3.19	2.42E-02
positive regulation of neuron projection development (GO:0010976)	223	39	12.33	3.16	3.92E-07
negative regulation of cell projection organization (GO:0031345)	212	37	11.72	3.16	9.26E-07
negative regulation of supramolecular fiber organization (GO:1902904)	172	30	9.51	3.16	1.68E-05
positive regulation of protein localization to cell periphery (GO:1904377)	69	12	3.81	3.15	2.63E-02
neuromuscular process (GO:0050905)	179	31	9.9	3.13	1.25E-05
positive regulation of neuron death (GO:1901216)	133	23	7.35	3.13	3.60E-04
neuron projection development (GO:0031175)	747	129	41.29	3.12	1.10E-23

learning (GO:0007612)	186	32	10.28	3.11	9.31E-06
positive regulation of dendritic spine development (GO:0060999)	64	11	3.54	3.11	4.23E-02
cellular component morphogenesis (GO:0032989)	653	112	36.1	3.1	1.97E-20
positive regulation of cell projection organization (GO:0031346)	438	75	24.21	3.1	1.87E-13
potassium ion transmembrane transport (GO:0071805)	146	25	8.07	3.1	1.83E-04
nucleotide biosynthetic process (GO:0009165)	228	39	12.6	3.09	6.26E-07
potassium ion transport (GO:0006813)	170	29	9.4	3.09	3.78E-05
nerve development (GO:0021675)	88	15	4.86	3.08	9.76E-03
cell junction organization (GO:0034330)	524	89	28.97	3.07	6.82E-16
axon guidance (GO:0007411)	242	41	13.38	3.06	3.62E-07
memory (GO:0007613)	160	27	8.84	3.05	1.02E-04
neuron projection guidance (GO:0097485)	243	41	13.43	3.05	3.92E-07
neuron development (GO:0048666)	921	154	50.91	3.02	1.75E-27
regulation of protein depolymerization (GO:1901879)	96	16	5.31	3.01	8.16E-03
nucleoside phosphate biosynthetic process (GO:1901293)	234	39	12.94	3.01	1.12E-06
regulation of regulated secretory pathway (GO:1903305)	186	31	10.28	3.01	2.51E-05
learning or memory (GO:0007611)	319	53	17.63	3.01	5.54E-09
regulation of nervous system development (GO:0051960)	554	92	30.63	3	6.57E-16
locomotory behavior (GO:0007626)	253	42	13.99	3	3.92E-07
regulation of synaptic transmission, glutamatergic (GO:0051966)	85	14	4.7	2.98	1.83E-02
regulation of oxidative stress-induced cell death (GO:1903201)	79	13	4.37	2.98	2.61E-02
neuron death (GO:0070997)	128	21	7.08	2.97	1.52E-03
negative regulation of neuron projection development (GO:0010977)	159	26	8.79	2.96	2.41E-04
negative regulation of nervous system development (GO:0051961)	172	28	9.51	2.94	1.22E-04
negative regulation of protein-containing complex disassembly (GO:0043242)	86	14	4.75	2.94	2.01E-02
positive regulation of transporter activity (GO:0032411)	142	23	7.85	2.93	8.39E-04
regulation of ion transmembrane transporter activity (GO:0032412)	291	47	16.09	2.92	1.20E-07
negative regulation of protein-containing complex assembly (GO:0031333)	143	23	7.91	2.91	9.15E-04

sensory perception of mechanical stimulus (GO:0050954)	199	32	11	2.91	3.24E-05
negative regulation of neurogenesis (GO:0050768)	168	27	9.29	2.91	2.14E-04
regulation of plasma membrane bounded cell projection organization (GO:0120035)	740	118	40.91	2.88	1.77E-19
neuron migration (GO:0001764)	157	25	8.68	2.88	5.05E-04
response to retinoic acid (GO:0032526)	82	13	4.53	2.87	3.37E-02
regulation of ion transmembrane transport (GO:0034765)	525	83	29.02	2.86	2.94E-13
regulated exocytosis (GO:0045055)	152	24	8.4	2.86	8.13E-04
regulation of cell size (GO:0008361)	209	33	11.55	2.86	3.13E-05
positive regulation of neurogenesis (GO:0050769)	298	47	16.47	2.85	2.16E-07
regulation of cell projection organization (GO:0031344)	756	119	41.79	2.85	2.79E-19
generation of precursor metabolites and energy (GO:0006091)	338	53	18.68	2.84	3.02E-08
positive regulation of ion transmembrane transporter activity (GO:0032414)	134	21	7.41	2.83	2.52E-03
regulation of transmembrane transporter activity (GO:0022898)	301	47	16.64	2.82	2.78E-07
neuron differentiation (GO:0030182)	1147	179	63.41	2.82	4.71E-29
regulation of cellular response to oxidative stress (GO:1900407)	90	14	4.98	2.81	2.74E-02
behavior (GO:0007610)	720	112	39.8	2.81	9.97E-18
regulation of cation transmembrane transport (GO:1904062)	412	64	22.78	2.81	7.72E-10
regulation of calcium ion transmembrane transporter activity (GO:1901019)	97	15	5.36	2.8	2.09E-02
cognition (GO:0050890)	356	55	19.68	2.79	2.31E-08
sensory perception of sound (GO:0007605)	169	26	9.34	2.78	5.73E-04
generation of neurons (GO:0048699)	1226	188	67.77	2.77	1.53E-29
negative regulation of cytoskeleton organization (GO:0051494)	170	26	9.4	2.77	6.22E-04
cell morphogenesis involved in differentiation (GO:0000904)	615	94	34	2.76	2.92E-14
regulation of transporter activity (GO:0032409)	315	48	17.41	2.76	3.72E-07
cell-cell adhesion (GO:0098609)	453	69	25.04	2.76	3.43E-10
positive regulation of developmental growth (GO:0048639)	217	33	12	2.75	6.36E-05
vesicle localization (GO:0051648)	178	27	9.84	2.74	5.02E-04
regulation of response to oxidative stress (GO:1902882)	99	15	5.47	2.74	2.42E-02

telencephalon development (GO:0021537)	258	39	14.26	2.73	8.95E-06
proteoglycan metabolic process (GO:0006029)	86	13	4.75	2.73	4.66E-02
signal release (GO:0023061)	206	31	11.39	2.72	1.49E-04
cell morphogenesis (GO:0000902)	785	118	43.4	2.72	9.95E-18
positive regulation of endocytosis (GO:0045807)	127	19	7.02	2.71	7.89E-03
regulation of neuron apoptotic process (GO:0043523)	288	43	15.92	2.7	4.31E-06
central nervous system neuron differentiation (GO:0021953)	201	30	11.11	2.7	2.39E-04
regulation of microtubule cytoskeleton organization (GO:0070507)	161	24	8.9	2.7	1.69E-03
regulation of protein localization to cell periphery (GO:1904375)	141	21	7.79	2.69	4.29E-03
cell junction assembly (GO:0034329)	262	39	14.48	2.69	1.75E-05
calcium ion transmembrane transport (GO:0070588)	162	24	8.96	2.68	1.83E-03
protein-containing complex localization (GO:0031503)	169	25	9.34	2.68	1.36E-03
regulation of neurogenesis (GO:0050767)	456	67	25.21	2.66	2.21E-09
cerebellum development (GO:0021549)	109	16	6.03	2.66	2.28E-02
positive regulation of plasma membrane bounded cell projection assembly (GO:0120034)	116	17	6.41	2.65	1.70E-02
sodium ion transmembrane transport (GO:0035725)	96	14	5.31	2.64	4.38E-02
inorganic cation transmembrane transport (GO:0098662)	460	67	25.43	2.63	4.57E-09
positive regulation of myeloid cell differentiation (GO:0045639)	112	16	6.19	2.58	2.80E-02
positive regulation of protein localization to membrane (GO:1905477)	112	16	6.19	2.58	2.79E-02
regulation of transmembrane transport (GO:0034762)	625	89	34.55	2.58	7.98E-12
exocytosis (GO:0006887)	253	36	13.99	2.57	9.20E-05
regulation of exocytosis (GO:0017157)	253	36	13.99	2.57	9.16E-05
cellular response to metal ion (GO:0071248)	169	24	9.34	2.57	3.99E-03
neurogenesis (GO:0022008)	1396	198	77.17	2.57	1.51E-27
positive regulation of cell growth (GO:0030307)	198	28	10.95	2.56	1.22E-03
regulation of ion transport (GO:0043269)	769	108	42.51	2.54	3.15E-14
regulation of protein localization to plasma membrane (GO:1903076)	114	16	6.3	2.54	3.23E-02

camera-type eye morphogenesis (GO:0048593)	150	21	8.29	2.53	1.09E-02
negative regulation of cell development (GO:0010721)	208	29	11.5	2.52	1.04E-03
protein localization to plasma membrane (GO:0072659)	216	30	11.94	2.51	8.10E-04
establishment of vesicle localization (GO:0051650)	166	23	9.18	2.51	6.57E-03
purine ribonucleotide metabolic process (GO:0009150)	356	49	19.68	2.49	4.09E-06
negative regulation of developmental growth (GO:0048640)	124	17	6.85	2.48	4.00E-02
positive regulation of cation transmembrane transport (GO:1904064)	190	26	10.5	2.48	3.08E-03
positive regulation of ion transmembrane transport (GO:0034767)	212	29	11.72	2.47	1.32E-03
circadian rhythm (GO:0007623)	139	19	7.68	2.47	2.26E-02
regulation of neuron death (GO:1901214)	397	54	21.95	2.46	1.82E-06
eye morphogenesis (GO:0048592)	177	24	9.78	2.45	5.88E-03
plasma membrane bounded cell projection organization (GO:0120036)	1174	159	64.9	2.45	3.27E-20
purine nucleotide metabolic process (GO:0006163)	371	50	20.51	2.44	7.10E-06
regulation of protein localization to membrane (GO:1905475)	201	27	11.11	2.43	2.86E-03
secretion by cell (GO:0032940)	432	58	23.88	2.43	6.56E-07
negative regulation of neuron apoptotic process (GO:0043524)	194	26	10.72	2.42	3.79E-03
inorganic ion transmembrane transport (GO:0098660)	516	69	28.52	2.42	4.41E-08
regulation of cellular component size (GO:0032535)	397	53	21.95	2.41	3.26E-06
cell projection organization (GO:0030030)	1225	163	67.72	2.41	5.25E-20
ribonucleotide metabolic process (GO:0009259)	376	50	20.79	2.41	8.32E-06
cation transmembrane transport (GO:0098655)	504	67	27.86	2.4	9.26E-08
positive regulation of cell development (GO:0010720)	377	50	20.84	2.4	8.62E-06
establishment of cell polarity (GO:0030010)	136	18	7.52	2.39	3.57E-02
response to metal ion (GO:0010038)	295	39	16.31	2.39	1.60E-04
hindbrain development (GO:0030902)	174	23	9.62	2.39	9.74E-03
calcium ion transport (GO:0006816)	235	31	12.99	2.39	1.58E-03
ribose phosphate metabolic process (GO:0019693)	387	51	21.39	2.38	7.28E-06

cardiac ventricle development (GO:0003231)	145	19	8.02	2.37	2.92E-02
nervous system development (GO:0007399)	2038	267	112.66	2.37	3.58E-33
export from cell (GO:0140352)	482	63	26.65	2.36	4.02E-07
cytoskeleton-dependent intracellular transport (GO:0030705)	199	26	11	2.36	7.18E-03
positive regulation of synaptic transmission (GO:0050806)	169	22	9.34	2.35	1.44E-02
cellular calcium ion homeostasis (GO:0006874)	200	26	11.06	2.35	7.40E-03
inner ear development (GO:0048839)	216	28	11.94	2.34	4.21E-03
regulation of metal ion transport (GO:0010959)	456	59	25.21	2.34	1.54E-06
brain development (GO:0007420)	673	87	37.2	2.34	1.16E-09
regulation of developmental growth (GO:0048638)	395	51	21.84	2.34	1.60E-05
cellular response to inorganic substance (GO:0071241)	194	25	10.72	2.33	1.00E-02
protein dephosphorylation (GO:0006470)	163	21	9.01	2.33	2.04E-02
regulation of muscle system process (GO:0090257)	257	33	14.21	2.32	1.25E-03
protein localization to cell periphery (GO:1990778)	265	34	14.65	2.32	9.69E-04
regulation of heart contraction (GO:0008016)	195	25	10.78	2.32	1.03E-02
positive regulation of cellular component biogenesis (GO:0044089)	535	68	29.57	2.3	2.71E-07
protein localization to membrane (GO:0072657)	473	60	26.15	2.29	2.56E-06
metal ion transport (GO:0030001)	608	77	33.61	2.29	3.56E-08
forebrain development (GO:0030900)	395	50	21.84	2.29	2.80E-05
cell-cell signaling (GO:0007267)	894	113	49.42	2.29	3.68E-12
purine-containing compound metabolic process (GO:0072521)	404	51	22.33	2.28	2.21E-05
regulation of cell development (GO:0060284)	596	75	32.95	2.28	7.28E-08
sensory organ morphogenesis (GO:0090596)	310	39	17.14	2.28	4.37E-04
regulation of supramolecular fiber organization (GO:1902903)	390	49	21.56	2.27	4.20E-05
regulation of calcium ion transmembrane transport (GO:1903169)	199	25	11	2.27	1.19E-02
regulation of protein polymerization (GO:0032271)	207	26	11.44	2.27	9.34E-03
positive regulation of cellular component organization (GO:0051130)	1180	148	65.23	2.27	4.71E-16

regulation of GTPase activity (GO:0043087)	351	44	19.4	2.27	1.76E-04
carbohydrate derivative biosynthetic process (GO:1901137)	538	67	29.74	2.25	7.63E-07
head development (GO:0060322)	731	91	40.41	2.25	2.43E-09
mitochondrion organization (GO:0007005)	452	56	24.99	2.24	1.10E-05
striated muscle tissue development (GO:0014706)	210	26	11.61	2.24	1.04E-02
calcium ion homeostasis (GO:0055074)	235	29	12.99	2.23	7.55E-03
regulation of endocytosis (GO:0030100)	235	29	12.99	2.23	7.53E-03
organophosphate biosynthetic process (GO:0090407)	471	58	26.04	2.23	7.57E-06
cardiac muscle tissue development (GO:0048738)	204	25	11.28	2.22	1.46E-02
regulation of vesicle-mediated transport (GO:0060627)	621	76	34.33	2.21	1.53E-07
central nervous system development (GO:0007417)	913	111	50.47	2.2	5.47E-11
regulation of plasma membrane bounded cell projection assembly (GO:0120032)	206	25	11.39	2.2	1.59E-02
negative regulation of neuron death (GO:1901215)	266	32	14.7	2.18	4.25E-03
secretion (GO:0046903)	550	66	30.4	2.17	2.99E-06
regulation of cell projection assembly (GO:0060491)	209	25	11.55	2.16	2.42E-02
localization within membrane (GO:0051668)	544	65	30.07	2.16	4.15E-06
positive regulation of growth (GO:0045927)	310	37	17.14	2.16	1.90E-03
cation transport (GO:0006812)	765	91	42.29	2.15	1.70E-08
muscle system process (GO:0003012)	253	30	13.99	2.15	8.06E-03
positive regulation of protein serine/threonine kinase activity (GO:0071902)	203	24	11.22	2.14	3.31E-02
regulation of cellular component biogenesis (GO:0044087)	983	116	54.34	2.13	8.22E-11
muscle organ development (GO:0007517)	297	35	16.42	2.13	3.46E-03
positive regulation of transmembrane transport (GO:0034764)	272	32	15.04	2.13	7.44E-03
cellular response to peptide (GO:1901653)	247	29	13.65	2.12	1.08E-02
positive regulation of ion transport (GO:0043270)	342	40	18.91	2.12	1.59E-03
negative regulation of cell motility (GO:2000146)	325	38	17.97	2.12	2.66E-03

muscle contraction (GO:0006936)	197	23	10.89	2.11	4.51E-02
regulation of cellular response to growth factor stimulus (GO:0090287)	317	37	17.52	2.11	3.46E-03
ear development (GO:0043583)	249	29	13.76	2.11	1.62E-02
divalent inorganic cation homeostasis (GO:0072507)	268	31	14.82	2.09	1.03E-02
second-messenger-mediated signaling (GO:0019932)	199	23	11	2.09	4.72E-02
cellular divalent inorganic cation homeostasis (GO:0072503)	225	26	12.44	2.09	2.41E-02
nucleotide metabolic process (GO:0009117)	477	55	26.37	2.09	9.56E-05
regulation of anatomical structure morphogenesis (GO:0022603)	989	114	54.67	2.09	5.83E-10
cellular response to organonitrogen compound (GO:0071417)	470	54	25.98	2.08	1.29E-04
actin filament-based process (GO:0030029)	592	68	32.73	2.08	7.84E-06
positive regulation of GTPase activity (GO:0043547)	262	30	14.48	2.07	1.41E-02
nucleoside phosphate metabolic process (GO:0006753)	484	55	26.76	2.06	1.68E-04
negative regulation of protein localization (GO:1903828)	221	25	12.22	2.05	3.48E-02
negative regulation of cellular component organization (GO:0051129)	718	81	39.69	2.04	1.32E-06
ion transmembrane transport (GO:0034220)	640	72	35.38	2.04	6.32E-06
regulation of transport (GO:0051049)	1940	218	107.24	2.03	2.74E-19
negative regulation of cell migration (GO:0030336)	312	35	17.25	2.03	7.53E-03
sensory system development (GO:0048880)	403	45	22.28	2.02	1.57E-03
negative regulation of locomotion (GO:0040013)	360	40	19.9	2.01	3.60E-03
locomotion (GO:0040011)	532	59	29.41	2.01	1.26E-04
regulation of anatomical structure size (GO:0090066)	561	62	31.01	2	9.24E-05
cell adhesion (GO:0007155)	887	98	49.03	2	9.98E-08
metal ion homeostasis (GO:0055065)	417	46	23.05	2	1.43E-03
small GTPase mediated signal transduction (GO:0007264)	246	27	13.6	1.99	3.62E-02
actin cytoskeleton organization (GO:0030036)	538	59	29.74	1.98	2.08E-04
cellular metal ion homeostasis (GO:0006875)	329	36	18.19	1.98	9.95E-03
regulation of cellular component organization (GO:0051128)	2474	270	136.76	1.97	1.09E-22

actin filament organization (GO:0007015)	266	29	14.7	1.97	3.36E-02
establishment of organelle localization (GO:0051656)	395	43	21.84	1.97	3.12E-03
eye development (GO:0001654)	396	43	21.89	1.96	3.21E-03
regulation of microtubule-based process (GO:0032886)	268	29	14.82	1.96	3.48E-02
negative regulation of transferase activity (GO:0051348)	259	28	14.32	1.96	4.41E-02
muscle structure development (GO:0061061)	518	56	28.64	1.96	4.93E-04
nucleobase-containing small molecule metabolic process (GO:0055086)	537	58	29.69	1.95	3.10E-04
regulation of cell growth (GO:0001558)	445	48	24.6	1.95	1.58E-03
visual system development (GO:0150063)	399	43	22.06	1.95	3.47E-03
renal system development (GO:0072001)	325	35	17.97	1.95	1.38E-02
regulation of intracellular transport (GO:0032386)	337	36	18.63	1.93	1.21E-02
chemotaxis (GO:0006935)	506	54	27.97	1.93	8.84E-04
taxis (GO:0042330)	508	54	28.08	1.92	9.14E-04
response to inorganic substance (GO:0010035)	461	49	25.48	1.92	1.98E-03
transmembrane receptor protein tyrosine kinase signaling pathway (GO:0007169)	387	41	21.39	1.92	8.44E-03
regulation of localization (GO:0032879)	2297	243	126.98	1.91	9.15E-19
positive regulation of protein localization (GO:1903829)	493	52	27.25	1.91	1.55E-03
negative regulation of phosphorylation (GO:0042326)	389	41	21.5	1.91	8.63E-03
positive regulation of hydrolase activity (GO:0051345)	544	57	30.07	1.9	7.72E-04
regulation of cytoskeleton organization (GO:0051493)	545	57	30.13	1.89	7.87E-04
regulation of system process (GO:0044057)	651	68	35.99	1.89	1.36E-04
cell development (GO:0048468)	1915	200	105.86	1.89	2.21E-14
ion homeostasis (GO:0050801)	527	55	29.13	1.89	1.24E-03
organelle localization (GO:0051640)	528	55	29.19	1.88	1.26E-03
cellular response to nitrogen compound (GO:1901699)	549	57	30.35	1.88	8.69E-04
negative regulation of organelle organization (GO:0010639)	357	37	19.74	1.87	1.63E-02
cation homeostasis (GO:0055080)	502	52	27.75	1.87	2.54E-03
regulation of protein-containing complex assembly (GO:0043254)	426	44	23.55	1.87	7.40E-03

urogenital system development (GO:0001655)	368	38	20.34	1.87	1.82E-02
positive regulation of developmental process (GO:0051094)	1505	155	83.2	1.86	2.25E-10
inorganic ion homeostasis (GO:0098771)	515	53	28.47	1.86	2.13E-03
kidney development (GO:0001822)	311	32	17.19	1.86	4.70E-02
camera-type eye development (GO:0043010)	350	36	19.35	1.86	2.12E-02
regulation of cellular localization (GO:0060341)	1051	108	58.1	1.86	5.83E-07
regulation of protein localization (GO:0032880)	944	97	52.18	1.86	2.57E-06
muscle tissue development (GO:0060537)	361	37	19.96	1.85	2.34E-02
sensory organ development (GO:0007423)	616	63	34.05	1.85	5.21E-04
positive regulation of transport (GO:0051050)	1076	110	59.48	1.85	4.19E-07
regulation of secretion (GO:0051046)	767	78	42.4	1.84	7.68E-05
cellular ion homeostasis (GO:0006873)	423	43	23.38	1.84	1.01E-02
regulation of biological quality (GO:0065008)	3833	389	211.89	1.84	4.17E-29
cellular cation homeostasis (GO:0030003)	404	41	22.33	1.84	1.51E-02
regulation of secretion by cell (GO:1903530)	681	69	37.65	1.83	2.98E-04
ion transport (GO:0006811)	1117	113	61.75	1.83	4.81E-07
cellular response to endogenous stimulus (GO:0071495)	931	94	51.47	1.83	8.85E-06
cellular response to growth factor stimulus (GO:0071363)	426	43	23.55	1.83	1.43E-02
negative regulation of phosphorus metabolic process (GO:0010563)	447	45	24.71	1.82	9.77E-03
negative regulation of phosphate metabolic process (GO:0045936)	447	45	24.71	1.82	9.74E-03
regulation of cell migration (GO:0030334)	987	99	54.56	1.81	6.45E-06
positive regulation of protein kinase activity (GO:0045860)	360	36	19.9	1.81	3.31E-02
cellular response to hormone stimulus (GO:0032870)	380	38	21.01	1.81	2.98E-02
negative regulation of protein phosphorylation (GO:0001933)	341	34	18.85	1.8	4.97E-02
anatomical structure morphogenesis (GO:0009653)	2337	233	129.19	1.8	4.76E-15
regulation of binding (GO:0051098)	404	40	22.33	1.79	2.19E-02
developmental growth (GO:0048589)	496	49	27.42	1.79	9.12E-03

cellular homeostasis (GO:0019725)	618	61	34.16	1.79	2.05E-03
regulation of cell motility (GO:2000145)	1044	103	57.71	1.78	6.52E-06
regulation of actin filament-based process (GO:0032970)	417	41	23.05	1.78	2.42E-02
positive regulation of molecular function (GO:0044093)	1506	148	83.25	1.78	1.42E-08
growth (GO:0040007)	500	49	27.64	1.77	9.66E-03
protein-containing complex assembly (GO:0065003)	1115	109	61.64	1.77	3.94E-06
organophosphate metabolic process (GO:0019637)	860	84	47.54	1.77	1.26E-04
response to growth factor (GO:0070848)	441	43	24.38	1.76	2.34E-02
protein-containing complex organization (GO:0043933)	1256	122	69.43	1.76	9.52E-07
regulation of multicellular organismal development (GO:2000026)	1545	150	85.41	1.76	2.21E-08
heart development (GO:0007507)	577	56	31.9	1.76	4.70E-03
regulation of protein kinase activity (GO:0045859)	598	58	33.06	1.75	4.25E-03
regulation of kinase activity (GO:0043549)	704	68	38.92	1.75	1.52E-03
supramolecular fiber organization (GO:0097435)	549	53	30.35	1.75	8.79E-03
cellular chemical homeostasis (GO:0055082)	518	50	28.64	1.75	1.16E-02
enzyme-linked receptor protein signaling pathway (GO:0007167)	602	58	33.28	1.74	4.44E-03
regulation of establishment of protein localization (GO:0070201)	582	56	32.17	1.74	6.79E-03
cytoskeleton organization (GO:0007010)	1185	114	65.51	1.74	4.35E-06
positive regulation of kinase activity (GO:0033674)	437	42	24.16	1.74	3.05E-02
positive regulation of catalytic activity (GO:0043085)	1083	104	59.87	1.74	1.47E-05
regulation of protein transport (GO:0051223)	553	53	30.57	1.73	9.22E-03
positive regulation of cell death (GO:0010942)	689	66	38.09	1.73	1.84E-03
system development (GO:0048731)	3813	365	210.78	1.73	1.16E-22
regulation of locomotion (GO:0040012)	1092	104	60.37	1.72	2.21E-05
organonitrogen compound biosynthetic process (GO:1901566)	1218	116	67.33	1.72	4.62E-06
establishment of localization in cell (GO:0051649)	1765	168	97.57	1.72	6.17E-09
regulation of DNA-binding transcription factor activity (GO:0051090)	435	41	24.05	1.71	4.17E-02

positive regulation of apoptotic process (GO:0043065)	606	57	33.5	1.7	8.64E-03
positive regulation of cell differentiation (GO:0045597)	991	93	54.78	1.7	1.45E-04
regulation of transferase activity (GO:0051338)	823	77	45.5	1.69	1.09E-03
carbohydrate derivative metabolic process (GO:1901135)	931	87	51.47	1.69	3.65E-04
nucleobase-containing compound biosynthetic process (GO:0034654)	793	74	43.84	1.69	1.53E-03
regulation of hydrolase activity (GO:0051336)	986	92	54.51	1.69	2.47E-04
cellular response to oxygen-containing compound (GO:1901701)	969	90	53.57	1.68	2.95E-04
regulation of growth (GO:0040008)	714	66	39.47	1.67	5.47E-03
positive regulation of programmed cell death (GO:0043068)	617	57	34.11	1.67	1.25E-02
regulation of molecular function (GO:0065009)	2583	238	142.79	1.67	7.88E-12
microtubule cytoskeleton organization (GO:0000226)	533	49	29.46	1.66	3.16E-02
phosphate-containing compound metabolic process (GO:0006796)	1772	162	97.96	1.65	2.00E-07
phosphorus metabolic process (GO:0006793)	1794	164	99.17	1.65	1.37E-07
regulation of developmental process (GO:0050793)	2652	242	146.6	1.65	1.04E-11
negative regulation of developmental process (GO:0051093)	999	91	55.22	1.65	5.15E-04
intracellular protein transport (GO:0006886)	651	59	35.99	1.64	1.64E-02
protein localization (GO:0008104)	1931	175	106.75	1.64	7.28E-08
regulation of signaling (GO:0023051)	3356	304	185.52	1.64	4.35E-15
apoptotic process (GO:0006915)	983	89	54.34	1.64	7.97E-04
cell death (GO:0008219)	1072	97	59.26	1.64	3.92E-04
cellular localization (GO:0051641)	2697	244	149.09	1.64	2.03E-11
cellular macromolecule localization (GO:0070727)	1935	175	106.97	1.64	7.60E-08
positive regulation of locomotion (GO:0040017)	622	56	34.38	1.63	2.24E-02
programmed cell death (GO:0012501)	1033	93	57.1	1.63	6.76E-04
regulation of cell communication (GO:0010646)	3348	301	185.08	1.63	1.99E-14
cellular component assembly (GO:0022607)	2204	198	121.84	1.63	1.03E-08
regulation of cell differentiation (GO:0045595)	1677	150	92.71	1.62	2.28E-06

regulation of organelle organization (GO:0033043)	1187	106	65.62	1.62	2.44E-04
response to endogenous stimulus (GO:0009719)	1156	103	63.9	1.61	3.38E-04
regulation of catalytic activity (GO:0050790)	1810	161	100.06	1.61	8.93E-07
transmembrane transport (GO:0055085)	972	86	53.73	1.6	2.14E-03
multicellular organism development (GO:0007275)	4559	403	252.02	1.6	8.05E-20
positive regulation of cell migration (GO:0030335)	578	51	31.95	1.6	4.63E-02
heterocycle biosynthetic process (GO:0018130)	864	76	47.76	1.59	6.14E-03
positive regulation of phosphorus metabolic process (GO:0010562)	924	81	51.08	1.59	4.27E-03
positive regulation of phosphate metabolic process (GO:0045937)	924	81	51.08	1.59	4.26E-03
positive regulation of cell motility (GO:2000147)	605	53	33.44	1.58	4.38E-02
intracellular transport (GO:0046907)	1303	114	72.03	1.58	2.52E-04
positive regulation of multicellular organismal process (GO:0051240)	1699	148	93.92	1.58	1.06E-05
vesicle-mediated transport (GO:0016192)	1414	123	78.17	1.57	1.45E-04
negative regulation of cell differentiation (GO:0045596)	714	62	39.47	1.57	2.59E-02
aromatic compound biosynthetic process (GO:0019438)	876	76	48.43	1.57	8.56E-03
cellular component organization (GO:0016043)	5412	469	299.18	1.57	2.64E-22
regulation of cell death (GO:0010941)	1767	153	97.68	1.57	9.64E-06
regulation of apoptotic process (GO:0042981)	1560	135	86.24	1.57	6.16E-05
regulation of phosphate metabolic process (GO:0019220)	1424	123	78.72	1.56	2.03E-04
establishment of protein localization (GO:0045184)	1228	106	67.88	1.56	7.62E-04
regulation of phosphorus metabolic process (GO:0051174)	1425	123	78.77	1.56	2.04E-04
microtubule-based process (GO:0007017)	812	70	44.89	1.56	1.51E-02
animal organ morphogenesis (GO:0009887)	1057	91	58.43	1.56	3.03E-03
regulation of programmed cell death (GO:0043067)	1592	137	88.01	1.56	5.91E-05
negative regulation of cell death (GO:0060548)	1118	96	61.8	1.55	2.12E-03
cell migration (GO:0016477)	945	81	52.24	1.55	8.12E-03

response to abiotic stimulus (GO:0009628)	983	84	54.34	1.55	6.46E-03
cellular component biogenesis (GO:0044085)	2437	208	134.72	1.54	1.56E-07
negative regulation of apoptotic process (GO:0043066)	962	82	53.18	1.54	8.92E-03
regulation of multicellular organismal process (GO:0051239)	2989	254	165.23	1.54	2.51E-09
cellular nitrogen compound biosynthetic process (GO:0044271)	1355	115	74.9	1.54	7.72E-04
regulation of cell adhesion (GO:0030155)	814	69	45	1.53	2.40E-02
cellular component organization or biogenesis (GO:0071840)	5606	475	309.9	1.53	7.10E-21
macromolecule localization (GO:0033036)	2329	197	128.75	1.53	6.37E-07
cellular developmental process (GO:0048869)	3702	313	204.65	1.53	7.40E-12
cell differentiation (GO:0030154)	3675	310	203.15	1.53	1.40E-11
negative regulation of programmed cell death (GO:0043069)	985	83	54.45	1.52	1.02E-02
localization (GO:0051179)	4500	379	248.76	1.52	5.72E-15
transport (GO:0006810)	3760	316	207.85	1.52	1.02E-11
establishment of localization (GO:0051234)	3923	329	216.86	1.52	3.53E-12
chemical homeostasis (GO:0048878)	942	79	52.07	1.52	1.56E-02
organelle organization (GO:0006996)	2886	242	159.54	1.52	2.51E-08
response to organonitrogen compound (GO:0010243)	802	67	44.33	1.51	4.38E-02
positive regulation of phosphorylation (GO:0042327)	839	70	46.38	1.51	3.38E-02
positive regulation of intracellular signal transduction (GO:1902533)	996	83	55.06	1.51	1.35E-02
regulation of intracellular signal transduction (GO:1902531)	1639	136	90.6	1.5	3.42E-04
regulation of phosphorylation (GO:0042325)	1270	105	70.21	1.5	3.86E-03
intracellular signal transduction (GO:0035556)	1456	119	80.49	1.48	2.09E-03
protein transport (GO:0015031)	1129	92	62.41	1.47	1.36E-02
circulatory system development (GO:0072359)	945	77	52.24	1.47	3.71E-02
anatomical structure development (GO:0048856)	5341	434	295.25	1.47	2.22E-15
response to oxygen-containing compound (GO:1901700)	1385	112	76.56	1.46	4.36E-03
organic substance biosynthetic process (GO:1901576)	2240	180	123.83	1.45	6.41E-05

negative regulation of cell communication (GO:0010648)	1397	112	77.23	1.45	7.02E-03
organic cyclic compound biosynthetic process (GO:1901362)	999	80	55.22	1.45	3.92E-02
regulation of signal transduction (GO:0009966)	2924	234	161.64	1.45	1.75E-06
regulation of protein phosphorylation (GO:0001932)	1125	90	62.19	1.45	2.42E-02
developmental process (GO:0032502)	5724	457	316.42	1.44	3.52E-15
negative regulation of molecular function (GO:0044092)	1031	82	56.99	1.44	4.44E-02
cell motility (GO:0048870)	1109	88	61.31	1.44	3.36E-02
animal organ development (GO:0048513)	3306	262	182.76	1.43	4.40E-07
negative regulation of signaling (GO:0023057)	1401	111	77.45	1.43	1.03E-02
cellular biosynthetic process (GO:0044249)	2150	170	118.85	1.43	3.09E-04
positive regulation of cell communication (GO:0010647)	1784	141	98.62	1.43	1.97E-03
negative regulation of signal transduction (GO:0009968)	1268	100	70.1	1.43	2.00E-02
negative regulation of multicellular organismal process (GO:0051241)	1154	91	63.79	1.43	3.31E-02
cellular response to chemical stimulus (GO:0070887)	2500	197	138.2	1.43	6.36E-05
positive regulation of signaling (GO:0023056)	1791	141	99.01	1.42	2.05E-03
biosynthetic process (GO:0009058)	2313	181	127.86	1.42	2.51E-04
cellular response to organic substance (GO:0071310)	1903	148	105.2	1.41	2.51E-03
regulation of protein modification process (GO:0031399)	1586	122	87.67	1.39	1.36E-02
homeostatic process (GO:0042592)	1469	113	81.21	1.39	1.95E-02
positive regulation of cellular process (GO:0048522)	5869	443	324.44	1.37	1.11E-10
positive regulation of signal transduction (GO:0009967)	1577	119	87.18	1.37	2.63E-02
negative regulation of cellular process (GO:0048523)	4808	362	265.79	1.36	5.26E-08
negative regulation of response to stimulus (GO:0048585)	1662	125	91.88	1.36	2.40E-02
organonitrogen compound metabolic process (GO:1901564)	4762	346	263.24	1.31	4.61E-06
response to chemical (GO:0042221)	3602	261	199.12	1.31	3.88E-04
positive regulation of biological process (GO:0048518)	6514	468	360.1	1.3	2.08E-08

negative regulation of biological process (GO:0048519)	5444	391	300.95	1.3	1.41E-06
regulation of response to stimulus (GO:0048583)	4140	288	228.86	1.26	1.84E-03
multicellular organismal process (GO:0032501)	7442	509	411.4	1.24	1.34E-06
protein metabolic process (GO:0019538)	3741	255	206.8	1.23	1.51E-02
cellular process (GO:0009987)	15352	1005	848.66	1.18	1.08E-20
regulation of cellular process (GO:0050794)	11607	751	641.64	1.17	1.09E-07
signaling (GO:0023052)	5487	354	303.32	1.17	3.49E-02
cellular metabolic process (GO:0044237)	6217	396	343.68	1.15	3.43E-02
biological regulation (GO:0065007)	12948	821	715.77	1.15	1.73E-07
regulation of biological process (GO:0050789)	12315	780	680.78	1.15	1.62E-06
biological_process (GO:0008150)	20785	1185	1149	1.03	9.19E-05

References

1. Purves D, ed. *Neuroscience*. 5th ed. Sinauer Associates; 2012.

2. Bharadwaj HM, Verhulst S, Shaheen L, Liberman MC, Shinn-Cunningham BG. Cochlear neuropathy and the coding of supra-threshold sound. *Front Syst Neurosci*. 2014;8. doi:10.3389/fnsys.2014.00026

3. Ryugo DK. The Auditory Nerve: Peripheral Innervation, Cell Body Morphology, and Central Projections. In: Webster DB, Popper AN, Fay RR, eds. *The Mammalian Auditory Pathway: Neuroanatomy*. Vol 1. Springer Handbook of Auditory Research. Springer New York; 1992:23-65. doi:10.1007/978-1-4612-4416-5_2

4. Liberman LD, Wang H, Liberman MC. Opposing Gradients of Ribbon Size and AMPA Receptor Expression Underlie Sensitivity Differences among Cochlear-Nerve/Hair-Cell Synapses. *Journal of Neuroscience*. 2011;31(3):801-808. doi:10.1523/JNEUROSCI.3389-10.2011

5. Sun S, Babola T, Pregernig G, et al. Hair Cell Mechanotransduction Regulates Spontaneous Activity and Spiral Ganglion Subtype Specification in the Auditory System. *Cell*. 2018;174(5):1247-1263.e15. doi:10.1016/j.cell.2018.07.008

6. Shrestha BR, Chia C, Wu L, Kujawa SG, Liberman MC, Goodrich LV. Sensory Neuron Diversity in the Inner Ear Is Shaped by Activity. *Cell*. 2018;174(5):1229-1246.e17. doi:10.1016/j.cell.2018.07.007

7. Petitpré C, Wu H, Sharma A, et al. Neuronal heterogeneity and stereotyped connectivity in the auditory afferent system. *Nat Commun*. 2018;9(1):3691. doi:10.1038/s41467-018-06033-3

8. Liu C, Glowatzki E, Fuchs PA. Unmyelinated type II afferent neurons report cochlear damage. *Proc Natl Acad Sci USA*. 2015;112(47):14723-14727. doi:10.1073/pnas.1515228112

9. Flores EN, Duggan A, Madathany T, et al. A Non-canonical Pathway from Cochlea to Brain Signals Tissue-Damaging Noise. *Current Biology*. 2015;25(5):606-612. doi:10.1016/j.cub.2015.01.009

10. Zhang KD, Coate TM. Recent advances in the development and function of type II spiral ganglion neurons in the mammalian inner ear. *Seminars in Cell & Developmental Biology*. 2017;65:80-87. doi:10.1016/j.semcdb.2016.09.017

11. Perkins RE, Morest DK. A study of cochlear innervation patterns in cats and rats with the Golgi method and Nomarski optics. *J Comp Neurol*. 1975;163(2):129-158. doi:10.1002/cne.901630202

12. Spoendlin H. Anatomy of Cochlear Innervation. *American Journal of Otolaryngology*. 1985;6(6):453-467. doi:10.1016/S0196-0709(85)80026-0

13. Liberman LD, Liberman MC. Postnatal maturation of auditory-nerve heterogeneity, as seen in spatial gradients of synapse morphology in the inner hair cell area. *Hearing Research*. 2016;339:12-22. doi:10.1016/j.heares.2016.06.002

14. Kiang N. *Discharge Patterns of Single Fibres in the Cat's Auditory Nerve*. Vol xvii, 154 p. illus. 25 cm. Cambridge, Mass., M.I.T. Press; 1965.

15. Wichmann C, Moser T. Relating structure and function of inner hair cell ribbon synapses. *Cell Tissue Res*. 2015;361(1):95-114. doi:10.1007/s00441-014-2102-7

16. Rutherford MA, von Gersdorff H, Goutman JD. Encoding sound in the cochlea: from receptor potential to afferent discharge. *The Journal of Physiology*. 2021;599(10):2527-2557. doi:10.1113/JP279189

17. Greenwood DD. A cochlear frequency-position function for several species—29 years later. *The Journal of the Acoustical Society of America*. 1990;87(6):2592-2605. doi:10.1121/1.399052

18. Müller M, Hünerbein K von, Hoidis S, Smolders JWT. A physiological place–frequency map of the cochlea in the CBA/J mouse. *Hearing Research*. 2005;202(1-2):63-73. doi:10.1016/j.heares.2004.08.011

19. Crozier RA, Davis RL. Unmasking of Spiral Ganglion Neuron Firing Dynamics by Membrane Potential and Neurotrophin-3. *Journal of Neuroscience*. 2014;34(29):9688-9702. doi:10.1523/JNEUROSCI.4552-13.2014

20. Markowitz AL, Kalluri R. Gradients in the biophysical properties of neonatal auditory neurons align with synaptic contact position and the intensity coding map of inner hair cells. *eLife*. 2020;9:e55378. doi:10.7554/eLife.55378

21. Liberman MC. Single-Neuron Labeling in the Cat Auditory Nerve. *Science*. 1982;216(4551):1239-1241. doi:10.1126/science.7079757

22. Meyer AC, Frank T, Khimich D, et al. Tuning of synapse number, structure and function in the cochlea. *Nat Neurosci*. 2009;12(4):444-453. doi:10.1038/nn.2293

23. Schmitz F, Königstorfer A, Südhof TC. RIBEYE, a Component of Synaptic Ribbons. *Neuron*. 2000;28(3):857-872. doi:10.1016/S0896-6273(00)00159-8

24. Frank T, Khimich D, Neef A, Moser T. Mechanisms contributing to synaptic Ca^{2+} signals and their heterogeneity in hair cells. *Proc Natl Acad Sci USA*. 2009;106(11):4483-4488. doi:10.1073/pnas.0813213106

25. Ohn TL, Rutherford MA, Jing Z, et al. Hair cells use active zones with different voltage dependence of Ca^{2+} influx to decompose sounds into complementary neural codes. *Proc Natl Acad Sci USA*. 2016;113(32). doi:10.1073/pnas.1605737113

26. Özçete ÖD, Moser T. A sensory cell diversifies its output by varying Ca^{2+} influx-release coupling among active zones. *The EMBO Journal*. 2021;40(5). doi:10.15252/embj.2020106010

27. Payne SA, Joens MS, Chung H, et al. Maturation of Heterogeneity in Afferent Synapse Ultrastructure in the Mouse Cochlea. *Front Synaptic Neurosci*. 2021;13:678575. doi:10.3389/fnsyn.2021.678575

28. Ruel J, Bobbin RP, Vidal D, Pujol R, Puel JL. The selective AMPA receptor antagonist GYKI 53784 blocks action potential generation and excitotoxicity in the guinea pig cochlea. *Neuropharmacology*. 2000;39(11):1959-1973. doi:10.1016/S0028-3908(00)00069-1

29. Ruel J, Chen C, Pujol R, Bobbin RP, Puel JL. AMPA-preferring glutamate receptors in cochlear physiology of adult guinea-pig. *The Journal of Physiology*. 1999;518(3):667-680. doi:10.1111/j.1469-7793.1999.0667p.x

30. Puel JL, Ruel J, Guitton M, Wang J, Pujol R. The Inner Hair Cell Synaptic Complex: Physiology, Pharmacology and New Therapeutic Strategies. *Audiol Neurotol*. 2002;7(1):49-54. doi:10.1159/000046864

31. Glowatzki E, Fuchs PA. Transmitter release at the hair cell ribbon synapse. *Nat Neurosci*. 2002;5(2):147-154. doi:10.1038/nn796

32. Hu N, Rutherford MA, Green SH. Protection of cochlear synapses from noise-induced excitotoxic trauma by blockade of Ca^{2+} -permeable AMPA receptors. *Proc Natl Acad Sci USA*. 2020;117(7):3828-3838. doi:10.1073/pnas.1914247117

33. Bonini D, Filippini A, La Via L, et al. Chronic glutamate treatment selectively modulates AMPA RNA editing and ADAR expression and activity in primary cortical neurons. *RNA Biology*. 2015;12(1):43-53. doi:10.1080/15476286.2015.1008365

34. Lomeli H, Mosbacher J, Melcher T, et al. Control of Kinetic Properties of AMPA Receptor Channels by Nuclear RNA Editing. *Science*. 1994;266(5191):1709-1713. doi:10.1126/science.7992055

35. Walia A, Lee C, Hartsock J, et al. Reducing Auditory Nerve Excitability by Acute Antagonism of Ca2+-Permeable AMPA Receptors. *Front Synaptic Neurosci*. 2021;13:680621. doi:10.3389/fnsyn.2021.680621

36. Yuan Y, Shi F, Yin Y, et al. Ouabain-Induced Cochlear Nerve Degeneration: Synaptic Loss and Plasticity in a Mouse Model of Auditory Neuropathy. *JARO*. 2014;15(1):31-43. doi:10.1007/s10162-013-0419-7

37. Niwa M, Young ED, Glowatzki E, Ricci AJ. Functional subgroups of cochlear inner hair cell ribbon synapses differently modulate their EPSC properties in response to stimulation. *Journal of Neurophysiology*. 2021;125(6):2461-2479. doi:10.1152/jn.00452.2020

38. Davis RL. Gradients of Neurotrophins, Ion Channels, and Tuning in the Cochlea. *Neuroscientist*. 2003;9(5):311-316. doi:10.1177/1073858403251986

39. Schmiedt RA, Mills JH, Boettcher FA. Age-related loss of activity of auditory-nerve fibers. *Journal of Neurophysiology*. 1996;76(4):2799-2803. doi:10.1152/jn.1996.76.4.2799

40. Sergeyenko Y, Lall K, Liberman MC, Kujawa SG. Age-Related Cochlear Synaptopathy: An Early-Onset Contributor to Auditory Functional Decline. *Journal of Neuroscience*. 2013;33(34):13686-13694. doi:10.1523/JNEUROSCI.1783-13.2013

41. Appler JM, Goodrich LV. Connecting the ear to the brain: Molecular mechanisms of auditory circuit assembly. *Progress in Neurobiology*. 2011;93(4):488-508. doi:10.1016/j.pneurobio.2011.01.004

42. Coate TM, Raft S, Zhao X, Ryan AK, Crenshaw EB, Kelley MW. Otic Mesenchyme Cells Regulate Spiral Ganglion Axon Fasciculation through a Pou3f4/EphA4 Signaling Pathway. *Neuron*. 2012;73(1):49-63. doi:10.1016/j.neuron.2011.10.029

43. Lu CC, Appler JM, Houseman EA, Goodrich LV. Developmental Profiling of Spiral Ganglion Neurons Reveals Insights into Auditory Circuit Assembly. *Journal of Neuroscience*. 2011;31(30):10903-10918. doi:10.1523/JNEUROSCI.2358-11.2011

44. Appler JM, Lu CC, Druckenbrod NR, Yu WM, Koundakjian EJ, Goodrich LV. Gata3 Is a Critical Regulator of Cochlear Wiring. *Journal of Neuroscience*. 2013;33(8):3679-3691. doi:10.1523/JNEUROSCI.4703-12.2013

45. Shrestha BR, Wu L, Goodrich LV. *Regulation of Auditory Sensory Neuron Diversity by Runx1*. Neuroscience; 2022. doi:10.1101/2022.08.02.502556

46. Yu WM, Goodrich LV. Morphological and physiological development of auditory synapses. *Hearing Research*. 2014;311:3-16. doi:10.1016/j.heares.2014.01.007

47. Sendin G, Bulankina AV, Riedel D, Moser T. Maturation of Ribbon Synapses in Hair Cells Is Driven by Thyroid Hormone. *Journal of Neuroscience*. 2007;27(12):3163-3173. doi:10.1523/JNEUROSCI.3974-06.2007

48. Huang LC, Barclay M, Lee K, et al. Synaptic profiles during neurite extension, refinement and retraction in the developing cochlea. *Neural Dev*. 2012;7(1):38. doi:10.1186/1749-8104-7-38

49. Michanski S, Smaluch K, Steyer AM, et al. Mapping developmental maturation of inner hair cell ribbon synapses in the apical mouse cochlea. *Proc Natl Acad Sci USA*. 2019;116(13):6415-6424. doi:10.1073/pnas.1812029116

50. Yu WM, Appler JM, Kim YH, Nishitani AM, Holt JR, Goodrich LV. A Gata3–Mafb transcriptional network directs post-synaptic differentiation in synapses specialized for hearing. *eLife*. 2013;2:e01341. doi:10.7554/eLife.01341

51. Rodríguez-Martínez JA, Reinke AW, Bhimsaria D, Keating AE, Ansari AZ. Combinatorial bZIP dimers display complex DNA-binding specificity landscapes. *eLife*. 2017;6:e19272. doi:10.7554/eLife.19272

52. Yang Y, Cvekl A. Large Maf Transcription Factors: Cousins of AP-1 Proteins and Important Regulators of Cellular Differentiation. *EJBM*. 2016;23(1):2. doi:10.23861/EJBM20072347

53. Suda N, Itoh T, Nakato R, et al. Dimeric combinations of MafB, cFos and cJun control the apoptosis-survival balance in limb morphogenesis. *Development*. 2014;141(14):2885-2894. doi:10.1242/dev.099150

54. Pogenberg V, Consani Textor L, Vanhille L, Holton SJ, Sieweke MH, Wilmanns M. Design of a bZip Transcription Factor with Homo/Heterodimer-Induced DNA-Binding Preference. *Structure*. 2014;22(3):466-477. doi:10.1016/j.str.2013.12.017

55. Wende H, Lechner SG, Cheret C, et al. The Transcription Factor c-Maf Controls Touch Receptor Development and Function. *Science*. 2012;335(6074):1373-1376. doi:10.1126/science.1214314

56. Pai ELL, Vogt D, Clemente-Perez A, et al. Mafb and c-Maf Have Prenatal Compensatory and Postnatal Antagonistic Roles in Cortical Interneuron Fate and Function. *Cell Reports*. 2019;26(5):1157-1173.e5. doi:10.1016/j.celrep.2019.01.031

57. Pai ELL, Chen J, Fazel Darbandi S, et al. Maf and Mafb control mouse pallial interneuron fate and maturation through neuropsychiatric disease gene regulation. *eLife*. 2020;9:e54903. doi:10.7554/eLife.54903

58. Becker L, Schnee ME, Niwa M, et al. The presynaptic ribbon maintains vesicle populations at the hair cell afferent fiber synapse. *eLife*. 2018;7:e30241. doi:10.7554/eLife.30241

59. Hickman TT, Hashimoto K, Liberman LD, Liberman MC. Synaptic migration and reorganization after noise exposure suggests regeneration in a mature mammalian cochlea. *Sci Rep*. 2020;10(1):19945. doi:10.1038/s41598-020-76553-w

60. Sobkowicz H, Rose J, Scott G, Slapnick S. Ribbon synapses in the developing intact and cultured organ of Corti in the mouse. *J Neurosci*. 1982;2(7):942-957. doi:10.1523/JNEUROSCI.02-07-00942.1982

61. Sherrill HE, Jean P, Driver EC, et al. Pou4f1 Defines a Subgroup of Type I Spiral Ganglion Neurons and Is Necessary for Normal Inner Hair Cell Presynaptic Ca^{2+} Signaling. *J Neurosci*. 2019;39(27):5284-5298. doi:10.1523/JNEUROSCI.2728-18.2019

62. Kane KL, Longo-Guess CM, Gagnon LH, Ding D, Salvi RJ, Johnson KR. Genetic background effects on age-related hearing loss associated with Cdh23 variants in mice. *Hearing Research*. 2012;283(1-2):80-88. doi:10.1016/j.heares.2011.11.007

63. Melcher JR, Kiang NYS. Generators of the brainstem auditory evoked potential in cat III: identified cell populations. *Hearing Research*. 1996;93(1-2):52-71. doi:10.1016/0378-5955(95)00200-6

64. Petitpré C, Faure L, Uhl P, et al. Single-cell RNA-sequencing analysis of the developing mouse inner ear identifies molecular logic of auditory neuron diversification. *Nat Commun*. 2022;13(1):3878. doi:10.1038/s41467-022-31580-1

65. Del Barrio MG, Bourane S, Grossmann K, et al. A Transcription Factor Code Defines Nine Sensory Interneuron Subtypes in the Mechanosensory Area of the Spinal Cord. Baccei ML, ed. *PLoS ONE*. 2013;8(11):e77928. doi:10.1371/journal.pone.0077928

66. Hafemeister C, Satija R. Normalization and variance stabilization of single-cell RNA-seq data using regularized negative binomial regression. *Genome Biol*. 2019;20(1):296. doi:10.1186/s13059-019-1874-1

67. Gall D, Roussel C, Susa I, et al. Altered Neuronal Excitability in Cerebellar Granule Cells of Mice Lacking Calretinin. *J Neurosci*. 2003;23(28):9320-9327. doi:10.1523/JNEUROSCI.23-28-09320.2003

68. Schwaller B. Calretinin: from a “simple” Ca2+ buffer to a multifunctional protein implicated in many biological processes. *Front Neuroanat*. 2014;8. doi:10.3389/fnana.2014.00003

69. Yamawaki TM, Lu DR, Ellwanger DC, et al. Systematic comparison of high-throughput single-cell RNA-seq methods for immune cell profiling. *BMC Genomics*. 2021;22(1):66. doi:10.1186/s12864-020-07358-4

70. Wiens KM. Rac1 Induces the Clustering of AMPA Receptors during Spinogenesis. *Journal of Neuroscience*. 2005;25(46):10627-10636. doi:10.1523/JNEUROSCI.1947-05.2005

71. Oh D, Han S, Seo J, et al. Regulation of Synaptic Rac1 Activity, Long-Term Potentiation Maintenance, and Learning and Memory by BCR and ABR Rac GTPase-Activating Proteins. *Journal of Neuroscience*. 2010;30(42):14134-14144. doi:10.1523/JNEUROSCI.1711-10.2010

72. Park P, Kang H, Sanderson TM, et al. The Role of Calcium-Permeable AMPARs in Long-Term Potentiation at Principal Neurons in the Rodent Hippocampus. *Front Synaptic Neurosci*. 2018;10:42. doi:10.3389/fnsyn.2018.00042

73. Gohla A, Bokoch GM. 14-3-3 Regulates Actin Dynamics by Stabilizing Phosphorylated Cofilin. *Current Biology*. 2002;12(19):1704-1710. doi:10.1016/S0960-9822(02)01184-3

74. Qiao H, Foote M, Graham K, Wu Y, Zhou Y. 14-3-3 Proteins Are Required for Hippocampal Long-Term Potentiation and Associative Learning and Memory. *J Neurosci*. 2014;34(14):4801-4808. doi:10.1523/JNEUROSCI.4393-13.2014

75. Finci L, Zhang Y, Meijers R, Wang JH. Signaling mechanism of the netrin-1 receptor DCC in axon guidance. *Progress in Biophysics and Molecular Biology*. 2015;118(3):153-160. doi:10.1016/j.pbiomolbio.2015.04.001

76. Kim YJ, Wang S zhi, Tymanskyj S, Ma L, Tao HW, Zhang LI. Dcc Mediates Functional Assembly of Peripheral Auditory Circuits. *Sci Rep*. 2016;6(1):23799. doi:10.1038/srep23799

77. Williams ME, Wilke SA, Daggett A, et al. Cadherin-9 Regulates Synapse-Specific Differentiation in the Developing Hippocampus. *Neuron*. 2011;71(4):640-655. doi:10.1016/j.neuron.2011.06.019

78. Cho IH, Panzera LC, Chin M, et al. The potassium channel subunit K_v β1 serves as a major control point for synaptic facilitation. *Proc Natl Acad Sci USA*. 2020;117(47):29937-29947. doi:10.1073/pnas.2000790117

79. Sun W, Maffie JK, Lin L, Petralia RS, Rudy B, Hoffman DA. DPP6 Establishes the A-Type K+ Current Gradient Critical for the Regulation of Dendritic Excitability in CA1 Hippocampal Neurons. *Neuron*. 2011;71(6):1102-1115. doi:10.1016/j.neuron.2011.08.008

80. Goel M, Aponte AM, Wistow G, Badea TC. Molecular studies into cell biological role of Copine-4 in Retinal Ganglion Cells. Agudo-Barriuso M, ed. *PLoS ONE*. 2021;16(11):e0255860. doi:10.1371/journal.pone.0255860

81. Ramirez MA, Ninoyu Y, Miller C, et al. Cochlear ribbon synapse maturation requires Nlgn1 and Nlgn3. *iScience*. 2022;25(8):104803. doi:10.1016/j.isci.2022.104803

82. Jean P, Özçete ÖD, Tarchini B, Moser T. Intrinsic planar polarity mechanisms influence the position-dependent regulation of synapse properties in inner hair cells. *Proc Natl Acad Sci USA*. 2019;116(18):9084-9093. doi:10.1073/pnas.1818358116

83. Joo JY, Schaukowitch K, Farbiak L, Kilaru G, Kim TK. Stimulus-specific combinatorial functionality of neuronal c-fos enhancers. *Nat Neurosci*. 2016;19(1):75-83. doi:10.1038/nn.4170

84. Sheng M, Greenberg ME. The regulation and function of c-fos and other immediate early genes in the nervous system. *Neuron*. 1990;4(4):477-485. doi:10.1016/0896-6273(90)90106-P